12-16-2015

Monitoring of Breathing Activity using Smartphone-acquired Signals

Bersain A. Reyes
University of Connecticut - Storrs, bersain.reyes@uconn.edu

Monitoring of Breathing Activity using Smartphone-acquired Signals

Bersain Alexander Reyes, PhD

University of Connecticut, 2015

Respiratory rate (RR) and tidal volume (V_T) are two parameters that a breathing monitor should provide. Several techniques have been developed for monitoring these parameters in clinical and research settings. However, as being designed for such settings, they employ specialized devices that are not translated easily to everyday use due to their high costs, need for skilled operators, or limited mobility. Hence, there is still a lack of portable monitoring devices that can noninvasively estimate RR and V_T on a daily basis for the general population. Among V_T and RR monitoring methods, respiratory acoustical and noncontact optical approaches have provided promising results. Nowadays it is recognized that more information beyond those parameters can be extracted from respiratory sounds via their digital analysis, which in turns involves the classification of their breath phases. Such classification is trivial when using an external reference like airflow/volume from spirometry, but generally this availability cannot be taken for granted outside clinical and research settings. In this dissertation, we explored the feasibility of developing a portable, accurate, and ease-of-use breathing monitoring device based on a smartphone. Smartphones are an enticing option for developing health applications due to their ubiquity, and software and hardware capabilities. First, we tested the reliability of acquiring real tracheal sounds using smartphones. Then, we performed the tracking of RR at each time instant (IRR) and the estimation of V_T from the smartphone-acquired tracheal sounds. Next, we estimated these parameters directly on the smartphone via a noncontact optical monitoring approach able to track the temporal variations of the volumetric changes produced while breathing. Finally, we explored the automatic breath-phase classification of smartphone-acquired respiratory sounds directly on a smartphone. The results obtained in this research regarding the acquisition of tracheal sounds via smartphones, the estimation of IRR and V_T via acoustical and optical approaches, and the automatic classification of respiratory breath phases directly on the smartphone, would help to provide the basis for developing a portable, easy-to-use, and reliable breathing monitoring system that would expand the monitoring options available on a daily-basis to the general population.

Monitoring of Breathing Activity using Smartphone-acquired Signals

Bersain Alexander Reyes

B.S., Universidad Autónoma Metropolitana, México, **2006**

M.S., Universidad Autónoma Metropolitana, México, **2010**

A Dissertation

Submitted in Partial Fulfillment of the

Requirements for the Degree of

Doctor of Philosophy

at the

University of Connecticut

2015

APPROVAL PAGE

Doctor of Philosophy Dissertation

Monitoring of Breathing Activity using Smartphone-acquired Signals

Presented by

Bersain Alexander Reyes, B.S., M.S.

Major Advisor _____
Dr. Ki H. Chon

Associate Advisor _____
Dr. Kazunori Hoshino

Associate Advisor _____
Dr. Sabato Santaniello

Associate Advisor _____
Dr. Sonia Charleston-Villalobos

University of Connecticut
2015

Acknowledgements

I would like to start thanking Dr. Ki Chon, for his constant guidance and support throughout the whole duration of my formation under his advice. I have learned from him not only technical or professional skills but also many positive attitudes towards the research process that would be very helpful in my upcoming career.

I appreciate and recognize the efforts made by my committee members Dr. Kazunori Hoshino, Dr. Sabato Santaniello, and Dr. Sonia Charleston-Villalobos for their feedback provided to improve this research, and for their support during my academic formation.

Thanks to the US Army Medical Research and Material Command (US-AMRMC) for partially supporting this research under grant No. W81XWH-12-1-0541.

I would like to thank the National Council of Science and Technology (Consejo Nacional de Ciencia y Tecnologia, CONACyT) of Mexico for the scholarship granted to me for pursing the Doctoral degree in the United States of America.

Thanks to the research group headed by Dr. Tomas Aljama-Corrales and Dr. Ramon Gonzalez-Camarena in Mexico City for being collaborative over the past years, in particular for sharing their sensors and signals, as well as for looking after me from the distance. Thanks also to Dr. Yunyoung Nam and Dr. Sangho Ha for their collaboration in this research.

I am very grateful to each postdoctoral, graduate and undergraduate researcher at the laboratory of Dr. Chon with whom I had the opportunity to share and learn experiences and thoughts in both professional and personal life aspects. Every day, I feel blessed for having such a good friends I can rely on.

Thanks to the many students at Worcester Polytechnic Institute and University of Connecticut with whom I shared courses, projects, and multiple activities throughout my stay at those institutions.

I would like to thank my parents and siblings for giving me support and stimulate me to pursue my goals. Finally, I want to especially acknowledge my wife, Beatriz, and my son, David, for their infinite love and comprehension that made easier this enriching period of my life.

Table of Contents

Table of Figures

Table of Tables

List of Abbreviations

BFD	Blanket fractal dimension
bpm	Breaths-per-minute
COPD	Chronic obstructive pulmonary disease
CORSA	Computerized respiratory sounds analysis
EAA	Extrinsic allergic alveolitis
EMD	Empirical mode decomposition
FFT	Fast Fourier transform
FIR	Finite impulse response
fps	Frames-per-second
HR	Heart rate
ICA	Independent component analysis
IMF	Intrinsic mode function
IRR	Instantaneous respiratory rate
IS	Incentive spirometer
NRMSE	Normalized root-mean-squared error
OS	Operating system
pdf	Probability density function
PSD	Power spectral density
RGB	Red-green-blue color channels of image
RMSE	Root-mean-squared error
ROI	Region of interest of image
RR	Respiratory rate
SE	Shannon entropy
SP	Spectrogram
SPWVD	Smoothed pseudo Wigner-Ville distribution
STFT	Short-time Fourier transform
TFR	Time-frequency representation
WVD	Wigner-Ville distribution
$\dot{V}_E$	Minute ventilation
V_T	Tidal volume

Chapter 1: Introduction

1.1 Overview

Breathing is an essential activity for human life [1]. While breathing, a variety of respiratory sounds are produced including breath sounds (basal or base sounds), adventitious sounds (added or superimposed sounds), and sounds from the respiratory muscles with exclusion of voiced sounds [2]. According to their recording location, respiratory sounds are classified as lung sounds, if heard or detected over the chest wall or within the chest, or as tracheal sounds if heard or detected over the extrathoracic part of the trachea or close to the mouth [2]. Among respiratory sounds, tracheal sounds are of particular interest in the detection of pulmonary diseases as well as monitoring of breathing activity [3]–[5]. An important step in the analysis of tracheal sounds involves the automatic classification of the recorded inspiratory and expiratory phases which is classically performed using an external reference signal like airflow or volume from a spirometer [6].

The monitoring of breathing activity has been recognized as critical in identifying and predicting adverse events [7], *e.g.*, in assessing risky situations involving respiratory failure [1], [8]. Two basic parameters that a breathing monitor should be able to provide are tidal volume (V_T) and respiration rate (RR) [1]. V_T provides information about the respiration depth and is defined as the volume of air moved with each breath; on the other hand, RR corresponds to the number of breaths per unit of time and it is commonly expressed in breaths-per-minute (bpm). In turn, the product of these two quantities defines the volume of gas moved by the respiratory system per minute, called minute ventilation ($\dot{V}_E$). Normal average values for a human man are around 0.5 L and 12 bpm for V_T and RR, respectively. These values are not fixed and $\dot{V}_E$ is determined by adjusting the combination of V_T and RR according to a body's requirements in response to different scenarios [9].

The most natural method for monitoring breathing activity is the qualified human observation. Although it has the advantages of being technology independent, adaptive, and fast responding; human

observation is subjective, time-consuming, and not always accurate [1]. Similar observations apply when breathing monitoring is aided with the mechanical stethoscope [10], [11]. Fortunately, the computerized monitoring of breathing activity has overcome some limitations of the human observation and mechanical stethoscope and accelerated the interest in the field over the last decades. As a side effect of this renaissance, the computerized respiratory sounds analysis (CORSA) has produced several different measurement systems by different laboratories [12]–[14] but standardization of CORSA systems has been addressed, and guidelines for the minimum requirements of systems have been provided [15], [16]. Current employment of computerized systems allows quantification of changes in breathing parameters, correlation of these quantities with other physiological signals, and generation of useful data representations [17]. Even with those advantages, qualified human observation and auscultation with the stethoscope still guides the physician when other tests are not available [18]. Ubiquity, low-cost, mobility, ease-of-use, and non-invasiveness are some characteristics that made the stethoscope the most widely used instrument in clinical practice. Such characteristics should remain when aiming for the development of a breathing monitoring system.

Nowadays, smartphones are widely available and their use for everyday activities, including vital sign measurements, has become popular as they have been found to be accurate and robust. In particular, our research group has made efforts to employ smartphones for health monitoring in the area of cardiac monitoring [19], [20]. Smartphones have fast microprocessors, large data storage, multiple sensors, peripheral connectivity, media capabilities, and software capabilities that give them advantages over other architectures in terms of implementation, upgrading, and integration with other health monitoring technologies. These characteristics make smartphones an enticing option for developing a ubiquitous breathing monitoring system.

1.2 Problem Statement

The need for reliable devices that can record and analyze respiratory sounds in a continuous and portable fashion stand still, and specialized committees have stated that “one goal of the current

technological developments is to combine processing power, storage, miniaturization of components and analysis programed into a small hand-held computerized stethoscope that will provide the clinician with much more useful information than the current simple mechanical stethoscope [21]." Efforts have been done to develop mobile CORSA systems with those characteristics [22]–[24]. However, these efforts have not questioned the reliability of the acquired respiratory sounds or have mainly focused on testing their subsystems via sounds obtained from databases. In addition, estimation of breathing activity parameters, like RR or V_T, from smartphone-acquired respiratory sounds has not been performed.

Currently, diverse clinical methods exist for monitoring RR [25]–[28] as well as V_T [29]–[34]. Each method has its own disadvantages. However flawed, at least clinical and research devices exist for monitoring RR and V_T parameters but having been designed for clinical settings or research centers, these methods employ specialized devices that are not translated easily to everyday use due to their high costs, need for skilled operators, or limited mobility. Outside clinical or research settings, there is still a lack of monitoring devices that can accurately determine RR and V_T in a noninvasive way and can be used on a daily basis.

In addition to the estimation of RR and V_T parameters, it is now recognized that more information can be obtained from respiratory sounds. In order to achieve that, an important step in respiratory sound analysis involves the classification of the breath phases recorded during the breathing maneuvers. The importance of this classification is exemplified by the recognition that the timing and the relationship of adventitious (superimposed) respiratory sounds to the breath phase must be characterized as they have been found to differ between different pulmonary disorders, reflecting different pathophysiology [35], [36]. Classically, this phase classification is performed by using phonopneumography –the simultaneous representation of respiratory sounds and airflow or volume signals- to accurate find the timing or volume level of occurrences of respiratory sounds and their relationship to the breath phases [35]. However, due to the current breathing monitoring limitations, outside clinical and research settings these airflow or

volume signals cannot always be taken for granted. Hence, a portable and low-cost phonopneumography system is still pending of development.

In this dissertation, we took advantage of the smartphone's processing power, peripheral noninvasive and cost-effective sensors to explore their use for breathing monitoring purposes. In particular, this research focused on the smartphone-acquisition of tracheal sounds and their use for estimating RR as well as V_T. In contrast to only average estimation, the temporal variation of RR at each time instant, *i.e.*, instantaneous RR (IRR) was tracked. In addition to estimate such parameters via the aforementioned acoustical approach, a non-contact optical approach was also explored for IRR and V_T estimation. Finally, both smartphone-based approaches, *i.e.*, the optical and the acoustical, were jointed for the task of automatically classify the tracheal sounds when an external temporal reference like the airflow is not available.

We consider that this research would provide some basis for developing a portable, reliable and inexpensive breathing monitoring system that would expand the monitoring options available to the general population. Also, it would allow practitioners in more health centers to undertake the quantitative analysis of respiratory sounds during the clinical examination. In particular, it would allow the monitoring of IRR and V_T parameters on a daily basis as well as the automatic classification of breath-phases without relying on the availability of airflow or volume signals from specialized devices. The low-cost and portability of the proposed system would aid in the acquisition of large-sample studies in locations not easily accessible nowadays with the currently used computerized systems.

1.3 Summary of Objectives

We hypothesize that a reliable breathing monitoring system with respiratory sound analysis capabilities can be implemented using a commercially available smartphone. First research question regards with the reliability of the proposed smartphone-based system to acquire real tracheal sounds during breathing maneuvers. To this end, the smartphone-acquired tracheal sounds should exhibit

characteristics in agreement to what has been reported in the literature when using classical CORSA systems. Second question regards with the feasibility of extracting information from the smartphone-acquired tracheal sounds that enables the estimation of IRR and V_T using a simple calibration procedure and without relying on the use of specialized devices. Third question involves the further exploitation of smartphone's sensors to estimate IRR and V_T directly on the smartphone without using an external sensor. Finally, we question if the automatic classification of respiratory sounds recorded under a diversity of scenarios found in practice can be fully performed on a smartphone so that a portable phonopneumogram system can be fully implemented on a smartphone. To this end, the **specific aims** of this thesis dissertation are:

Aim 1. Reliable acquisition of tracheal sounds via smartphone-based system.

Aim 2. Estimation of breathing parameters using the smartphone-acquired tracheal sounds.

Aim 3. Estimation of breathing parameters using an optical approach implemented on a smartphone.

Aim 4. Automatic breath-phase classification of tracheal sounds using smartphone-acquired signals.

To achieve **Aim 1**, the reliability of our proposed smartphone-based system will be tested on the well-known characteristics of the tracheal sounds like well-defined breath phases, similar frequency content for the inspiratory and expiratory phases, and in more detail the airflow-dependent amplitude relationship. This amplitude-airflow relationship will be helpful to detect the breath-phase onsets from the smartphone-acquired tracheal sounds and these detection results will be compared with those obtained using the airflow from a spirometer considered as reference. Achieving of this aim will provide the foundations to extract breathing monitoring parameters from smartphone-acquired tracheal sounds.

Aim 2 will be partially achieved by tracking the temporal evolution of the respiration rates (IRR estimation) from smartphone-acquired tracheal sounds and by validating the estimation using the corresponding IRR obtained from the volume signal acquired via spirometry. Remaining portion of Aim 2 will be achieved with the estimation of V_T from smartphone-acquired tracheal sounds. In particular, a

novel approach based on fractal analysis will be applied to the tracheal sounds to extract nonlinear features from which V_T could be possible. Smartphone-based V_T estimates from tracheal sounds will be validated by using a calibrated inductance plethysmography system as reference due to experimental restrictions. An easy-to-use calibration procedure will be proposed for this acoustical approach with the potential of allowing V_T estimation outside research and clinical settings on a daily basis.

To achieve **Aim 3**, we will apply a noncontact optical approach directly implemented in a smartphone that provides information about IRR as well as V_T when calibrated. In this dissertation, the proposed breathing monitoring approach will be implemented on commercially-available Android smartphone, but it can be implemented in smartphones running other operating systems. We will acquire the chest movement signals from healthy volunteers and test the performance of this optical approach for the tasks of IRR and V_T estimation, considering the spirometer-acquired volume signal as reference. In contrast with the breathing monitoring performed during Aim 2, the optical monitoring proposed has the advantage of being done without plugging an additional sensor to the smartphone. Achievement of Aim 3 could not be completed without proposing an easy-to-do calibration procedure without using expensive specialized devices. To this end, we proposed to take advantage of the linearity of the smartphone-acquired signal and reference tidal volume to construct a linear calibration model based on two data points obtained while breathing through an inexpensive and widely available incentive spirometer.

Finally, in **Aim 4** as an alternative to the challenging breath-phase classification using only tracheal sounds information, we propose to perform the classification of tracheal sounds directly on a smartphone by simultaneously acquiring an additional respiratory-related signal that can be used as a temporal reference as it is done in classic phonopneumography. In particular, we propose using the smartphone-acquired optical signal used in Aim 3 from which the correct detection of the inspiratory and expiratory phases could be achieved by a simple processing technique. Here, as a reference to compare the classification results, spirometer-based airflow and volume signals will be simultaneously collected. This aim will involve the collection of signals during noise-free recordings and also while the subjects

make non-breath noises (swallow, cough, and talk) and perform both regular (alternate phases) and irregular breathing patterns to analyze the performance of the proposed classification method in such scenarios.

1.4 Dissertation Organization

This dissertation is structured in the chapters described below to report the background, methodology and experimental results in accordance to the specific aims. A diagram of the general methodology and structure of this thesis is shown in Figure 1.1. It is worth mentioning that Chapters 3-7 follow the structure of a general Journal paper, each one.

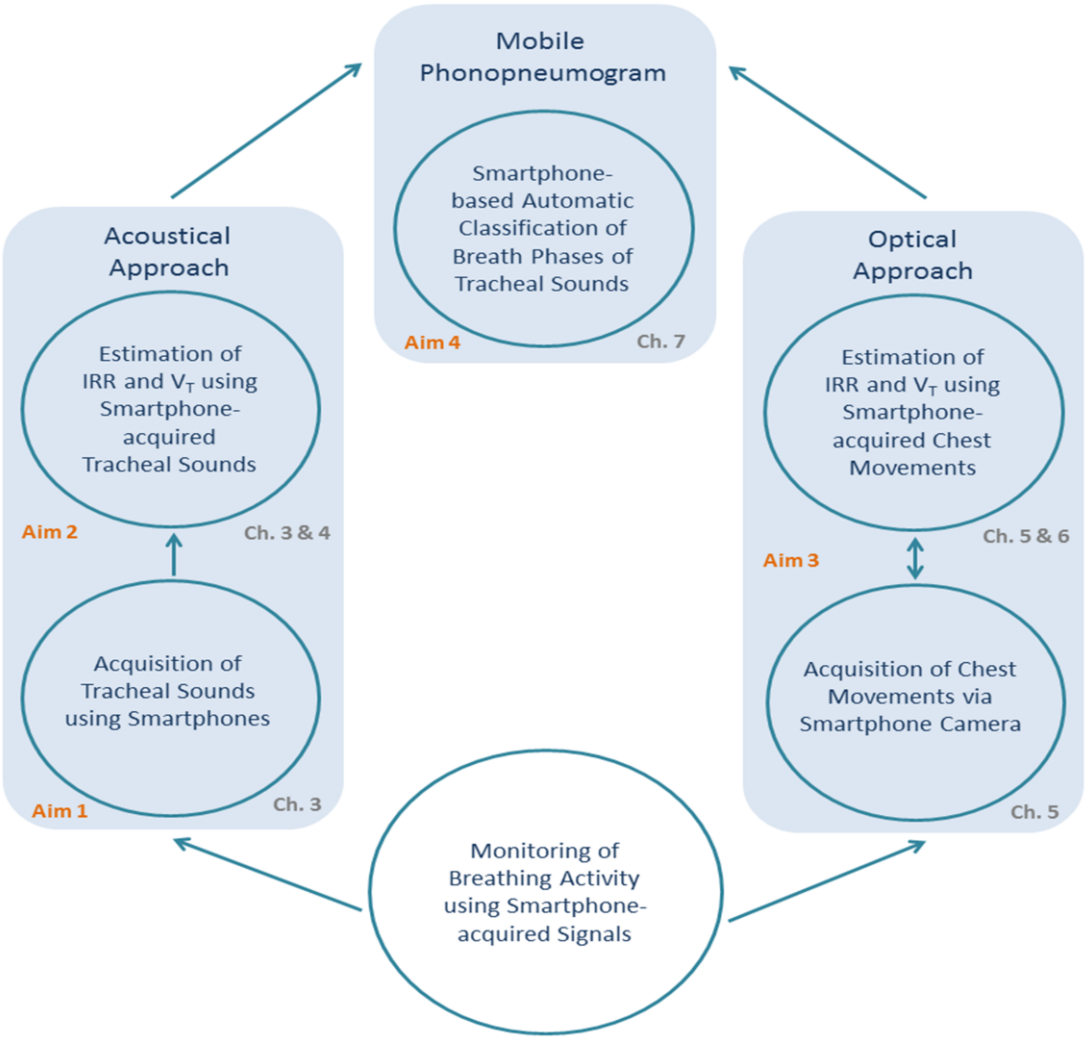

Figure 1.1 – Diagram of the methodology of this research.

Chapter 2: Background

Presents general information about the physiology of the respiratory system, definition and genesis of tracheal sounds, previous efforts on the use of tracheal sounds for breathing monitoring via computerized analysis (acoustical approach), as well as previous efforts on the noncontact optical monitoring of breathing activity (optical approach).

Chapter 3: Tracheal Sounds Acquisition using Smartphones

Describes the methodology and experimental results regarding the achievement of **Aim 1**, *i.e.*, the reliable acquisition of tracheal sounds via a smartphone-based system, as well as half of **Aim 2**, *i.e.*, the estimation of IRR breathing parameter using the smartphone-acquired tracheal sounds. Description of the employed signal processing techniques based on spectral and time-frequency analysis of tracheal sounds will be done. (*B. A. Reyes, N. Reljin, and K. H. Chon, "Tracheal Sounds Acquisition Using Smartphones," Sensors, vol. 14, no. 8, pp. 13830–13850, 2014*).

Chapter 4: Tidal Volume Estimation Using Smartphone-acquired Tracheal Sounds

Describes the methodology and experimental results regarding the achievement of the remaining portion of **Aim 2**, *i.e.*, the estimation of V_T breathing parameter using the smartphone-acquired tracheal sounds. A signal processing approach based on fractal analysis in junction with a simple calibration procedure will be introduced. The signal processing techniques used to achieve Aim 2 and based on fractal analysis will be described in this chapter together with the proposed calibration models. (*N. Reljin, B. A. Reyes, and K. H. Chon, "Tidal Volume Estimation Using the Blanket Fractal Dimension of the Tracheal Sounds Acquired by Smartphone," Sensors, vol. 15, no. 8, pp. 9773-9790, 2015*).

Chapter 5: Tidal Volume and Instantaneous Respiration Rate Estimation using a Smartphone-acquired Camera Signal

Describes the methodology and experimental results regarding the **Aim 3**, *i.e.*, the estimation of IRR and V_T parameters using a noncontact optical approach implemented on a smartphone. Here, the acquisition of the chest movement signal via smartphone's camera will be described. As in previous Aim, a time-frequency representation technique will be used to track temporal variations of IRR from the chest movement signal. Regarding, V_T estimation, at this point the calibration of the smartphone-acquired optical signal for V_T estimation will be performed using spirometry to construct a linear model that allows the mapping of the chest movement displacements to tidal volume. (*B. A. Reyes, N. Reljin, Y. Kong, Y. Nam, and K. H. Chon, "Tidal Volume and Instantaneous Respiration Rate Estimation using a Volumetric Surrogate Signal Acquired via a Smartphone Camera," Under revision, December 2015*).

Chapter 6: Calibration via an Incentive Spirometer for Smartphone-based Tidal Volume Estimation from Optical Approach

Describes the methodology and experimental results regarding the use of an easy-calibration procedure for the task of V_T estimation directly on a smartphone that does not employ a specialized device like spirometry or inductance plethysmography. This chapter fulfills **Aim 3** via the use of an inexpensive volume-oriented incentive spirometer together with the linearity found in terms of the smartphone-acquired the chest displacements with respect to spirometry-based reference tidal volume as reported in previous chapter. (*B. A. Reyes, N. Reljin, Y. Kong, Y. Nam, S. Ha, and K. H. Chon, "Calibration via an Incentive Spirometer for Smartphone-based Tidal Volume Estimation"; Under revision, December 2015*).

Chapter 7: Automatic Breath-Phase Classification using Smartphones to Develop a Mobile Phonopneumogram

Describes the methodology and experimental results regarding the achievement of **Aim 4**, *i.e.*, the automatic breath-phase classification of tracheal sounds using smartphone-acquired optical signals as a surrogate of the volume signal classically used as reference. To this end, tracheal sounds will be acquired together with the chest movement signal using smartphones and the classification of the breath phases will be performed via the slope of the simple linear regression of the acquired optical signal of each consecutive two phase onsets. Examples of the proposed classification in different scenarios found in practice are also presented. (*B. A. Reyes, N. Reljin, Y. Kong, Y. Nam, S. Ha, and K. H. Chon, "Towards the Development of a Mobile Phonopneumogram: Automatic Breath-Phase Classification using Smartphones"; Under revision, December 2015*).

Chapter 8: Conclusions and Future work

Summarizes the main findings of this dissertation as well as the limitations and areas of future development and application of the methods proposed in this research.

1.5 References

[1] M. Folke, L. Cernerud, M. Ekström, and B. Hök, "Critical review of non-invasive respiratory monitoring in medical care," *Med. Biol. Eng. Comput.*, vol. 41, no. 4, pp. 377–383, Jul. 2003.

[2] A. R. A. Sovijarvi, F. Dalmasso, J. Vanderschoot, L. P. Malmberg, G. Righini, and S. A. T. Stoneman, "Definition of terms for applications of respiratory sounds," *Eur. Respir. Rev.*, vol. 10, no. 77, pp. 597–610, 2000.

[3] A. R. A. Sovijarvi, F. Dalmasso, J. Vanderschoot, L. P. Malmberg, G. Righini, and S. A. T. Stoneman, "Definition of terms for applications of respiratory sounds," *Eur. Respir. Rev.*, vol. 10, no. 77, pp. 597–610, 2000.

[4] Z. Moussavi, *Fundamentals of Respiratory System and Sounds Analysis*. Morgan & Claypool.

[5] A. R. A. Sovijarvi, L. P. Malmberg, G. Charbonneau, J. Vanderschoot, F. Dalmasso, C. Sacco, M. Rossi, and J. E. Earis, "Characteristics of breath sounds and adventitious respiratory sounds," *Eur. Respir. Rev.*, vol. 10, no. 77, pp. 591–596, 2000.
[6] S. Huq and Z. Moussavi, "Acoustic breath-phase detection using tracheal breath sounds," *Med. Biol. Eng. Comput.*, vol. 50, no. 3, pp. 297–308, Feb. 2012.
[7] F. Q. Al-Khalidi, R. Saatchi, D. Burke, H. Elphick, and S. Tan, "Respiration rate monitoring methods: A review," *Pediatr. Pulmonol.*, vol. 46, no. 6, pp. 523–529, Jun. 2011.
[8] G. Chen, I. de la Cruz, and E. Rodriguez-Villegas, "Automatic lung tidal volumes estimation from tracheal sounds," *Conf. Proc. Annu. Int. Conf. IEEE Eng. Med. Biol. Soc. IEEE Eng. Med. Biol. Soc. Annu. Conf.*, vol. 2014, pp. 1497–1500, Aug. 2014.
[9] B. M. Koeppen and B. A. Stanton, *Berne & Levy Physiology, Updated Edition*. Elsevier Health Sciences, 2009.
[10] H. Pasterkamp, S. S. Kraman, and G. R. Wodicka, "Respiratory Sounds: Advances Beyond the Stethoscope," *Am. J. Respir. Crit. Care Med.*, vol. 156, no. 3, pp. 974–987, Sep. 1997.
[11] G. Charbonneau, E. Ademovic, B. M. G. Cheetham, L. P. Malmberg, J. Vanderschoot, and A. R. A. Sovijarvi, "Basic techniques for respiratory sound analysis," *Eur. Respir. Rev.*, vol. 10, no. 77, pp. 625–635, 2000.
[12] F. Dalmay, M. T. Antonini, P. Marquet, and R. Menier, "Acoustic properties of the normal chest," *Eur. Respir. J.*, vol. 8, no. 10, pp. 1761–1769, Oct. 1995.
[13] J. E. Earis and B. M. G. Cheetham, "Current methods used for computerized respiratory sound analysis," *Eur. Respir. Rev.*, vol. 10, no. 77, pp. 586–590, 2000.
[14] D. M. J. Mussell, "The need for standards in recording and analysing respiratory sounds," *Med. Biol. Eng. Comput.*, vol. 30, no. 2, pp. 129–139, Mar. 1992.
[15] B. M. G. Cheetham, G. Charbonneau, A. Giordano, P. Helisto, and J. Vanderschoot, "Digitization of data for respiratory sound recordings," *Eur. Respir. Rev.*, vol. 10, no. 77, pp. 621–624, 2000.
[16] L. Vannuccini, J. E. Earis, P. Helisto, B. M. G. Cheetham, M. Rossi, A. R. A. Sovijarvi, and J. Vanderschoot, "Capturing and preprocessing of respiratory sounds," *Eur. Respir. Rev.*, vol. 10, no. 77, pp. 616–620, 2000.
[17] J. E. Earis and B. M. G. Cheetham, "Current methods used for computerized respiratory sound analysis," *Eur. Respir. Rev.*, vol. 10, no. 77, pp. 586–590, 2000.
[18] H. Pasterkamp, C. Carson, D. Daien, and Y. Oh, "Digital respirosonography. New images of lung sounds.," *Chest*, vol. 96, no. 6, pp. 1405–1412, Dec. 1989.
[19] J. Lee, B. A. Reyes, D. D. McManus, O. Mathias, and K. H. Chon, "Atrial Fibrillation Detection Using an iPhone 4S," *IEEE Trans. Biomed. Eng.*, vol. 60, no. 1, pp. 203–206, 2013.
[20] C. G. Scully, J. Lee, J. Meyer, A. M. Gorbach, D. Granquist-Fraser, Y. Mendelson, and K. H. Chon, "Physiological Parameter Monitoring from Optical Recordings with a Mobile Phone," *IEEE Trans. Biomed. Eng.*, vol. 59, no. 2, pp. 303–306, Feb. 2012.
[21] J. E. Earis and B. M. G. Cheetham, "Future perspectives for respiratory sound research," *Eur. Respir. Rev.*, vol. 10, no. 77, pp. 641–646, 2000.
[22] L. Guangbin, C. Shaoqin, Z. Jingming, C. Jinzhi, and W. Shengju, "The development of a portable breath sounds analysis system," presented at the 1992 14th Annual International Conference of the IEEE Engineering in Medicine and Biology Society, 1992, vol. 6, pp. 2582–2583.
[23] K. Hung, B. L. Luk, W. H. Choy, B. Tai, and S. K. Tso, "Multifunction stethoscope for telemedicine," presented at the 2003 IEEE International Workshop on Computer Architectures for Machine Perception, 2004, pp. 87–89.
[24] D. Oletic, M. Skrapec, and V. Bilas, "Monitoring Respiratory Sounds: Compressed Sensing Reconstruction via OMP on Android Smartphone," in *Wireless Mobile Communication and Healthcare*, B. Godara and K. S. Nikita, Eds. Springer Berlin Heidelberg, 2013, pp. 114–121.
[25] K. P. Cohen, W. M. Ladd, D. M. Beams, W. S. Sheers, R. G. Radwin, W. J. Tompkins, and J. G. Webster, "Comparison of impedance and inductance ventilation sensors on adults during breathing,

motion, and simulated airway obstruction," *IEEE Trans. Biomed. Eng.*, vol. 44, no. 7, pp. 555–566, Jul. 1997.
[26] G. B. Drummond, A. F. Nimmo, and R. A. Elton, "Thoracic impedance used for measuring chest wall movement in postoperative patients.," *Br. J. Anaesth.*, vol. 77, no. 3, pp. 327–332, Sep. 1996.
[27] M. A. E. Ramsay, M. Usman, E. Lagow, M. Mendoza, E. Untalan, and E. De Vol, "The Accuracy, Precision and Reliability of Measuring Ventilatory Rate and Detecting Ventilatory Pause by Rainbow Acoustic Monitoring and Capnometry:," *Anesth. Analg.*, vol. 117, no. 1, pp. 69–75, Jul. 2013.
[28] J. J. Vargo, G. Zuccaro Jr., J. A. Dumot, D. L. Conwell, J. B. Morrow, and S. S. Shay, "Automated graphic assessment of respiratory activity is superior to pulse oximetry and visual assessment for the detection of early respiratory depression during therapeutic upper endoscopy," *Gastrointest. Endosc.*, vol. 55, no. 7, pp. 826–831, Jun. 2002.
[29] K. Ashutosh, R. Gilbert, J. H. Auchincloss, J. Erlebacher, and D. Peppi, "Impedance pneumograph and magnetometer methods for monitoring tidal volume," *J Appl Physiol*, vol. 37, no. 6, pp. 964–966, 1974.
[30] P. Grossman, M. Spoerle, and F. H. Wilhelm, "Reliability of respiratory tidal volume estimation by means of ambulatory inductive plethysmography," *Biomed. Sci. Instrum.*, vol. 42, pp. 193–198, 2006.
[31] A. Johansson and P. P. Å. Öberg, "Estimation of respiratory volumes from the photoplethysmographic signal. Part I: experimental results," *Med. Biol. Eng. Comput.*, vol. 37, no. 1, pp. 42–47, Jan. 1999.
[32] G. Li, N. C. Arora, H. Xie, H. Ning, W. Lu, D. Low, D. Citrin, A. Kaushal, L. Zach, K. Camphausen, and R. W. Miller, "Quantitative prediction of respiratory tidal volume based on the external torso volume change: a potential volumetric surrogate," *Phys. Med. Biol.*, vol. 54, no. 7, pp. 1963–1978, Apr. 2009.
[33] M. R. Miller, J. Hankinson, V. Brusasco, F. Burgos, R. Casaburi, A. Coates, R. Crapo, P. Enright, C. P. M. van der Grinten, P. Gustafsson, and others, "Standardisation of spirometry," *Eur. Respir. J.*, vol. 26, no. 2, pp. 319–338, 2005.
[34] C.-L. Que, C. Kolmaga, L.-G. Durand, S. M. Kelly, and P. T. Macklem, "Phonospirometry for noninvasive measurement of ventilation: methodology and preliminary results," *J. Appl. Physiol. Bethesda Md 1985*, vol. 93, no. 4, pp. 1515–1526, Oct. 2002.
[35] P. Piirila and A. R. Sovijarvi, "Crackles: recording, analysis and clinical significance," *Eur. Respir. J.*, vol. 8, no. 12, pp. 2139–2148, Dec. 1995.
[36] N. Meslier, G. Charbonneau, and J. L. Racineux, "Wheezes," *Eur. Respir. J.*, vol. 8, no. 11, pp. 1942–1948, Nov. 1995.

Chapter 2: Background

2.1 Relevant physiology

The main function of the respiratory system is the delivering of oxygen (O_2) to the blood and the removal of carbon dioxide (CO_2), and other waste gases, from the body [1]. The inhalation of O_2 and exhalation of CO_2 is achieved through breathing, and the lungs are the organs where gas exchange takes place. Lung structure shows a gas exchange surface divided into small subunits connected to a branched conduction airway system. The respiratory system begins at the nose and ends in the most distal alveolus, being its main parts the airways, the lungs and linked blood vessels, and the muscles used for breathing [2]. Figure 2.1 shows a schematic of the respiratory system.

The upper airways condition the inspired air and include the nose, sinuses and larynx; while the lower airways consist of the trachea and all its bifurcations until reach the alveolus [2]. The tracheobronchial tree has features common to fractal objects and has been modeling accordingly [3], [4]. The trachea bifurcates into two stem bronchi, which bifurcate into lobar bronchi, which bifurcate into segmental bronchi. The anatomic unit of the lung is its region supplied by a segmental bronchus. The segmental bronchus bifurcates into smaller branches called bronchioles. The bronchioles continue bifurcating until small airways without alveoli called terminal bronchioles. Branching of respiratory alveoli allows increasing the total surface area by increasing the size and number until opening to a group of alveoli [2]. The alveolus is the smallest gas exchange unit within the respiratory parenchyma. To be efficient, an average of 480 million of alveoli is found in an adult human lung , resulting in a large lung surface area for gas exchange of approximately 85 m^2, where each alveolus has a polygonal shape of about 250 μm in diameter [5]. The physiological unit of the lung, called respiratory or gas-exchange unit, is composed of the respiratory bronchioles, the alveolar ducts, and the alveoli [2]. The alveolar-capillary network is the place where gas exchange occurs in the alveoli via passive diffusion of O_2 and CO_2 [6]. The lung has a dual circulation; the bronchial circulation provides nourishment to the lung parenchyma,

and the pulmonary circulation provides deoxygenated blood from the right ventricle to the respiratory units for gas exchange [2]. Deoxygenated blood is pumped from the heart through the pulmonary artery to the lungs, where in turn it diffuses CO_2 through the wall membranes of the alveoli and takes up O_2 from the air in the alveolar lumen [1]. The oxygenated blood is returned to the heart through the pulmonary vein and it is pumped to the tissues for cell use throughout the body [1]. Connective tissue, smooth muscle, lymphatics, capillaries, and other cells compose the lung interstitium which is very small under normal conditions but it can become enlarged with influx of inflammatory cells and edema fluid due to pathological conditions [2].

The lungs occupy the majority of the thoracic (chest) cavity volume. The thorax, *i.e.*, outer chest wall, is formed by the rib cage that join the sternum anteriorly and the thoracic vertebrae posteriorly. Skeletal muscles connect the bony structure to enclosure the thoracic cavity, at the floor of which there is a large dome-shaped skeletal muscle called diaphragm [6].

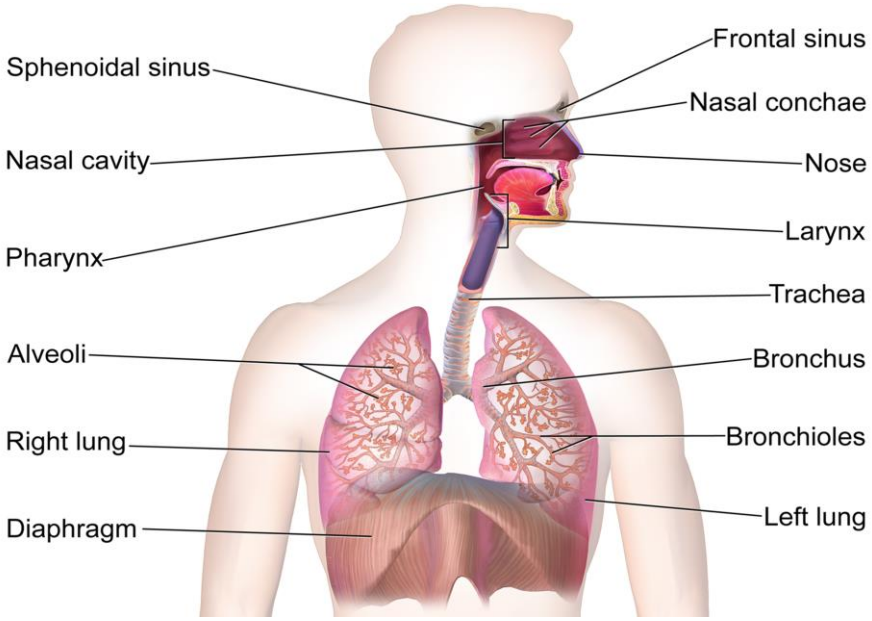

Figure 2.1 – Basic schematic of the respiratory system
Figure from: *"Respiratory system," Blausen gallery 2014. Figure labeled for reuse and available at: https://en.wikiversity.org/wiki/Wikiversity_Journal_of_Medicine/Blausen_gallery_2014*

2.1.1 Chest wall movements

The diaphragm and the external intercostal muscles are the major muscles during the inspiration [6]. At the beginning of the inspiration, the respiratory muscles are relaxed. During the inspiration, the inspiratory muscles are stimulated to contract, resulting in an enlarged thoracic cavity [6]; the diaphragm has a convex upper surface that flattens when contracted and descends downward increasing the vertical dimension of the thoracic cavity. Also, the external intercostal muscles contract and elevate the ribs and move the sternum upward and outward increasing the thoracic cavity in the horizontal axis [6]. Due to these contractions, the lungs expand to fill the larger thoracic cavity, resulting in a drop of the intra-alveolar pressure, which is now less than the atmospheric pressure, causing a flow of air into the lungs until the intra-alveolar pressure equals the atmospheric pressure [6]. During a forced inspiration, accessory inspiratory muscles located in the neck are used to further enlarge the thoracic cavity [6]. Inspiratory muscles relax during the expiration, restoring the chest wall and stretched lungs to their preinspiratory sizes, due to their elastic properties, and causing a rise in the intra-alveolar pressure above atmospheric level forcing the air to leave the lungs [6]. In contrast to expiration, inspiration is always an active process. The passive expiration during quite breathing can become active during a forced expiration when the abdominal muscles and the internal intercostal muscles are employed to further reduce the thoracic cavity and lungs volumes [6].

The rib cage and abdomen compartments of the chest wall are the major breathing contributors [7]. A relationship between volume displacement and linear motion exist during breathing, as this system belongs to mechanical systems involvement volume displacements [7]. The chest wall movements in the anteroposterior direction are greater than those in the vertical or transverse directions, with an increase of around 3 cm in the anteroposterior diameter over the vital capacity range [7]. Recent studies have shown a one-to-one relationship between changes of the external torso and tidal volume corresponding to internal lung air content [8].

Changes of postures can modify the contribution of the rib cage and abdomen compartments. A decreased rib cage excursion and an increased abdominal excursion have been found in the supine position compared to the sitting or standing postures [9], [10]. Normally, the expansion of the rib cage and abdomen during the inspiration is almost synchronous but during upper airway obstruction and/or lung restriction movements can become asynchronous, *i.e.*, the rib cage moves inwards/outwards and abdomen moves outward/inward during the inspiration/expiration, due to a change in the phase angle and timing of their movements [11]. This asynchrony is augmented by respiratory muscle weakness or respiratory disease [12].

2.1.2 Tracheal sounds

A variety of sounds are produced while breathing. Tracheal sounds belong to the class of respiratory sounds. The respiratory sounds include breath sounds (or basal sounds), adventitious sounds (added or superimposed sounds), and sounds from the respiratory muscles, excluding voiced sounds during breathing [13]. Depending on their location, respiratory sounds are denoted as lung sounds if heard or detected over the chest wall or within the chest, or as tracheal sounds if heard or detected over the extrathoracic part of the trachea or close to the mouth [13]. Both lung and tracheal sounds enclose the breathing sounds and adventitious sounds detected at their corresponding locations. A diagram showing the relationship between all these terms is shown in Figure 2.1.

Tracheal sounds have characteristics of broad-band noise and exhibit several resonance peaks in their spectra which depend airway dimensions and gas density [14], [15]. These sounds exhibit a hollow or tubular character, which according to Laennec, father of the auscultation and inventor of the stethoscope, reflects the movement of air through a wider channel than the alveolar one [16]. Tracheal sounds show well defined inspiratory and expiratory phases with a silent period in between, when represented in temporal or time-frequency domains [15], and their inspiratory and expiratory phases have similar frequency contents for same airflow levels [17]. Due to the short distance between the acoustical

sources in the upper airways and the location of the sensors over the neck, and without the interposition of the pulmonary parenchyma and the chest wall, tracheal sounds have been interpreted as more pure or less filtered than lung sounds [18]. Accordingly, the frequency content of tracheal sounds are higher than those from lung sounds [15]. Figure 2.2 shows the waveform of a tracheal sound together with the airflow, called phonopneumogram, and its time-frequency representation, called respirosonogram.

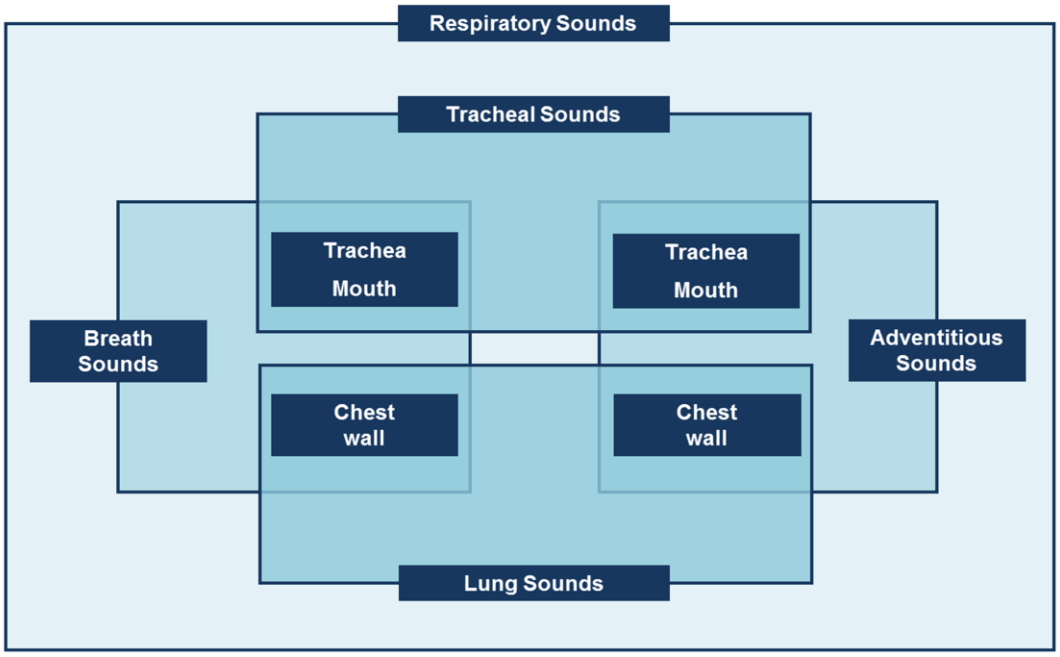

Figure 2.2 – Relationship between respiratory sounds, tracheal sounds, lung sounds, breath sounds and adventitious sounds

Figure based on: *A. R. A. Sovijarvi, F. Dalmasso, J. Vanderschoot, L. P. Malmberg, G. Righini, and S. A. T. Stoneman,"Definition of terms for applications of respiratory sounds," Eur. Respir. Rev., vol. 10, no. 77, pp. 597–610, 2000*.

Regarding the genesis of tracheal sounds, a turbulent flow in upper airways, including the pharynx and glottis, is considered the primary responsible [19]. A dominating local turbulent eddy and a propagating acoustic component with resonances are the major constituents of tracheal sounds [14]. The tracheal sounds recorded over the external surface of the neck are due to the turbulent airflow in the upper airways that appears to produce pressure fluctuations inside these airways and also to the movement of

the airway walls that produce vibrations that reach the acquisition site. Spectral analysis has shown results compatible with sounds generated during inspiration via turbulent flow in a bifurcated network [20]. Dimensions of the airways have influence on tracheal sound's acoustical characteristics [19].

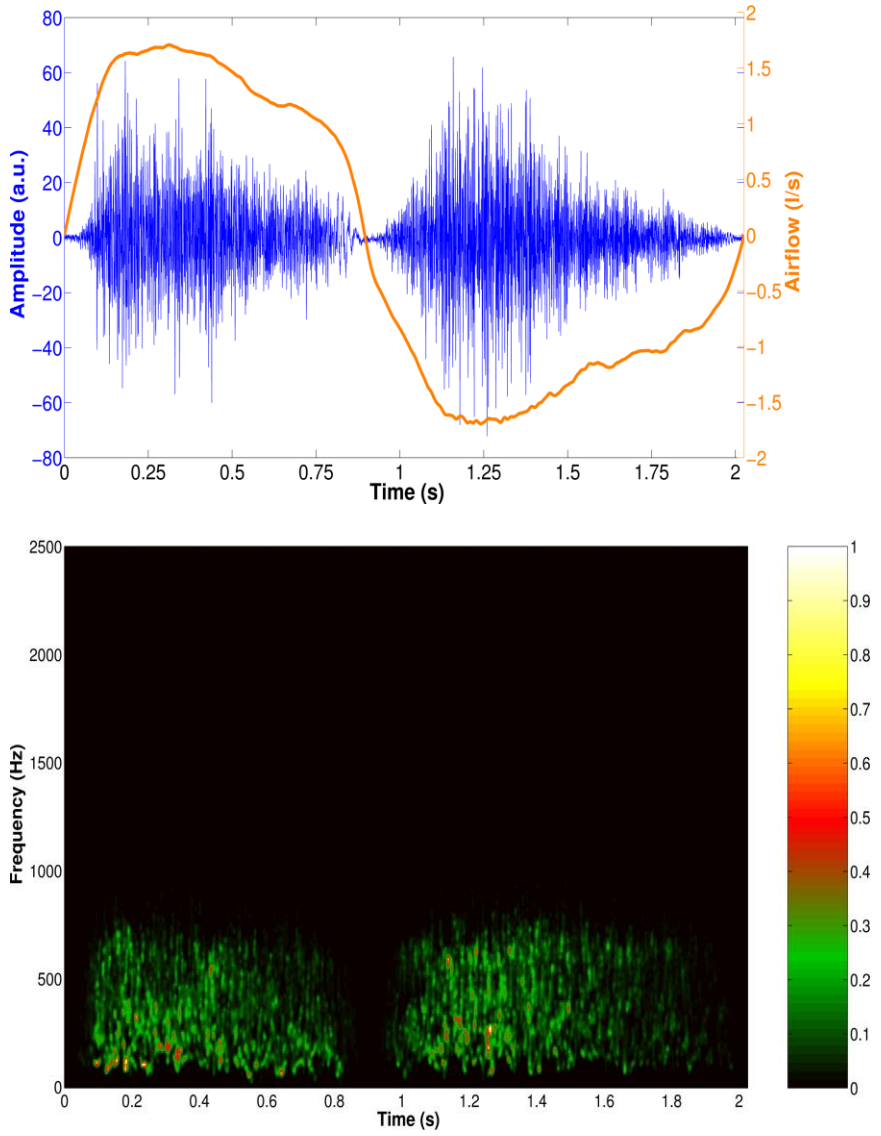

Figure 2.3 – Tracheal sounds recorded from a healthy subject
Top: phonopneumogram displaying the tracheal sound waveform (blue) and the simultaneously recorded airflow signal from spirometry. *Bottom*: respirosonogram of the tracheal sound obtained via the Hilbert-Huang time-frequency representation. Image reproduced with permission from: *Reyes, B. A. "Time-frequency representations for thoracic sound analysis", Master Thesis, In Spanish, 2010.*

Nowadays it is well-recognized that the relationship between respiratory airflow, *F*, and tracheal sound's amplitude, *A*, is best fitted by a power law of the form $A = kF^{\alpha}$, where *k* and α are constants, where different values having been found for the exponent by different research groups [14], [20]–[23]. This sound's amplitude-airflow relationship has been exploited for breathing monitoring, particularly for qualitative and quantitative assessment of respiratory airflow [24], and more recently continuous respiratory rate estimation [25].

2.2 Breathing monitoring

Monitoring of breathing status has been recognized as critical to identify and predict serious adverse events [11] like risky situations involving respiratory failure or sleep-related breathing disorders [26]–[28]. Accordingly, the monitoring of breathing status could be potentially life-saving in such situations [26]. Ideally, a breathing monitoring should be able to provide information about three basic parameters in a noninvasive fashion: respiratory frequency, breathing depth, and the degree of gas exchange actually taking place in the body [26]. In this thesis we will focus on the first two parameters, to say, respiratory rate (RR) and tidal volume (V_T). V_T provides information about the respiration depth and is defined as the volume of air moved with each breath and it is commonly expressed in liters (L); on the other hand, RR corresponds to the number of breaths per unit of time and it is commonly expressed in breaths-per-minute (bpm). In turn, the product of these two quantities defines the volume of gas moved by the respiratory system per minute, called minute ventilation ($\dot{V}_E$). Normal average values for a human man are around 0.5 L and 12 bpm for V_T and RR, respectively. These values are not fixed and the mechanism of respiratory control is crucial in determining $\dot{V}_E$ by adjusting the combination of V_T and RR according to a body's requirements in response to different scenarios like exercising or sleeping [2].

Breathing monitoring methods can be categorized according to their detection or sensing principles in three classes: 1) movement, volume and tissue composition detection, 2) airflow sensing, and 3) blood gas measurement. Inductance plethysmography, transthoracic impedance, strain-gauge

transducers, Doppler radar, sensors in mattress, electromyography, and optical monitoring are included in the first category. Airflow sensing includes temperature, humidity, carbon dioxide, and acoustical sensing via tracheal sounds. Blood gas measurement methods and devices include pulse oximetry, end-tidal O_2, end tidal CO_2, and transcutaneous CO_2 measurements. An extensive review of the monitoring devices and methods in each of these categories can be found in reference [26]. Below we present a brief summary of the current clinical and research devices and methods used for RR and V_T monitoring. Next we discuss in more detail the acoustical and optical breathing monitoring approaches as they will be employed in this thesis.

Nowadays, RR monitoring methods commonly used include qualified human observation [26], transthoracic impedance [29], impedance plethysmography [30], inductance plethysmography [31], capnography monitoring [32], photoplethysmography [33], and acoustical monitoring [25]. Each method has its own disadvantages, *e.g.*, human observation is technology independent and could allow an immediate response to risk events but it is time consuming and subjective, capnography is more accurate but patients usually show a low tolerance for using the nasal cannula [26].

V_T estimation results, in general, more challenging than RR estimation. Despite this challenge, several efforts have been made towards V_T estimation and current clinical and research methods include spirometry [34], impedance pneumography [35], inductance plethysmography [36], optical tracking of reflective markers place on the body [37], photoplethysmography [38], computed tomography [8], phonospirometry [39], Doppler radar [28], and more recently electrocardiography [40]. As in RR monitoring, limitations arise when estimating V_T, *e.g.*, the use of high doses of ionizing radiation in computed tomography, or alteration in the natural breathing depth due to spirometer use [41].

In this thesis, we will employ two approaches for monitoring of breath parameters: 1) an acoustical, and 2) a noncontact optical approach. Following subsections describes these approaches with emphasis on the estimation of RR and V_T parameters.

2.2.1 Acoustical approach

In the field of Computerized Respiratory Sound Analysis (CORSA), tracheal sounds are recorded using a sensors placed over the extrathoracic part of the trachea, *e.g.*, at the suprasternal or jugular notch [13]. Sensors used for tracheal sound analysis correspond to microphones following a kinematic approach (contact sensor) or an acoustical approach (air-coupled sensor) to convert mechanical vibrations into electrical signals [42]. Both a condenser microphone using an air cavity for air-coupling and a piezoelectric contact sensor are recommended to be used in CORSA systems as similar performance and signal-to-noise ratio has been found in frequency range of respiratory sounds [42]–[44]. A detailed list of the recommendations for sensors specifications, coupling, fixing methods, noise and interference, filtering, and digitization of the sound signal can be found in reference [42], [45]. A list of these minimum requirements for CORSA systems, focused on the parameters pertinent to this dissertation, is shown in Table 2.1.

The use of CORSA systems allows to store the acquired sounds for further analysis, to quantify changes in respiratory sound characteristics, to correlate the recorded sounds with other physiological signals, and to aid in the diagnosis and treatment of patients with pulmonary diseases by mean of useful data representations [46], [47]. The use of CORSA systems has not replaced the mechanical stethoscope in but has overcome some of its known disadvantages [15], [46], [48]. Auscultation with the stethoscope is a subjective process that depends on the skills of the physician [49], it is limited by human audition [50], depends on the different stethoscopes used with the stethoscope itself being more adequate for cardiac auscultation [15], and also the lung sounds are not permanent recorded for further analysis. Even with the advantage of CORSA systems, the auscultation with the stethoscope still guides in diagnosis when other pulmonary tests are not available [51]. Ubiquity, low-cost, mobility, ease-of-use, and non-invasiveness are some characteristics that made the stethoscope the most widely used instrument in clinical practice. Such characteristics should remain when aiming for the development of a CORSA system.

Table 2.1 – Minimum requirements of Computerized Respiratory Sound Analysis systems.

Requirement	Recomendations
Sensor	Flat response in the frequency range of the respitory sound Maximum deviation of 6dB allowed
Sensitivity	Independent of frequency Minimum of 1 mV/Pa
SNR	> 20 dB in-situ
Type of sensor	Electret or condenser Piezoelectric
Coupling	Condenser: Air-coupled in a conical shape Depth: 2.5-5 mm. Diameter at skin: 10-25 mm
Fixing method	Adhesive ring
High-pass filtering	Cut-off frequency 60 Hz Roll-off > 18 dB/octave Minimized ripple
Low-pass filtering	Cut-off frequency above upper frequency of signal Roll-off > 24 dB/octave Minimized ripple
Sampling frequency	Depending of the application Recommended 11.025 Hz
ADC resolution	At least 16 bits

Tracheal sounds are of particular interest for the estimation of breathing parameters. They have been used in phonospirometry for airflow estimation [52] as well as for volume estimation [39]. In particular, the Shannon entropy (SE) of tracheal sounds was computed and then calibrated using data from pneumotachograph for airflow estimation [52]. In a subsequent study, the Shannon entropy method was simplified to reduced computational cost by simply obtaining the range of the tracheal sound signal

[24]. A similar approach has been used for volume estimation. The envelope of the tracheal sound, obtained via the Hilbert transform, was first used to estimate airflow, after a linear calibration using pneumotachograph data, and then the estimated airflow was integrated to obtain volume parameters [39]. A recent study also reported the used of tracheal sounds for tidal volume estimation by integrating their acoustic energy and after calibration using respirometry data [27]. An acoustic monitoring system has been released by Masimo Corp. for the task of RR monitoring [53]. This system has been tested under different clinical conditions and good agreement has been found for the RR estimates when compared to capnography and thoracic impedance methods [25], [54], [55].

Use of tracheal sounds in phonospirometry has provided promising results. However, both the airflow and volume estimation involves a classification step in which the inspiratory and expiratory phases should be accurately labeled. This automatic classification is trivial when an external breathing-related signal like airflow or volume from spirometry is employed. However, the latter is not usually the case, especially outside specialized clinical and research centers. Given that the acquisition of tracheal sounds is noninvasive and less intrusive when compared to the use of nasal cannulas, mouth piece or facemask connected to a pneumotachograph, the classification of breath phases via automatic analysis of tracheal sounds has been proposed. In a first attempt, a multichannel CORSA system was used so that classification was performed by first detection the breath-phase onsets using tracheal sound and then by analyzing the inspiratory/expiratory power different of lung sounds [45]. Even when 100% accuracy was achieved, the proposed methodology requires the acquisition of an additional channel, *i.e.*, lung sounds, to the tracheal sounds. The use of only tracheal sounds to completely perform the breath-phase classification has been also studied. Temporal and spectral methods that analyze the fast changes in tracheal sounds have been proposed but without reporting the accuracy in terms of the breath-phase classification [57]. An accuracy of 97% have been reported by using a ratio of frequency magnitudes at high and low frequency bands of tracheal sounds [58]. The logarithm of the variance of tracheal sounds has been proposed for breath-phase classification, and an accuracy of 95.6% has been reported

independently of the measured airflow level [59]. Finally, Mel-frequency cepstral coefficients of tracheal sounds has been proposed, with a reported 90% classification accuracy [60].

As can be noticed, the use of only tracheal sounds to completely perform the automatic classification of breath phases is challenging and still under exploration. Despite the approach used, the accurate labeling and timing of the breath phases is relevant in the field of respiratory analysis. In addition to provide the correct polarity of the estimated airflow [24] or volume signals [39], the timing of adventitious sounds, both discontinuous and continuous, must be characterized with respect to the breath phase as it has been found to differ between different pulmonary disorders [50], [61]. In the case of crackle sounds, *i.e.*, discontinuous adventitious sounds with a short duration and explosive character [13], it has been found that those occurring at the end of the inspiration (late inspiratory crackles) are associated with restrictive pulmonary diseases while crackles occurring at the beginning of the inspiration (early inspiratory crackles) are associated with severe airway obstruction [62]. Also, the early timing of crackles found in chronic obstructive pulmonary disease did not overlapped with the late timing of crackles in fibrosing alveolitis [63]. Expiratory crackles are in general less commonly found than inspiratory crackles [64] but they can still occur in many respiratory diseases [65]. Regarding the wheeze sounds, *i.e.*, continuous adventitious sounds with a long duration and a musical character [13], the severity of bronchial obstruction has been found to be higher in asthmatic patients with both inspiratory and expiratory wheezes than in those patients with only expiratory wheezes [66]. During pulmonary fibrosing diseases and pneumonia, it is common to hear short duration wheezes, called squawks, during the inspiratory phase [67], [68]. The timing and labeling of breath phases is not only relevant in the analysis of adventitious sounds but also when studying breath (base) lung sounds. In a recent study, statistically-significant differences were found between breath sounds from healthy subjects and patients with extrinsic allergic alveolitis patients, where the differences were more consistent during the expiratory phase presumably. It was proposed that due to the more central source of the expiratory breath sounds, they can carry out more information about the surrounding tissue between their source location and the recording site. It is worth mentioning that these findings were possible due to the simultaneous

acquisition and representation of the respiratory sounds and the airflow or volume signal, method called phonopneumography, that allows an accurate timing and level of occurrence of the sounds [65].

2.2.2 Noncontact optical approach

The acoustical breathing monitoring, as previously described, requires a microphone to be attached to the subject's body on the detection site of interest [11]. In contrast, in the noncontact monitoring of breathing the subject's body is not in contact with the measurement device. A detailed description of the diverse contact and noncontact breathing monitoring methods can be found in reference [11]. In this thesis we will focus on the noncontact optical breathing monitoring where a video camera placed at distance from the subject's body captures the changes in the intensity of reflected light caused by his/her chest wall movements as they modify the path length of the illumination light [69]. Figure 2.3 shows a schematic representation of the classical noncontact breathing monitoring method.

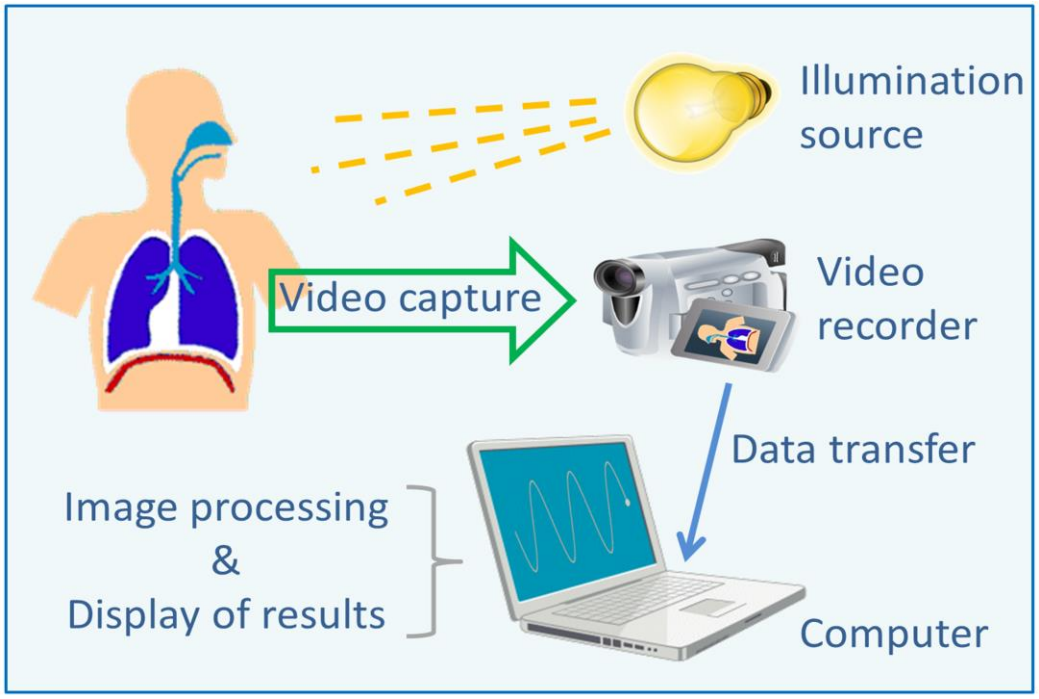

Figure 2.4 – Schematic of a classical noncontact breathing monitoring approach
Image based on *D. Shao, Y. Yang, C. Liu, F. Tsow, H. Yu, and N. Tao, "Noncontact Monitoring Breathing Pattern, Exhalation Flow Rate and Pulse Transit Time," IEEE Trans. Biomed. Eng., vol. 61, no. 11, pp. 2760–2767, Nov. 2014.*

There have been efforts for monitoring of breathing using video cameras but most of them have focused on average RR estimation [69]–[74] despite the importance of monitoring breathing depth. High agreement between the proposed noncontact methods and the specialized breathing monitoring sensors has been found for the task of RR estimation. A webcam focused on the subject's face have been employed for RR estimation via independent component analysis (ICA) of the red, green and blue (RGB) color channels of videos recorded indoors and using ambient sunlight as source of illumination [70]. The single channel ICA of video recordings, obtained via a monochrome CMOS camera faced on the subject's face and a custom-built infrared source of illumination, was used for RR estimation under rest and motion conditions [71]. An Eulerian-based method was used to magnify small motions from video recordings. RR estimation was not extensively studied but authors indicated that their algorithm can enhance the subtle chest motions of a baby while breathing [72]. A delay-coordinate transformation and ICA were applied to video recordings, obtained using a near-infrared camera and using indoor ambient light and near infrared as sources of illumination, for the task of RR estimation [69]. Video images obtained from internet were also analyzed in the latter study [69]. The autoregressive modeling and a pole selection method were used to estimate RR from RGB video recordings obtained with a high-quality 5 megapixel camera under fluorescent and natural light sources of illumination [73]. More recently, a webcam was used to acquire video recordings from the subject's shoulder [74]. The acquired videos were processed via differential signal processing and motion tracking to detect the shoulder movements from which the RR was estimated [74]. It is worth mentioning that the above studies employed a personal computer or laptop to process the video recordings in order to extract the RR estimates.

Regarding the estimation of V_T via a noncontact optical approach, the studies are more limited in comparison to RR estimation [37], [74], [75]. Nevertheless, accurate V_T estimates were found when surface markers placed on the chest wall were tracked by an optical reflectance system using an array of video cameras placed in front and behind of the subject [37], [75]. In a first study, several (up to 100) passive plastic hemispheres coated with reflective paper were tracked via four especial television cameras

and parallel processing to compute their spatial coordinates in real-time [75]. A grid tracking on a known geometry was used for calibration [75]. In a similar way, 86 infrared reflective markers were placed on the chest wall and tracked by four infrared charge-coupled device cameras [37]. Calibration was performed by computing the spatial position of an array of sensors placed on a known grid [37]. In both cases, good correlation of the volume estimates was found with respect to spirometry. A respiratory movement measuring instrument, consisting of 6 lightweight sensors placed on the surface of the upper and lower thorax and on abdominal region and 6 video monitoring cameras, has been also used for studying the respiratory movements in terms of chest wall excursion [76], [77]. The results found with the systems for tracking of reflective markers on the chest wall have been supported by a recent study using computed tomography that has shown a linear relationship between volume changes in the external torso and V_T regarded as the internal lung air content, the so-called volume conservation hypothesis [8]. Although promising, the use of those optical reflective tracking systems is not widely available to the general population. More recently, in addition to RR estimation, the detection of shoulder displacements via webcam and image processing techniques showed a good correlation (r^2=0.81) between these displacements and exhaled breath volume measured with a commercial metabolic analysis device [74]. However, no further analysis was done regarding V_T estimation and its calibration. As in previous cases, an external video camera was used; the video data was then transferred to a personal computer or laptop where the processing and final estimation was performed.

2.3 Breathing monitoring using smartphones

Besides their limitations, the abovementioned RR and V_T breathing monitoring devices are currently being used in clinical and research environments where they have shown their relevance. With some exceptions, the translation of the clinical and research breathing monitoring methods to everyday by the general population is not easy due, for example, to the high costs of the devices employed, the level of skills required to use them, or their limited mobility. Exceptions include the acoustical monitoring via tracheal sounds or the noncontact optical systems employing simple video cameras, *e.g.*, webcams, and

ambient light illumination sources. However, their successful implementation on low-cost handheld systems is still pending, particularly for the task of V_T estimation.

Smartphones result an attractive option for the development of a mobile breathing monitor that provides useful information beyond the mechanical stethoscope given their advanced state-of-the art and near-ubiquity characteristics. According to statistics reported by leading analytics companies on the internet, the number of smartphones sold to end users worldwide quadrupled from 2010 (296.65 million units) to 2014 (1,2444.89 million units), meaning that around 20% of the world's total population owns a smartphone nowadays [78]. Currently, Google's Android operating system (OS) and Apple's iOS lead the smartphone global market, with a respective share of around 80% and 15% [79], [80]. The market share is almost equally divided by Android and iOS in the United States [79], [81]. The penetration of the smartphones among mobile users is expected to keep increasing, *e.g.*, it is predicted to increase to almost 80% by 2017 compared to the 26.9% users in 2010 [78].

Factors contributing to the increased application of smartphones in everyday life include [82] the comparable processing and memory capabilities to the ones found in personal computers, the number of cost-effective sensors built into the devices, the advanced OS that allow to take advantage of the smartphone hardware and software capabilities, their higher portability and lower prices compared to personal computers, and the easy access to software applications and OS upgrades. Nowadays smartphone applications also include healthcare, and the abovementioned factors give them advantages over other architectures in terms of implementation and integration with other health monitoring technologies.

The use of smartphones for professional purposes among physicians has increased in the last years, going from 68% in 2012 to 84% in 2015, reflecting the increased interest in mobile health technologies [83]. The global mobile health industry is expected to increase and reach more than 55 billion U.S dollars in the next five years, an increase more than eightfold in comparison to 2013 [84]. Nowadays, consumers/patients are the main target by mobile applications rather than healthcare

professionals, almost in a 3:1 ratio [85]. From the point of view of the patient, main reasons to adopt mobile health applications include [86] the ability to access their healthcare providers in effectively and conveniently way, the ability to reduce their own healthcare costs, ability to take greater control over their own health, the ability to obtain information that is difficult or impossible for them from other sources, and the ability to access better quality healthcare. Mobile healthcare applications have potential to improve costs, convenience, and quality of healthcare to costumers/patients. Reports from a recent survey performed this year indicate that the use of health and wellbeing mobile applications have positively impacted their users in United Kingdom [87].

Summarizing, smartphone health care applications are on the rise, healthcare professionals are already adopting them, and, simultaneously, patients are also willing to use them to actively participate in their own care [88]. Given the current state, smartphones have the potential to become ubiquitous standalone devices that provide point-of-care monitoring and diagnosis to anyone [89]. On the way, they can help to reduce the costs and burden on health care systems by providing early monitoring and reducing frequency of patient transport [89].

A diversity of smartphone-based healthcare applications for on-demand self-monitoring have been developed by taking advantage of the smartphone's processing power, sensors, and multimedia and wireless communications capabilities. Extensive reviews of the smartphone applications in healthcare can be found in references [85], [88], [90]–[94]. Perhaps the most widely known smartphone healthcare application for monitoring purposes refers to cardiac monitoring via a contact optical approach using the built camera of the device [95]–[98]. Another smartphone application currently under research refers to RR estimation via a contact optical approach [99], [100]. The noncontact optical approach has been also employed on smartphones for cardiac and respiratory monitoring. In particular, a smartphone application for iOS devices has been released by Philips [101]. According to the available information, Philips vital signs camera application allows the estimation of HR and RR; HR by analyzing color changes in the subject's face, and RR by analyzing the up and down chest movements while breathing [101].

Regarding the analysis of respiratory sounds based on smartphones, there have been some efforts. The concept of a digital stethoscope using a palmtop has been proposed [102]. Unfortunately, the technical detail provided about the characteristics of the system was limited and there were no reports on the reliability of the acquired respiratory sounds or examples of the acquired signals. A smartphone-based asthma monitoring system has been proposed by using wireless communications [103], [104]. In a first study, respiratory sounds were processed via custom designed hardware and the obtained information was transmitted to the smartphone using wireless protocols. The smartphone was used to display the processed data and as a gateway between the obtained information and a medical database via Internet [103]. In a subsequent study, sounds obtained from Internet sources were transmitted to the smartphone and different reconstruction techniques were tested to analyze the performance of the wireless transmission stage [104]. The employment smartphones to record respiratory efforts, via respiratory sounds, together with body movements and oxygen saturation measurements, via accelerometers and a wireless pulse oximeter, respectively, has been proposed for the detection of obstructive sleep apnea [105]. A digital stethoscope, called One, has been developed by Thinklabs and it is commercially available for around $500 U.S. dollars [106]. It allows connection to smartphones via companion software applications and a custom designed wired connector. Additional wireless Bluetooth transmitter-receiver can be acquired at additional cost. Available documentation on their webpage mostly focuses on heart sounds recording but their sound library also includes examples of respiratory sounds [106]. The extraction of breathing parameters using this digital stethoscope system has not been reported. In particular, to our best knowledge, there are no applications regarding the estimation of V_T using smartphone-acquired acoustical or optical signals directly on the device.

Next chapters of this dissertation will introduce the smartphone-based breathing monitoring methods via the acoustical and noncontact optical approaches proposed in this dissertation research. It is worth mentioning that the devices and sensors were selected so that the minimum requirements for CORSA systems summarized in Table 2.1 were satisfied.

2.4 References

[1] Z. Moussavi, *Fundamentals of Respiratory System and Sounds Analysis*. Morgan & Claypool.

[2] B. M. Koeppen and B. A. Stanton, *Berne & Levy Physiology, Updated Edition*. Elsevier Health Sciences, 2009.

[3] H. Kitaoka, R. Takaki, and B. Suki, "A three-dimensional model of the human airway tree," *J. Appl. Physiol.*, vol. 87, no. 6, pp. 2207–2217, Dec. 1999.

[4] T. R. Nelson and D. K. Manchester, "Modeling of lung morphogenesis using fractal geometries," *IEEE Trans. Med. Imaging*, vol. 7, no. 4, pp. 321–327, 1988.

[5] M. Ochs, J. R. Nyengaard, A. Jung, L. Knudsen, M. Voigt, T. Wahlers, J. Richter, and H. J. G. Gundersen, "The Number of Alveoli in the Human Lung," *Am. J. Respir. Crit. Care Med.*, vol. 169, no. 1, pp. 120–124, Jan. 2004.

[6] L. Sherwood, *Fundamentals of Human Physiology*, 4th ed. Boston, MA, USA: Cengage Learning, 2011.

[7] K. Konno and J. Mead, "Measurement of the separate volume changes of rib cage and abdomen during breathing," *J. Appl. Physiol.*, vol. 22, no. 3, pp. 407–422, Mar. 1967.

[8] G. Li, N. C. Arora, H. Xie, H. Ning, W. Lu, D. Low, D. Citrin, A. Kaushal, L. Zach, K. Camphausen, and R. W. Miller, "Quantitative prediction of respiratory tidal volume based on the external torso volume change: a potential volumetric surrogate," *Phys. Med. Biol.*, vol. 54, no. 7, pp. 1963–1978, Apr. 2009.

[9] V. P. Vellody, M. Nassery, W. S. Druz, and J. T. Sharp, "Effects of body position change on thoracoabdominal motion," *J. Appl. Physiol.*, vol. 45, no. 4, pp. 581–589, Oct. 1978.

[10] W. S. Druz and J. T. Sharp, "Activity of respiratory muscles in upright and recumbent humans," *J. Appl. Physiol.*, vol. 51, no. 6, pp. 1552–1561, Dec. 1981.

[11] F. Q. Al-Khalidi, R. Saatchi, D. Burke, H. Elphick, and S. Tan, "Respiration rate monitoring methods: A review," *Pediatr. Pulmonol.*, vol. 46, no. 6, pp. 523–529, Jun. 2011.

[12] N. O. T. Strömberg and N. Nelson, "Thoracoabdominal asynchrony in small children with lung disease – methodological aspects and the relationship to lung mechanics," *Clin. Physiol.*, vol. 18, no. 5, pp. 447–456, Oct. 1998.

[13] A. R. A. Sovijarvi, F. Dalmasso, J. Vanderschoot, L. P. Malmberg, G. Righini, and S. A. T. Stoneman, "Definition of terms for applications of respiratory sounds," *Eur. Respir. Rev.*, vol. 10, no. 77, pp. 597–610, 2000.

[14] R. Beck, G. Rosenhouse, M. Mahagnah, R. M. Chow, D. W. Cugell, and N. Gavriely, "Measurements and Theory of Normal Tracheal Breath Sounds," *Ann. Biomed. Eng.*, vol. 33, no. 10, pp. 1344–1351, Oct. 2005.

[15] H. Pasterkamp, S. S. Kraman, and G. R. Wodicka, "Respiratory Sounds: Advances Beyond the Stethoscope," *Am. J. Respir. Crit. Care Med.*, vol. 156, no. 3, pp. 974–987, Sep. 1997.

[16] R. Laennec, *Treatise' is De l'Auscultation Médiate ou Traité du Diagnostic des Maladies des Poumons et du Coeu. Paris: Brosson & Chaudé, 1819*, English translation by J. Forbes. London: Underwood, 1821.

[17] V. A. McKusick, J. T. Jenkins, and G. N. Webb, "The acoustic basis of the chest examination; studies by means of sound spectrography," *Am Rev Tuberc*, vol. 72, no. 1, pp. 12–34, Jul. 1955.

[18] A. R. A. Sovijarvi, L. P. Malmberg, G. Charbonneau, J. Vanderschoot, F. Dalmasso, C. Sacco, M. Rossi, and J. E. Earis, "Characteristics of breath sounds and adventitious respiratory sounds," *Eur. Respir. Rev.*, vol. 10, no. 77, pp. 591–596, 2000.

[19] F. Dalmay, M. T. Antonini, P. Marquet, and R. Menier, "Acoustic properties of the normal chest," *Eur. Respir. J.*, vol. 8, no. 10, pp. 1761–1769, Oct. 1995.

[20] N. Gavriely and D. W. Cugell, "Airflow effects on amplitude and spectral content of normal breath sounds," *J. Appl. Physiol.*, vol. 80, no. 1, pp. 5–13, Jan. 1996.

[21] P. Leblanc, P. T. Macklem, and W. R. Ross, “Breath sounds and distribution of pulmonary ventilation,” *Am. Rev. Respir. Dis.*, vol. 102, no. 1, pp. 10–16, Jul. 1970.
[22] D. Olson and J. Hammersley, “Mechanisms of Lung Sound Generation,” *Semin. Respir. Crit. Care Med.*, vol. 6, no. 03, pp. 171–179, 1985.
[23] B. E. Shykoff, Y. Ploysongsang, and H. K. Chang, “Airflow and Normal Lung Sounds,” *Am. Rev. Respir. Dis.*, vol. 137, no. 4, pp. 872–876, Apr. 1988.
[24] A. Yadollahi and Z. M. K. Moussavi, “Acoustical Respiratory Flow,” *IEEE Eng. Med. Biol. Mag.*, vol. 26, no. 1, pp. 56–61, 2007.
[25] M. A. E. Ramsay, M. Usman, E. Lagow, M. Mendoza, E. Untalan, and E. De Vol, “The Accuracy, Precision and Reliability of Measuring Ventilatory Rate and Detecting Ventilatory Pause by Rainbow Acoustic Monitoring and Capnometry:,” *Anesth. Analg.*, vol. 117, no. 1, pp. 69–75, Jul. 2013.
[26] M. Folke, L. Cernerud, M. Ekström, and B. Hök, “Critical review of non-invasive respiratory monitoring in medical care,” *Med. Biol. Eng. Comput.*, vol. 41, no. 4, pp. 377–383, Jul. 2003.
[27] G. Chen, I. de la Cruz, and E. Rodriguez-Villegas, “Automatic lung tidal volumes estimation from tracheal sounds,” *Conf. Proc. Annu. Int. Conf. IEEE Eng. Med. Biol. Soc. IEEE Eng. Med. Biol. Soc. Annu. Conf.*, vol. 2014, pp. 1497–1500, Aug. 2014.
[28] Y. S. Lee, P. N. Pathirana, C. L. Steinfort, and T. Caelli, “Monitoring and Analysis of Respiratory Patterns Using Microwave Doppler Radar,” *IEEE J. Transl. Eng. Health Med.*, vol. 2, pp. 1–12, 2014.
[29] G. B. Drummond, A. F. Nimmo, and R. A. Elton, “Thoracic impedance used for measuring chest wall movement in postoperative patients.,” *Br. J. Anaesth.*, vol. 77, no. 3, pp. 327–332, Sep. 1996.
[30] S. Hoffman, R. Jedeikin, and D. Atlas, “Respiratory monitoring with a new impedance plethysmograph,” *Anaesthesia*, vol. 41, no. 11, pp. 1139–1142, 1986.
[31] K. P. Cohen, W. M. Ladd, D. M. Beams, W. S. Sheers, R. G. Radwin, W. J. Tompkins, and J. G. Webster, “Comparison of impedance and inductance ventilation sensors on adults during breathing, motion, and simulated airway obstruction,” *IEEE Trans. Biomed. Eng.*, vol. 44, no. 7, pp. 555–566, Jul. 1997.
[32] J. J. Vargo, G. Zuccaro Jr., J. A. Dumot, D. L. Conwell, J. B. Morrow, and S. S. Shay, “Automated graphic assessment of respiratory activity is superior to pulse oximetry and visual assessment for the detection of early respiratory depression during therapeutic upper endoscopy,” *Gastrointest. Endosc.*, vol. 55, no. 7, pp. 826–831, Jun. 2002.
[33] J. Lázaro, E. Gil, R. Bailón, A. Mincholé, and P. Laguna, “Deriving respiration from photoplethysmographic pulse width,” *Med. Biol. Eng. Comput.*, vol. 51, no. 1–2, pp. 233–242, Sep. 2012.
[34] M. R. Miller, J. Hankinson, V. Brusasco, F. Burgos, R. Casaburi, A. Coates, R. Crapo, P. Enright, C. P. M. van der Grinten, P. Gustafsson, and others, “Standardisation of spirometry,” *Eur. Respir. J.*, vol. 26, no. 2, pp. 319–338, 2005.
[35] K. Ashutosh, R. Gilbert, J. H. Auchincloss, J. Erlebacher, and D. Peppi, “Impedance pneumograph and magnetometer methods for monitoring tidal volume,” *J Appl Physiol*, vol. 37, no. 6, pp. 964–966, 1974.
[36] B. J. Semmes, M. J. Tobin, J. V. Snyder, and A. Grenvik, “Subjective and objective measurement of tidal volume in critically ill patients.,” *Chest*, vol. 87, no. 5, pp. 577–579, 1985.
[37] S. J. Cala, C. M. Kenyon, G. Ferrigno, P. Carnevali, A. Aliverti, A. Pedotti, P. T. Macklem, and D. F. Rochester, “Chest wall and lung volume estimation by optical reflectance motion analysis,” *J. Appl. Physiol.*, vol. 81, no. 6, pp. 2680–2689, Dec. 1996.
[38] A. Johansson and P. P. Å. Öberg, “Estimation of respiratory volumes from the photoplethysmographic signal. Part I: experimental results,” *Med. Biol. Eng. Comput.*, vol. 37, no. 1, pp. 42–47, Jan. 1999.

[39] C.-L. Que, C. Kolmaga, L.-G. Durand, S. M. Kelly, and P. T. Macklem, "Phonospirometry for noninvasive measurement of ventilation: methodology and preliminary results," *J. Appl. Physiol. Bethesda Md 1985*, vol. 93, no. 4, pp. 1515–1526, Oct. 2002.
[40] O. Sayadi, E. H. Weiss, F. M. Merchant, D. Puppala, and A. A. Armoundas, "An Optimized Method for Estimating the Tidal Volume from Electrocardiographic Signals: Implications for Estimating Minute Ventilation," *Am. J. Physiol. - Heart Circ. Physiol.*, vol. 307, pp. H426–H436, 2014.
[41] R. Gilbert, J. H. Auchincloss, J. Brodsky, and W. Boden, "Changes in tidal volume, frequency, and ventilation induced by their measurement.," *J. Appl. Physiol.*, vol. 33, no. 2, pp. 252–254, Aug. 1972.
[42] L. Vannuccini, J. E. Earis, P. Helisto, B. M. G. Cheetham, M. Rossi, A. R. A. Sovijarvi, and J. Vanderschoot, "Capturing and preprocessing of respiratory sounds," *Eur. Respir. Rev.*, vol. 10, no. 77, pp. 616–620, 2000.
[43] C. K. Druzgalski, R. L. Donnerberg, and R. M. Campbell, "Techniques of recording respiratory sounds," *J. Clin. Eng.*, vol. 5, no. 4, pp. 321–330, 1980.
[44] D. M. J. Mussell, "The need for standards in recording and analysing respiratory sounds," *Med. Biol. Eng. Comput.*, vol. 30, no. 2, pp. 129–139, Mar. 1992.
[45] B. M. G. Cheetham, G. Charbonneau, A. Giordano, P. Helisto, and J. Vanderschoot, "Digitization of data for respiratory sound recordings," *Eur. Respir. Rev.*, vol. 10, no. 77, pp. 621–624, 2000.
[46] A. R. A. Sovijarvi, J. Vanderschoot, and J. E. Earis, "Standardization of computerized respiratory sound analysis," *Eur. Respir. Rev.*, vol. 10, no. 77, pp. 585–585, 2000.
[47] J. E. Earis and B. M. G. Cheetham, "Current methods used for computerized respiratory sound analysis," *Eur. Respir. Rev.*, vol. 10, no. 77, pp. 586–590, 2000.
[48] P. Forgacs, "The functional basis of pulmonary sounds.," *Chest*, vol. 73, no. 3, pp. 399–405, 1978.
[49] D. Brooks and J. Thomas, "Interrater Reliability of Auscultation of Breath Sounds Among Physical Therapists," *Phys. Ther.*, vol. 75, no. 12, pp. 1082–1088, Dec. 1995.
[50] P. Piirila and A. R. Sovijarvi, "Crackles: recording, analysis and clinical significance," *Eur. Respir. J.*, vol. 8, no. 12, pp. 2139–2148, Dec. 1995.
[51] H. Pasterkamp, C. Carson, D. Daien, and Y. Oh, "Digital respirosonography. New images of lung sounds.," *Chest*, vol. 96, no. 6, pp. 1405–1412, Dec. 1989.
[52] A. Yadollahi and Z. M. K. Moussavi, "A robust method for estimating respiratory flow using tracheal sounds entropy," *IEEE Trans. Biomed. Eng.*, vol. 53, no. 4, pp. 662–668, Apr. 2006.
[53] Masimo, Corp., "RRa. Noninvasive Acoustic Respiration Rate." [Online]. Available: http://www.masimo.com/rra/.
[54] Y. Guechi, A. Pichot, D. Frasca, F. Rayeh-Pelardy, J.-Y. Lardeur, and O. Mimoz, "Assessment of noninvasive acoustic respiration rate monitoring in patients admitted to an Emergency Department for drug or alcoholic poisoning," *J. Clin. Monit. Comput.*, vol. 29, no. 6, pp. 721–726, Dec. 2015.
[55] M. Patino, D. T. Redford, T. W. Quigley, M. Mahmoud, C. D. Kurth, and P. Szmuk, "Accuracy of acoustic respiration rate monitoring in pediatric patients," *Paediatr. Anaesth.*, vol. 23, no. 12, pp. 1166–1173, Dec. 2013.
[56] Z. K. Moussavi, M. T. Leopando, H. Pasterkamp, and D. G. Rempel, "Computerised acoustical respiratory phase detection without airflow measurement," *Med. Biol. Eng. Comput.*, vol. 38, no. 2, pp. 198–203, Mar. 2000.
[57] P. Hult, B. Wranne, and P. Ask, "A bioacoustic method for timing of the different phases of the breathing cycle and monitoring of breathing frequency," *Med. Eng. Phys.*, vol. 22, no. 6, pp. 425–433, Jul. 2000.
[58] H. Alshaer, G. R. Fernie, and T. D. Bradley, "Monitoring of breathing phases using a bioacoustic method in healthy awake subjects," *J. Clin. Monit. Comput.*, vol. 25, no. 5, pp. 285–294, Sep. 2011.
[59] S. Huq and Z. Moussavi, "Acoustic breath-phase detection using tracheal breath sounds," *Med. Biol. Eng. Comput.*, vol. 50, no. 3, pp. 297–308, Feb. 2012.
[60] A. Abushakra and M. Faezipour, "Acoustic signal classification of breathing movements to virtually aid breath regulation," *IEEE J. Biomed. Health Inform.*, vol. 17, no. 2, pp. 493–500, Mar. 2013.

[61] N. Meslier, G. Charbonneau, and J. L. Racineux, “Wheezes,” *Eur. Respir. J.*, vol. 8, no. 11, pp. 1942–1948, Nov. 1995.
[62] A. R. Nath and L. H. Capel, “Inspiratory crackles—early and late,” *Thorax*, vol. 29, no. 2, pp. 223–227, Mar. 1974.
[63] P. Piirilä, A. R. Sovijärvi, T. Kaisla, H. M. Rajala, and T. Katila, “Crackles in patients with fibrosing alveolitis, bronchiectasis, COPD, and heart failure,” *Chest*, vol. 99, no. 5, pp. 1076–1083, May 1991.
[64] A. Vyshedskiy, R. M. Alhashem, R. Paciej, M. Ebril, I. Rudman, J. J. Fredberg, and R. Murphy, “Mechanism of inspiratory and expiratory crackles,” *Chest*, vol. 135, no. 1, pp. 156–164, Jan. 2009.
[65] P. Piirila and A. R. Sovijarvi, “Crackles: recording, analysis and clinical significance,” *Eur. Respir. J.*, vol. 8, no. 12, pp. 2139–2148, Dec. 1995.
[66] C. S. Shim and M. H. Williams, “Relationship of wheezing to the severity of obstruction in asthma,” *Arch. Intern. Med.*, vol. 143, no. 5, pp. 890–892, May 1983.
[67] J. E. Earis, K. Marsh, M. G. Pearson, and C. M. Ogilvie, “The inspiratory ‘squawk’ in extrinsic allergic alveolitis and other pulmonary fibroses.,” *Thorax*, vol. 37, no. 12, pp. 923–926, Dec. 1982.
[68] R. Paciej, A. Vyshedskiy, D. Bana, and R. Murphy, “Squawks in pneumonia,” *Thorax*, vol. 59, no. 2, pp. 177–178, Feb. 2004.
[69] F. Zhao, M. Li, Y. Qian, and J. Z. Tsien, “Remote Measurements of Heart and Respiration Rates for Telemedicine,” *PLoS ONE*, vol. 8, no. 10, p. e71384, Oct. 2013.
[70] M.-Z. Poh, D. J. McDuff, and R. W. Picard, “Advancements in Noncontact, Multiparameter Physiological Measurements Using a Webcam,” *IEEE Trans. Biomed. Eng.*, vol. 58, no. 1, pp. 7–11, Jan. 2011.
[71] Y. Sun, S. Hu, V. Azorin-Peris, S. Greenwald, J. Chambers, and Y. Zhu, “Motion-compensated noncontact imaging photoplethysmography to monitor cardiorespiratory status during exercise,” *J. Biomed. Opt.*, vol. 16, no. 7, pp. 077010–077010, 2011.
[72] H.-Y. Wu, M. Rubinstein, E. Shih, J. Guttag, F. Durand, and W. Freeman, “Eulerian Video Magnification for Revealing Subtle Changes in the World,” *ACM Trans Graph*, vol. 31, no. 4, pp. 65:1–65:8, Jul. 2012.
[73] L. Tarassenko, M. Villarroel, A. Guazzi, J. Jorge, D. A. Clifton, and C. Pugh, “Non-contact video-based vital sign monitoring using ambient light and auto-regressive models,” *Physiol. Meas.*, vol. 35, no. 5, p. 807, 2014.
[74] D. Shao, Y. Yang, C. Liu, F. Tsow, H. Yu, and N. Tao, “Noncontact Monitoring Breathing Pattern, Exhalation Flow Rate and Pulse Transit Time,” *IEEE Trans. Biomed. Eng.*, vol. 61, no. 11, pp. 2760–2767, Nov. 2014.
[75] G. Ferrigno, P. Carnevali, A. Aliverti, F. Molteni, G. Beulcke, and A. Pedotti, “Three-dimensional optical analysis of chest wall motion,” *J. Appl. Physiol. Bethesda Md 1985*, vol. 77, no. 3, pp. 1224–1231, Sep. 1994.
[76] M. Ragnarsdóttir, A. KristjAnsdóttir, I. Ingvarsdóttir, P. Hannesson, B. Torfason, and L. Cahalin, “Short-term changes in pulmonary function and respiratory movements after cardiac surgery via median sternotomy,” *Scand. Cardiovasc. J. SCJ*, vol. 38, no. 1, pp. 46–52, Mar. 2004.
[77] M. Ragnarsdóttir and E. K. Kristinsdóttir, “Breathing movements and breathing patterns among healthy men and women 20-69 years of age. Reference values,” *Respir. Int. Rev. Thorac. Dis.*, vol. 73, no. 1, pp. 48–54, 2006.
[78] Statista, Inc., “Global smartphone sales to end users since 2007.” [Online]. Available: http://www.statista.com/statistics/263437/global-smartphone-sales-to-end-users-since-2007/.
[79] Statista, Inc., “Global market share held by smartphone operating systems.” [Online]. Available: http://www.statista.com/statistics/263453/global-market-share-held-by-smartphone-operating-systems/.
[80] IDC Research, Inc., “Smartphone OS Market Share, 2015 Q2.” [Online]. Available: http://www.idc.com/prodserv/smartphone-os-market-share.jsp.

[81] comScore, Inc., “comScore Reports January 2015 U.S. Smartphone Subscriber Market Share.” [Online]. Available: https://www.comscore.com/Insights/Market-Rankings/comScore-Reports-January-2015-US-Smartphone-Subscriber-Market-Share.
[82] Phys.org, “Smart phone functions seep into all sectors.” [Online]. Available: http://phys.org/news/2011-01-smart-functions-seep-sectors.html.
[83] Statista, Inc., “Physicians’ usage of smartphones for professional purposes in the U.S. from 2012 to 2015.” [Online]. Available: http://www.statista.com/statistics/416951/smartphone-use-for-professional-purposes-among-us-physicians/.
[84] Statista, Inc., “Global digital health market from 2013 to 2020, by segment (in billion U.S. dollars).” [Online]. Available: http://www.statista.com/statistics/387867/value-of-worldwide-digital-health-market-forecast-by-segment/.
[85] IMS Institute for Healthcare Informatics, “Patient Apps for Improved Healthcare (October 2013). From Novelty to Mainstream.” [Online]. Available: http://www.imshealth.com/deployedfiles/imshealth/Global/Content/Corporate/IMS%20Health%20Institute/Reports/Patient_Apps/IIHI_Patient_Apps_Report.pdf.
[86] Statista, Inc., “Top drivers for adoption of mHealth applications and services by patients as of 2012.” [Online]. Available: http://www.statista.com/statistics/328661/reasons-for-patient-use-of-mhealth-apps-and-services/.
[87] Statista, Inc., “Impact of health and wellbeing mobile apps use in the United Kingdom (UK) in 2015, by mobile app type.” [Online]. Available: http://www.statista.com/statistics/472899/impact-of-health-and-wellbeing-mobile-apps-use-in-the-uk-by-mobile-app-type/.
[88] M. N. Boulos, S. Wheeler, C. Tavares, and R. Jones, “How smartphones are changing the face of mobile and participatory healthcare: an overview, with example from eCAALYX,” *Biomed. Eng. OnLine*, vol. 10, no. 1, p. 24, Apr. 2011.
[89] G. Kiss, “Using Smartphones in Healthcare and to Save Lives,” in *Internet of Things (iThings/CPSCom), 2011 International Conference on and 4th International Conference on Cyber, Physical and Social Computing*, 2011, pp. 614–619.
[90] J. Behar, A. Roebuck, J. S. Domingos, E. Gederi, and G. D. Clifford, “A review of current sleep screening applications for smartphones,” *Physiol. Meas.*, vol. 34, no. 7, p. R29, 2013.
[91] A. Kho, L. E. Henderson, D. D. Dressler, and S. Kripalani, “Use of Handheld Computers in Medical Education,” *J. Gen. Intern. Med.*, vol. 21, no. 5, pp. 531–537, May 2006.
[92] S. Krishna, S. A. Boren, and E. A. Balas, “Healthcare via Cell Phones: A Systematic Review,” *Telemed. E-Health*, vol. 15, no. 3, pp. 231–240, Apr. 2009.
[93] A. Kailas, C.-C. Chong, and F. Watanabe, “From Mobile Phones to Personal Wellness Dashboards,” *IEEE Pulse*, vol. 1, no. 1, pp. 57–63, Jul. 2010.
[94] M. Terry, “Medical Apps for Smartphones,” *Telemed. J. E-Health Off. J. Am. Telemed. Assoc.*, vol. 16, no. 1, pp. 17–22, Feb. 2010.
[95] M. J. Gregoski, M. Mueller, A. Vertegel, A. Shaporev, B. B. Jackson, R. M. Frenzel, S. M. Sprehn, and F. A. Treiber, “Development and Validation of a Smartphone Heart Rate Acquisition Application for Health Promotion and Wellness Telehealth Applications,” *Int J Telemed. Appl*, vol. 2012, pp. 1:1–1:1, Jan. 2012.
[96] R.-C. Peng, X.-L. Zhou, W.-H. Lin, and Y.-T. Zhang, “Extraction of heart rate variability from smartphone photoplethysmograms,” *Comput. Math. Methods Med.*, vol. 2015, p. 516826, 2015.
[97] C. G. Scully, J. Lee, J. Meyer, A. M. Gorbach, D. Granquist-Fraser, Y. Mendelson, and K. H. Chon, “Physiological Parameter Monitoring from Optical Recordings with a Mobile Phone,” *IEEE Trans. Biomed. Eng.*, vol. 59, no. 2, pp. 303–306, Feb. 2012.
[98] J. Lee, B. A. Reyes, D. D. McManus, O. Mathias, and K. H. Chon, “Atrial Fibrillation Detection Using an iPhone 4S,” *IEEE Trans. Biomed. Eng.*, vol. 60, no. 1, pp. 203–206, 2013.
[99] Y. Nam, J. Lee, and K. H. Chon, “Respiratory Rate Estimation from the Built-in Cameras of Smartphones and Tablets,” *Ann. Biomed. Eng.*, vol. 42, no. 4, pp. 885–898, Nov. 2013.

[100] J. Lázaro, Y. Nam, E. Gil, P. Laguna, and K. H. Chon, “Respiratory rate derived from smartphone-camera-acquired pulse photoplethysmographic signals,” *Physiol. Meas.*, vol. 36, no. 11, p. 2317, 2015.
[101] Philips, “Philips Vital Signs Camera.” [Online]. Available: http://www.vitalsignscamera.com/.
[102] K. Hung, B. L. Luk, W. H. Choy, B. Tai, and S. K. Tso, “Multifunction stethoscope for telemedicine,” in *Proceedings of the 2003 IEEE International Workshop on Computer Architectures for Machine Perception*, 2004, pp. 87–89.
[103] D. Oletic, B. Arsenali, and V. Bilas, “Towards Continuous Wheeze Detection Body Sensor Node as a Core of Asthma Monitoring System,” in *Wireless Mobile Communication and Healthcare*, K. S. Nikita, J. C. Lin, D. I. Fotiadis, and M.-T. A. Waldmeyer, Eds. Springer Berlin Heidelberg, 2012, pp. 165–172.
[104] D. Oletic, M. Skrapec, and V. Bilas, “Monitoring Respiratory Sounds: Compressed Sensing Reconstruction via OMP on Android Smartphone,” in *Wireless Mobile Communication and Healthcare*, B. Godara and K. S. Nikita, Eds. Springer Berlin Heidelberg, 2013, pp. 114–121.
[105] M. Al-Mardini, F. Aloul, A. Sagahyroon, and L. Al-Husseini, “Classifying obstructive sleep apnea using smartphones,” *J. Biomed. Inform.*, vol. 52, pp. 251–259, Dec. 2014.
[106] Thinklabs, “Thinklabs One - Digital Stethoscope.” [Online]. Available: http://www.thinklabs.com/.

Chapter 3: Tracheal Sounds Acquisition using Smartphones

(B. A. Reyes, N. Reljin, and K. H. Chon, "Tracheal Sounds Acquisition Using Smartphones," *Sensors*, vol. 14, no. 8, pp. 13830–13850, 2014; reused with permission from MDPI - Open Access Publishing)

3.1 Introduction

In this dissertation, we will concentrate only on the study of tracheal sounds recorded from healthy subjects. Main characteristics of tracheal sounds were introduced in previous chapter but it is worth mentioning here that their inspiratory and expiratory phases have similar frequency contents [1], [2], as well as that the relationship between airflow, F, and tracheal sound's amplitude, A, is relevant; being a power law of the form $A = kF^{\alpha}$ considered as the typical best fit, where k and α are constants with varying values having been found from different research groups [3]–[7]. Those characteristics will be analyzed in this chapter.

The stethoscope remains the most widely used instrument in clinical medicine and its use during auscultation still guides in diagnosis when other pulmonary function testing is not available [8]. However, auscultation with the mechanical stethoscope has limitations [2], [9], [10]. Many of these limitations have been overcome by using CORSA systems. Computerized analysis of respiratory sounds has led to the renaissance of lung auscultation over the last decades but this renewed interest has also produced several different measurement systems by different laboratories [11]–[13]. Fortunately, standardization of CORSA has been addressed, and guidelines for the minimum requirements of CORSA systems have been provided [14], [15]. The European Community financed the CORSA project, which explicitly expressed that [16] "one goal of the current technological developments is to combine processing power, storage, miniaturization of components and analysis programed into a small hand-held computerized stethoscope that will provide the clinician with much more useful information than the current simple mechanical stethoscope." Given the need for reliable devices that can record and

analyze respiratory sounds in a continuous, non-invasive, and portable fashion, we propose to develop a respiratory sound system based on a smartphone platform.

The development of an inexpensive, reliable, and portable CORSA system would expand the noninvasive diagnostic capabilities of the auscultation procedure when used by general practitioners and pneumologists in the diagnosis of respiratory diseases during the clinical examination. The use of an inexpensive, reliable, and portable system would also enable more health centers to undertake the quantitative analysis of respiratory sounds for diagnosis of respiratory diseases. We hypothesize that a CORSA system that satisfies these characteristics can be implemented using a smartphone.

There have been attempts to develop a portable system for the analysis of respiratory sounds. In particular, the concept of a portable device based on a microcontroller, memory arrays, and liquid crystal displays has been proposed but without sufficient details about implementation results [17]. The concept of a digital stethoscope using a palmtop computer has been also proposed but neither technical detail about the characteristics of the system that guarantee the reliability of the acquired respiratory sound signals nor examples of the acquired signals were provided [18]. Recently, the concept of a smartphone-based asthma monitoring system has been proposed [19], [20]. The sounds were processed via custom-designed hardware and the obtained information was wirelessly transmitted to the smartphone to display the processed data. The processed data were then transmitted to a medical database via the Internet [19]. Sounds obtained from Internet sources were transmitted to smartphone and reconstruction techniques were tested [20]. However, like in the previous attempts, no information was provided about the reliability of the system when acquiring real respiratory sounds.

The smartphone-based CORSA system we propose in this dissertation differs from the existing systems in two main ways. First, the signal processing of the acquired respiratory sounds will be performed directly on the smartphone, without the employment of complicated secondary devices with microcontroller-based architectures that increase the energy consumption and the cost of

maintenance/upgrade. The smartphone will be used not only to display the respiratory sound signal, but will also control the acquisition stage and perform the signal processing. Second, no wireless communication will be used to transmit the acquired respiratory sounds to the smartphone in order to avoid losses in the quality of the transmitted information and to reduce the energy consumption in the preprocessing stage. The proposed mobile system will be designed to satisfy the standard requirements for a CORSA system and will take advantage of the already available hardware characteristics of the smartphone for the acquisition, visualization, and processing of the respiratory sounds. The proposed system will have the advantage of being non-invasive, low cost, and a portable device which can be used to monitor anytime and anywhere. It should be noted that the developed system was only used to acquire tracheal sounds while the raw recordings were transferred and processed on a computer.

In this dissertation, the reliability of our proposed smartphone-based system will be tested on the well-known characteristics of the tracheal sounds: well-defined breath phases, similar frequency content for the inspiratory and expiratory phases, and a flow-dependent amplitude relationship. In addition, we aim to detect the breath-phase onsets from the smartphone-acquired tracheal sounds and compare the results with those obtained using the flow signal from a spirometer which is considered the reference. Finally, we will estimate respiration rates from the smartphone-acquired tracheal sound signals and validate them using the respiration rates estimated from the volume changes derived from a spirometer.

3.2 Material and Methods

3.2.1 Subjects

Nine healthy non-smoker volunteers (seven males and two females) ages ranging from 23 to 35 years (mean ± standard deviation: 27.9 ± 5.1), weight 68.7 ± 8.1 kg and height 170.7 ± 6.7 cm, were recruited for this study. The study group consisted of students and staff members from Worcester Polytechnic Institute, MA, USA. All volunteers were invited to participate in the study and each

consented to be a subject and signed the study protocol approved by the Institutional Review Board of WPI.

3.2.2 Tracheal Sounds Data Acquisition

Equipment

Tracheal sounds were acquired using an acoustical sensor composed of a subminiature electret microphone BT-21759-000 (Knowles Electronics, Itasca, IL, USA) encased in a plastic bell. This microphone operates with a voltage supply ranging from 1.3 to 10 V with a low amplifier current drain of 50 μA, provides a flat frequency response between 50 and 3000 Hz, and offers advantages in terms of high durability compared to contact sensors. A light plastic bell was used for air-coupling between the sensor and the recording area on the surface over the trachea. The plastic bell consisted of a conical coupler chamber. This shape provides an efficient transducer of air pressure fluctuations from the skin over the trachea to the microphone [2]. This acoustic sensor was developed by our colleagues at the Metropolitan Autonomous University at Mexico City, Mexico, and had been successfully used for respiratory sound acquisition applications [21], [22]. Acoustical sensors of similar characteristics have been found to be adequate for respiratory sound research [14], [23], [24]. To minimize power line electrical interference, shielded twisted pair cables were used to connect the acoustical sensor to the standard 3.5 mm audio jack in the smartphone. In order to provide impedance matching and to obtain a balance between saturation and sensitivity, a simple voltage divider composed of two resistors of 2.2 kΩ was used before transmitting the recorded tracheal sounds to the smartphone. We cabled to the standard 3.5 mm audio connector to avoid high power consumption or loss of quality due to wireless communication.

Two smartphones were selected for this research: (1) the Galaxy S4 manufactured by Samsung (Samsung Electronics Co., Seoul, South Korea) and running an Android v4.4.2 operating system, and (2) the iPhone 4s manufactured by Apple (Apple, Inc., Cupertino, CA, USA) and running an

iOS 6.1 operating system. Selection of the devices was made based on the high market share of each phone's product family, and the dominant combined market share of their operating systems. In addition, each device contains a high-fidelity audio system that satisfies the minimum requirements recommended by the ERS Task Force Report [15]. The tracheal sounds were recorded using the corresponding built-in audio recorder application of each smartphone (Voice Recorder in the Galaxy S4, and Voice Memos in the iPhone 4s) using the predetermined 16-bit per sample and 44.1 kHz sampling rate and saved in the native .m4a format in each device. Recorded audio files were transferred to a personal computer and converted to .wav format preserving the same bits per sample and sampling rate using a conversion software (Free Audio Converter v.5.0.33, DVDVideoSoft Ltd., United Kingdom) and stored for further processing in Matlab (R2012a, The Mathworks, Inc., Natick, MA, USA).

Simultaneously with the tracheal sounds, the airflow was recorded using a spirometer system consisting of a respiratory flow head (MLT1000L, ADInstruments, Inc., Dunedin, New Zealand) connected to a differential pressure transducer to measure airflow (FE141 Spirometer, ADInstruments, Inc., Dunedin, New Zealand). The airflow signal was digitized using a 16-bit A/D converter PowerLab/4SP, ADInstruments, Inc., Dunedin, New Zealand) at 10 kHz sampling rate by using the manufacturer's software (LabChart 7, ADInstruments, Inc., Dunedin, New Zealand). The volume signal was computed online as the integral of the airflow. Prior to each day of recordings, the spirometer system was calibrated using a 3 L calibration syringe (Hans Rudolph, Inc., Shawnee, KS, USA). A new set of disposable filter, reusable mouthpiece, and disposable nose clip (MLA304, MLA1026, MLA1008, ADInstruments, Inc., Dunedin, New Zealand) was given to each subject.

Acquisition Protocol

Experiments were performed not in an anechoic chamber but in an office room held quiet. The acoustical sensor was fixed to the neck of the volunteers at the anterior cervical triangle using a double-sided adhesive ring (BIOPAC Systems, Goleta, CA, USA) to avoid pressure variations if hand-placed.

Subjects were asked to breathe through a spirometer for approximately 2 min at airflow levels above 0.5 L/s and at maximum of around 2.5 to 3.0 L/s; varying among subjects. The subjects were instructed to breathe first by increasing volumetric flow rates with each breath, and then with decreasing volumetric flow rates with each breath. The airflow was displayed on a 40" monitor placed in front of the subject in order to provide visual feedback. Visual markers were placed between −0.5 to 0.5 L/s and the subjects were instructed to keep the airflow peaks of each respiratory phase outside this boundary area. Initial inspiratory and final expiratory apnea phases of approximately 5 s were acquired in order to record the ambient noise levels. Nose clips were used to clamp the nostrils during the respiratory maneuver. An example of the acquisition protocol is shown in Figure 3.1. A respiratory maneuver was acquired using each smartphone in a sequential way, where the order of the devices was randomized between subjects.

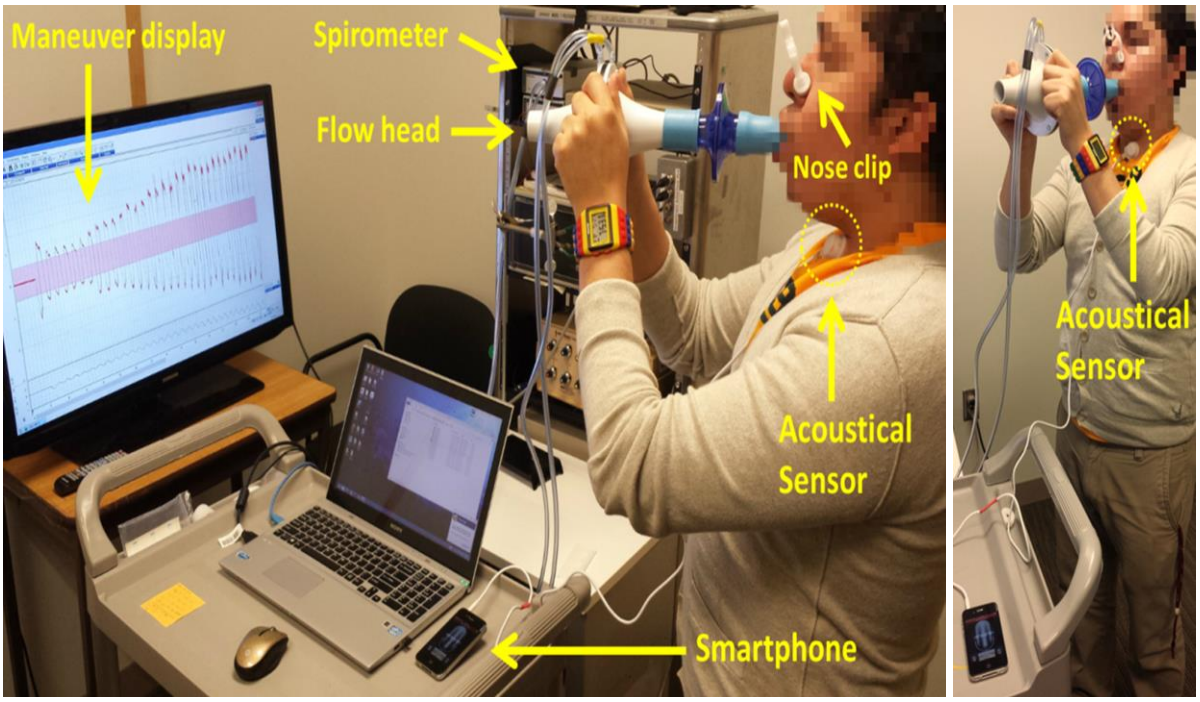

Figure 3.1 - Recording of tracheal sounds using smartphones.
Tracheal sound recording using a smartphone and simultaneous recording of the airflow signal via spirometer during the respiratory maneuver. The acoustical sensor transmitted the tracheal sound to the smartphone via the standard 3.5 mm audio connector.

3.2.3 Data Preprocessing

The acquired tracheal sounds were initially down-sampled from 44.1 kHz to 6300 Hz as this frequency still satisfies the Nyquist criteria and reduces the computational burden. Then, the tracheal sounds were digitally filtered using a 4^{th}-order Butterworth filter with a passband between 100 to 3000 Hz to minimize the heart sounds and muscle interferences. The filter was applied in forward and backward scheme to produce zero-phase distortion and minimize the start and end transients. The airflow and the volume signal were down-sampled to 5 kHz and then interpolated to achieve the same sampling frequency of 6300 Hz, and finally they were lowpass filtered at 20 Hz to minimize high frequency components due the interpolation processes that are not related to the respiratory maneuver.

(a)

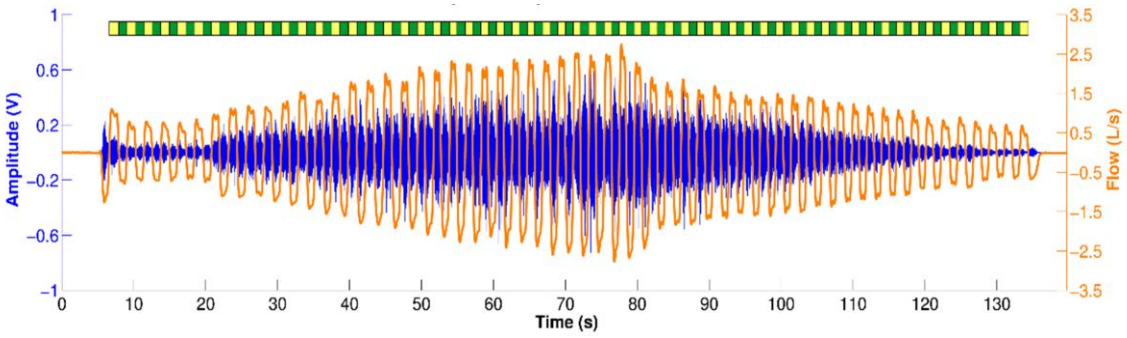

(b)

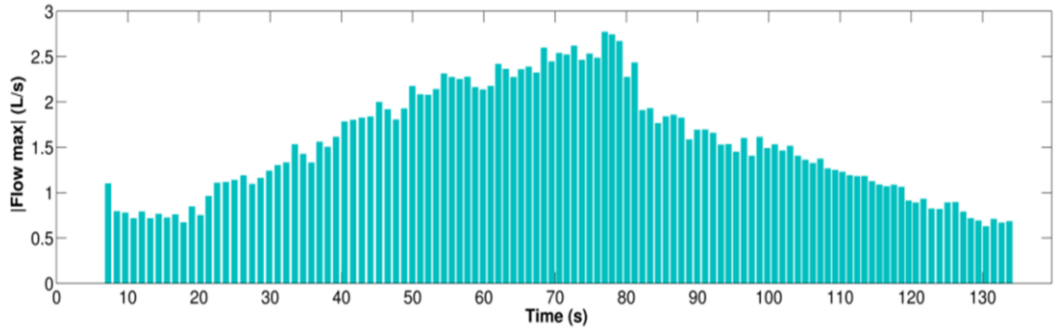

Figure 3.2 - Tracheal sounds acquired using a smartphone during a respiratory maneuver
(a) Preprocessed tracheal sound (in Volts) aligned with the corresponding spirometer's airflow signal. Yellow and green bars on top indicate the inspiratory and expiratory phases, respectively. (b) Corresponding absolute airflow peaks for each respiratory phase of the maneuver.

The volume signal was used for automatic segmentation of the inspiratory and expiratory phases by finding its corresponding local maxima and minima during the respiratory maneuver (breath-phase onsets) and by computing the volume slope between both consecutive onsets (positive for inspiration and negative for expiration). Although both the tracheal sounds and the volumetric flow rate were simultaneously recorded, due to different time delays and press start button times of the smartphone, these signals were manually aligned and their durations corrected to the minimum length of both. An example of the filtered, aligned and segmented tracheal sounds and airflow measured via spirometer is shown in Figure 3.2 for the respiratory maneuver performed by one subject

3.2.4 Tracheal Sound Amplitude and Airflow Relationship

Although visual inspection of the acquired tracheal sounds indicates that their amplitude increases as airflow increases, and decreases as airflow decreases, we used the information from automatically extracted inspiratory and expiratory phases to quantify this relationship. At each respiratory phase, the peak airflow was found and a time window of 400 ms was created starting at the time instant when the airflow signal reached the upper 10% of the airflow, where it reached its plateau. The tracheal sound segments within these windows were extracted and their corresponding power spectral density (PSD) was computed using the fast Fourier transform (FFT) with $NFFT = 1024$. The PSD of the initial apnea period was also computed and subtracted from each PSD of the tracheal sounds segment. The area under the curve of the resulting PSD was computed and regarded as the amplitude of the tracheal sound for that corresponding respiratory breath-phase. For each subject, the inspiratory/expiratory amplitudes were normalized by dividing them by the average inspiration/expiration amplitude [3]. Finally, for each subject, the best fitting curve of the form $A = kF^{\alpha}$ was computed separately for the inspiratory and expiratory phases.

3.2.5 Breath-Phase Onset Detection using Tracheal Sounds

Tracheal sounds acquired with the smartphones were used to estimate the breath-phase onset via the Shannon entropy approach. The Shannon entropy of tracheal sounds has been used as a method for estimating the airflow [25], [26]. The Shannon entropy (SE) of a random signal with probability density function (pdf) p is defined as

$$SE(p) = -\sum_{i=1}^{N} p_i \cdot log(p_i) \quad (1)$$

where N is the number of outcomes of the random variable with pdf p. The SE is used to quantify the uncertainty or irregularity of the process [27]. It has been found that the entropy values quantify the standard deviation and correlation properties of the signal where the individual weight contributions are not trivial to separate [28], [29].

As proposed for the airflow estimation from tracheal sounds, we applied the Shannon entropy in a moving window scheme as follows. First, the recorded tracheal sounds were sequestered into 25 ms windows with 50% overlap between successive windows. For each of the resulting windows, the Shannon entropy was computed. One way to estimate the pdf p is to use the histogram. However, due to the low number of samples within each overlapping window (n = 157 samples) its accuracy would be low. Instead, the pdf of each windowed tracheal sound was computed using the Parzen-window density estimation method with a Gaussian kernel [30], [31]. This non-parametric method estimates the pdf p of the random sample x from which the sample was derived, by superposing window functions placed at each of n observations and determining how many observations x_i fall within the specified window h, *i.e.*, the contribution of each observation x_i within this window h. Then, the pdf is estimated as the sum of the total of the contributions from the observations to this window, and the Parzen-window estimate $\hat{p}$ is given by

$$\hat{p}(x) = \frac{1}{n}\sum_{i=1}^{n}\frac{1}{h}K\left(\frac{x - x_i}{h}\right) \tag{2}$$

where $h > 0$ is the window width of the kernel K, which is typically a pdf itself. When a Gaussian kernel is used, the Parzen-window estimate becomes

$$\hat{p}(x) = \frac{1}{n}\sum_{i=1}^{n}\frac{1}{h\sqrt{2\pi}}exp\left(-\frac{1}{2}\left(\frac{x - x_i}{h}\right)^2\right) \tag{3}$$

where h is the standard deviation of the Gaussian kernel, and was set to [32]

$$h = 1.06 \cdot SD(x) \cdot n^{-\frac{1}{5}} \tag{4}$$

with $SD(\cdot)$ being the standard deviation of the windowed tracheal sound.

The SE estimated from each windowed tracheal sound was assigned to the middle time point of the window, and was interpolated using cubic spline in order to recover the original duration of the tracheal and volumetric flow rate signals. Figure 3.3 shows an example of the computed SE using the described approach for a tracheal sound segment acquired using a smartphone. Observe that this SE signal from a smartphone resembles a rectified airflow signal, as has previously been found when the SE of tracheal sounds are used for airflow estimation purposes [25], [26]. In order to estimate the breath-phase onset, the SE signal was inverted and the corresponding local maxima were automatically detected. First, the SE signal was normalized between [0–1] and down-sampled to 7.875 Hz. The PSD of the down-sampled SE signal was computed with Welch's modified periodogram method with a Hamming window, with 50% overlap, and *NFFT* = 512 bins. The peak of the PSD and its corresponding frequency f_{peak} were found. The local maxima of the SE signal were found and all those maxima that did not satisfy the threshold values criteria were removed. The amplitude threshold was set to $thr_1 = 0.1$, and the time threshold was set to $thr_2 = 0.5 * 1/f_{peak}$. Finally, the corresponding time onsets computed from the down-sampled SE were mapped to the closest point of the original SE time series which had a time resolution of $\Delta_t \approx 0.159\, ms$ given the sampling frequency $f_s = 6300\, Hz$. The detected breath-phase

onsets from tracheal sounds acquired from each smartphone were compared to those computed from volume.

3.2.6 Instantaneous Respiratory Rate Estimation using Tracheal Sounds

As previously stated, the SE of the tracheal sounds resembles the rectified airflow signal. This SE has two lobes for each breathing cycle indicated by the volume signal; see Figure 3.3. We took advantage of this fact to estimate the instantaneous respiratory rate from tracheal sounds acquired with the smartphone. In particular, we employed a joint time-frequency representation (TFR) approach. In general, a TFR allows one to analyze which frequencies of a signal under study are present at a certain time, *i.e.*, a TFR describes the energy density of a signal simultaneously in the time and frequency domains [33]. This characteristic is useful when analyzing signals whose frequency content varies with time, as is the case for the respiratory rate.

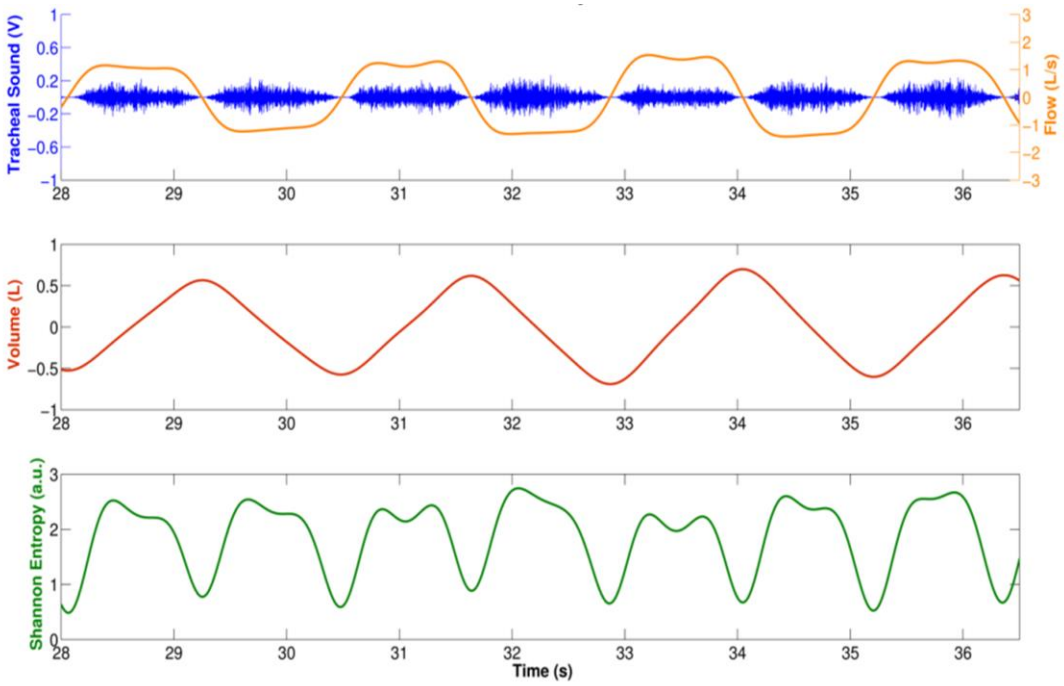

Figure 3.3 - Shannon Entropy of the tracheal sounds acquired using a smartphone.
Top: Segment of tracheal sound and corresponding airflow from spirometer (positive lobes are inspirations and negative lobes are expirations). *Middle:* Volume signal obtained with the spirometer as the integral of the flow. *Bottom:* Shannon entropy of tracheal sound. Observe that local minima of the Shannon entropy are obtained around the onset of each respiratory phase.

The most widely-used TFR in the respiratory sounds field is the spectrogram (SP) given by the magnitude square of the short time Fourier transform (STFT) [1], [8]. The idea behind the SP is that in order to study the properties of the signal s around time t, the original signal around that time is emphasized but it is suppressed at other times by multiplying by a window function $w(t)$ centered at t, to produce a modified signal $s_t(\tau)$ given by [33], [34]

$$s_t(\tau) = s(\tau)w(\tau - t) \tag{5}$$

where the modified signal is a function of two times, the fixed time t of interest, and the time τ. The window function allows the modified signal to satisfy

$$s_t(\tau) = \begin{cases} s(\tau) & for\ \tau\ close\ to\ t \\ 0 & for\ \tau\ far\ away\ from\ t \end{cases} \tag{6}$$

Given that the modified signal emphasizes the original signal around time t, its Fourier transform reflects the frequency distribution around that time

$$\begin{aligned} S_t(\omega) &= \frac{1}{\sqrt{2\pi}} \int e^{-j\omega\tau} s_t(\tau) d\tau \\ S_t(\omega) &= \frac{1}{\sqrt{2\pi}} \int e^{-j\omega\tau} s(\tau) w(\tau - t) d\tau \end{aligned} \tag{7}$$

and hence the name of STFT. The corresponding spectral density at time t is given by

$$SP(t,\omega) = |S_t(\omega)|^2 = \left| \frac{1}{\sqrt{2\pi}} \int e^{-j\omega\tau} s(\tau) w(\tau - t) d\tau \right|^2 \tag{8}$$

where a spectrum is obtained at each time instant and the total of that spectrum is the time-frequency distribution of the original signal $SP(t,\omega)$. This distribution has received different names depending on the application field, *e.g.*, respirosonogram in the respiratory sounds field [8], but the most common is simply spectrogram.

The SP was applied to the volume signal and to the SE of the acquired tracheal sounds. Due to the very low frequency content of the respiratory rate compared to the original sampling frequency, both signals were down-sampled to 7.875 Hz. The SP was computed using *NFFT* = 512 frequency bins, and a Hamming window of 10 s duration. The resulting TFR was normalized between [0–1] and at each time instant, the maximum peak was computed around the central frequency of the whole signal and the corresponding frequency vector was extracted. Due to the discussion mentioned above, the frequency vector extracted from the volume was regarded as the reference instantaneous respiratory frequency, while the half of the frequency vector extracted from the SE signal corresponded to the instantaneous frequency estimated from each smartphone. All instantaneous respiratory frequencies were converted from Hz to breaths-per-minute (bpm).

For each smartphone, three performance indices were computed for the instantaneous respiratory rate (IRR) of each subject. The first index corresponds to the cross-correlation coefficient ρ between the IRR obtained with the corresponding smartphone and the one obtained from the volume from spirometer given by

$$\rho = \frac{\sum_{i=1}^{N} IRR_{volume}(i) \cdot IRR_{smartphone}(i)}{\sqrt{\sum_{i=1}^{N} (IRR_{volume}(i))^2 \cdot \sum_{i=1}^{N} \left(IRR_{smartphone}(i)\right)^2}} \tag{9}$$

where IRR_{volume} represents the instantaneous respiratory rate obtained from the volume, $IRR_{smartphone}$ the corresponding IRR estimated from the tracheal sound acquired with the iPhone 4s or Galaxy S4 smartphone, and *N* is the length of the time vector of the signal. Observe that if the IRR_{volume} and $IRR_{smartphone}$ are the same, the value of ρ is unitary. Therefore, ρ values close to 1 reflect a good estimation performance. The remaining two indices computed were the root-mean-squared error $RMSE$, and the normalized root-mean-squared error $NRMSE$, given by

$$RMSE = \sqrt{\frac{\sum_{i=1}^{N}\left(IRR_{volume}(i) - IRR_{smartphone}(i)\right)^2}{N}} \quad (10)$$

$$NRMSE = \frac{RMSE}{mean(IRR_{volume})}\ x\ 100\% \quad (11)$$

respectively.

3.3 Results and Discussion

The tracheal sound signals acquired using both the Galaxy S4 and the iPhone 4s showed a temporal intensity variation related to the airflow during the respiratory phases as shown in Figure 3.4. The TFR of the smartphone-acquired tracheal sounds (bottom panel of Figure 3.4) shows characteristics of broad band noise where both inspiratory and expiratory phases have their main frequency components not higher than 1.5 kHz, with a sharp drop in power around 800 Hz, which is in agreement with other studies [35]. In addition, both respiratory phases have similar frequency content for similar airflow peaks and a silent period separating both phases could also be observed from both the tracheal sound waveform as well as its TFR. These results are in agreement with the findings reported in the literature when using CORSA systems [1], [2], [8].

In the next subsections we present the results obtained for both smartphones for the tracheal sound's amplitude with airflow, the breath-phase onset detection, and the respiratory rate estimation.

3.3.1 Tracheal Sound Amplitude and Airflow Relationship

A representative example of the curve fitting of the tracheal sound *versus* airflow acquired with an iPhone 4s and spirometer, respectively, for the inspiration and expiration phases is shown in Figure 3.5. We observe that during the inspiratory and expiratory phases, the increasing tracheal sounds' amplitudes as flow increases follow a power law relationship. The results of the power law model fitting parameters for the smartphone-acquired tracheal sounds' amplitude and airflow are presented in Table 3.1 for each respiratory phase and the two models of smartphones. The mean values of the exponent α were

between $\alpha = 1$ and $\alpha = 3$ for both smartphones. It is worth mentioning that different values of the exponent have been found in different studies, ranging from $\alpha = 1$ [5], $\alpha = 2$ [7], $\alpha = 3$ [6], and values in between this range [3], [4]. No statistically significant differences were found between the power law parameters obtained from the Galaxy S4 and the iPhone 4s smartphones with a two-tailed paired t-test with $p < 0.05$ considered as statistically significant (SPSS Statistics 17, IBM Corporation, Armonk, NY, USA).

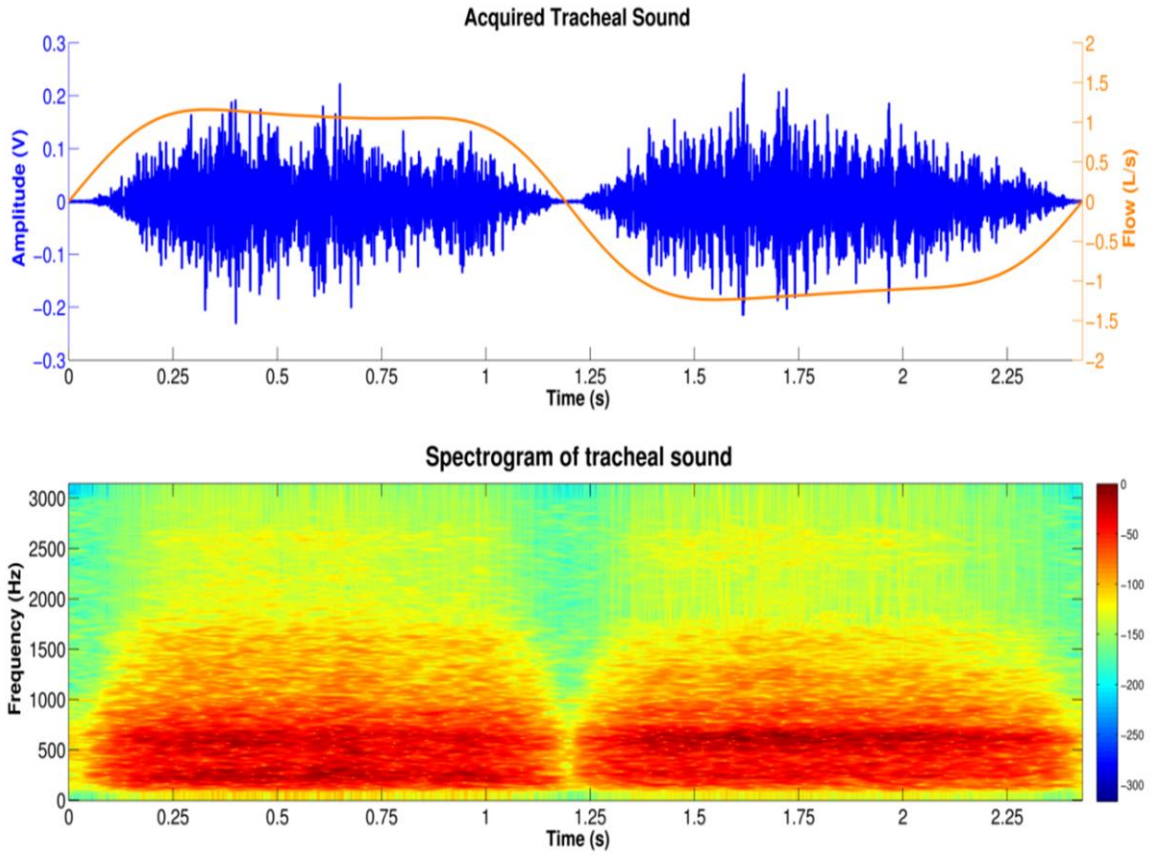

Figure 3.4 - Time-frequency characteristics of the tracheal sounds acquired using the smartphone during a respiratory cycle.
Top: Tracheal sound waveform together with its corresponding airflow signal (positive and negative lobes indicate the inspiration and expiration, respectively). *Bottom:* Time-frequency representation of the acquired tracheal sound computed via the spectrogram using a 100 ms Hamming window. Red/blue color in the color map indicates high/low intensity in decibels.

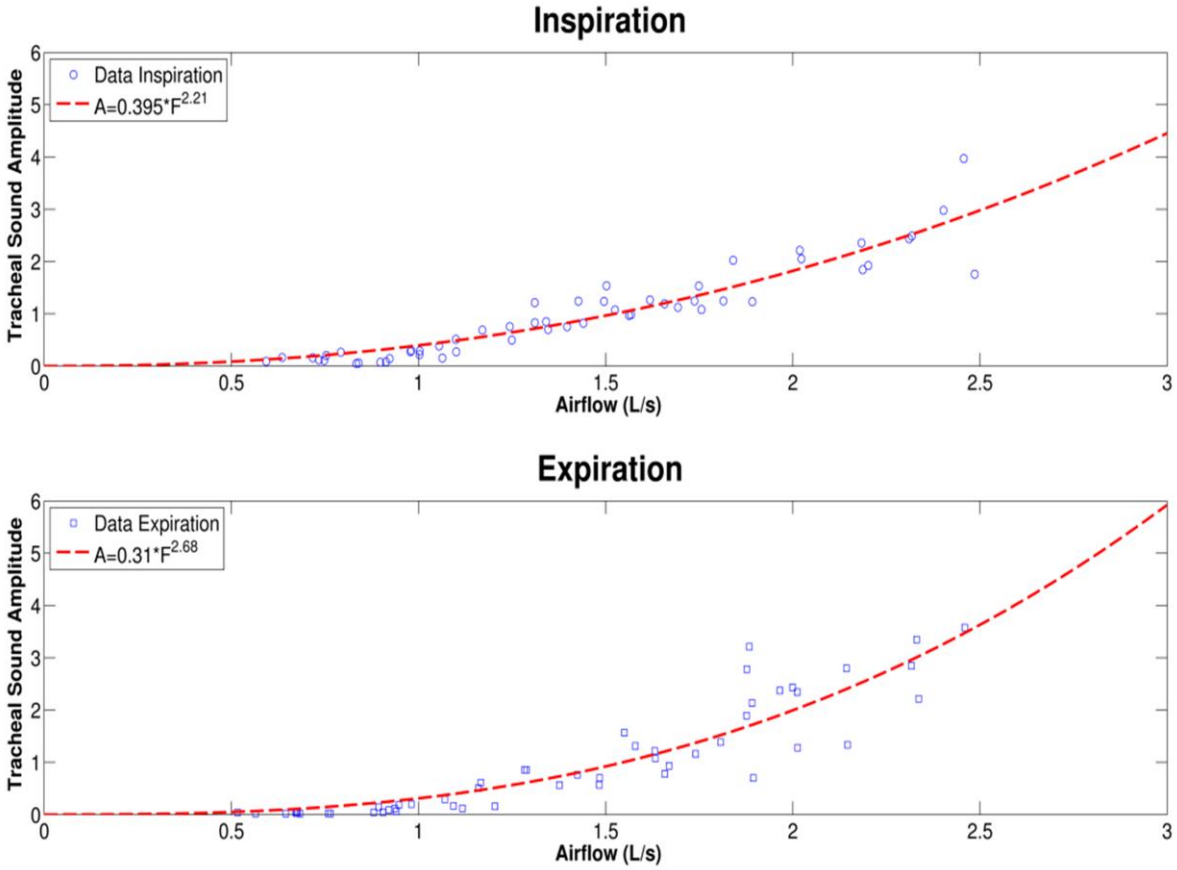

Figure 3.5 – Amplitude of smartphone-acquired tracheal sounds versus airflow.
Example of smartphone-acquired tracheal sounds amplitude as a function of airflow during the inspiratory and expiratory phases for one subject. Red dashed lines correspond to the best fit curves of the form $A = kF^{\alpha}$.

Table 3.1 - Results of the smartphone-acquired tracheal sounds amplitude and airflow relationship using a model of the form $A = kF^{\alpha}$ (N = 9 subjects).

Respiratory Phase	Parameter	Galaxy S4	iPhone 4s
Inspiration	k	0.450 ± 0.218	0.371 ± 0.197
	α	2.380 ± 1.077	2.686 ± 0.959
Expiration	k	0.523 ± 0.181	0.349 ± 0.162
	α	1.939 ± 0.900	2.632 ± 0.711

Values presented as mean ± standard deviation

3.3.2 Breath-Phase Onset Detection Using Tracheal Sounds

Table 3.2 summarizes the results obtained for the breath-onset detection using each smartphone for all volunteers. The absolute time difference between the reference breath-phase onsets from the volume via the spirometer and the estimated breath-phase onsets from the SE of the acquired tracheal sound, $|\Delta_{onset}|$, was computed. In addition, the total number of true breath-phase onsets computed from the volume is presented together with the corresponding extra and missed breath-phase onsets computed from the tracheal sounds. Note that the total number of true onsets is not the same for both smartphones given that different maneuver trials were performed for each subject. An example of the breathing onset using the iPhone 4s smartphone is shown in Figure 3.6. As shown, the Δ_{onset} is not consistently positive or negative. The distribution of time onsets was computed via the histogram and is shown in Figure 3.7 for each smartphone. We found that on average the breath-phase onsets $|\Delta_{onset}|$ detected with the smartphones have a time difference of approximately 50 ms from the onsets detected from the volume. Since some onsets were detected before or after the reference onsets, overall these Δ_{onset} values compensate and the mean onsets differ 9 ms and 14 ms for Samsung S4 and iPhone 4s, respectively. A two-tailed two-sample t-test was performed for Δ_{onset} and $|\Delta_{onset}|$ obtained from both smartphones for the total number of onsets. No statistically significant differences ($p > 0.05$) were found between Δ_{onset} and $|\Delta_{onset}|$ computed from the Galaxy S4 and iPhone 4s.

Table 3.2 - Results of the breath-phase onset detection using smartphone-acquired tracheal sounds in comparison to those detected from volume signal (N = 9 subjects).

Parameter		Galaxy S4	iPhone 4s
$\|\Delta_{onset}\|$	*[s]*	0.052 ± 0.051	0.051 ± 0.048
Total onsets		767	854
Extra onsets		12	5
Missed onsets		5	6

Values presented as mean ± standard deviation

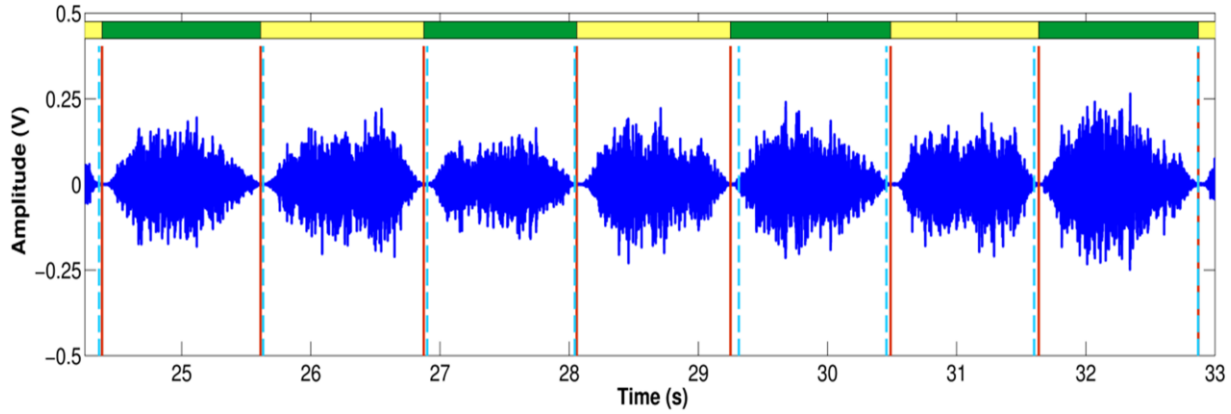

Figure 3.6 - Breath-phase onset detection using smartphone-acquired tracheal sound.
Example of breath-phase onset detection using the tracheal sounds acquired with a smartphone. Solid red lines indicate the breath-phase onsets detected using the volume signal from the spirometer. Dashed blue lines indicate the breath-phase onsets detected using only the information from the acquired tracheal sound.

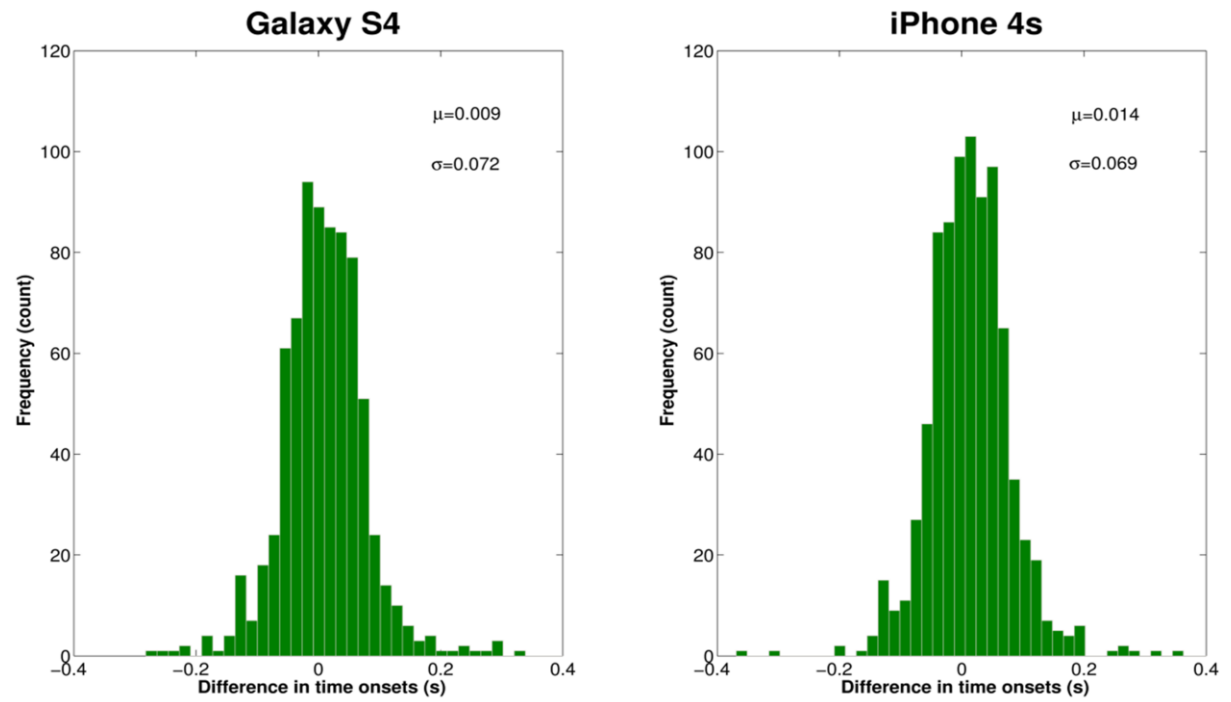

Figure 3.7 - Differences of breath-phase onsets detected from spirometer and from smartphones.
Distribution of the time differences of breath-phase onsets (Δ_{onset}) detected using the volume signal from the spirometer and breath-phase onsets detected using tracheal sounds acquired with the smartphones.

3.3.3 Instantaneous Respiratory Rate (IRR) Estimation Using Tracheal Sounds

The IRR estimation process using the spectrogram is illustrated in Figure 3.8 for a tracheal sound acquired using the iPhone 4s. It can be seen that the main frequency of the SE of the tracheal sound (Figure 3.8b), is located at twice the main frequency of the volume (Figure 3.8a), which is considered as reference, as the SE resembles a rectified airflow signal. At each time instant, the frequency at which the maximum energy of the TFR occurs was extracted from the corresponding spectrogram (white dashed lines superimposed on TFRs). Comparison of the estimated instantaneous frequencies of the SE of tracheal sound and volume of the spirometer is shown in Figure 3.8c. In most cases, we found that the discrepancies were more notable at the beginning and the end of the signal where the airflow levels were lower which in turn provided tracheal sound signals with small amplitudes. These are reflected as dispersion points in Figure 3.9. Table 3.3 summarizes the IRR results for all the subjects in terms of the performance indices for each smartphone. For both smartphones we found high cross correlation coefficients between the IRR estimated from tracheal sounds and volume. This is also reflected in the regression lines in Figures 3.9a and c for the Galaxy S4 (r^2 = 0.9693) and iPhone 4s (r^2 = 0.9672), respectively. High linear correlation has been also found between a tracheal acoustical method and pneumotachometer (r^2 = 0.98) [36]. A two-tailed paired t-test was performed for each performance index obtained from both smartphones for all subjects. For all performance indices, no statistically significant differences ($p > 0.05$) were found between the results from Galaxy S4 and iPhone 4s for the estimation of IRR considering the volume from spirometer as reference. The regression lines and the Bland-Altman plots between the estimated instantaneous respiration rate from tracheal sounds and the reference instantaneous respiration rate from volume signals are presented in Figure 3.9 for the Galaxy S4 and iPhone 4s smartphones. Compared to the spirometer, the bias ± 1.96SD and 95% limits of agreement were 0.11 ± 1.52 bpm and −1.41 to 1.63 bpm for the Galaxy S4, and 0.097 ± 1.47 bpm and −1.38 to 1.57 bpm for the iPhone 4s. Similar correlations and limits of agreement have been reported for a commercial device in post-anesthesia patients in comparison to capnography [37].

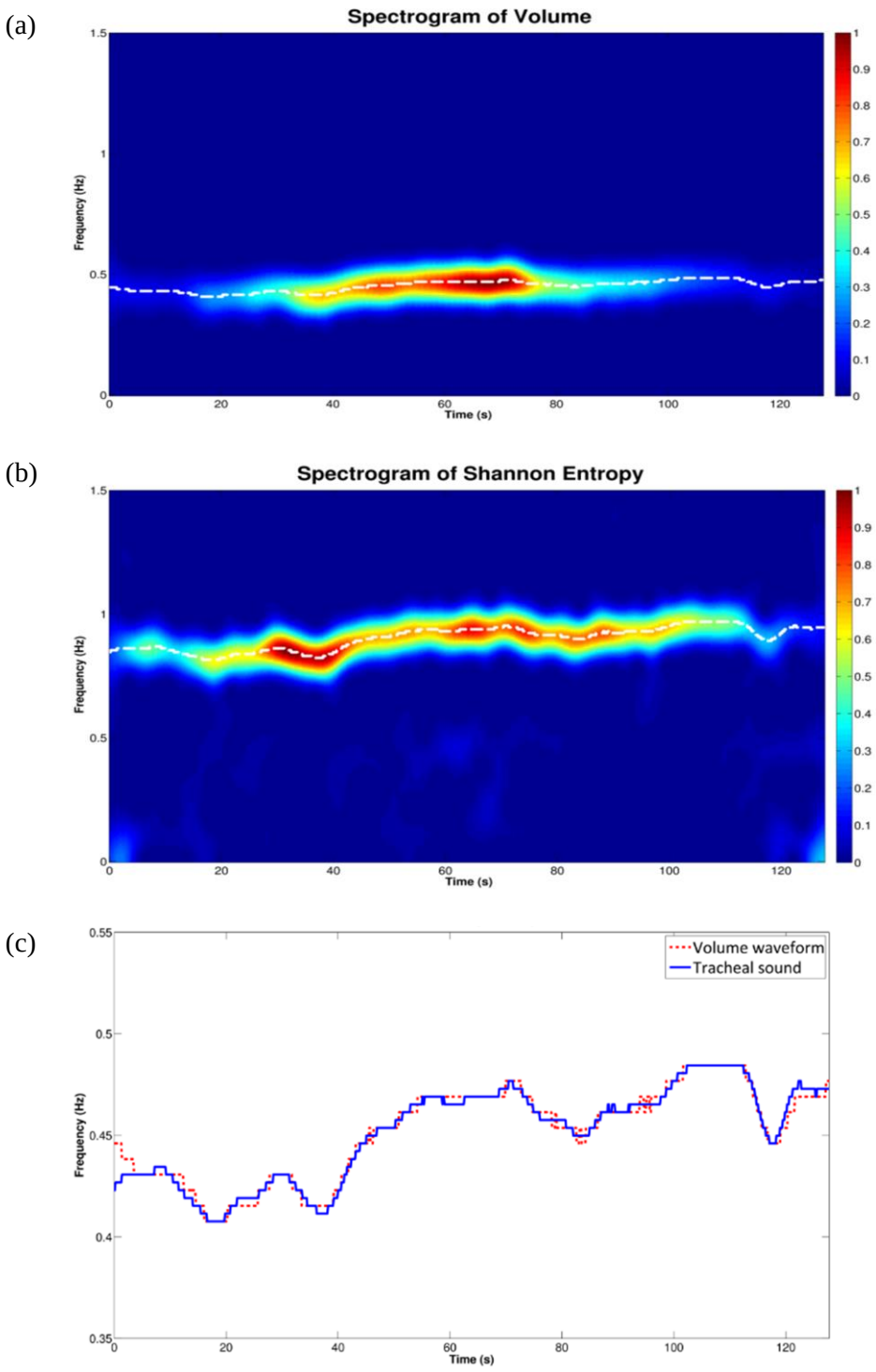

Figure 3.8 - Estimation of instantaneous respiratory rate using tracheal sounds acquired with a smartphone.

(a) Spectrogram of the volume signal from spirometer. (b) Spectrogram of the Shannon entropy of tracheal sound acquired with a smartphone. Observe that the main frequency content of the entropy signal is located at twice the frequency of that from the volume signal. White dashed lines indicate the maximum peak at each time instant. (c) Instantaneous respiratory rate computed from corresponding spectrograms of volume and Shannon entropy of tracheal sound.

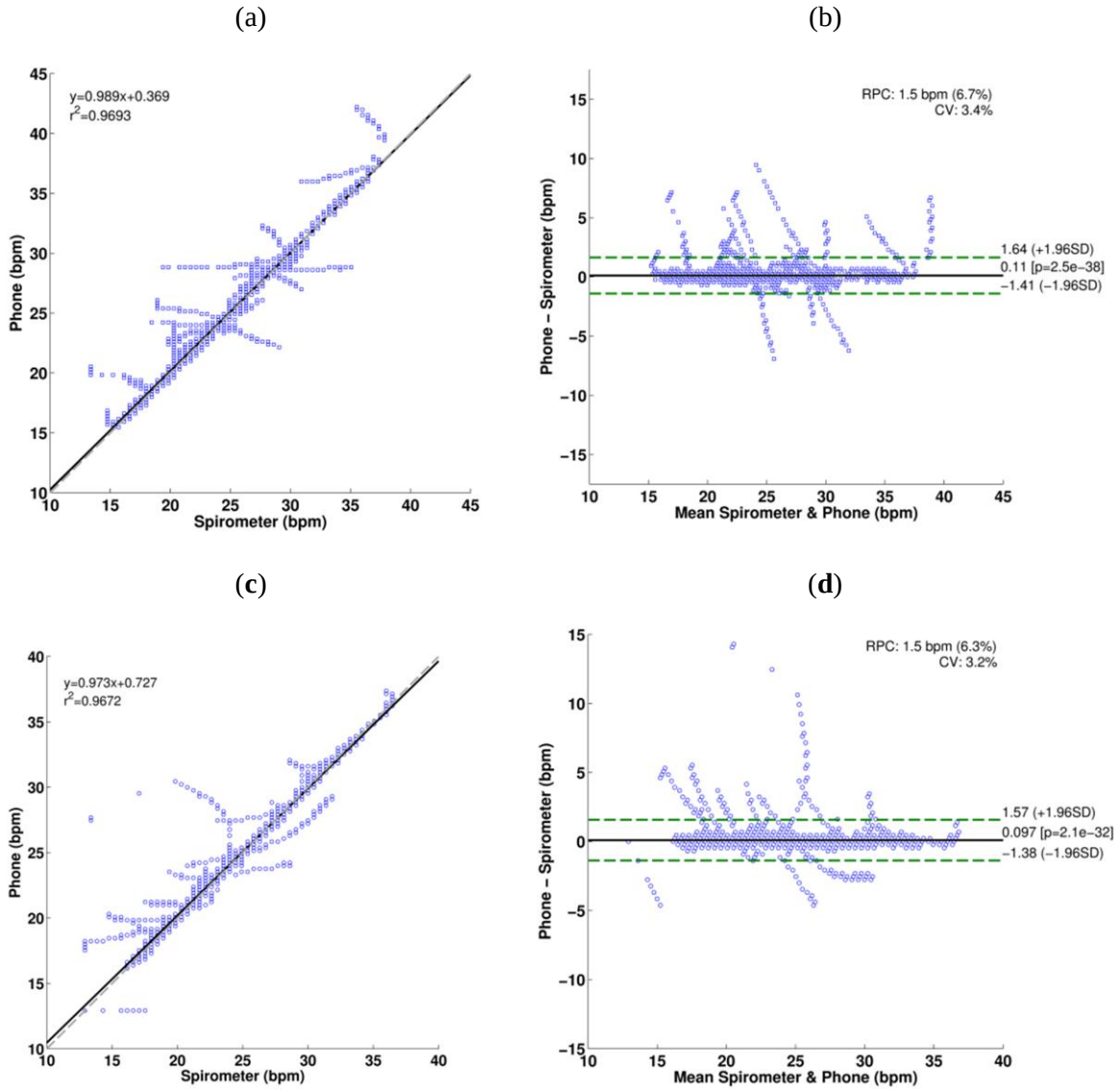

Figure 3.9 - Comparison of instantaneous respiratory rate estimated from tracheal sounds acquired with smartphones and estimated from volume signals (*N*=9 subjects).
(a) Regression line for estimation from Galaxy S4. (b) Bland-Altman plot for estimation from Galaxy S4. (c) Regression line for estimation from iPhone 4s. (d) Bland-Altman plot for estimation from iPhone 4s. In regression plots, the grey dashed line indicates the identity line and the solid black the regression line. In Bland-Altman plots, the solid black line indicates the bias while the dashed green lines indicate the 95% limits of agreement.

Table 3.3 - Results of the instantaneous respiratory rate estimation using tracheal sounds acquired with the smartphones in comparison to those from volume signals (N = 9 subjects).

Parameter		Galaxy S4	iPhone 4s
ρ	*[unitless]*	0.9994 ± 0.0004	0.9995 ± 0.0004
RMSE	*[bpm]*	0.731 ± 0.2878	0.700 ± 0.367
NRMSE	*[%]*	3.218 ± 1.297	2.957 ± 1.322

Values presented as mean ± standard deviation

3.4 Conclusions

In this dissertation, we propose the use of smartphones to develop a CORSA system that satisfies the current standards in the field. In particular, we employed two market-leading smartphones, the Galaxy S4 and iPhone 4s, and specifically-designed respiratory acoustical sensors for the acquisition of tracheal sounds. We obtained tracheal sounds from healthy volunteers in airflow controlled conditions from 0.5 to 2.5 L/s in a quiet room, but not an anechoic chamber.

The relationship between amplitude of tracheal sounds and airflow has been shown to be useful for respiratory health monitoring [25], [26], [38]. Tracheal sounds have been used for estimation of the airflow and volume in a non-invasive way [25], [26], [38]. The tracheal sounds have been used to estimate ventilation parameters by first estimating the airflow and then integrating this signal to estimate the volume [38]. Several features have been used to estimate the airflow from the tracheal acoustical information, and the Shannon entropy of the tracheal sounds was found to provide better performance compared to other models based on the signal envelope and average power [25], [26]. In this work, we found that smartphone-acquired tracheal sounds' amplitude is proportional to the airflow from a spirometer in a power law relationship which is in agreement to prior studies [3]–[7]. The power law models found for the inspiratory phase were $A = (0.450 \pm 0.218)F^{(2.380 \pm 1.077)}$ for the Galaxy S4, and $A = (0.371 \pm 0.197)F^{(2.686 \pm 0.959)}$ for the iPhone 4s, while for the expiratory phase they were $A = (0.523 \pm 0.181)F^{(1.939 \pm 0.900)}$ for the Galaxy S4, and $A = (0.349 \pm 0.162)F^{(2.632 \pm 0.711)}$ for the iPhone 4s.

Apnea monitoring and automatic breath-phase detection have been other applications of tracheal sounds analysis [39], [40]. In particular, information from the logarithm of the variance of the tracheal sounds was used as a way to detect the breath-phase onset which becomes a crucial part in an automatic acoustical system. Towards this goal, we tested the ability of the smartphone-acquired tracheal sounds to detect the breath-phase onsets, as this processing stage is important when the acoustical approach is used for airflow measurement and automatic breath-phase classification. Our results indicate that on average the onsets estimated from the smartphone-acquired tracheal sounds differ by only 52 ± 51 ms for Galaxy S4, and 51 ± 48 ms for iPhone 4s, from the corresponding onsets detected from the spirometer reference signal.

Estimation of the respiratory rate using an acoustical approach has recently gained popularity in clinical settings. As a vital sign, respiration rate can be used to predict serious clinical events [41]. In particular, continuous monitoring of breathing status becomes relevant to identify and predict risk situations both inside and outside clinical settings. Current clinical continuous monitoring methods include qualified human observation, impedance pneumography, and capnography monitoring. However, these methods have disadvantages, *e.g.* low tolerance of the patient for using the nasal cannula, or leaks around this cannula in capnography. As an alternative, respiratory rate estimation based on tracheal sound has been proposed [36]. Recently, a commercial device that monitors the respiratory rate via tracheal sounds was introduced for clinical settings (Masimo Rainbow SET® Acoustic Monitoring, Masimo Corp., Irvine, CA, USA). The accuracy of this device has been tested against capnography and good correlation has been found between both methods [37], [42]. However, there is still a need for a small and discrete device for everyday use, able to estimate the respiration rate in a continuous and non-invasive way outside the clinical setting [43]. Towards addressing this need, we found good correlation between the smartphone-based respiratory rate estimates and the spirometer-based ones ($r^2 \approx 0.97$), as well as 95% limits of agreement ranging approximately from −1.4 to 1.6 bpm for subjects breathing in a range from 15

to 35 bpm. Overall we did not find statistically significant differences between the results from the Galaxy S4 and iPhone 4s devices.

By employing smartphone devices we were able to reproduce major findings in the tracheal sounds field obtained with conventional CORSA systems. We foresee that efforts similar to the one performed in this dissertation would result in a reliable, low-cost, and easy-to-upgrade portable system that could aid not only general practitioners but also serve as on-demand health monitors outside clinical settings. In addition, systems with such characteristics would aid in the acquisition of large-sample studies in locations not easily accessible nowadays with the currently-used CORSA systems.

Our future work includes implementation of the presented signal processing techniques into applications on the smartphone operating systems, *i.e.*, Android and iOS, which will govern the acquisition, processing and display of the tracheal sounds information.

3.5 Acknowledgments

This work is supported in part by the US Army Medical Research and Material Command (US-AMRMC) under grant No. W81XWH-12-1-0541.

The authors would like to thank Professors Sonia Charleston-Villalobos, Tomas Aljama-Corrales, and Ramon Gonzalez-Camarena for introducing a microphone sensor used in this research work.

Bersain Reyes was supported by a Consejo Nacional de Ciencia y Tecnologia (CONACyT) Scholarship from the Mexican Government.

3.6 References

[1] V. A. McKusick, J. T. Jenkins, And G. N. Webb, “The acoustic basis of the chest examination; studies by means of sound spectrography,” *Am. Rev. Tuberc.*, vol. 72, no. 1, pp. 12–34, Jul. 1955.

[2] H. Pasterkamp, S. S. Kraman, and G. R. Wodicka, “Respiratory Sounds: Advances Beyond the Stethoscope,” *Am. J. Respir. Crit. Care Med.*, vol. 156, no. 3, pp. 974–987, Sep. 1997.

[3] R. Beck, G. Rosenhouse, M. Mahagnah, R. M. Chow, D. W. Cugell, and N. Gavriely, "Measurements and Theory of Normal Tracheal Breath Sounds," *Ann. Biomed. Eng.*, vol. 33, no. 10, pp. 1344–1351, Oct. 2005.
[4] N. Gavriely and D. W. Cugell, "Airflow effects on amplitude and spectral content of normal breath sounds," *J. Appl. Physiol.*, vol. 80, no. 1, pp. 5–13, Jan. 1996.
[5] P. Leblanc, P. T. Macklem, and W. R. Ross, "Breath sounds and distribution of pulmonary ventilation," *Am. Rev. Respir. Dis.*, vol. 102, no. 1, pp. 10–16, Jul. 1970.
[6] D. Olson and J. Hammersley, "Mechanisms of Lung Sound Generation," *Semin. Respir. Crit. Care Med.*, vol. 6, no. 03, pp. 171–179, 1985.
[7] B. E. Shykoff, Y. Ploysongsang, and H. K. Chang, "Airflow and Normal Lung Sounds," *Am. Rev. Respir. Dis.*, vol. 137, no. 4, pp. 872–876, Apr. 1988.
[8] H. Pasterkamp, C. Carson, D. Daien, and Y. Oh, "DIgital respirosonography. new images of lung sounds.," *Chest*, vol. 96, no. 6, pp. 1405–1412, Dec. 1989.
[9] P. Forgacs, "The functional basis of pulmonary sounds," *Chest*, vol. 73, no. 3, pp. 399–405, 1978.
[10] G. Charbonneau, E. Ademovic, B. M. G. Cheetham, L. P. Malmberg, J. Vanderschoot, and A. R. A. Sovijarvi, "Basic techniques for respiratory sound analysis," *Eur. Respir. Rev.*, vol. 10, no. 77, pp. 625–635, 2000.
[11] F. Dalmay, M. T. Antonini, P. Marquet, and R. Menier, "Acoustic properties of the normal chest," *Eur. Respir. J.*, vol. 8, no. 10, pp. 1761–1769, Oct. 1995.
[12] J. E. Earis and B. M. G. Cheetham, "Current methods used for computerized respiratory sound analysis," *Eur. Respir. Rev.*, vol. 10, no. 77, pp. 586–590, 2000.
[13] D. M. J. Mussell, "The need for standards in recording and analysing respiratory sounds," *Med. Biol. Eng. Comput.*, vol. 30, no. 2, pp. 129–139, Mar. 1992.
[14] B. M. G. Cheetham, G. Charbonneau, A. Giordano, P. Helisto, and J. Vanderschoot, "Digitization of data for respiratory sound recordings," *Eur. Respir. Rev.*, vol. 10, no. 77, pp. 621–624, 2000.
[15] L. Vannuccini, J. E. Earis, P. Helisto, B. M. G. Cheetham, M. Rossi, A. R. A. Sovijarvi, and J. Vanderschoot, "Capturing and preprocessing of respiratory sounds," *Eur. Respir. Rev.*, vol. 10, no. 77, pp. 616–620, 2000.
[16] J. E. Earis and B. M. G. Cheetham, "Future perspectives for respiratory sound research," *Eur. Respir. Rev.*, vol. 10, no. 77, pp. 641–646, 2000.
[17] L. Guangbin, C. Shaoqin, Z. Jingming, C. Jinzhi, and W. Shengju, "The development of a portable breath sounds analysis system," presented at the 1992 14th Annual International Conference of the IEEE Engineering in Medicine and Biology Society, 1992, vol. 6, pp. 2582–2583.
[18] K. Hung, B. L. Luk, W. H. Choy, B. Tai, and S. K. Tso, "Multifunction stethoscope for telemedicine," presented at the 2003 IEEE International Workshop on Computer Architectures for Machine Perception, 2004, pp. 87–89.
[19] D. Oletic, B. Arsenali, and V. Bilas, "Towards Continuous Wheeze Detection Body Sensor Node as a Core of Asthma Monitoring System," in *Wireless Mobile Communication and Healthcare*, K. S. Nikita, J. C. Lin, D. I. Fotiadis, and M.-T. A. Waldmeyer, Eds. Springer Berlin Heidelberg, 2012, pp. 165–172.
[20] D. Oletic, M. Skrapec, and V. Bilas, "Monitoring Respiratory Sounds: Compressed Sensing Reconstruction via OMP on Android Smartphone," in *Wireless Mobile Communication and Healthcare*, B. Godara and K. S. Nikita, Eds. Springer Berlin Heidelberg, 2013, pp. 114–121.
[21] S. Charleston-Villalobos, G. Martinez-Hernandez, R. Gonzalez-Camarena, G. Chi-Lem, J. G. Carrillo, and T. Aljama-Corrales, "Assessment of multichannel lung sounds parameterization for two-class classification in interstitial lung disease patients," *Comput. Biol. Med.*, vol. 41, no. 7, pp. 473–482, Jul. 2011.
[22] S. Charleston-Villalobos, L. Albuerne-Sanchez, R. Gonzalez-Camarena, M. Mejia-Avila, G. Carrillo-Rodriguez, and T. Aljama-Corrales, "Linear and Nonlinear Analysis of Base Lung Sound in Extrinsic Allergic Alveolitis Patients in Comparison to Healthy Subjects:," *Methods Inf. Med.*, vol. 52, no. 3, pp. 266–276, Apr. 2013.

[23] C. K. Druzgalski, R. L. Donnerberg, And R. M. Campbell, “Techniques of recording respiratory sounds,” *J. Clin. Eng.*, vol. 5, no. 4, pp. 321–330, 1980.
[24] S. S. Kraman, G. R. Wodicka, G. A. Pressler, and H. Pasterkamp, “Comparison of lung sound transducers using a bioacoustic transducer testing system,” *J. Appl. Physiol.*, vol. 101, no. 2, pp. 469–476, Aug. 2006.
[25] A. Yadollahi and Z. M. K. Moussavi, “A robust method for estimating respiratory flow using tracheal sounds entropy,” *IEEE Trans. Biomed. Eng.*, vol. 53, no. 4, pp. 662–668, Apr. 2006.
[26] A. Yadollahi and Z. M. K. Moussavi, “Acoustical Respiratory Flow,” *IEEE Eng. Med. Biol. Mag.*, vol. 26, no. 1, pp. 56–61, 2007.
[27] A. Papoulis and S. U. Pillai, *Probability, Random Variables, and Stochastic Processes*. Tata McGraw-Hill, 2002.
[28] M. Costa, A. L. Goldberger, and C.-K. Peng, “Multiscale Entropy Analysis of Complex Physiologic Time Series,” *Phys. Rev. Lett.*, vol. 89, no. 6, p. 068102, Jul. 2002.
[29] M. Costa, A. L. Goldberger, and C.-K. Peng, “Multiscale entropy analysis of biological signals,” *Phys. Rev. E*, vol. 71, no. 2, p. 021906, Feb. 2005.
[30] E. Parzen, “On Estimation of a Probability Density Function and Mode,” *Ann. Math. Stat.*, vol. 33, no. 3, pp. 1065–1076, Sep. 1962.
[31] R. O. Duda, P. E. Hart, and D. G. Stork, *Pattern Classification*, 2 edition. New York: Wiley-Interscience, 2000.
[32] A. Yadollahi and Z. M. K. Moussavi, “A robust method for heart sounds localization using lung sounds entropy,” *IEEE Trans. Biomed. Eng.*, vol. 53, no. 3, pp. 497–502, Mar. 2006.
[33] L. Cohen, *Time-frequency analysis*, vol. 778. Prentice Hall PTR New Jersey, 1995.
[34] B. Boashash, *Time Frequency Analysis*. Gulf Professional Publishing, 2003.
[35] N. Gavriely, Y. Palti, and G. Alroy, “Spectral characteristics of normal breath sounds,” *J. Appl. Physiol.*, vol. 50, no. 2, pp. 307–314, Feb. 1981.
[36] G. Sierra, V. Telfort, B. Popov, M. Pelletier, P. Despault, R. Agarwal, and V. Lanzo, “Comparison of respiratory rate estimation based on tracheal sounds versus a capnograph,” *Conf. Proc. Annu. Int. Conf. IEEE Eng. Med. Biol. Soc. IEEE Eng. Med. Biol. Soc. Conf.*, vol. 6, pp. 6145–6148, 2005.
[37] O. Mimoz, T. Benard, A. Gaucher, D. Frasca, and B. Debaene, “Accuracy of respiratory rate monitoring using a non-invasive acoustic method after general anaesthesia,” *Br. J. Anaesth.*, p. aer510, Feb. 2012.
[38] C.-L. Que, C. Kolmaga, L.-G. Durand, S. M. Kelly, and P. T. Macklem, “Phonospirometry for noninvasive measurement of ventilation: methodology and preliminary results,” *J. Appl. Physiol.*, vol. 93, no. 4, pp. 1515–1526, Oct. 2002.
[39] A. Yadollahi, E. Giannouli, and Z. Moussavi, “Sleep apnea monitoring and diagnosis based on pulse oximetery and tracheal sound signals,” *Med. Biol. Eng. Comput.*, vol. 48, no. 11, pp. 1087–1097, Nov. 2010.
[40] S. Huq and Z. Moussavi, “Acoustic breath-phase detection using tracheal breath sounds,” *Med. Biol. Eng. Comput.*, vol. 50, no. 3, pp. 297–308, Mar. 2012.
[41] F. q. AL-Khalidi, R. Saatchi, D. Burke, H. Elphick, and S. Tan, “Respiration rate monitoring methods: A review,” *Pediatr. Pulmonol.*, vol. 46, no. 6, pp. 523–529, Jun. 2011.
[42] M. A. E. Ramsay, M. Usman, E. Lagow, M. Mendoza, E. Untalan, and E. De Vol, “The accuracy, precision and reliability of measuring ventilatory rate and detecting ventilatory pause by rainbow acoustic monitoring and capnometry,” *Anesth. Analg.*, vol. 117, no. 1, pp. 69–75, Jul. 2013.
[43] P. Corbishley and E. Rodriguez-Villegas, “Breathing Detection: Towards a Miniaturized, Wearable, Battery-Operated Monitoring System,” *IEEE Trans. Biomed. Eng.*, vol. 55, no. 1, pp. 196–204, Jan. 2008.

Chapter 4: Tidal Volume Estimation Using Smartphone-acquired Tracheal Sounds

(N. Reljin, B. A. Reyes, and K. H. Chon, "Tidal Volume Estimation Using the Blanket Fractal Dimension of the Tracheal Sounds Acquired by Smartphone," *Sensors*, vol. 15, no. 8, pp. 9773-9790, 2015; reused with permission from MDPI - Open Access Publishing)

4.1 Introduction

Tracheal sounds, as part of the respiratory sounds, play an important role in monitoring respiratory activity, as well as in detection of pulmonary diseases [1]–[3]. Respiratory activity is one of the vital signs, and as such requires an adequate attention. Tidal volume is one of the parameters for monitoring respiratory activity [4]. It plays an important role for both healthy people and people with respiratory diseases, hence measuring and checking volume's values can be helpful, especially in assessing risky situations involving respiratory failure [4]–[6]. Tidal volume is defined as the volume of air exchanged in one breath, and is commonly measured at the mouth [1], [2], [7]. The average value is about 500 mL per breath at rest [2], [7]. Various methods exist for measuring the tidal volume, such as spirometry, whole-body plethysmography, inductance plethysmography, and electrocardiography [2], [8]–[10]. However, these methods require the use of specialized equipment, and cannot be easily applied in nonclinical settings. Therefore, there is a need for a miniature monitoring device that can be used in everyday situations and not only in clinical and/or research settings [11]. In addition, with an extensive growth of electronic devices and their computational capabilities, the development of portable tidal volume estimation systems is now possible [12].

Several efforts have been made in the research oriented towards the estimation of tidal volume. In [13], the authors estimated volume by optically tracking reflective markers in three dimensions. Petrovic *et al*. proposed a technique for measuring tidal volumes by using a single fiber-grating sensor [14], while

in [15] the authors estimated the tidal volume using Doppler radar signals. Chen *et al*. estimated tidal volume from the energy of the tracheal sounds [6]. To the best of our knowledge, there are no studies exploring the possibility to estimate tidal volume directly from smartphone-acquired tracheal sounds.

Smartphones are widely used nowadays. They have fast microprocessors, large storage capacities and a lot of media capabilities. In addition, the mobility of the smartphones is making them more popular for usage outside the clinics or research facilities, when they can be used for measuring vital signs and health monitoring, as shown in some of the previous works of our research group [16]–[18].

In this dissertation, we propose the use of blanket fractal dimension (BFD) for estimating the tidal volume from tracheal sounds acquired by a commercially available Android smartphone. Tracheal sounds, as part of respiratory sounds, are non-stationary and stochastic signals [2], [19]. The nonlinear analysis of respiratory sounds is still an open research field [20]. The genesis of the respiratory sounds is closely related to the interaction between the airflow and the bronchial tree, which can be assumed as a fractal geometry [19] and has been modeled accordingly as fractal [21], where this interaction could plausibly generate a nonlinear process that explain better the chaotic dynamic behavior [20]. Due to this fact, some past studies investigated the fractality of respiratory sounds and also have reported successful applications of fractal analysis of them [22]–[26]. None of these efforts was concerned with the tidal volume estimation using fractal analysis. In this dissertation, we explore the possibility to estimate tidal volume using BFD, which, to the best of our knowledge, was not used for respiratory sound analysis. The estimated volumes were compared to peak-to-peak volumes obtained from a Respitrace signal, which was considered as a reference. In addition, we estimated volumes by obtaining Shannon entropy (SE) from the same tracheal sounds, and compared them to reference volumes. For testing the proposed method and comparing it with SE method, we collected signals from healthy and non-smoker volunteers for six days, for a total of 30 recordings. As a figure of merit, the normalized root-mean-squared errors (NRMSEs) were calculated in both cases. Repeated experiments were performed to investigate if the models for

fitting data obtained during the first day of collecting signals could be successfully used on the data from the remaining days.

4.2 Material and Methods

4.2.1 Subjects

Five healthy non-smoker volunteers (four males and one female), with the mean age and standard deviation of 27 ± 7.5 years, weight of 63.5 ± 5 kg, and height 173.2 ± 8.4 cm, were asked to participate in this study. Individuals with previous pneumothorax, chronic respiratory illnesses, and common cold were excluded from the study. This group of participants consisted of students and staff members from the University of Connecticut (UConn, Storrs, CT, USA). All participants signed a consent form approved by the Institutional Review Board of UConn.

4.2.2 Equipment and Acquisition of the Signals

In this dissertation, two signals were acquired simultaneously: tracheal sounds and Respitrace signal. The tracheal sounds were collected using an acoustical sensor, which contained a subminiature electret microphone BT-21759-000 (Knowles Electronics, Itasca, IL, USA) placed in a plastic bell, which consisted of a conical coupler chamber [20], in accordance to previous findings [27]. The importance of this shape is that it provides an efficient transducer of air pressure fluctuations from the skin over the trachea to the microphone [28]. The acoustic sensor used in this dissertation was developed by our colleagues at the Metropolitan Autonomous University at Mexico City, Mexico, and have been successfully applied for respiratory sound acquisitions [18], [20], [29]. The acoustic sensor was connected to the audio jack of the Samsung Galaxy S4 smartphone (Samsung Electronics Co., Seoul, Korea). The tracheal sounds were recorded using the built-in audio recorder application (Voice Recorder), with 16-bit per sample and 44.1 kHz sampling rate, and saved in the .wav format. Afterwards, the recorded files were transferred to a personal computer and processed offline using Matlab (R2012a, The Mathworks, Inc., Natick, MA, USA).

The Respitrace (nowadays known as Inductotrace) signal was obtained simultaneously with the tracheal sounds, from two Respibands (Ambulatory Monitoring, Inc., Ardsley, NY, USA), placed over the rib cage and abdomen. Respibands' signals were digitized using 16-bit A/D converter (PowerLab/4SP, ADInstruments, Inc., Dunedin, New Zealand) at 10 kHz sampling rate, using the manufacturer's software (LabChart 7, ADInstruments, Inc.). Prior to every participant's recording, the Respibands were calibrated using a spirometer system (FE141 Spirometer, ADInstruments, Inc.) following the manufacturer's manual, and the corresponding signal was considered as the reference for volume estimation. Calibration errors between Respibands and spirometer were obtained for every recording, and were less than 10%, which is in accordance to the manufacturer's manual.

Experiments were performed in a regular dry lab which was held quiet. Respibands were placed over the participant's rib cage and abdomen, while the acoustical sensor was fixed at the suprasternal notch using a double-sided adhesive ring (BIOPAC Systems, Goleta, CA, USA). The experiment consisted of three stages, and all were performed in standing posture:

1. Participants were asked to breathe through an 800 mL Spirobag (Ambulatory Monitoring, Inc., Ardsley, NY, USA) for about six respiratory cycles;

2. Participants were asked to follow a maneuver that consisted of increasing tidal volumes and then decreasing with each breath, ranging from participant's comfortable lowest to highest volume, while breathing through a paper tube (tube's length: 20 cm, internal diameter: 1.5 cm, external diameter: 2 cm), for approximately 2 min;

3. Participants were asked to repeat the same maneuver as in the second stage while breathing without the tube.

In everyday situations people do not have access to spirometers or Respibands, and the lack of portable and easily accessible device with possibility to control and limit the tidal volume is needed. Thus, in this research, we use a Spirobag, since it is easy to find and carry, and has an almost fixed

volume (800 mL). The exact volume of the bag changes at each volunteers' breathe. Hence, we used the Respitrace system as reference in order to know this volume, since the use of spirometer with a bag was practically prohibited in the experimental setup.

Since breathing through a tube adds some resistance to the respiratory tract and changes the natural way of breathing, one of the objectives was to investigate if this apparatus influences the estimation results. This was the reason for recording the third stage of the experiment.

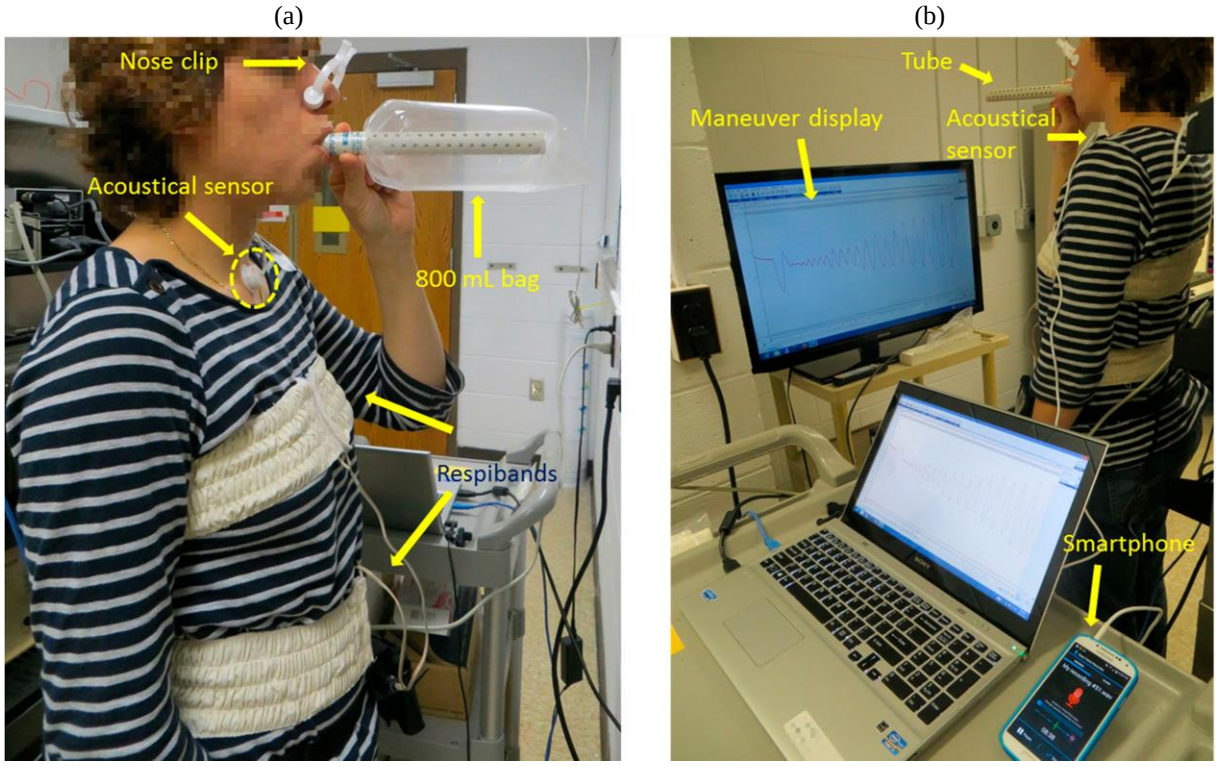

Figure 4.1 – Simultaneous recording of tracheal sound (using a smartphone) and volume signal (using Respibands).
(a) The participant is breathing through 800 mL bag; (b) The participant is breathing through a tube while performing the respiratory maneuver.

In all three stages, initial and final apnea phases of approximately 5 s were acquired for automatic alignment purposes between the two recordings, as well as for recording the ambient noise levels. In the last two stages, after the initial apnea, participants were instructed to take a forced respiration cycle before

performing the maneuver. In order to provide the visual feedback during the second and the third stage, the volume signal was displayed on a 40” monitor, placed in front of the participant. During the experiment, nose clips (MLA1008, ADInstruments, Inc.) were used to clamp the nostrils. An example of the set-up of the experiment is shown in Figure 4.1. Figure 4.1a depicts the first stage of the experiment, when the 800 mL bag was used, while Figure 4.1b shows the breathing maneuver through a tube (the second stage of the experiment).

4.2.3 Data Processing

Figure 4.2 shows the flowchart of the data processing steps. The acquired tracheal sounds were first downsampled from 44.1 kHz to 6.3 kHz, and then digitally filtered with a 4th order bandpass Butterworth filter with cutoff frequencies 100 and 3000 Hz to minimize the effects of heart sounds and muscle interferences [28], [30]. The volume signal was first downsampled from 10 kHz to 5 kHz, and then interpolated to 6.3 kHz in order to achieve the same sampling frequency as the tracheal sounds. Lastly, the volume signal was lowpass filtered at 2 Hz with a 4th order Butterworth filter.

The automatic extraction of the breathing phases (inspiration/expiration) was performed from the volume signal, by finding its corresponding local maxima and minima during the respiratory maneuver and computing the slope of the volume at each phase [18]. The tracheal sounds and the volume signal were recorded simultaneously, however, due to the different times of pressing the start buttons, the two signals were aligned manually. Figure 4.3 depicts an example of the filtered, detrended and aligned tracheal sounds and volume signal during the respiratory maneuver.

The volume signal, acquired with the Respibands, was assumed as the reference. For every breathing phase, the absolute volume difference between two consecutive extrema from the volume signal was calculated, and was considered as the true tidal volume value, V_T. Two features were used for estimating the tidal volume from the tracheal sounds acquired by smartphone: blanket fractal dimension (BFD) and the integral of the Shannon entropy (SE). Every breathing phase (inspiration/expiration) from

the tracheal sound was represented with one BFD and one SE value. In order to estimate the volume from these features, linear and exponential fitting curves were used. The estimated volumes are defined with the following:

$$V_{est\_l} = a \cdot F + b$$
$$V_{est\_e} = c \cdot e^{d \cdot F} \quad (1)$$

where V_{est_l} and V_{est_e} are the estimated volumes with linear and exponential models, respectively, a, b, c and d are coefficients, and F is the value of the BFD or SE feature computed from the tracheal sounds.

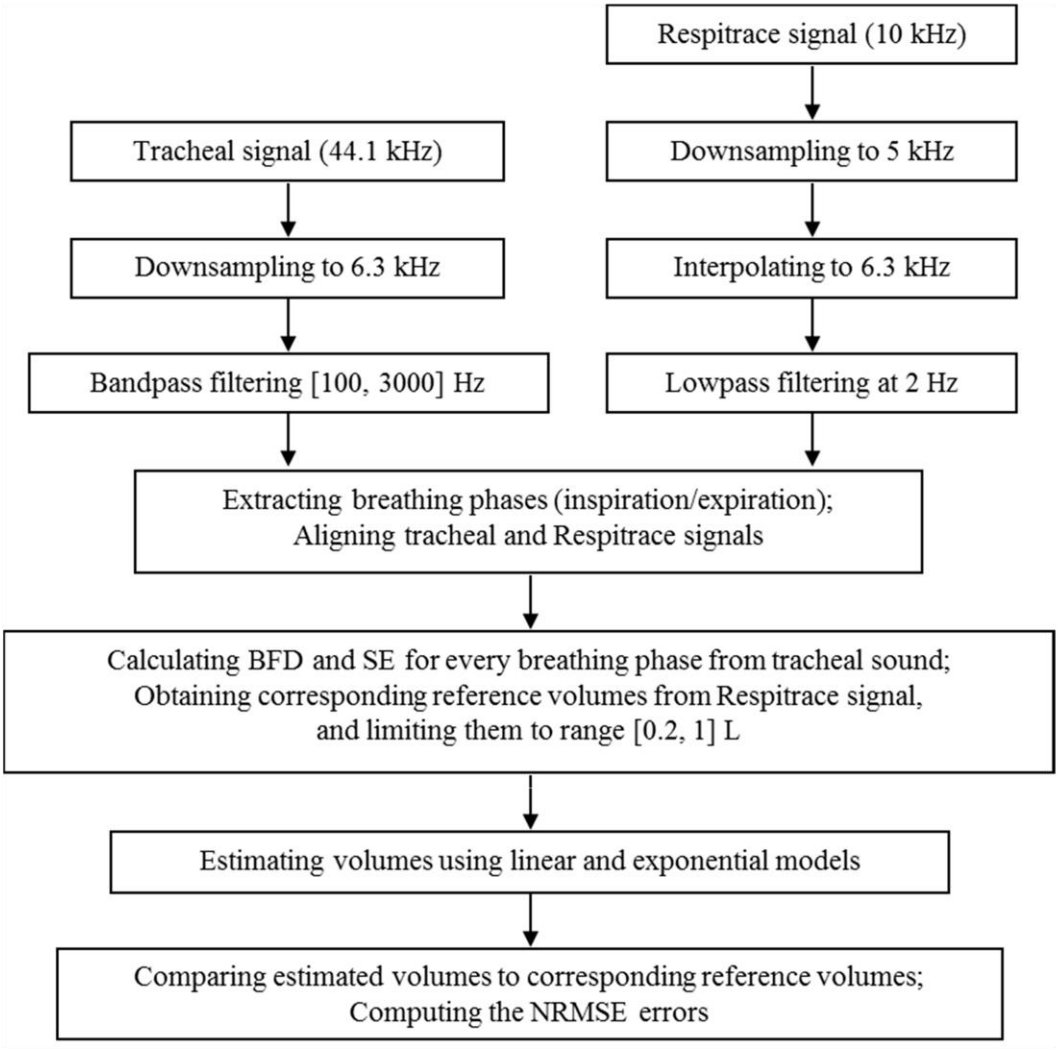

Figure 4.2 - The flowchart showing the steps for tracheal sounds' and Respitrace signal's processing.

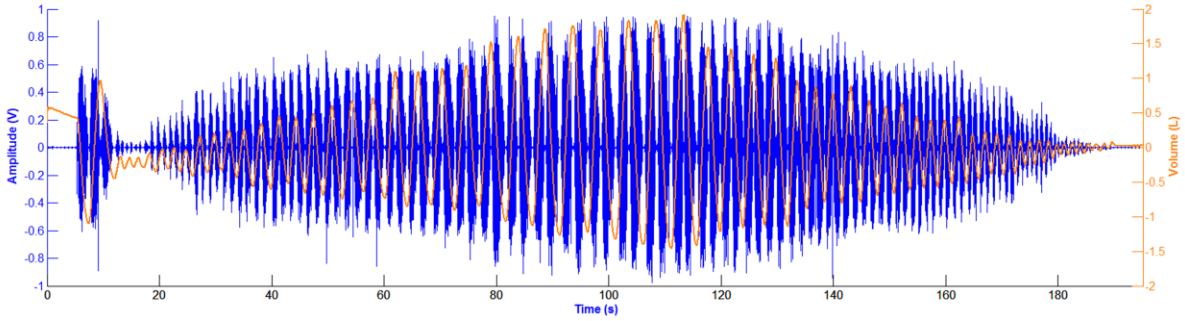

Figure 4.3 - Filtered, detrended and aligned tracheal sounds and volume signal during the respiratory maneuver.
Tracheal sound (in volts) is represented in blue, while volume signal (in liters) is in orange.

The last step in the data processing is the comparison of the estimated volumes to the corresponding reference volume values, and the evaluation of the performed estimation via computation of the normalized root-mean-squared error (NRMSE) defined as follows:

$$NRMSE = \frac{RMSE}{mean(V_T)} \cdot 100\%$$
$$RMSE = \sqrt{\frac{\sum_{i=1}^{N} (V_T(i) - V_{est}(i))^2}{P}} \quad (2)$$

where V_T is the volume obtained from Respitrace, V_{est} denotes the estimated volume, *i.e.*, V_{est_l} or V_{est_e}, and P is the number of breathing phases during the maneuver.

Shannon entropy is a measure of uncertainty or irregularity of a process [31]. It is one of the features frequently used for analysis of respiratory sounds, and has been successfully applied to airflow estimation in the field of tracheal sound analysis [32]. For a random signal with a probability density function (pdf), p, SE is defined as:

$$SE(p) = -\sum_{i=1}^{M} p_i \cdot \log p_i \quad (3)$$

where M is the number of outcomes of the random variable with pdf p. In this dissertation, pdf is estimated using the method of Parzen's windows with a Gaussian kernel [33], [34]. More details on this method can be found in [18], [32]. In this dissertation we were concerned with the tidal volume estimation rather than respiratory airflow, and based on the relationship between these two variables over time, the integral of the SE over each corresponding breathing phase was used as feature for tidal volume estimation.

4.2.4 Blanket Fractal Dimension

Fractals are defined as "a set having the fractal dimension strictly greater than its integer dimension", and are used to describe non-regular and non-stationary structures [35]–[37]. There are two types of fractals: natural and deterministic. Natural fractals are structures that could be found in the nature, such as lungs, while deterministic fractals are constructed artificially, by applying predetermined replicating rules (*e.g.*, the Von Koch curve, the Cantor set) [37], [38]. Fractal structures may be quantified by fractal dimension, which is a number (usually non-integer) expressing the manner in which the irregular structure replicates itself through different scales [37], [38]. As stated before, the genesis of tracheal sounds is related to the airflow in the airways, and a monotonically increasing relationship in the form of a power law exist between tracheal sound's intensity and the airflow, which in turns is the temporal derivative of the respiratory volume. In accordance, in this dissertation we hypothesize that as the tidal volume increases, the fractal dimension of the simultaneously-acquired tracheal sounds will also increase as a reflection of their increased intensity and dynamic behavior. Among various fractal dimensions, in this dissertation we used blanket fractal dimension. The BFD was initially proposed for estimating fractal dimension of digital images (2D signals) [39], and is further extended to 1D signals [40].

In the case of 1D signals, the set of points within maximal distance ε from a curve is considered. Therefore, a strip of width 2ε that surrounds the curve is observed [41]. Blanket method creates the strip around the signal, defined by the upper and lower limiting lines, defined as follows [40]:

$$\begin{aligned} u_\varepsilon(i) &= \max\left\{u_{\varepsilon-1}(i)+1, \max_{|m-i|\le 1} u_{\varepsilon-1}(m)\right\} \\ b_\varepsilon(i) &= \min\left\{b_{\varepsilon-1}(i)-1, \min_{|m-i|\le 1} b_{\varepsilon-1}(m)\right\} \\ u_0(i) &= b_0(i) = x(i) \end{aligned} \tag{4}$$

where *x(i)* represents the observed 1D signal, and are the upper and lower lines, respectively, *i* is the current sample of the signal, m denotes samples within the window around the current sample of the signal, and ε is the predefined maximal distance of upper/lower line from the signal. As can be noted from Equation (4), the upper/lower line is always calculated for the three consecutive samples: $i-1$, i, and $i+1$.

The area of the strip between upper and lower lines is defined as:

$$A_\varepsilon = \sum_i \left\{u_\varepsilon(i) - b_\varepsilon(i)\right\} \tag{5}$$

from which the length of the curve *x* can be estimated as [39]:

$$L(\varepsilon) = \frac{A_\varepsilon - A_{\varepsilon-1}}{2} \tag{6}$$

On the other hand, the length of the curve follows the power law [37]:

$$L(\varepsilon) = C \cdot \varepsilon^{1-D} \tag{7}$$

where *C* is the constant and *D* is the blanket fractal dimension. By combining Equations (6) and (7), and using the least square approximation, blanket fractal dimension is calculated.

4.3 Results

All five participants performed the experiments described in Section 2.2 six times in six distinct days, thus creating a database of 30 recordings. The data collected on the first day were used for obtaining

the linear and exponential models, while the data from the remaining five days were used for testing the previously obtained models. Each breathing phase, inspiration and expiration, was analyzed separately.

The linear and exponential fitting curves were calculated only from the first stage of the experiment performed during the first day, using two and three points, respectively, when the participant was breathing through an 800 mL bag for about six respiratory cycles. BFD and SE features were calculated from the smartphone acquired tracheal sounds, while the reference volume values were obtained from the Respitrace signal. This was performed for every inspiratory and expiratory phase, as well as for the portion of the signal during the initial apnea (denoted as background). For the linear fitting curve, for both BFD and SE features, it was found, experimentally, that two points, *A* and *B*, with the following coordinates:

$$\begin{aligned} A &= (x_1, y_1) = (\text{mean}(\text{feature values for 800 mL}), \text{mean}(\text{volumes for 800 mL})) \\ B &= (x_2, y_2) = (\text{feature value of background for 800 mL}, \text{volume of background for 800 mL}) \end{aligned} \tag{8}$$

are sufficient for determining the fitting line.

Similarly, for exponential fitting curves, we found empirically that three points are sufficient, as follows. When using BFD features, the three points (*C*, *D*, *E*) are:

$$\begin{aligned} C &= (x_3, y_3) = (\text{mean}(\text{BFD for 800 mL}), \text{mean}(\text{volumes for 800 mL})) \\ D &= (x_4, y_4) = (0.8, 0) \\ E &= (x_5, y_5) = (2, 2) \end{aligned} \tag{9}$$

and with SE features (points *F*, *G*, *H*):

$$\begin{aligned} F &= (x_6, y_6) = (\text{mean}(\text{SE for 800 mL}), \text{mean}(\text{volumes for 800 mL})) \\ G &= (x_7, y_7) = (0, 0.2) \\ H &= (x_8, y_8) = (6, 2) \end{aligned} \tag{10}$$

After investigating values of the BFD and SE features from all participants, we noticed that the upper limits were 2 and 6, for BFD and SE respectively. Therefore, we used these asymptotic values as abscissae of points *E* and *H*. Figure 4.4 illustrates the computation of the linear and exponential models.

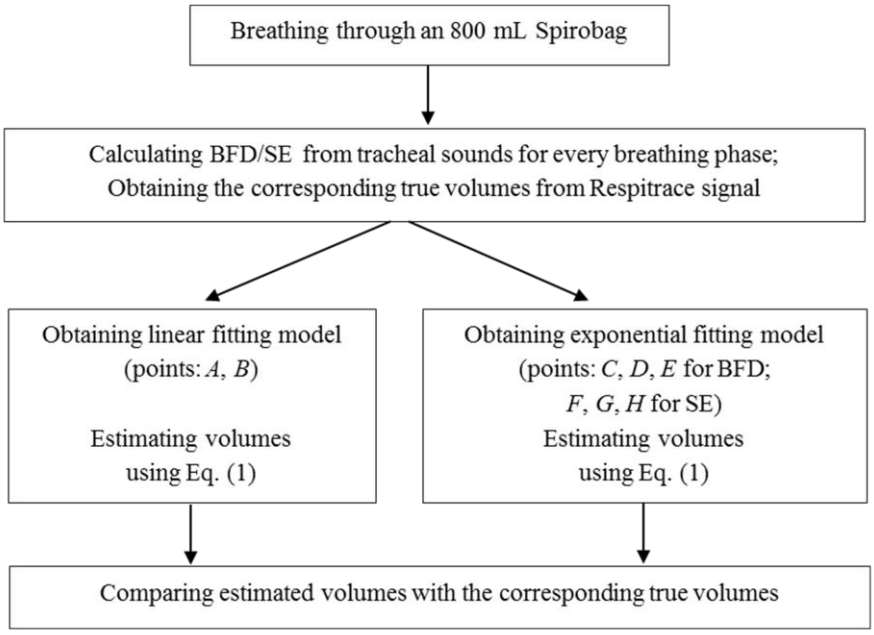

Figure 4.4 - The flowchart showing the computation of the fitting models.

After the linear and exponential curves are calculated, data from the second and the third stages of the experiment (breathing with and without a tube) were used to fit the curves, separately. BFD and SE features were calculated from the smartphone acquired tracheal sounds, and the corresponding volumes were estimated using Equation (1) for the linear and exponential models. Simultaneously, the true volume values were obtained from the reference Respitrace signal. Since the volume range for normal breathing is between 0.2 and 1 L [7], we limited the true volume values to this range, and used only the corresponding portions of tracheal sounds for analysis.

An example of the volume estimation from smartphone acquired tracheal sounds using BFD features and exponential model, for both inspiration and expiration, of one subject is shown in Figure 4.5. The true tidal volume values (from Respitrace system) and their corresponding BFD values when breathing through 800 mL bag and tube are represented in blue squares and green circles, respectively,

while the estimated volumes and their corresponding BFD features are depicted as brown triangles. The three points, shown as black marks in Figure 4.5 and given with Equation (9), are used for obtaining the exponential fitting curve, which is shown as a solid red curve.

For every inspiration and expiration phase, when a true volume value was between 0.2 and 1 L, the estimated volumes were compared to their corresponding true volumes, and NRMSEs were calculated using Equation (2). In Figure 4.6 are shown the estimated and reference volumes, as well as the corresponding NRMSE errors for every inspiratory and expiratory phase for the same example as in Figure 4.5.

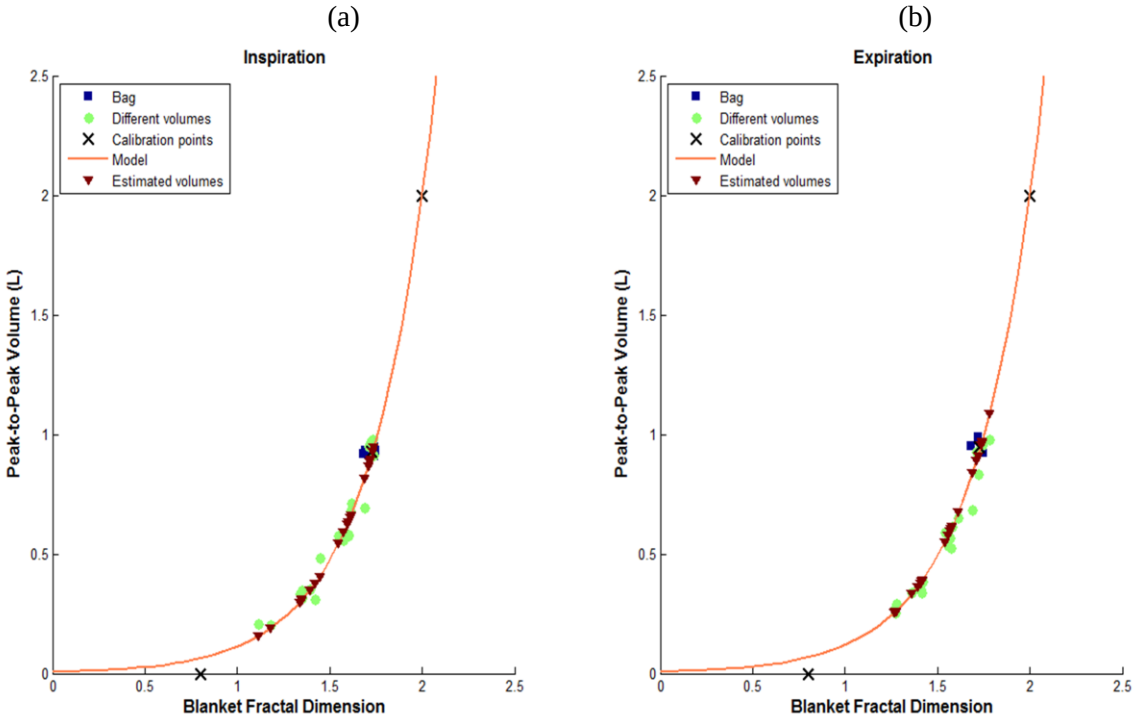

Figure 4.5 – An example of the volume estimation from smartphone acquired tracheal sounds using BFD features and exponential model of one subject.
The true volumes while breathing through a tube (green circles) are limited to a range from 0.2 to 1 L. (a) The inspiratory phase; (b) The expiratory phase.

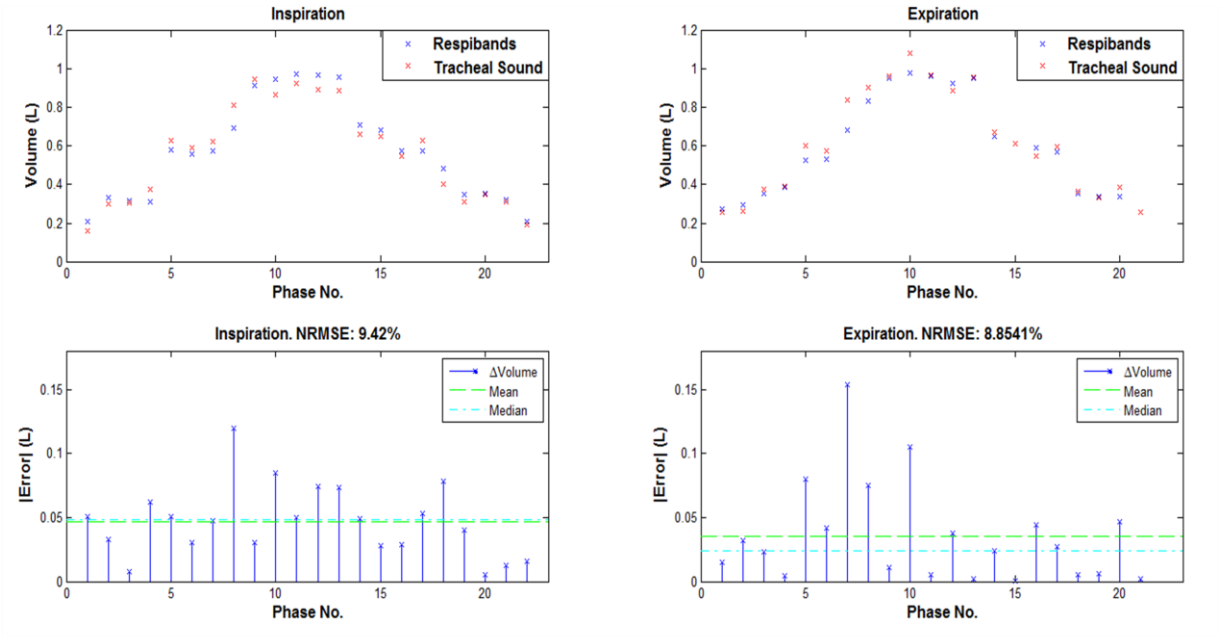

Figure 4.6 – Example of estimated tidal volume from smartphone-acquired tracheal sounds and reference volume from Respibands.
Top: Reference and estimated volumes for the same example as in Figure 4.5. *Bottom*: The corresponding NRMSE errors.

As can be noted from Figure 4.6, values of the volumes estimated from a smartphone acquired tracheal sounds using the BFD features are very similar to the volume values obtained from a Respitrace (reference) signal; and the NRMSE errors in both inspiration and expiration phases are low (less than 10%).

After the first day of experiments (later denoted as training), the participants repeated breathing maneuvers with and without a tube for five days (denoted as tests 1–5). The BFD and SE features were calculated from the tracheal sounds, and the volumes were estimated using the first day's fitting curves. Simultaneously, the true volume values were obtained from the Respitrace signal. Again, the estimated volumes were compared to the true volumes, and NRMSEs were calculated.

In this dissertation, we compared the volume estimation results when the proposed blanket fractal dimension is used as feature, with results obtained with Shannon entropy. Conditions of comparisons

included: the type of the model (exponential, linear), the type of the apparatus (tube, no tube), and the breathing phase (inspiration, expiration). All combinations of conditions were made, and the corresponding ones were tested statistically, using the two-tailed paired *t*-tests (SPSS Statistics 20, IBM Corporation, Armonk, NY, USA). Table 4.1 contains the list of combinations and their corresponding *p*-values when statistically significant differences occurred ($p < 0.05$).

In addition, for each combination, the comparisons between results (NRMSE errors) of the training day and the five test days were performed, and tested statistically using the repeated measures ANOVA with Bonferroni *post-hoc* tests (SPSS Statistics 20). The NRMSE errors are grouped into four parts, based on the apparatus and breathing phase, so that comparisons between features and models can be performed, and are depicted in Figure 4.7. These graphs show the changes in NRMSE errors throughout six days of experiments for all combinations of features and models simultaneously.

As can be concluded from the graphs in Figure 4.7, when blanket fractal dimension was used for volume estimation (red and green lines), the errors were lower at least two times than when Shannon entropy was used (blue and black lines), especially with the exponential model (red circles). Moreover, note that standard errors are also smaller when BFD is used. Statistically significant differences between the two features appeared during the fourth test day (for: exponential and linear models, with tube and both inspiration and expiration phases; and for both models, without tube and expiration) and the fifth test day (for: both models, with tube and expiration phase; and linear model, without a tube and expiration), as shown in Table 4.1.

The smallest NRMSE error, with mean and standard deviation of 15.877 ± 9.246%, was obtained during the first day of experiments (training), when BFD feature with the exponential model was used, for expiratory phase, while the participants were breathing without a tube, Figure 4.7b. The Bland-Altman analysis showed a bias and standard deviation of 0.0226 ± 0.0918 L, and the corresponding results are presented in Figure 4.8.

Table 4.1 – Combinations of conditions when statistically significant differences were obtained, and their corresponding *p*-values.

Type	Day	Conditions	*p*-value
BFD vs. SE	Test 4	Exponential, tube, inspiration	0.049
		Exponential, tube, expiration	0.015
		Exponential, no tube, expiration	0.011
		Linear, tube, inspiration	0.037
		Linear, tube, expiration	0.013
		Linear, no tube, expiration	0.002
	Test 5	Exponential, tube, expiration	0.017
		Linear, tube, expiration	0.006
		Linear, no tube, expiration	0.007
Inspiration vs. Expiration	Test 1	BFD, linear, tube	0.033
	Test 4	SE, linear, tube	0.025
	Test 5	BFD, linear, tube	0.022
		SE, exponential, tube	0.029
		SE, linear, tube	0.031
No tube vs. Tube	Training	SE, exponential, inspiration	0.016
	Test 4	BFD, linear, inspiration	0.042
	Test 5	BFD, linear, inspiration	0.033
Exponential vs. Linear	Training	BFD, tube, expiration	0.008
		BFD, no tube, expiration	0.038
	Test 4	BFD, tube, expiration	0.028
		SE, tube, expiration	0.018
	Test 5	SE, tube, expiration	0.028

Note: Results are grouped into 4 groups, based on the type of comparisons performed in the study, *i.e.*, BFD vs. SE; inspiration vs. expiration; no tube vs. tube; exponential vs. linear model.

By looking at the NRMSEs calculated for the remaining 5 days (test days), one can conclude that the smallest was always obtained with the BFD feature, exponential model and inspiration while breathing through a tube (errors ranging from 20% to 27%), Figure 4.7c, except for the fifth day, when linear model provided better estimation (error around 21%). No statistically significant differences were found between BFD exponential model from inspiratory and expiratory phases, as deduced from Table 4.1.

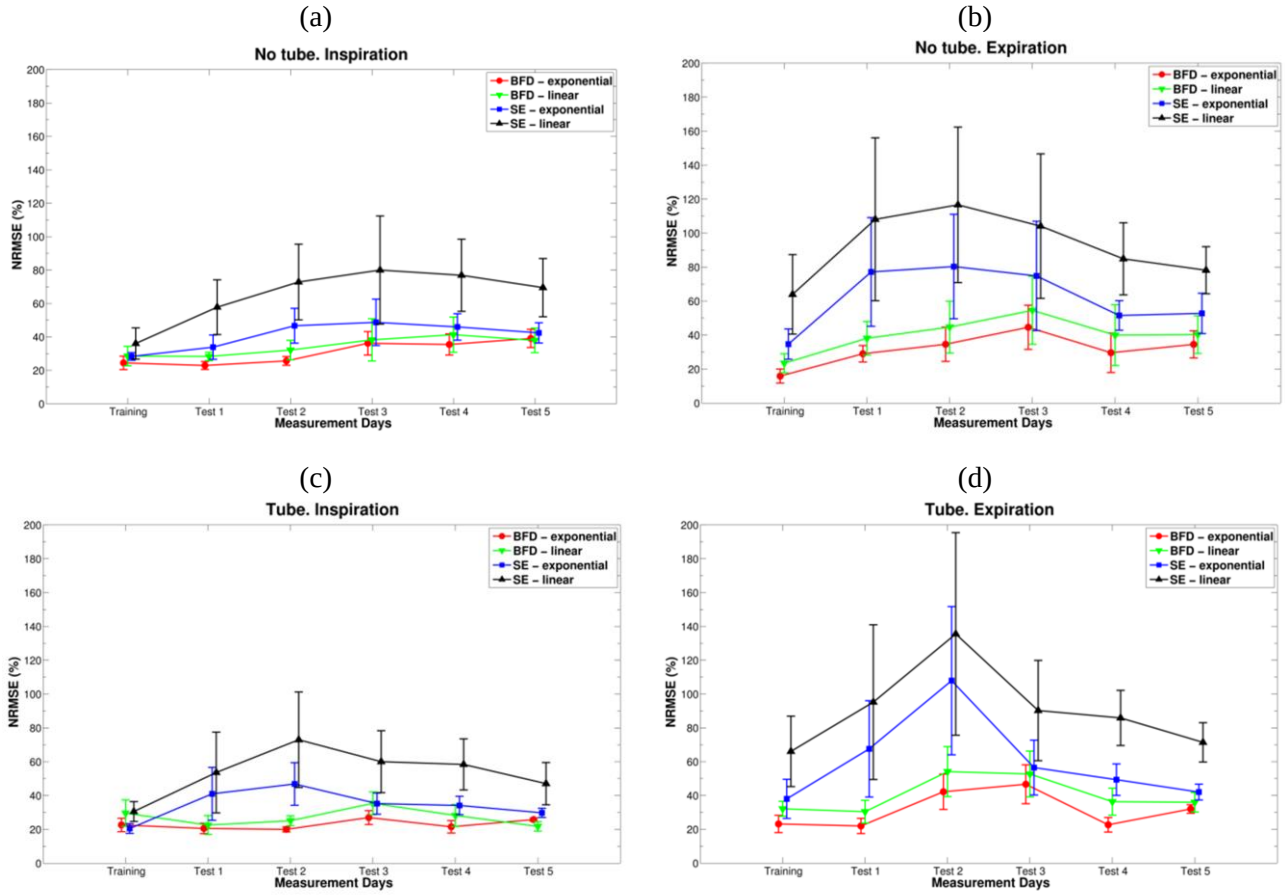

Figure 4.7 - NRMSE errors when BFD and SE with exponential and linear models are used.
NRMSE errors (represented with its mean and standard error of the mean) when: BFD and exponential model (red circles), BFD and linear model (green downward triangles), SE and exponential model (blue squares), and SE and linear model (black triangles) are used. (a) No tube and inspiration; (b) No tube and expiration; (c) Tube and inspiration; (d) Tube and expiration.

As was mentioned above, when BFD feature was used the errors were always smaller than with SE. In addition, one can conclude that the fitting curves obtained during the first day of experiments (training) can be successfully used for the following test days. This way, the participants do not need to perform all three stages of the experiments, and the fitting curves do not need to be calculated every day, as the previously determined could be used. In order to statistically compare errors throughout all six days of experiments, repeated measures ANOVA with Bonferroni *post-hoc* tests were performed, and was

determined that there were no statistically significant differences between the days of experiments when BFD or SE was used as feature. According to Table 4.1, for the BFD using exponential model, no statistically significant differences were found between breathing through the tube or not.

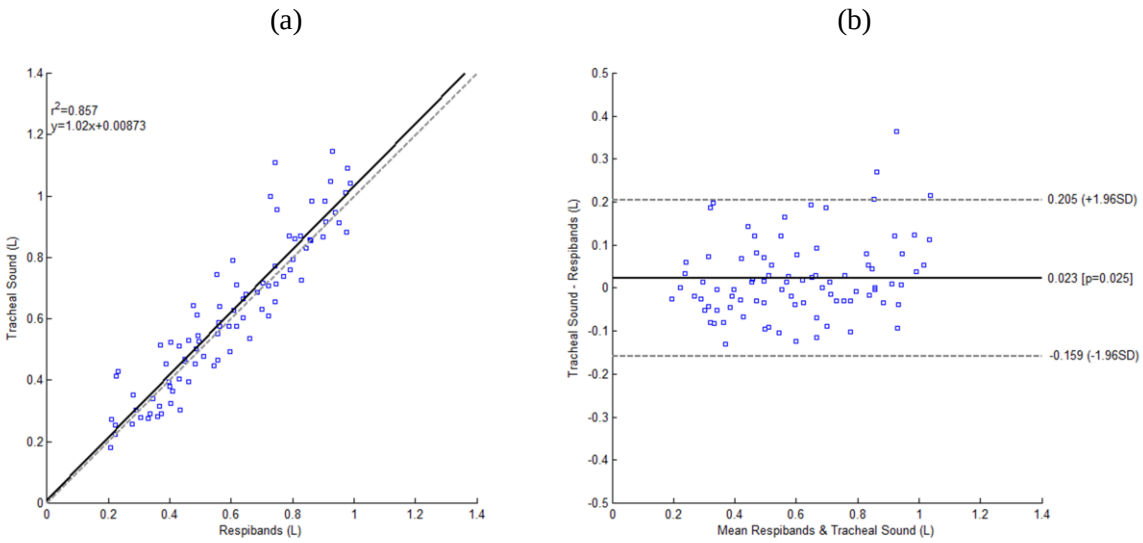

Figure 4.8 - Bland-Altman plot for BFD feature with the exponential model, for expiratory phase, while the participants (*N* = 5) were breathing without a tube during the first day of experiments.
(a) The regression plot: The unitary line is shown as gray dashed line, while the regression line is represented as black solid line; (b) Bland-Altman plot: The bias is represented as a solid black line and the 95% limits of agreement as gray dashed lines.

4.4 Discussions and Conclusions

The goal of this dissertation was to estimate tidal volume from the smartphone acquired tracheal sounds. The main challenge was to find a suitable feature to describe these sounds, such that the volume could be estimated directly from the sounds as accurate as possible. Respiratory sounds, and hence tracheal sounds, are non-stationary and stochastic signals [2], and as such they are suitable for fractal analysis [37]. We tested several ways for estimating fractal dimension, and decided to use the blanket

fractal dimension because it was more suitable for describing and following the dynamics of the tracheal sounds, which was evident after exploring the results. Possible explanation could be the definition of the blanket fractal dimension itself. Blanket method creates a strip around the tracheal signal, closely following the changes in the signal. As the signal changes faster, the value of blanket fractal dimension becomes higher. In some past studies fractal analysis and fractal dimensions were used for analyzing tracheal and lung sounds [22]–[26]. Moreover, blanket fractal dimension was not used in respiratory sound analysis yet, and especially not for estimating the tidal volume, which are some of the novelties of this dissertation. In addition, to the best of our knowledge, none of the studies on tidal volume estimation has reported results based on tracheal sounds acquired by a smartphone.

In addition to BFD features, we used Shannon entropy (SE), as it is one of the features frequently used for analysis of respiratory sounds. In [42], the authors proposed a method to estimate airflow from tracheal sounds using SE. In [43], the authors proposed tidal volume estimation method by integrating airflow derived from tracheal sounds, which takes advantage of airflow/sound intensity relationship. As can be noted, the straightforward comparison between our method and method used in [43] is difficult to perform, since the conditions are not exactly the same. We estimated the tidal volume directly from tracheal sounds, using BFD as a feature, while Que *et al.* [43] obtained first the relationship between sounds' amplitude and airflow, and then the volume by integrating the flow. Consequently, according to the provided results, the range of volume values in [43] was roughly between 0.3 and 0.8 L, while we limited volumes to a broader range [0.2, 1] L. That being said, the Bland-Altman analysis results of [43] were 0.009 ± 0.046 L (bias ± SD), while we found a bias and standard deviation of 0.0226 ± 0.0918 L. Chen *et al*. estimated tidal volume from the energy of the tracheal sounds [6]. The comparison of our results with those reported in [6] is not easy to perform since they are reported separately for each individual participant. If we compute the average results from the provided individually-based values reported in Table 1 [6]), we can conclude that the results are comparable. The volumes ranged from 0.15 to 0.5 L in [6], which is notably smaller range than the one used in this dissertation. Note that in contrast

to these two studies, the only external information needed to compute the calibration model with our proposed method was obtained with a simple bag at a known fixed value and not from a spirometer-like device.

After volumes were estimated from the smartphone acquired tracheal sounds, they were compared to the true volume values, obtained from Respitrace signal, which was considered as a reference in this dissertation. The Respitrace signal was calibrated against the spirometer signal prior every recording and the obtained calibration errors were less than 10%, which is in accordance to the manufacturer's manual. These reference volumes were limited to a range from 0.2 to 1 L, as it is the normal breathing range [7]. Inspiratory and expiratory phases were analyzed separately. Two fitting models, exponential and linear, were used for estimation. Our results indicate that the best estimation was obtained using blanket fractal dimension with exponential model, during expiratory phase, while participants were breathing without a tube, when the NRMSE error was 15.877 ± 9.246% (expressed as mean ± standard deviation). In addition, when the BFD is used as a feature, the NRMSEs were always smaller, at least twice, compared to the SE.

The experiments involved acquisition during six days. Data from the first day of experiments were used to construct estimation models, while the data from the remaining five days were plotted against the obtained models. The results show the possibility to successfully apply previously obtained fitting curves and to monitor tidal volume for at least five days. This way we introduce an easy calibration procedure, where there is no need to calculate fitting curves prior every consecutive experiment. In our future work, we plan to determine for how many days the existing models can be used.

This dissertation research is a preliminary study, with the objective to estimate tidal volume in healthy participants, and not in patients with pulmonary diseases. Therefore, it was performed on five healthy participants, and for the future work we plan to expand the group. This dissertation was limited to acquisition of tracheal sounds in standing posture without head movements. We expect that the results

obtained with the proposed methodology would be in agreement with the study reported in [43], where the effects of body movements and posture changes on tidal volume estimates were investigated. Accordingly, we foresee that head movements without neck extension will not modify the obtained results and we do not anticipate an increase in estimation errors when moving to seated posture, but we do when moving from standing to supine posture, where a new calibration in latter posture would be required. It is worth to mention that all recordings were made in a regular dry lab, that was held quiet, and not in a special soundproof environment, hence making it applicable to real-life situations. Since spirometer is not a portable device, not easily accessed and fixed values of tidal volumes are hard to control, which results in additional turbulences and changes in breathing patterns, we used a Spirobag in order to obtain information at a known volume which in turn was employed in the estimation model. In addition, due to high performance capabilities of smartphones, by connecting an adequate acoustical sensor to a smartphone and using a Spirobag, a portable system for tidal volume estimation can be obtained.

In summary, in this dissertation we proposed a novel technique for estimation of tidal volume directly from the blanket fractal dimension of the tracheal sounds. The proposed method provided promising results and outperformed a method based on the Shannon entropy, which is frequently used in tracheal sounds analysis. Furthermore, we introduced an easy calibration procedure that does not require specialized devices and when combined with the proposed signal processing technique allows reasonable estimation for at least five days, which makes this method easier to use in everyday situations. The employment of smartphone-acquired tracheal sounds was also introduced for all of the above mentioned purposes. We foresee that similar efforts to the one presented here represent a step forward to the development of a mobile breathing monitoring system easily available for the general population.

4.5 Acknowledgments

This work is supported in part by the US Army Medical Research and Material Command (US-AMRMC) under grant No. W81XWH-12-1-0541.

The authors would like to thank Sonia Charleston-Villalobos, Thomas Aljama-Corrales, and Ramon Gonzales-Camarena for introducing a microphone sensor used in this research work. The authors would also like to thank Milorad Paskas for his help in programs for calculating blanked fractal dimension. We also acknowledge the feedback provided by the reviewers and editor to improve the quality of this manuscript.

Bersain Reyes was supported by a Consejo Nacional de Ciencia y Tecnologia (CONACyT) Scholarship from the Mexican Government.

4.6 References

[1] A. R. A. Sovijarvi, F. Dalmasso, J. Vanderschoot, L. P. Malmberg, G. Righini, and S. A. T. Stoneman, "Definition of terms for applications of respiratory sounds," *Eur. Respir. Rev.*, vol. 10, no. 77, pp. 597–610, 2000.

[2] Z. Moussavi, *Fundamentals of Respiratory System and Sounds Analysis*. Morgan & Claypool.

[3] A. R. A. Sovijarvi, L. P. Malmberg, G. Charbonneau, J. Vanderschoot, F. Dalmasso, C. Sacco, M. Rossi, and J. E. Earis, "Characteristics of breath sounds and adventitious respiratory sounds," *Eur. Respir. Rev.*, vol. 10, no. 77, pp. 591–596, 2000.

[4] M. Folke, L. Cernerud, M. Ekström, and B. Hök, "Critical review of non-invasive respiratory monitoring in medical care," *Med. Biol. Eng. Comput.*, vol. 41, no. 4, pp. 377–383, Jul. 2003.

[5] Y. Kuratomi, N. Okazaki, T. Ishihara, T. Arai, and S. Kira, "Variability of breath-by-breath tidal volume and its characteristics in normal and diseased subjects. Ventilatory monitoring with electrical impedance pneumography," *Jpn. J. Med.*, vol. 24, no. 2, pp. 141–149, May 1985.

[6] G. Chen, I. de la Cruz, and E. Rodriguez-Villegas, "Automatic lung tidal volumes estimation from tracheal sounds," *Conf. Proc. Annu. Int. Conf. IEEE Eng. Med. Biol. Soc. IEEE Eng. Med. Biol. Soc. Annu. Conf.*, vol. 2014, pp. 1497–1500, Aug. 2014.

[7] L. Sherwood, *Fundamentals of Human Physiology*, 4th ed. Boston, MA, USA: Cengage Learning, 2011.

[8] B. J. Semmes, M. J. Tobin, J. V. Snyder, and A. Grenvik, "Subjective and objective measurement of tidal volume in critically ill patients.," *Chest*, vol. 87, no. 5, pp. 577–579, 1985.

[9] P. Grossman, M. Spoerle, and F. H. Wilhelm, "Reliability of respiratory tidal volume estimation by means of ambulatory inductive plethysmography," *Biomed. Sci. Instrum.*, vol. 42, pp. 193–198, 2006.

[10] O. Sayadi, E. H. Weiss, F. M. Merchant, D. Puppala, and A. A. Armoundas, "An Optimized Method for Estimating the Tidal Volume from Electrocardiographic Signals: Implications for Estimating Minute Ventilation," *Am. J. Physiol. - Heart Circ. Physiol.*, vol. 307, pp. H426–H436, 2014.

[11] P. Corbishley and E. Rodriguez-Villegas, “Breathing Detection: Towards a Miniaturized, Wearable, Battery-Operated Monitoring System,” *IEEE Trans. Biomed. Eng.*, vol. 55, no. 1, pp. 196–204, Jan. 2008.
[12] J. E. Earis and B. M. G. Cheetham, “Future perspectives for respiratory sound research,” *Eur. Respir. Rev.*, vol. 10, no. 77, pp. 641–646, 2000.
[13] S. J. Cala, C. M. Kenyon, G. Ferrigno, P. Carnevali, A. Aliverti, A. Pedotti, P. T. Macklem, and D. F. Rochester, “Chest wall and lung volume estimation by optical reflectance motion analysis,” *J. Appl. Physiol.*, vol. 81, no. 6, pp. 2680–2689, Dec. 1996.
[14] M. D. Petrović, J. Petrovic, A. Daničić, M. Vukčević, B. Bojović, L. Hadžievski, T. Allsop, G. Lloyd, and D. J. Webb, “Non-invasive respiratory monitoring using long-period fiber grating sensors,” *Biomed. Opt. Express*, vol. 5, no. 4, p. 1136, Apr. 2014.
[15] Y. S. Lee, P. N. Pathirana, C. L. Steinfort, and T. Caelli, “Monitoring and Analysis of Respiratory Patterns Using Microwave Doppler Radar,” *IEEE J. Transl. Eng. Health Med.*, vol. 2, pp. 1–12, 2014.
[16] C. Scully, J. Lee, J. Meyer, A. M. Gorbach, D. Granquist-Fraser, Y. Mendelson, and K. H. Chon, “Physiological parameter monitoring from optical recordings with a mobile phone,” *Biomed. Eng. IEEE Trans. On*, vol. 59, no. 2, pp. 303–306, 2012.
[17] J. Lee, B. A. Reyes, D. D. McManus, O. Mathias, and K. H. Chon, “Atrial Fibrillation Detection Using an iPhone 4S,” *IEEE Trans. Biomed. Eng.*, vol. 60, no. 1, pp. 203–206, 2013.
[18] B. A. Reyes, N. Reljin, and K. H. Chon, “Tracheal Sounds Acquisition Using Smartphones,” *Sensors*, vol. 14, no. 8, pp. 13830–13850, Jul. 2014.
[19] C. Ahlstrom, A. Johansson, P. Hult, and P. Ask, “Chaotic dynamics of respiratory sounds,” *Chaos Solitons Fractals*, vol. 29, no. 5, pp. 1054–1062, Sep. 2006.
[20] S. Charleston-Villalobos, L. Albuerne-Sanchez, R. Gonzalez-Camarena, M. Mejia-Avila, G. Carrillo-Rodriguez, and T. Aljama-Corrales, “Linear and Nonlinear Analysis of Base Lung Sound in Extrinsic Allergic Alveolitis Patients in Comparison to Healthy Subjects,” *Methods Inf. Med.*, vol. 52, no. 3, pp. 266–276, Apr. 2013.
[21] H. Kitaoka, R. Takaki, and B. Suki, “A three-dimensional model of the human airway tree,” *J. Appl. Physiol.*, vol. 87, no. 6, pp. 2207–2217, Dec. 1999.
[22] Y. L. Yap and Z. Moussavi, “Respiratory onset detection using variance fractal dimension,” in *Proceedings of the 23rd Annual International Conference of the IEEE Engineering in Medicine and Biology Society, 2001.*, 2001, vol. 2, pp. 1554–1556 vol.2.
[23] J. Gnitecki and Z. Moussavi, “Variance fractal dimension trajectory as a tool for hear sound localization in lung sounds recordings,” in *Proceedings of the 25th Annual International Conference of the IEEE Engineering in Medicine and Biology Society, 2003.*, 2003, vol. 3, pp. 2420–2423 Vol.3.
[24] L. J. Hadjileontiadis and I. T. Rekanos, “Detection of explosive lung and bowel sounds by means of fractal dimension,” *IEEE Signal Process. Lett.*, vol. 10, no. 10, pp. 311–314, 2003.
[25] J. Gnitecki and Z. Moussavi, “The fractality of lung sounds: A comparison of three waveform fractal dimension algorithms,” *Chaos Solitons Fractals*, vol. 26, no. 4, pp. 1065–1072, Nov. 2005.
[26] L. J. Hadjileontiadis, “A Novel Technique for Denoising Explosive Lung Sounds: Empirical Mode Decomposition and Fractal Dimension Filter,” *IEEE Eng. Med. Biol. Mag.*, vol. 26, no. 1, pp. 30–39, Jan. 2007.
[27] C. K. Druzgalski, R. L. Donnerberg, and R. M. Campbell, “Techniques of recording respiratory sounds,” *J. Clin. Eng.*, vol. 5, no. 4, pp. 321–330, 1980.
[28] H. Pasterkamp, S. S. Kraman, and G. R. Wodicka, “Respiratory Sounds: Advances Beyond the Stethoscope,” *Am. J. Respir. Crit. Care Med.*, vol. 156, no. 3, pp. 974–987, Sep. 1997.
[29] S. Charleston-Villalobos, G. Martinez-Hernandez, R. Gonzalez-Camarena, G. Chi-Lem, J. G. Carrillo, and T. Aljama-Corrales, “Assessment of multichannel lung sounds parameterization for two-class classification in interstitial lung disease patients,” *Comput. Biol. Med.*, vol. 41, no. 7, pp. 473–482, Jul. 2011.

[30] S. Reichert, R. Gass, C. Brandt, and E. Andres, “Analysis of Respiratory Sounds: State of the Art,” *Clin. Med. Circ. Respir. Pulm. Med.*, vol. 2, pp. 45–58, May 2008.
[31] A. Papoulis and S. U. Pillai, *Probability, Random Variables and Stochastic Processes*. New York, NY, USA: McGraw-Hill, 2002.
[32] A. Yadollahi and Z. M. K. Moussavi, “A robust method for heart sounds localization using lung sounds entropy,” *IEEE Trans. Biomed. Eng.*, vol. 53, no. 3, pp. 497–502, Mar. 2006.
[33] E. Parzen, “On Estimation of a Probability Density Function and Mode,” *Ann. Math. Stat.*, vol. 33, no. 3, pp. 1065–1076, Sep. 1962.
[34] R. O. Duda, P. E. Hart, and D. G. Stork, *Pattern Classification*. New York, NY, USA: Wiley-Interscience, 2000.
[35] B. Mandelbrot, “How Long Is the Coast of Britain? Statistical Self-Similarity and Fractional Dimension,” *Science*, vol. 156, no. 3775, pp. 636–638, May 1967.
[36] B. B. Mandelbrot, “Stochastic models for the Earth’s relief, the shape and the fractal dimension of the coastlines, and the number-area rule for islands,” *Proc. Natl. Acad. Sci. U. S. A.*, vol. 72, no. 10, pp. 3825–3828, Oct. 1975.
[37] B. B. Mandelbrot, *The Fractal Geometry of Nature*. San Francisco: W. H. Freeman and Company, 1982.
[38] H.-O. Peitgen, H. Jürgens, and D. Saupe, *Chaos and Fractals: New Frontiers of Science*. New York, NY, USA: Springer, 2004.
[39] S. Peleg, J. Naor, R. Hartley, and D. Avnir, “Multiple Resolution Texture Analysis and Classification,” *IEEE Trans. Pattern Anal. Mach. Intell.*, vol. PAMI-6, no. 4, pp. 518–523, Jul. 1984.
[40] M. P. Paskas, A. M. Gavrovska, and N. B. Reljin, “Identification of fundamental heart sounds from PCG using blanket fractal dimension,” in *Proceedings of the 8th Conference of the European Study Group on Cardiovascular Oscillations*, Trento, Italy, 2014, pp. 123–124.
[41] M. J. Turner and J. M. Blackledge, “Analysis of the limitations of fractal dimension texture segmentation for image characterization,” in *Fractal Geometry: Mathematical Methods, Algorithms, Applications*, Chichester, England: Horwood Publishing Limited, 2002, pp. 114–137.
[42] A. Yadollahi and Z. M. K. Moussavi, “A robust method for estimating respiratory flow using tracheal sounds entropy,” *IEEE Trans. Biomed. Eng.*, vol. 53, no. 4, pp. 662–668, Apr. 2006.
[43] C.-L. Que, C. Kolmaga, L.-G. Durand, S. M. Kelly, and P. T. Macklem, “Phonospirometry for noninvasive measurement of ventilation: methodology and preliminary results,” *J. Appl. Physiol.*, vol. 93, no. 4, pp. 1515–1526, Oct. 2002.

Chapter 5: Tidal Volume and Instantaneous Respiration Rate Estimation using a Smartphone-acquired Camera Signal

(B. A. Reyes, N. Reljin, Y. Kong, Y. Nam, and K. H. Chon, "Tidal Volume and Instantaneous Respiration Rate Estimation using a Volumetric Surrogate Signal Acquired via a Smartphone Camera; Under revision, December 2015)

5.1 Introduction

Monitoring of respiration status has been recognized as critical for identifying and predicting serious adverse events [1]. Two basic parameters that a breathing monitor should be able to provide are tidal volume (V_T) and respiration rate (RR) [2]. Normal average values for a human man are around 0.5 L and 12 bpm for V_T and RR, respectively. These values are not fixed and the mechanism of respiratory control is crucial in determining $\dot{V}_E$ by adjusting the combination of V_T and RR according to a body's requirements in response to different scenarios [3].

Currently, there are several clinical RR monitoring methods including qualified human observation, transthoracic impedance, inductance plethysmography, capnography monitoring, and tracheal sound monitoring [4]–[7]. Also, there are several methods for measuring V_T including spirometry, impedance pneumography, inductance plethysmography, photoplethysmography, computed tomography, phonospirometry, Doppler radar, and more recently electrocardiography [8]–[16]. Each method has its own disadvantages, *e.g.*, human observation is time consuming and subjective to do, patients have a low tolerance for wearing the nasal cannula in capnography [2], high doses of ionizing radiation in computed tomography, or alteration in both natural RR and V_T due to spirometer use [17]. However flawed, at least clinical devices exist for monitoring. Outside clinical or research settings, there is still a lack of monitoring devices that can accurately determine RR and V_T in a non-contact way and can be used on a daily basis. Moreover, having been designed for clinical settings or research centers,

these methods employ specialized devices that are not translated easily to everyday use due to their high costs, need for skilled operators, or limited mobility.

Nowadays, smartphones have software and hardware capabilities that make them an enticing option for developing a ubiquitous mobile respiration monitoring system. In an attempt to develop such a mobile system, we analyzed an acoustical approach and found good correlation between the smartphone-based respiration rate estimates and the spirometer-based ones ($r^2 \approx 0.97$), as well as 95% limits of agreement ranging approximately from -1.4 to 1.6 bpm for a breathing range from 15 to 35 bpm [18]. However, the last approach requires plugging an additional acoustical sensor into the smartphone in order to extract information from tracheal sounds and just provides estimates of RR.

Previous two chapters of this dissertation focused on the estimation of respiratory rate and tidal volume via an acoustical monitoring approach using smartphones. In this chapter of the dissertation we will focus on the estimation of these two breathing parameters using a non-contact optical approach implemented on a smartphone.

In order to overcome the need for an external sensor for the task of RR estimation, *i.e.*, the acoustical sensor, more recently our research group studied a noncontact optical approach that takes advantage of a smartphone's cameras. In particular, an algorithm that allows the real time acquisition of a surrogate signal from breathing-related light intensity changes due to chest wall movements was implemented on a smartphone and its performance was tested in healthy volunteers breathing at a metered pace and spontaneously, while seated. Under these paced breathing, we found that the smartphone-based estimates of average RR were accurate when compared to those obtained from inductance plethysmography. Note that in the noncontact optical breathing monitoring approach, volume changes are not directly measured but a surrogate signal is obtained from the analysis of the variations in the reflected light due to chest wall movements captured by the system's camera while breathing.

There have been efforts to perform breathing monitoring via the noncontact optical approach described above but most of them have focused on average RR estimation [19]–[25] despite the importance of monitoring breathing depth. Still, noncontact optical methods have been proposed for V_T estimation which is more challenging than average RR estimation. In particular, chest wall surface markers tracked by an optical reflectance system have shown promising results [20]. Those findings have been supported by studies that showed a one-to-one relationship between changes of the external torso and V_T corresponding to internal lung air content [12]. More recently, a webcam and image processing technique based on the detection of shoulder displacements were implemented for breathing pattern tracking [22]. However, to the best of our knowledge, a smartphone-based system that uses a noncontact optical approach together with an algorithm implemented directly in the smartphone for the task of V_T estimation is not available yet.

Further observation of the smartphone-acquired signals during our previous study pointed us to the possibility of obtaining more valuable information than the average RR. Namely, we noticed that our algorithm was capable of monitoring the increased amplitude of the chest movements when volunteers took deeper breaths.

In this dissertation we propose a mobile system based on a noncontact optical approach implemented in a smartphone that provides information, from a volume surrogate, about both RR at each time instant (IRR) as well as V_T (when calibrated), in contrast to just average RR. For this dissertation, the proposed breathing monitoring system was implemented on a commercially-available Android smartphone, but could of course be implemented in smartphones using other operating systems. We collected signals from healthy volunteers and tested the performance of the proposed smartphone system for the tasks of IRR and V_T estimation, using the spirometer-acquired volume signal as reference.

5.2 Material and Methods

5.2.1 Subjects

For this study, fifteen (N=15) healthy and non-smoker volunteers (fourteen males) aged 19 to 52 years (mean ± standard deviation: 28.73 ± 9.27), weight 70.14 ± 19.83 kg and height 175.67 ± 5.94 cm, were recruited. Exclusion criteria included individuals with previous pneumothorax, those with chronic respiratory illnesses such as asthma, and anyone who was currently ill with common cold or an upper respiratory infection. Each volunteer consented to participate and signed the study protocol approved by the Institutional Review Board of the University of Connecticut (UConn), USA.

5.2.2 Respiration Signals Acquisition

Equipment

The HTC One M8 smartphone (HTC Corporation, New Taipei City, Taiwan) running the Android v4.4.2 (KitKat) operating system was selected for this research as it is one of the state-of-the-art Android smartphones which is nowadays the dominant operating system in mobile devices. The HTC One M8 allows simultaneous dual camera recording supported by its processor running a 2.3 GHz quad-core CPU (Snapdragon 801, Qualcomm Technologies Inc., San Diego, CA, USA). For this dissertation, the chest movement signal of interest was collected via the frontal camera consisting of a 5 MP, backside-illumination sensor with wide angle lens and 1080p full HD video recording capabilities at 30 frames-per-second. The video recording was processed in real time using a smartphone application specifically designed and implemented in the smartphone to obtain a volumetric surrogate signal, referred in this dissertation as chest movement signal, of the subject as discussed in the next section. After finishing the maneuver, the chest movement signal and corresponding time vector were saved into a text file in the smartphone and transferred to a personal computer for offline analysis of results using Matlab (R2012a, The Mathworks, Inc., Natick, MA, USA).

Together with the smartphone-recorded chest signal, a spirometer system consisting of a respiration flow head connected to a differential pressure transducer to measure airflow was used to record the airflow signal (MLT1000L, FE141 Spirometer, ADInstruments, Dunedin, New Zealand). The volume signal, regarded as reference for V_T and IRR estimation, was computed in the phone as the integral of the airflow over time. Both the airflow and volume signals were sampled at 1 kHz using a 16-bit A/D converter (PowerLab/4SP, ADInstruments). A 3.0 L calibration syringe (Hans Rudolph, Inc., Shawnee, KS, USA) was used to calibrate the spirometer system prior to recording each volunteer. A new set consisting of disposable filter, reusable mouthpiece, and disposable nose clip was given to each volunteer (MLA304, MLA1026, MLA1008, ADInstruments).

Maneuver

Each maneuver lasted approximately 2 minutes during which the volunteers were asked to breathe through the spirometer system at different volume levels ranging from around 300 mL to 3 L depending on was what manageable for that individual. Each volunteer was instructed to breathe while first increasing their V_T with each breath for around 1 minute, and then decreasing their V_T with each breath for the remaining time. To provide visual feedback of the maneuver to the volunteers, their volume signal was displayed on a 40" monitor placed in front of them. Nose clips were used to clamp the nostrils during the respiration maneuver. Volunteers were standing still during signal collection. The smartphone was positioned in front of the volunteer at approximately 60 cm in a 3-pronged clamp placed at thorax level so that the frontal camera recorded chest wall movements associated with breathing during the maneuver. All signals were recorded in a regular dry lab with the ambient light consisting majorly of ordinary fluorescent lamps located in the ceiling approximately 2.5 m above floor level and, in a lower degree, sunlight entering through lab's windows. Although the smartphone and spirometer recordings were simultaneously started, 5s of initial and final apnea segments were acquired for automatic alignment purposes between both recordings. After initial apnea, volunteers took a forced respiration cycle before performing the described respiration maneuver. Figure 5.1 shows an example of the smartphone

recording together with acquired raw data as explained in next subsection. It is worth mentioning that volunteers were not restricted in wearing any color/pattern of their clothes during the maneuvers but instructed not to wear loose clothes.

5.2.3 Chest Movement Recording using Smartphone Camera

The two major contributors to breathing are the rib cage and abdomen compartments of the chest wall, whose movements in the anteroposterior direction are greater than those in the vertical or transverse directions, with an increase of around 3 cm in the anteroposterior diameter over the vital capacity range [26]. There is a relationship between volume displacement and linear motion during breathing [26], and a one-to-one relationship between changes of the external torso and tidal volume corresponding to internal lung air content has been found [12]. The proposed smartphone algorithm is intended to take advantage of this relationship to obtain a volume surrogate by analyzing the changes in the intensity of the reflected light caused by the breathing-related chest wall movements captured at distance with the device's camera. In particular, the algorithm processes video recordings in real time, where at each time instant t, the intensities of the red, green and blue (RGB) channels are averaged within a rectangular region of interest (ROI) according to

$$I(t) = \left(\frac{1}{3D}\right)\left(\sum_{\{m,n\}\in D} i_R(m,n,t) + \sum_{\{m,n\}\in D} i_G(m,n,t) + \sum_{\{m,n\}\in D} i_B(m,n,t)\right) \quad (1)$$

where $i_x(m,n,t)$ is the intensity value of the pixel at the m-th row and n-th column of the red, green or blue channel within the ROI containing a total of D pixels. For this dissertation, a region of 49×90 pixels was selected in a resolution of 320×240 pixels and was focused on the thoracic area of the volunteer. This reduced resolution and ROI size were selected so that they do not compromise the sampling rate during the real time monitoring in the smartphone app. With these settings, the frame rate dropped to around 25 frames-per-second. The average intensity waveform $I(t)$ was regarded as the chest movement signal, *i.e.*,

the volume surrogate, from which the tidal volume and respiratory rates were estimated. As shown in Figure 5.1, despite the DC values all channels carry similar information, and hence their average was taken to avoid channel selection. An example of the raw volume acquired with a spirometer and the corresponding chest movement signal acquired online with the smartphone's camera and chest movement app is shown in Figure 5.2 for the respiration maneuver performed by one subject. It is worth mentioning that similarly to other monitoring methods, *e.g.*, inductance plethysmography, in this proposed noncontact optical approach the smartphone-acquired volumetric surrogate signal might be very weak if the clothes worn by the subject are not tight to his/her thorax, and hence resulting in an increased estimation error of breathing parameters.

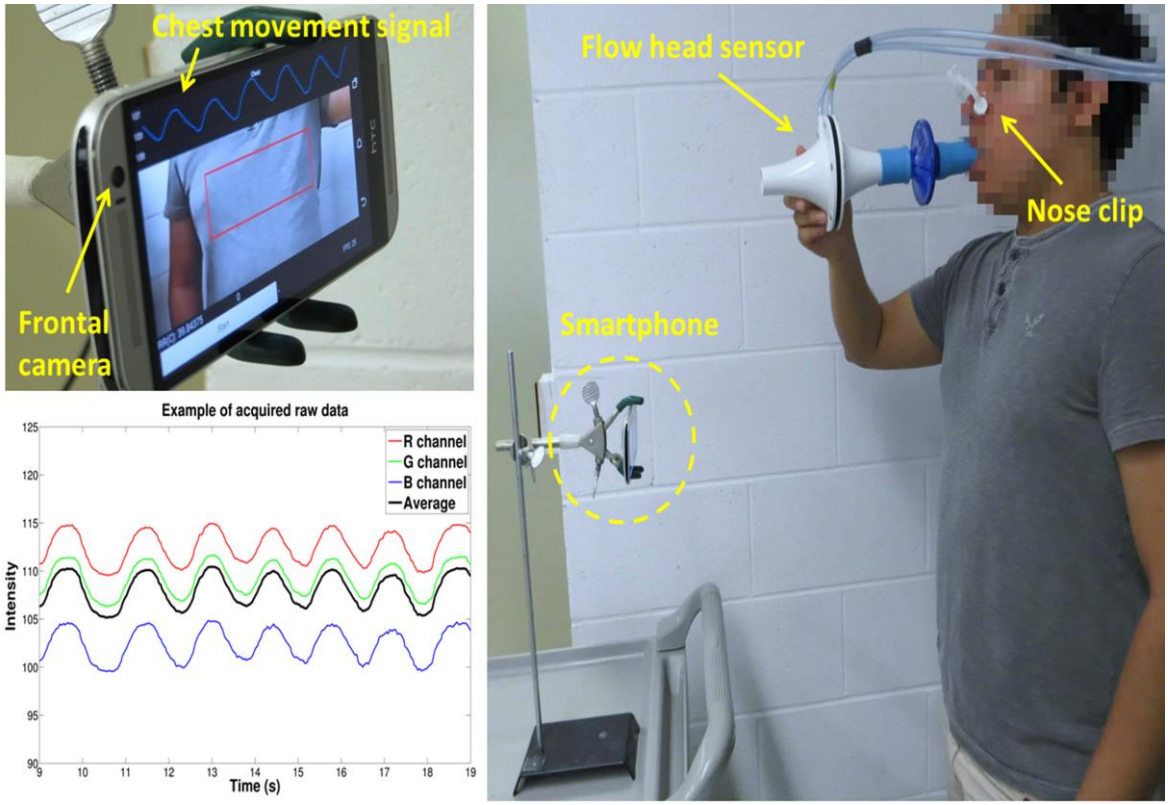

Figure 5.1 – Recording of chest movement signal using a smartphone's camera during a respiration maneuver.
Right: Smartphone placed in front of the volunteer at thorax level in order to record chest movements which were later compared to the reference volume signal from the spirometer. *Top left*: Zoomed view of the developed smartphone app. *Bottom left*: A segment of the raw signals extracted from the RGB channels and their average.

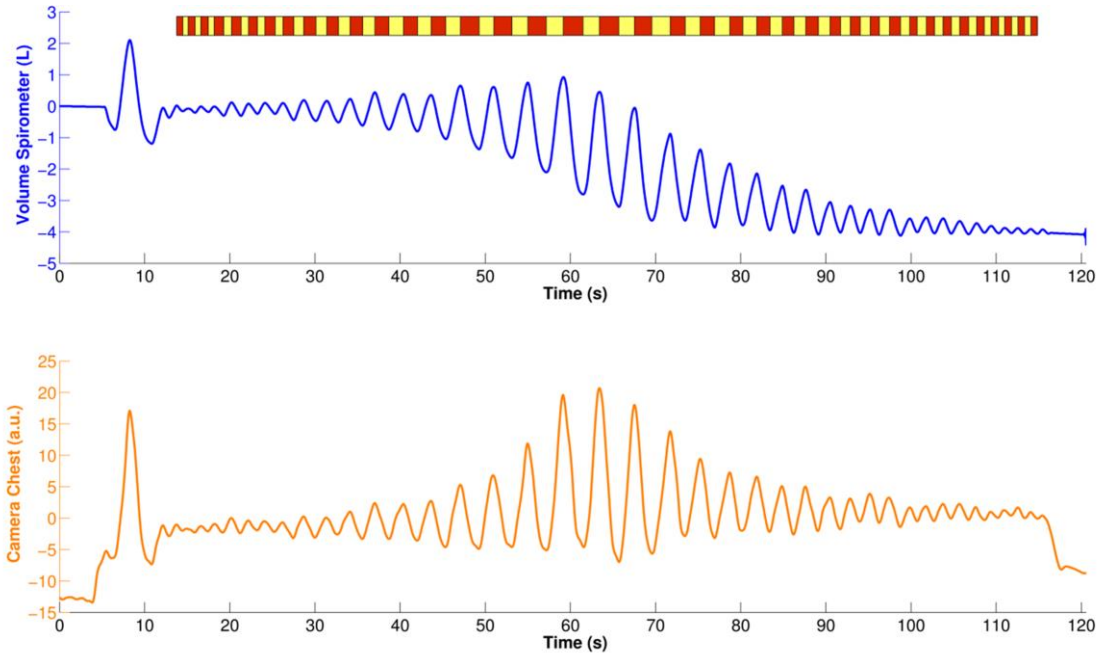

Figure 5.2 - Example of the acquired signals during the respiration maneuver of one volunteer.
Top: volume signal from spirometer. *Bottom*: chest movement signal from smartphone's camera. Positive and negative deflections indicate inspiratory and expiratory phases and are indicated by yellow and red bars displayed on top of the signals, respectively.

5.2.4 Data Preprocessing

The acquired chest movement signal was interpolated at 25 Hz via a cubic spline algorithm to achieve a uniform sampling rate that corrects fluctuations around this value during the real time acquisition in the smartphone. The reference volume signal was down-sampled to 25 Hz to achieve the same sampling frequency as the chest movement signal. In order to minimize high frequency components not related to the respiration maneuver, the chest movement and reference volume signals were filtered with a 4th-order Butterworth lowpass filter at 2 Hz that was applied in a forward and backward scheme to produce zero-phase distortion and minimize the start and end transients.

After filtering, chest movement and reference volume signals were automatically aligned using the cross-correlation function, where 20 seconds in the central portion of the maneuver were extracted from each recording to compute the cross-correlation sequence in order to obtain the sample lag providing

the maximum cross-correlation value that indicates the required samples to be shifted. This alignment was required because of different starting times and delays of the smartphone and AD converter acquisition systems during the simultaneous recording of the maneuver. The duration of the signals was set accordingly, to the minimum duration of both types of recordings.

Finally, both signals, the surrogate and the actual volume, were detrended via the Empirical Mode Decomposition (EMD) method [27]. The essence of this decomposition is to identify the intrinsic oscillatory modes, called IMFs, of a signal through the time scales present in it. Its principal attractiveness resides in obtaining the IMFs directly from the signal without the use of any kernel. All the IMFs of the signal *s(t)* under analysis are extracted automatically by a shifting process intended to eliminate riding waveforms and to produce close to zero mean value as defined by upper and lower envelope signals. The EMD sifting process allows representation of the original signal in term of its extracted components as

$$s(t) = \sum_{k=1}^{K} IMF_k(t) + r_K(t) \tag{2}$$

where *K* is the total number of IMFs, and $r_K(t)$ is the residual signal. EMD has the characteristic of being a complete decomposition [27].

5.2.5 Tidal Volume Estimation using Smartphone Camera Signal

The volume signal from the spirometer was used to automatically determine the breath-phase onsets during the maneuver by finding their local maxima and minima. Inspiratory/expiratory phases corresponded to positive/negative traces of the volume signal. The reference V_T of each phase was computed as the absolute volume difference between two consecutive breath-phase onsets. In the aligned chest movement signal from smartphone, the corresponding extrema were located and the amplitude difference between two consecutive breath-phase onsets was used for V_T estimation via the smartphone.

For calibration, a least-squares linear regression between the reference V_T and the absolute peak-to-peak amplitude of chest movement was performed for each volunteer; half of the data points of the maneuver were randomly selected for calibration purposes and regarded as a training data set, while the remaining half were used as a test data set to which the computed linear model was applied in order to map the smartphone-based measurements to volume estimates in liters.

The performance of the V_T estimation was measured on the test data using the regression parameter r^2, the root-mean-squared error RMSE, and the normalized root-mean-squared error NRMSE, defined as follows

$$RMSE = \sqrt{\frac{\sum_{i=1}^{N}\left(V_{T_{spirometer}}(i) - V_{T_{smartphone}}(i)\right)^2}{N}} \tag{3}$$

$$NRMSE = \frac{RMSE}{\text{mean}\left(V_{T_{spirometer}}\right)} \text{ x } 100\% \tag{4}$$

where $V_{T_{spirometer}}$ indicates the tidal volume obtained from the spirometer-acquired volume signal, $V_{T_{smartphone}}$ the tidal volume estimated from smartphone-acquired chest movements after calibration, and *N* is the number of breath-phases of the analyzed maneuver used for testing.

Figure 5.3 shows an example of the preprocessed reference volume and chest movement signals. The breath-phase onsets and respiration phases as computed from the volume signal are indicated on top. The corresponding maxima and minima are superimposed on each signal. The reference V_T of each breath phase is also shown below the respiratory maneuver.

5.2.6 Instantaneous Respiration Rate Estimation using Smartphone Camera Signal

To estimate IRR from the smartphone-acquired chest movement signal, a time-varying spectral technique was used. In this dissertation, the smoothed pseudo Wigner-Ville distribution (SPWVD) time-frequency representation (TFR) was employed. A TFR is a function that simultaneously describes the energy density of a signal in the time and frequency domains, allowing one to analyze which frequencies

of the signal are present at a certain time [28]. TFR analysis is useful for analyzing signals whose frequency content varies over time, as is the case with respiration signals.

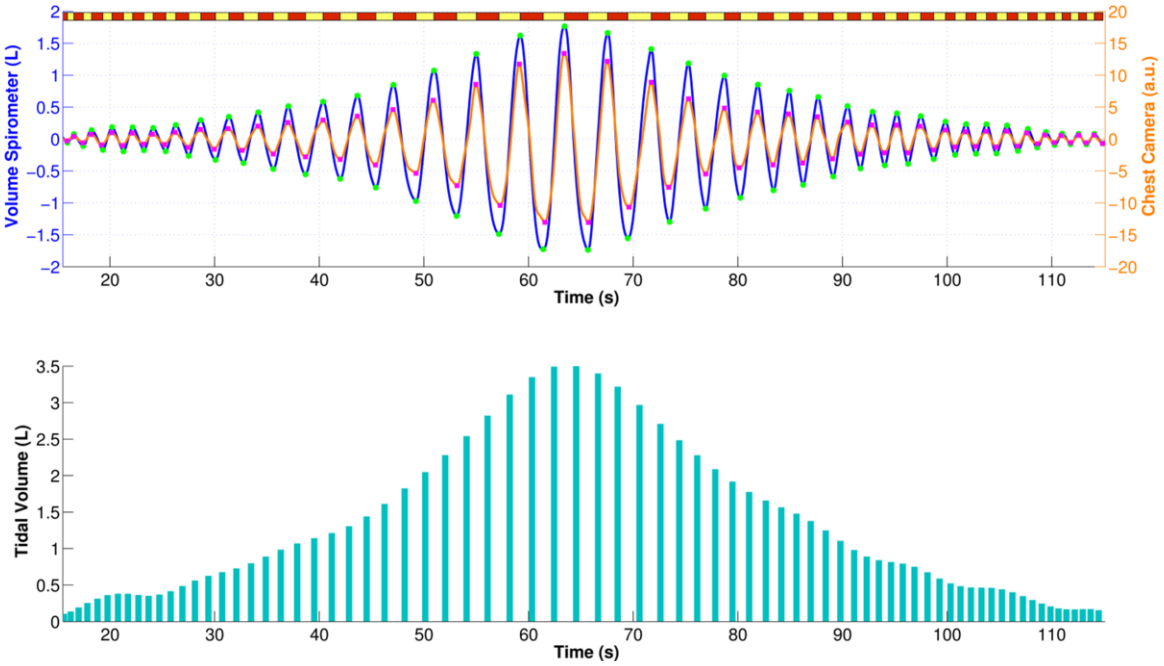

Figure 5.3 - Example of pre-processed signals during the respiration maneuver of one volunteer. *Top*: Detrended versions of a volume signal from the spirometer and the chest movement signal from a smartphone camera. Green and magenta dots indicate the maxima and minima of volume and chest movement signals, respectively. *Bottom*: Tidal volume of each respiration phase computed as the absolute difference between the volumes at two consecutive breath-phase onsets.

The Wigner-Ville distribution (WVD) belongs to the Cohen's class of bilinear time-frequency representations [28]; it possesses several interesting properties, and in particular provides the highest time-frequency resolution. The main limitation of the WVD is the presence of cross-terms that obscure its readability, and several techniques have been proposed to reduce the number of cross-terms; however, there is a tradeoff between the amount of cross-term interference and the time-frequency resolution. The spectrogram is one such attempt, a joint time-frequency smoothing window is applied and hence the performance in one direction is enhanced at the expense of degrading the performance in the other. In contrast, the SPWVD employs independent time and frequency smoothing windows [29], as follows:

$$SPWVD(t,f) = \int_{-\infty}^{\infty} h(\tau) \int_{-\infty}^{\infty} g(\eta - t) s\left(\eta + \frac{\tau}{2}\right) s^*\left(\eta + \frac{\tau}{2}\right) d\eta e^{-j2\pi f\tau} d\tau \quad (5)$$

where *s(t)* is the signal under analysis, *g(·)* is the time smoothing window, and *h(·)* is the frequency smoothing window in the time-domain [30].

The SPWVD was applied to the volume and chest movement signals. The SPWVD was computed using *NFFT*=1024 frequency bins, a 5.12 second Hamming window as the time smoothing window, and a 10.24 second Hamming window as the frequency smoothing window. After computing, the SPWVD was normalized between [0-1]. The Welch modified periodogram was used to compute the spectrum of the whole maneuver in order to obtain the central or average respiration frequency as the maximum spectral peak. The periodogram was computed using 50% overlap, 512 frequency bins, and a Hamming window. Then, at each time instant the maximum peak around the central frequency was computed and the frequency at which that maximum occurs was regarded as the respiration frequency at that instant, so that a vector of instantaneous respiration frequency was returned from each SWPVD. The frequency vector extracted from the spirometer-based volume was regarded as the reference instantaneous respiration frequency and was compared against the frequency vector extracted from the corresponding smartphone-based chest movement signal. All instantaneous respiration frequencies were converted from hertz to bpm to obtain IRR.

Similar to V_T estimation, the performance of IRR estimation using the smartphone-acquired chest movement signal was tested using three performance indices by considering the IRR from spirometer-acquired volume as reference: the root-mean-squared error RMSE, the normalized root-mean-squared error NRMSE, and the cross-correlation index ρ defined as follows

$$\rho = \frac{\sum_{i=1}^{N}\left(\mathrm{IRR}_{\mathrm{spirometer}}(i) \cdot \mathrm{IRR}_{\mathrm{smartphone}}(i)\right)}{\sqrt{\sum_{i=1}^{N}\left(\mathrm{IRR}_{\mathrm{spirometer}}(i)\right)^2 \cdot \sum_{i=1}^{N}\left(\mathrm{IRR}_{\mathrm{smartphone}}(i)\right)^2}} \quad (6)$$

where $IRR_{spirometer}$ indicates the IRR obtained from the spirometer-acquired volume, $IRR_{smartphone}$ is the IRR estimated from smartphone-acquired chest movements, and *N* is the number of samples of the analyzed signal, *i.e.*, time instants. RMSE and NRMSE were computed via Equations (3) and (4), by replacing the V_T values at each breath-phase by the IRR values at each time instant.

5.3 Results

The smartphone-acquired chest movement signal showed temporal amplitude variation related to the volume from spirometer during the breathing maneuver as shown in Figure 5.2 and more evidently in Figure 5.3 after detrending. In the following subsections we present the results in terms of tidal volume estimation and instantaneous respiration rate estimation using this smartphone-acquired chest movement signal. The distribution of the number of breathing cycles, average V_T, and average RR performed by volunteers during the breathing maneuvers are shown in Table 5.1. As can be seen, the maneuvers included a wide range of breathing cycles, rates and depths.

5.3.1 Tidal Volume Estimation using Smartphone Camera Signal

Figure 5.4 shows the relationship between the absolute peak-to-peak amplitude of smartphone-acquired chest movement acquired and the reference V_T acquired with the spirometer for each breath phase of the maneuver performed by one volunteer. As shown in this figure, the amplitude differences of smartphone-based chest movement signals linearly correlate to reference V_T from the spirometer. The regression parameter r^2 between the absolute peak-to-peak amplitude of chest movement and reference V_T was computed for all breath-phases of each volunteer (r^2=0.951 ± 0.042, mean ± SD). The corresponding boxplot for all volunteers is also shown in Figure 5.4. Strong linear relationship (r^2>0.9) was found between the smartphone-based amplitude measurements and the reference V_T from spirometer, as tested via a one-sample Wilcoxon signed rank test (p=6.41x10-4) after the normality assumption did not hold (one-sample Kolmogorov-Smirnov test, p=0.002).

Table 5.1 – Distribution of breathing cycles, tidal volume and respiration rate measured by spirometer during breathing maneuvers (*N*=15 volunteers).

Parameter		Min	Max	Average
Breathing cycles	[*cycles*]	16	51	31.40 ± 10.25
Maneuver tidal volume	[*L*]	0.24 ± 0.11	3.11 ± 0.67	1.32 ± 0.26
Maneuver respiration rate	[*bpm*]	11.08 ± 3.69	35.45 ± 13.04	17.12 ± 5.28

Values presented as mean ± standard deviation

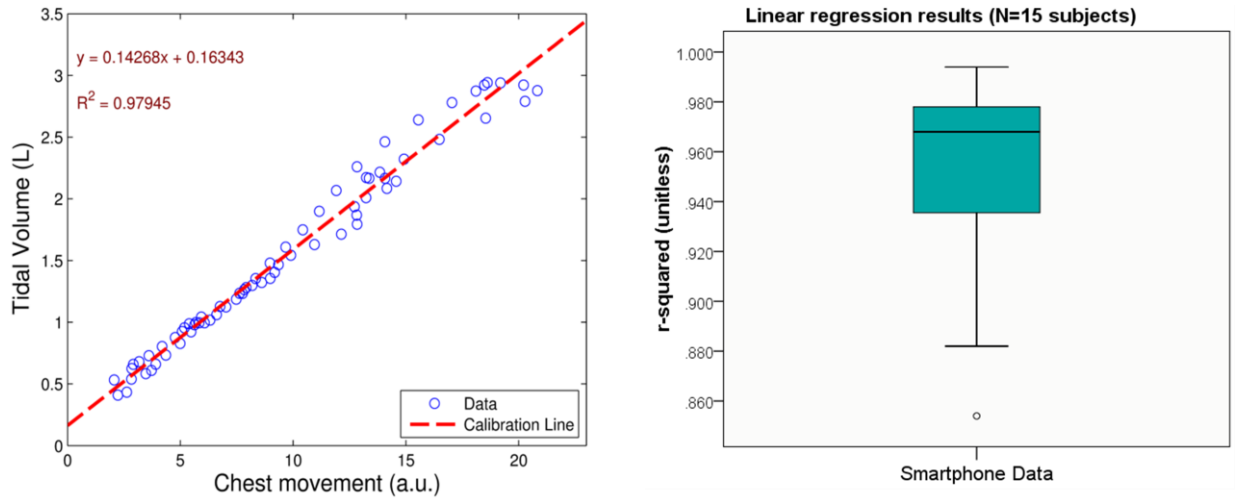

Figure 5.4 - Least-squares linear regression between the chest movement amplitude differences from smartphone and reference tidal volume from spirometer.
Left: Example of regression for all data from one volunteer. *Right*: Boxplot of r^2 regression parameter for all volunteers.

An example of the V_T estimation procedure from smartphone-acquired data is shown in Figure 5.5. From left to right, the first two plots of Figure 5.5 correspond to the calibration process using the training data set, and the testing process using the remaining randomly-selected breath-phase data points, respectively. The calibration parameters were computed via least-squares linear regression. The middle plot shows the corresponding smartphone-based V_T estimates, after using the calibration parameters, next to the corresponding spirometer V_T values for each breathing phase of the maneuver of one volunteer. Below these estimates, the bottom plot shows the corresponding error differences with respect to the reference V_T from spirometry are displayed.

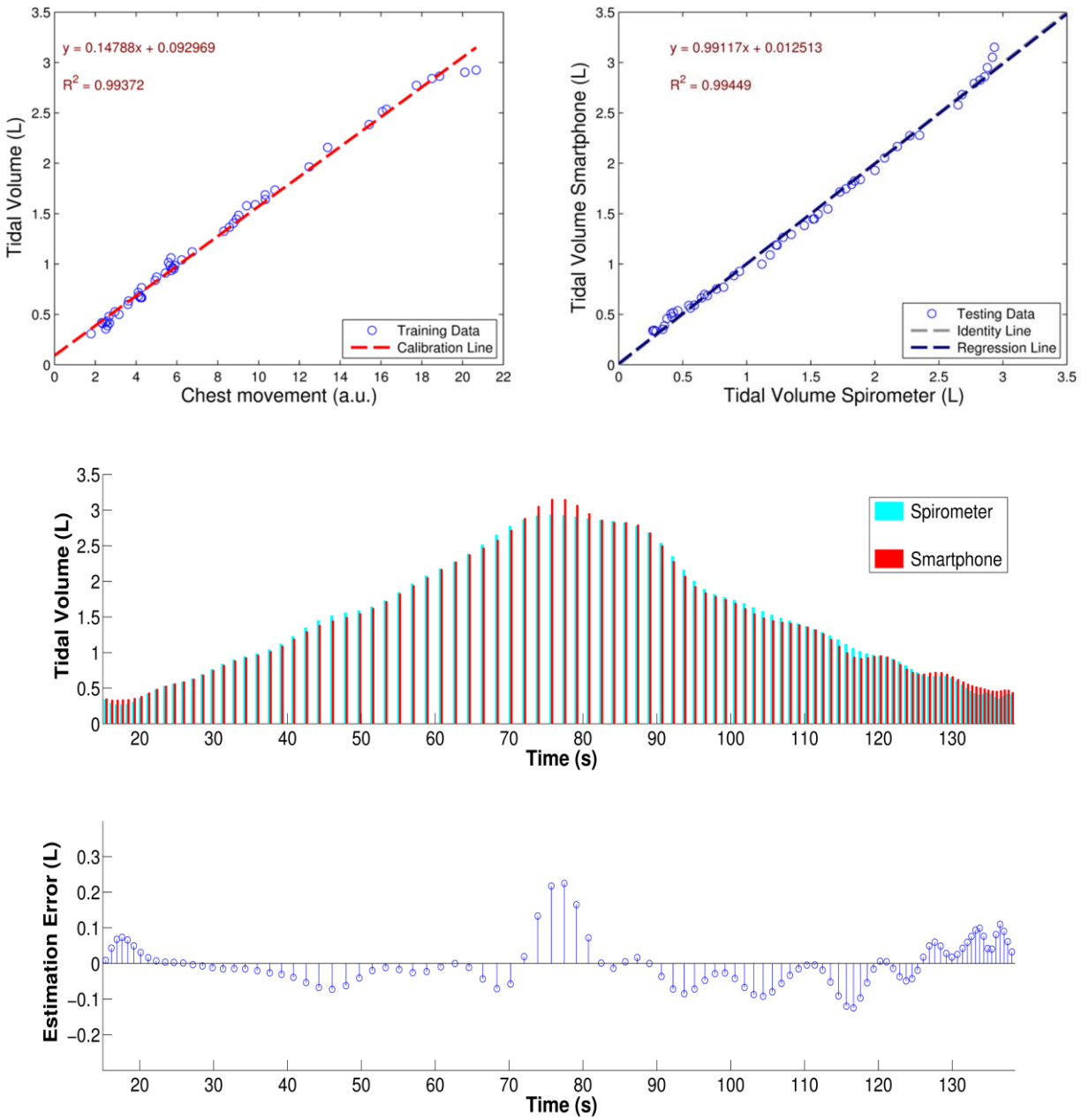

Figure 5.5 – Example of tidal volume estimation using smartphone for one volunteer.
Top Left: Calibration curve between chest movement amplitude differences from smartphone and tidal volume from spirometer for half of data randomly selected as training data. *Top Right*: Linear regression between smartphone-estimated tidal volume, after applying the calibration linear model, and reference tidal volume for the remaining half. *Middle*: Estimated tidal volumes from smartphone throughout the whole breathing maneuver and the corresponding true volumes from spirometer. *Bottom*: Corresponding differences between tidal volume derived from smartphone and reference tidal volume from spirometer throughout the whole breathing maneuver.

The performance indices for smartphone-based V_T estimation are presented in Table 5.2 for the testing data set of all the volunteers, using the spirometer measurements as reference. The linear regression results shown in Figure 5.5, for one volunteer, hold for all volunteers, as shown in Figure 5.6, when a linear regression was applied to all the V_T estimates from all volunteers. The figure also presents the corresponding Bland-Altman plot. We found that when calibrated on a subject-by-subject basis, the smartphone-based V_T estimation produced a bias of 0.014 liters and a standard deviation of 0.185 liters, however the bias was not found to be statistically significant from a zero bias. Accordingly, the 95% limits of agreements were -0.348 to 0.376 liters.

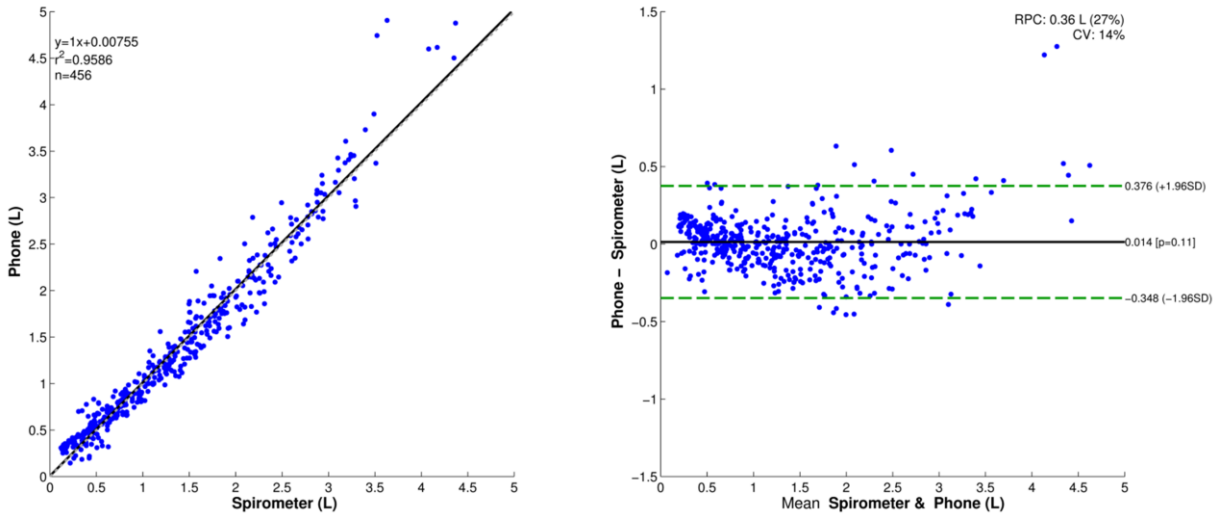

Figure 5.6 – Tidal volume estimation using smartphone (*N*=15 volunteers).
Left: Regression curve. Grey dashed line indicates the identity line and the solid black the regression line. *Right*: Bland-Altman plot. Solid black line indicates the bias and dashed green lines indicate the 95% limits of agreement.

Table 5.2 – Results of tidal volume estimation using smartphone-acquired chest movement signals compared to the reference volume from the spirometer (*N*=15 volunteers).

Parameter		Values		
r^2	[*unitless*]	0.961	±	0.026
RMSE	[*L*]	0.182	±	0.107
NRMSE	[*%*]	14.998	±	5.171

Values presented as mean ± standard deviation

5.3.2 Instantaneous Respiration Rate Estimation using Smartphone Camera Signal

Figure 5.7 shows an example of IRR estimation via the SPWVD technique applied to volume from the spirometer and chest movements from the smartphone for the respiration maneuver of one volunteer. The superimposed white dashed curve indicates the frequency at which the maximum energy of the SPWVD occurs at each time instant. Side-by-side comparison of the extracted IRR from spirometer and smartphone signals is also presented.

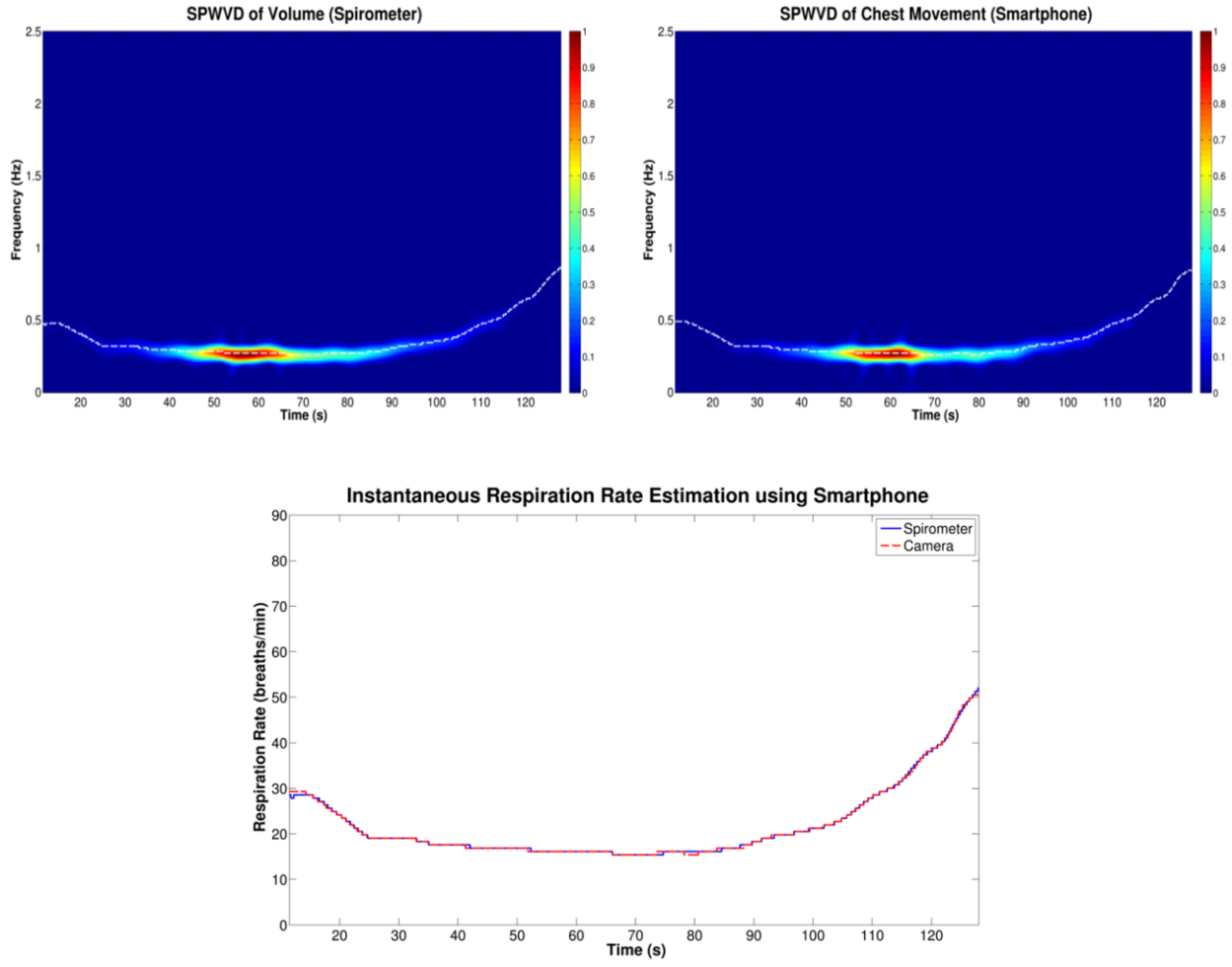

Figure 5.7 - Example of IRR estimation using smartphone-acquired chest movement signals.
Top left: SPWVD of the volume signal from the spirometer. *Top right*: SPWVD of the chest movement signal from smartphone. White dashed lines indicate the maximum peak at each time instant. Bottom: Instantaneous respiration rate computed from corresponding SPWVD of volume and chest movement signals.

Table 5.3 presents the performance indices of smartphone-based IRR estimation for all volunteers, using the spirometer values as reference. High cross-correlation coefficients were found between the IRR smartphone-based estimates and volume from spirometer. Figure 5.8 reflects this high correlation as shown by the regression line parameters (r^2=0.9973). The corresponding Bland-Altman plot is also presented in Figure 5.8. Compared to the spirometer, the bias ± standard deviation and the 95% limits of agreement were -0.024 ± 0.421 bpm and -0.850 to 0.802 bpm, respectively, in the range of approximately 7 to 50 bpm.

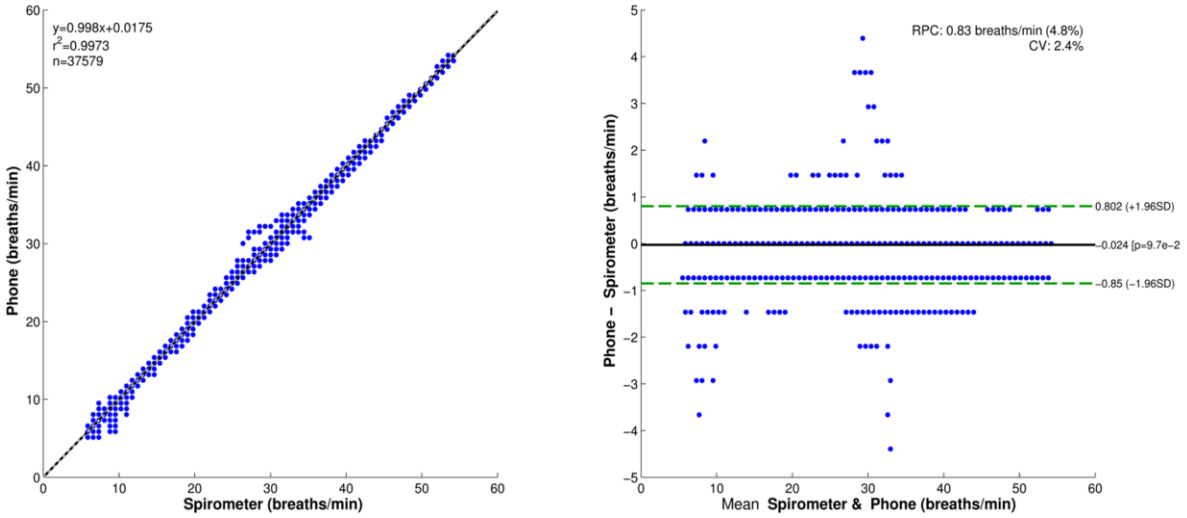

Figure 5.8 - Instantaneous respiration rate estimation using smartphone (*N*=15 volunteers).
Left: Calibration curve. Grey dashed line indicates the identity line and the solid black the calibration line. *Right*: Bland-Altman plot. Solid black line indicates the bias and dashed green lines indicate the 95% limits of agreement.

Table 5.3 – Results of the instantaneous respiration rate estimation using smartphone-acquired chest movement signal compared to volume signal from spirometer (*N*=15 volunteers).

Parameter		Values		
ρ	[*unitless*]	0.9992	±	0.0019
RMSE	[*bpm*]	0.414	±	0.178
NRMSE	[*%*]	3.031	±	2.873

Values presented as mean ± standard deviation

5.4 Discussions and Conclusions

In this dissertation we propose a smartphone-based respiration monitoring system for both instantaneous respiration rate estimation and tidal volume estimation via an algorithm that tracks chest movement directly from a smartphone's camera. The HTC One M8 Android smartphone was used in this dissertation and the algorithm was implemented in this device so that recordings of the chest movement signals were made directly on the phone. Together with this smartphone signal, airflow and volume signals were recorded with a spirometer and the latter was used as reference for IRR and V_T estimation. Recordings from fifteen healthy volunteers were obtained in a regular dry lab illuminated with fluorescent light while the volunteers were standing still and breathing at tidal volumes ranging from 300 mL to 3 L. Volunteers wore clothes with different colors and patterns. The developed algorithm can still detect the chest movements even if single color clothes are worn.

There have been several efforts to develop monitors that provide information about breathing status via optical approaches [19]–[25], most of them monitoring only average RR. In our previous study, we implemented an algorithm that is able to track chest movements directly on a smartphone and found promising results in terms of average RR estimation [31]. That study provided motivation to explore whether information beyond the average RR can be obtained from the smartphone-acquired chest movement signal. In particular, it appeared that the smartphone app provided a signal whose peak-to-peak amplitude was an indicator of the tidal volume of the volunteers. This hypothesis was corroborated in this dissertation as exemplified in the recorded reference volume and chest movement signals, especially after detrending to remove existing drift in both signals. We also analyzed the correlation of the peak-to-peak amplitude of smartphone-acquired signals with the corresponding reference V_T acquired via a spirometer, and we found that a strong correlation existed between both measurements (r^2=0.951 ± 0.042, mean ± SD). Given these correlation results, for each volunteer we randomly selected 50% of the data points for training the linear model during the calibration process, and the remaining 50% of the data for testing the V_T estimation based on the computed model. Once calibrated on an individual basis using

the reference volume signal, when we mapped the chest movement amplitude differences at each breath-phase of the testing data set, we found an RMSE of 0.182 ± 0.107 liters which corresponded to 14.998 ± 5.171 % when normalized to the mean value of the reference V_T of the testing data set of the maneuver. Overall, we found that a linear regression model fitted well the calibrated peak-to-peak amplitude of smartphone signals for the task of V_T estimation ($V_{Tsmartphone}$=1.005·$V_{Tspirometer}$+0.008). We did not find statistically-significant bias in the V_T estimation using smartphones and the 95% limits of agreement were -0.348 to 0.376 liters. At this point we do not know if this difference in tidal volume can be acceptable for monitoring breathing status to make it comparable to spirometer. Other popular methods for tidal volume estimation also suffer from high estimation errors, for example respiratory inductance plethysmography (RIP), where even when calibration is performed according to the manual (usually stating that 10% error difference is acceptable), it is common to have much higher errors when measuring. Researchers have reported these findings with respect to errors, *e.g.*, in reference [4] a bias and 95% limits of agreement in RIP sensors of approximately 0.4 L, and -0.3 to 1.1 L for a breathing range of 360 mL to 3.5 L, were found. As noticed, that error using RIP is even higher than reported in this dissertation using smartphones. As stated by other authors, in order for two instruments to be comparable, they should lead to same actions and decisions regarding the subject. We recognize that this is just an initial step and further studies are required to analyze the relevance of this and similar efforts.

By taking advantage of the high correlation between detrended smartphone signals and volume from the spirometer, we analyzed using the smartphone signal for the task of RR estimation at each time instant. Due to the time-varying characteristics of the signals, we employed the smoothed pseudo Wigner-Ville distribution. We found high correlation between the smartphone-based IRR estimates and the spirometer-based values (r^2=0.9992 ± 0.0019). We found an RMSE of 0.414 ± 0.178 bpm which corresponds to an NRMSE of 3.031 ± 2.783 %. The linear relationship between IRR estimated from the smartphone and IRR from reference volume was IRRsmartphone=0.9980·IRRspirometer+0.0175. The 95% limits of agreement ranged from -0.850 to 0.802 bpm, while there was a statistically-significant bias of -0.024 bpm. Other studies have reported the estimation of respiratory rate using noncontact optical

approaches, *e.g.*, in [19] the bias and standard deviation were found to be 0.19 bpm and 2.46 bpm, respectively, in the range of approximately 10-70 bpm, in [21] the RMSE, bias, and standard deviation were 1.28 bpm, 0.12 bpm, and 1.33 bpm, respectively, in the range of approximately 10-22 bpm, in [22] the RMSE, bias and 95% limits of agreement were 1.20 bpm, 0.02 bpm, -2.40 to 2.45 bpm, respectively, in the range of approximately 10-24 bpm; while in [25] the RMSE, bias, and 95% limits of agreement were found to be 0.09 bpm, -0.02 bpm, and -1.69 to 1.65 bpm, respectively in the range of approximately 7-24 bpm. Interestingly, the results reported in [25] during the night conditions outperformed those mentioned above during daylight conditions. Although a straightforward comparison is not possible due to the differences in the measurement devices and ranges tested, in general, note that the proposed noncontact optical monitoring of respiratory rate based on smartphones performs as well as, if not outperforms, that reported in the abovementioned literature.

Limitations of this dissertation include the recording of the breathing maneuvers while the subjects were standing still, *i.e.*, the subjects were instructed not to move. As found in other noncontact optical approaches, the main challenge comes from motion artifacts, especially when both the volumetric surrogate signal obtained from the chest wall movements and the motion artifacts lie in a similar low frequency range (<2 Hz). Hence, it is expected that motion artifacts deteriorate the performance of the smartphone-based breathing estimates. Implementation of body tracking and artifact removal schemes similar to the ones reported in the literature to improve respiratory rate estimation [22], [32] are expected to reduce the effect of body motion not related to the breathing maneuver. Implementation and testing of such algorithms in the smartphone for breathing monitoring, especially for the task of tidal volume estimation, should be explored in future studies.

Another major challenge regards the variations of the ambient illumination at different times of the day due to fluctuations in the amount of sunlight, for example. The experiments presented here were performed at different times of the day and while the main illumination source came from the ceiling fluorescent lamps, the window shades of the laboratory were kept open or closed accordingly to the needs of its users. Despite that we did not noticed that these variations disturbs the acquisition of the volumetric

surrogate signal, perhaps due to the dominance of the fluorescent source, we recognize that systematic studies must analyze the performance of the proposed system in different levels of ambient illumination as well as to explore ways to account for these illumination variations.

The chest wall area of interest monitored during the breathing maneuver also represents another limitation. Classically, chest wall movements are attributed to two mechanical degrees of freedom due to contributions from rib cage and abdomen, which can be used to estimate tidal volume [26]. Although 1D or 2D displacements of these two compartments account for the majority of tidal volume, the algorithm ignores systematic effects of rib cage distortions [20]. In this dissertation, the chest movement signal used as volume surrogate was extracted from an image's rectangular area centered on the anterior chest wall portion of the volunteer that visually provided the most dominant displacements while breathing. Accordingly, our approach ignores those small contributions due to rib cage distortions and only constructs the chest movement signal from the chest wall displacements monitored by the camera.

It is also expected that postural changes and airway obstruction impact the performance of the estimates as it has been found in other breathing monitoring techniques [33], [34]. Changes of postures can modify the contribution of the rib cage and abdomen compartments to tidal volume. A decreased rib cage excursion and an increased abdominal excursion have been found in the supine position compared to the sitting or standing postures [35], [36]. Accordingly, it is likely that another area of the thorax would provide a stronger surrogate signal when monitoring breathing in the supine position.

Another limitation regards the restriction given to the subjects of not wearing loose clothes during the experiments. As pointed out by other researchers, if the clothes are not tight to the subject's body a weak breathing-related signal might be obtained using the noncontact optical monitoring approach. Note that this is also the case in other breathing monitoring methods based on chest wall displacements, like inductance plethysmography, where the sensors are recommended to be worn over bare skin or ultimately tight clothes. Observe that in general, the noncontact optical approach looks for changes in the light intensity due to the modification of the path length caused by breathing displacements of the chest wall, not limited to movements of clothes features. To this end, the authors have been able to obtain volume

surrogate signals using the smartphone method proposed here by monitoring subject's bare skin but a systematic study is required to analyze the effect of wearing loose, tight and not wearing top clothes. Finally, at this research point, note that to estimate tidal volume via the smartphone's camera, the measurement conditions should match those during which calibration was performed. Although we found that a linear model fitted well between peak-to-peak amplitude of chest movement signals from a smartphone and tidal volume from a spirometer, so that it can be used to calibrate the smartphone measurements to obtain tidal volume on an individual basis, a new calibration should be performed prior to acquisition if the subject's chest wall position monitored by the smartphone's camera displaces with respect to the one used for calibration. Other tidal volume estimation techniques suffer similar issues, *e.g.,* displacement of elastic belts wrapped around the rib cage and abdomen from the position employed when calibration was performed deteriorates the performance of the measurements in inductance plethysmography.

Several monitoring techniques for breathing status in clinical and research settings currently exist. This dissertation and similar works are steps towards the developing of an inexpensive and mobile breathing monitoring system that can be translated outside research settings for on-demand health applications. By taking advantage of their ubiquity, smartphone-based systems could aid in the monitoring of breathing status of the general population, where this general practice remains unclear if we consider that these parameters are not always recorded on a daily basis even in clinical settings. The results obtained in this dissertation point out the feasibility of developing a mobile system being able to provide information about instantaneous respiration rate and tidal volume when calibrated on an individual basis. It is foreseen that when calibration is not possible to be performed, this smartphone approach could still be used as a qualitative indicator of changes in tidal volume due to the high correlation between the chest movement signal and tidal volume that reflects the major contribution of chest wall displacements to tidal volume. To this end, this dissertation reports our initial step towards the estimation of V_T from a surrogate signal obtained with a smartphone. We cannot make conclusions about

the robustness in terms of measurement conditions such as gender, body mass index or lighting conditions given the small sample size and conditions tested.

Currently, we are running a study regarding an easy-to-use calibration procedure that can be performed with an incentive spirometer (IS) with the potential to be translated outside research settings due to their availability and low cost. Briefly, by taking advantage of the high linear relationship between smartphone measurements and tidal volume, the calibration model is computed while breathing at only two reference volume points through the IS. Preliminary results have shown to be comparable to those presented in this dissertation which would allow a fast and easy-to-perform calibration procedure. In parallel, we are currently working on the implementation of the proposed signal processing techniques, currently developed for Android, on iOS to cover the two dominant smartphone operating systems. Future work of our research group includes study of body tracking and motion artifact algorithms to address some of the limitations mentioned above.

5.5 Acknowledgments

This work is supported in part by the US Army Medical Research and Material Command (US-AMRMC) under grant No. W81XWH-12-1-0541.

5.6 References

[1] F. Q. Al-Khalidi, R. Saatchi, D. Burke, H. Elphick, and S. Tan, "Respiration rate monitoring methods: A review," *Pediatr. Pulmonol.*, vol. 46, no. 6, pp. 523–529, Jun. 2011.

[2] M. Folke, L. Cernerud, M. Ekström, and B. Hök, "Critical review of non-invasive respiratory monitoring in medical care," *Med. Biol. Eng. Comput.*, vol. 41, no. 4, pp. 377–383, Jul. 2003.

[3] B. M. Koeppen and B. A. Stanton, *Berne & Levy Physiology, Updated Edition*. Elsevier Health Sciences, 2009.

[4] K. P. Cohen, W. M. Ladd, D. M. Beams, W. S. Sheers, R. G. Radwin, W. J. Tompkins, and J. G. Webster, "Comparison of impedance and inductance ventilation sensors on adults during breathing, motion, and simulated airway obstruction," *IEEE Trans. Biomed. Eng.*, vol. 44, no. 7, pp. 555–566, Jul. 1997.

[5] G. B. Drummond, A. F. Nimmo, and R. A. Elton, "Thoracic impedance used for measuring chest wall movement in postoperative patients.," *Br. J. Anaesth.*, vol. 77, no. 3, pp. 327–332, Sep. 1996.

[6] M. A. E. Ramsay, M. Usman, E. Lagow, M. Mendoza, E. Untalan, and E. De Vol, "The Accuracy, Precision and Reliability of Measuring Ventilatory Rate and Detecting Ventilatory Pause by

Rainbow Acoustic Monitoring and Capnometry:," *Anesth. Analg.*, vol. 117, no. 1, pp. 69–75, Jul. 2013.
[7] J. J. Vargo, G. Zuccaro Jr., J. A. Dumot, D. L. Conwell, J. B. Morrow, and S. S. Shay, "Automated graphic assessment of respiratory activity is superior to pulse oximetry and visual assessment for the detection of early respiratory depression during therapeutic upper endoscopy," *Gastrointest. Endosc.*, vol. 55, no. 7, pp. 826–831, Jun. 2002.
[8] K. Ashutosh, R. Gilbert, J. H. Auchincloss, J. Erlebacher, and D. Peppi, "Impedance pneumograph and magnetometer methods for monitoring tidal volume," *J Appl Physiol*, vol. 37, no. 6, pp. 964–966, 1974.
[9] P. Grossman, M. Spoerle, and F. H. Wilhelm, "Reliability of respiratory tidal volume estimation by means of ambulatory inductive plethysmography," *Biomed. Sci. Instrum.*, vol. 42, pp. 193–198, 2006.
[10] A. Johansson and P. P. Å. Öberg, "Estimation of respiratory volumes from the photoplethysmographic signal. Part I: experimental results," *Med. Biol. Eng. Comput.*, vol. 37, no. 1, pp. 42–47, Jan. 1999.
[11] Y. S. Lee, P. N. Pathirana, C. L. Steinfort, and T. Caelli, "Monitoring and Analysis of Respiratory Patterns Using Microwave Doppler Radar," *IEEE J. Transl. Eng. Health Med.*, vol. 2, pp. 1–12, 2014.
[12] G. Li, N. C. Arora, H. Xie, H. Ning, W. Lu, D. Low, D. Citrin, A. Kaushal, L. Zach, K. Camphausen, and R. W. Miller, "Quantitative prediction of respiratory tidal volume based on the external torso volume change: a potential volumetric surrogate," *Phys. Med. Biol.*, vol. 54, no. 7, pp. 1963–1978, Apr. 2009.
[13] M. R. Miller, J. Hankinson, V. Brusasco, F. Burgos, R. Casaburi, A. Coates, R. Crapo, P. Enright, C. P. M. van der Grinten, P. Gustafsson, and others, "Standardisation of spirometry," *Eur. Respir. J.*, vol. 26, no. 2, pp. 319–338, 2005.
[14] C.-L. Que, C. Kolmaga, L.-G. Durand, S. M. Kelly, and P. T. Macklem, "Phonospirometry for noninvasive measurement of ventilation: methodology and preliminary results," *J. Appl. Physiol. Bethesda Md 1985*, vol. 93, no. 4, pp. 1515–1526, Oct. 2002.
[15] O. Sayadi, E. H. Weiss, F. M. Merchant, D. Puppala, and A. A. Armoundas, "An Optimized Method for Estimating the Tidal Volume from Electrocardiographic Signals: Implications for Estimating Minute Ventilation," *Am. J. Physiol. - Heart Circ. Physiol.*, vol. 307, pp. H426–H436, 2014.
[16] B. J. Semmes, M. J. Tobin, J. V. Snyder, and A. Grenvik, "Subjective and objective measurement of tidal volume in critically ill patients.," *Chest*, vol. 87, no. 5, pp. 577–579, 1985.
[17] R. Gilbert, J. H. Auchincloss, J. Brodsky, and W. Boden, "Changes in tidal volume, frequency, and ventilation induced by their measurement.," *J. Appl. Physiol.*, vol. 33, no. 2, pp. 252–254, Aug. 1972.
[18] B. A. Reyes, N. Reljin, and K. H. Chon, "Tracheal Sounds Acquisition Using Smartphones," *Sensors*, vol. 14, no. 8, pp. 13830–13850, Jul. 2014.
[19] M. Bartula, T. Tigges, and J. Muehlsteff, "Camera-based system for contactless monitoring of respiration," in *2013 35th Annual International Conference of the IEEE Engineering in Medicine and Biology Society (EMBC)*, 2013, pp. 2672–2675.
[20] S. J. Cala, C. M. Kenyon, G. Ferrigno, P. Carnevali, A. Aliverti, A. Pedotti, P. T. Macklem, and D. F. Rochester, "Chest wall and lung volume estimation by optical reflectance motion analysis," *J. Appl. Physiol.*, vol. 81, no. 6, pp. 2680–2689, Dec. 1996.
[21] M.-Z. Poh, D. J. McDuff, and R. W. Picard, "Advancements in Noncontact, Multiparameter Physiological Measurements Using a Webcam," *IEEE Trans. Biomed. Eng.*, vol. 58, no. 1, pp. 7–11, Jan. 2011.
[22] D. Shao, Y. Yang, C. Liu, F. Tsow, H. Yu, and N. Tao, "Noncontact Monitoring Breathing Pattern, Exhalation Flow Rate and Pulse Transit Time," *IEEE Trans. Biomed. Eng.*, vol. 61, no. 11, pp. 2760–2767, Nov. 2014.

[23] L. Tarassenko, M. Villarroel, A. Guazzi, J. Jorge, D. A. Clifton, and C. Pugh, “Non-contact video-based vital sign monitoring using ambient light and auto-regressive models,” *Physiol. Meas.*, vol. 35, no. 5, p. 807, 2014.
[24] H.-Y. Wu, M. Rubinstein, E. Shih, J. Guttag, F. Durand, and W. Freeman, “Eulerian Video Magnification for Revealing Subtle Changes in the World,” *ACM Trans Graph*, vol. 31, no. 4, pp. 65:1–65:8, Jul. 2012.
[25] F. Zhao, M. Li, Y. Qian, and J. Z. Tsien, “Remote Measurements of Heart and Respiration Rates for Telemedicine,” *PLoS ONE*, vol. 8, no. 10, p. e71384, Oct. 2013.
[26] K. Konno and J. Mead, “Measurement of the separate volume changes of rib cage and abdomen during breathing,” *J. Appl. Physiol.*, vol. 22, no. 3, pp. 407–422, Mar. 1967.
[27] N. E. Huang, Z. Shen, S. R. Long, M. C. Wu, H. H. Shih, Q. Zheng, N.-C. Yen, C. C. Tung, and H. H. Liu, “The empirical mode decomposition and the Hilbert spectrum for nonlinear and non-stationary time series analysis,” *Proc. R. Soc. Lond. Ser. Math. Phys. Eng. Sci.*, vol. 454, no. 1971, pp. 903–995, 1998.
[28] L. Cohen, “Time-frequency distributions-a review,” *Proc. IEEE*, vol. 77, no. 7, pp. 941–981, Jul. 1989.
[29] W. Martin and P. Flandrin, “Wigner-Ville spectral analysis of nonstationary processes,” *IEEE Trans. Acoust. Speech Signal Process.*, vol. 33, no. 6, pp. 1461–1470, Dec. 1985.
[30] F. Hlawatsch, T. G. Manickam, R. L. Urbanke, and W. Jones, “Smoothed pseudo-Wigner distribution, Choi-Williams distribution, and cone-kernel representation: Ambiguity-domain analysis and experimental comparison,” *Signal Process.*, vol. 43, no. 2, pp. 149–168, May 1995.
[31] Y. Nam, Y. Kong, B. Reyes, N. Reljin, and K. H. Chon, “Monitoring of Heart and Respiratory Rates using Dual Cameras on a Smartphone,” vol. In revision, 2015.
[32] Y. Sun, S. Hu, V. Azorin-Peris, S. Greenwald, J. Chambers, and Y. Zhu, “Motion-compensated noncontact imaging photoplethysmography to monitor cardiorespiratory status during exercise,” *J. Biomed. Opt.*, vol. 16, no. 7, pp. 077010–077010, 2011.
[33] T. M. Baird and M. R. Neuman, “Effect of infant position on breath amplitude measured by transthoracic impedance and strain gauges,” *Pediatr. Pulmonol.*, vol. 10, no. 1, pp. 52–56, 1991.
[34] M. J. Tobin, S. M. Guenther, W. Perez, and M. J. Mador, “Accuracy of the respiratory inductive plethysmograph during loaded breathing,” *J Appl Physiol*, vol. 62, no. 2, pp. 497–505, 1987.
[35] V. P. Vellody, M. Nassery, W. S. Druz, and J. T. Sharp, “Effects of body position change on thoracoabdominal motion,” *J. Appl. Physiol.*, vol. 45, no. 4, pp. 581–589, Oct. 1978.
[36] W. S. Druz and J. T. Sharp, “Activity of respiratory muscles in upright and recumbent humans,” *J. Appl. Physiol.*, vol. 51, no. 6, pp. 1552–1561, Dec. 1981.

Chapter 6: Calibration via an Incentive Spirometer for Smartphone-based Tidal Volume Estimation from Optical Approach

(B. A. Reyes, N. Reljin, Y. Kong, Y. Nam, S. Ha, and K. H. Chon, "Calibration via an Incentive Spirometer for Smartphone-based Tidal Volume Estimation"; Under revision, December 2015)

6.1 Introduction

Tidal volume (V_T) provides information about the breathing depth and is defined as the volume of air moved with each breath. V_T value is around 0.5 L but is not fixed as the mechanism of respiratory control adjust it together with respiratory rate (RR) in response to different scenarios, *e.g.*, exercise or sleep, to deal with body's requirements [1]. Several clinical and research methods currently exist to estimate V_T [2]–[10]. However, these methods have been designed for clinical or research centers and hence they are not easily translated to everyday use due to the employment of specialized devices, high costs, need for skilled operators, or limited mobility.

An interesting approach to develop a system that overcome some of the abovementioned limitations consists in the optical monitoring of breathing status by means of general purpose video cameras. Although most of efforts in this area have focused on estimate the RR [11]–[16], there have been also studies to estimate V_T [17]–[20]. Recently, a volume conservation hypothesis was proposed and validated by establishing a one-to-one linear relationship between changes of the external torso volume and V_T corresponding to internal lung air content [6]. Those findings validates previous studies that found accurate V_T estimation results by tracking markers placed on the chest wall surface via an optical reflectance system [17], [18]. Although promising, the use of former system is not widely available to the general population. More recently, a good correlation (r^2=0.81) between shoulder displacements obtained by processing webcam video recordings and exhaled breath volume measured with a commercial metabolic analysis device was obtained [19]. Besides the promising results, analysis in terms of V_T estimation was limited to the correlation between the video amplitudes and reference

volumes. In addition, the implementation was done in a personal computer and with the aid of an external digital camera.

Current smartphones are attractive for developing monitoring systems with ubiquitous and mobile characteristics. Accordingly, their applications have been found to be accurate in a diversity of vital signs monitoring applications [21]–[24]. Recently, our research group proposed a dual approach consisting of contact and noncontact monitoring directly implemented on a smartphone for the tasks of heart rate (HR) and average RR estimation, respectively [16]. In turn, the algorithm for the noncontact approach provided a waveform whose amplitude increased with deeper breaths. Accordingly, in a subsequent study we analyzed the employment of the non-contact algorithm for the task of V_T estimation and tracking of RR at each time instant [20]. We found that the peak-to-peak amplitude of the smartphone-acquired chest movement signal was highly correlated with the V_T from spirometer regarded as reference (r^2=0.951 ± 0.042, mean ± SD). We found that when calibrated on an individual basis, the root-mean-squared error was 0.182 ± 0.107 L equivalent to 14.998 ± 5.171 % when normalized. Besides this former effort, we are not aware of a smartphone-based system for V_T estimation using a noncontact optical approach together with an algorithm directly implemented on a smartphone. However, we recognize that in order to be used outside research and clinical settings by the general population a simple calibration procedure that does not employ a specialized device is required.

In this dissertation we propose a calibration procedure using a volume-oriented incentive spirometer (IS) for the task of V_T estimation from the smartphone-acquired chest movement signal. To this end, we computed the V_T estimates after calibration from data computed while breathing through an IS, and compared them to simultaneously acquired volume from a spirometer as reference. The performance of the V_T estimation from the proposed calibration via IS was also compared to the best estimation that could be obtained via linear regression between reference volume and smartphone data. The smartphone application used in this dissertation was implemented in a commercially available Android smartphone. Its main screens used for V_T estimation are presented.

6.2 Material and Methods

6.2.1 Subjects

Twelve (*N*=12) healthy and non-smoker volunteers (eleven males) aged 27.7 ± 9.5 years (mean ± standard deviation), weight 71.6 ± 7.8 kg, and height 174.5 ± 6.0 cm, were recruited for this study. Individuals with previous pneumothorax, those with chronic respiratory illnesses such as asthma, and anyone who was currently ill with the common cold or an upper respiratory infection were excluded from this study. Each volunteer consented to be a subject and signed the study protocol approved by the Institutional Review Board of University of Connecticut (UConn, Storrs, CT, USA).

6.2.2 Signals Acquisition

Equipment

The algorithm for recording the chest movement signal was implemented in a HTC One M8 smartphone (HTC Corporation, New Taipei City, Taiwan) running the Android v4.4.2 operating system. The frontal camera of this smartphone was used and consisted of a 5 MP, backside-illumination sensor with wide angle lens and 1080p full HD video recording capabilities at 30 frames-per-second. The implemented app processed the video data in real time to obtain the chest movement signal used for estimation of V_T. Collected data were saved into a text file for offline analysis of results in Matlab (R2012a, The Mathworks, Natick, MA, USA).

To test the smartphone-based V_T estimates, a reference volume signal was collected with a spirometer system consisting of a respiration flow head connected to a differential pressure transducer to the measure airflow signal (MLT1000L, FE141 Spirometer, ADInstruments, Dunedin, New Zealand). The integral of the airflow over time was computed to generate the volume signal. Both the airflow and volume signals were sampled at 1 kHz using a 16-bit A/D converter (PowerLab/4SP, ADInstruments). Prior recording, the spirometer system was calibrated using a 3.0 L calibration syringe (Hans Rudolph, Inc., Shawnee, KS, USA). Each volunteer was provided with a new set consisting of a disposable filter,

mouthpiece, and nose clip (MLA304, MLA1026, MLA1008, ADInstruments). For calibration of the smartphone-based V_T estimates, a new volumetric incentive spirometer (IS) was provided to each volunteer (AirlifeTM, Carefusion, Yorba Linda, CA, USA).

Breathing Maneuvers

Each experiment consisted of two phases with the corresponding maneuvers as follows:

I. *Calibration maneuver*. Volunteers were asked to breathe four times through the IS at the first target of 250 mL, hold their breath for a couple seconds, and finally breathe four times through the IS at the second target of 500 mL.

II. *Test breathing maneuver*. Volunteers were asked to hold their breaths for a couple seconds, take a deep breathing, and then breathe through the spirometer system at different volume levels ranging from around 200 mL to 2.5 L; first increasing their V_T with each breath for around one minute, and finally decreasing their V_T with each breathe for another minute. Subjects breathed at their own pace, *i.e.*, we did not use a metronome to control their respiratory frequency. Reference volume was recorded for this maneuver using spirometry.

Data from the calibration maneuver was used to compute the calibration model for the smartphone-based V_T estimates. As seen in Figure 6.1, the IS we used has increments of 250 mL, a volume indicator, and a flow rate guide. Volunteers were asked to hold the IS in its upright position and then breathe through the mouthpiece of the IS so that at each inspiration the top of the volume indicator lined up with the corresponding target mark, while the flow rate indicator was kept in between the two arrow guides to maintain an adequate inspiration speed as indicated in the manufacturer's manual. While the volunteers performed the calibration maneuver, the chest movement signal was recorded using the smartphone placed in front of the subject at approximately 60 cm in a 3-pronged clamp at their thoracic level. The smartphone application we developed allows a remote Start/Stop recording option via a generic Bluetooth® camera shutter (I Shutter, Shanghai, China).

The second (test) maneuver provided a wide range of V_T to test the computed calibration model. Simultaneous recording of the smartphone-based chest movement signal and spirometer-acquired reference volume was performed. The chest movement signal was recorded in the same manner as it had been for the calibration maneuver. Visual feedback was provided to the volunteers by displaying the reference volume on a 40" monitor placed in front of them, where visual marks were used to indicate the tidal volume's range of interest.

Both maneuvers were recorded in a regular dry lab using ambient light from ceiling fluorescent lamps. During both maneuvers, subjects were asked to stand still and not to change position in between maneuvers. Nose clips were used to clamp the nostrils during both maneuvers. During the experiments, volunteers worn different color/pattern of their clothes and were only asked not to wear loose clothes. An example of the acquisition setup is shown in Figure 6.1 for a subject breathing through the IS.

6.2.3 Smartphone Algorithm for Recording Chest Movements

The chest movement signal *I(t)* was computed in real time in the smartphone app by averaging the intensity within a rectangular region of interest (ROI) of the red, green and blue (RGB) channels at each time instant *t*, according to

$$I(t) = \left(\frac{1}{3D}\right)\left(\sum_{\{m,n\}\in ROI} i_R(m,n,t) + \sum_{\{m,n\}\in ROI} i_G(m,n,t) + \sum_{\{m,n\}\in ROI} i_B(m,n,t)\right) \quad (1)$$

where $i_x(m,n,t)$ is the intensity value of the pixel at the *m*-th row and *n*-th column of the RGB channel within the ROI containing a total of *D* pixels. The camera resolution was set to 320x240 pixels, and the ROI of 49x90 pixels was focused on the thoracic area of the volunteer. The sampling rate fluctuated around 25 frames-per-second during the real time monitoring. Hence, after stopping the recording, the recorded signal was cubic splined to obtain a uniform sampling rate of 25 Hz. Finally, a bandpass filtering was applied to the chest movement signal between 0.01 to 2 Hz using a 50^{th} order finite impulse response (FIR) filter, designed with a Hamming window, to minimize the high frequency components not

related to the breathing maneuvers and the trend in the signal. Both the cubic spline and bandpass filtering were performed in the smartphone app.

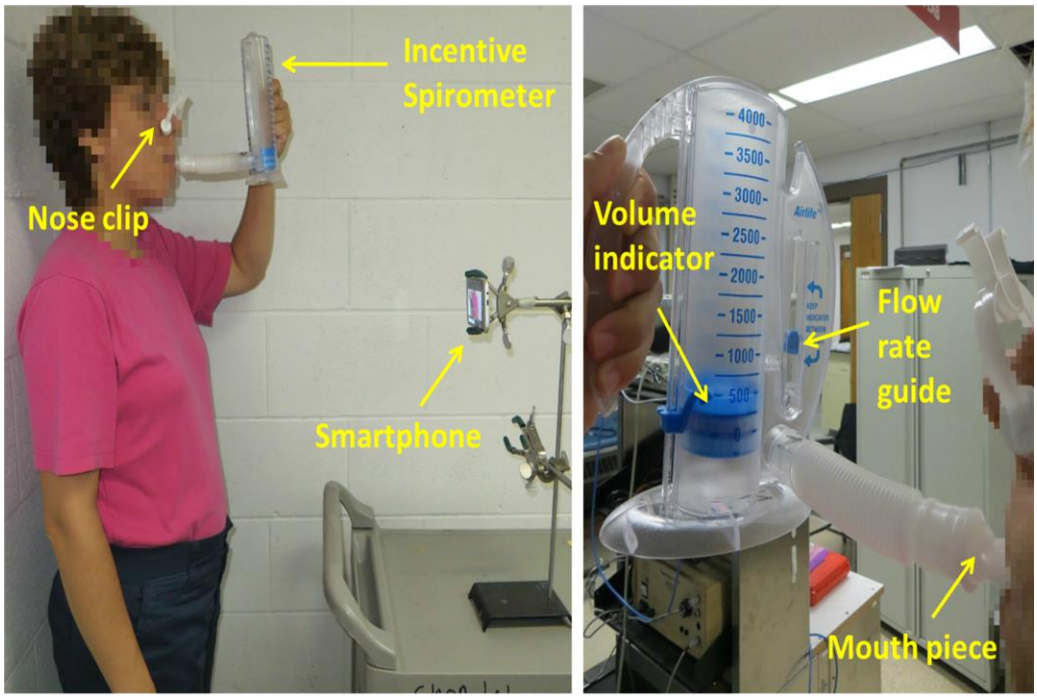

Figure 6.1 – Experimental setup to record the chest movements using the smartphone camera while volunteers breathe through an incentive spirometer (IS) for calibration.
Right: Detailed view of the IS while the subject is inspiring at to reach a volume target. Subjects were asked to inspire so that the top of the piston was lined up with the desired blue mark and at a rate that kept the indictor between the two blue guide arrows.

6.2.4 Data Preprocessing

Reference volume signal recorded during the second phase of the experiment was conditioned offline in Matlab. First, it was down-sampled to 25 Hz in to achieve the same sampling frequency as the corresponding chest movement signal, and then bandpass filtered using a 4th-order Butterworth bandpass between 0.01 to 2 Hz applied in a forward and backward scheme to produce zero-phase distortion and minimize the start and end transients.

Due to differences in the starting times and delays between the smartphone and spirometer systems, both types of simultaneous recorded signals were aligned using the initial breath holding and

deep inspiration portion and also by using the cross-correlation function, where 20 seconds in the central portion of the maneuver were extracted from each recording to compute the cross-correlation sequence and find the sample lag with the maximum cross-correlation value indicating the required samples to be shifted. Figure 6.2 shows an example of the acquired signals using smartphone and spirometer after alignment for the maneuvers performed by one subject.

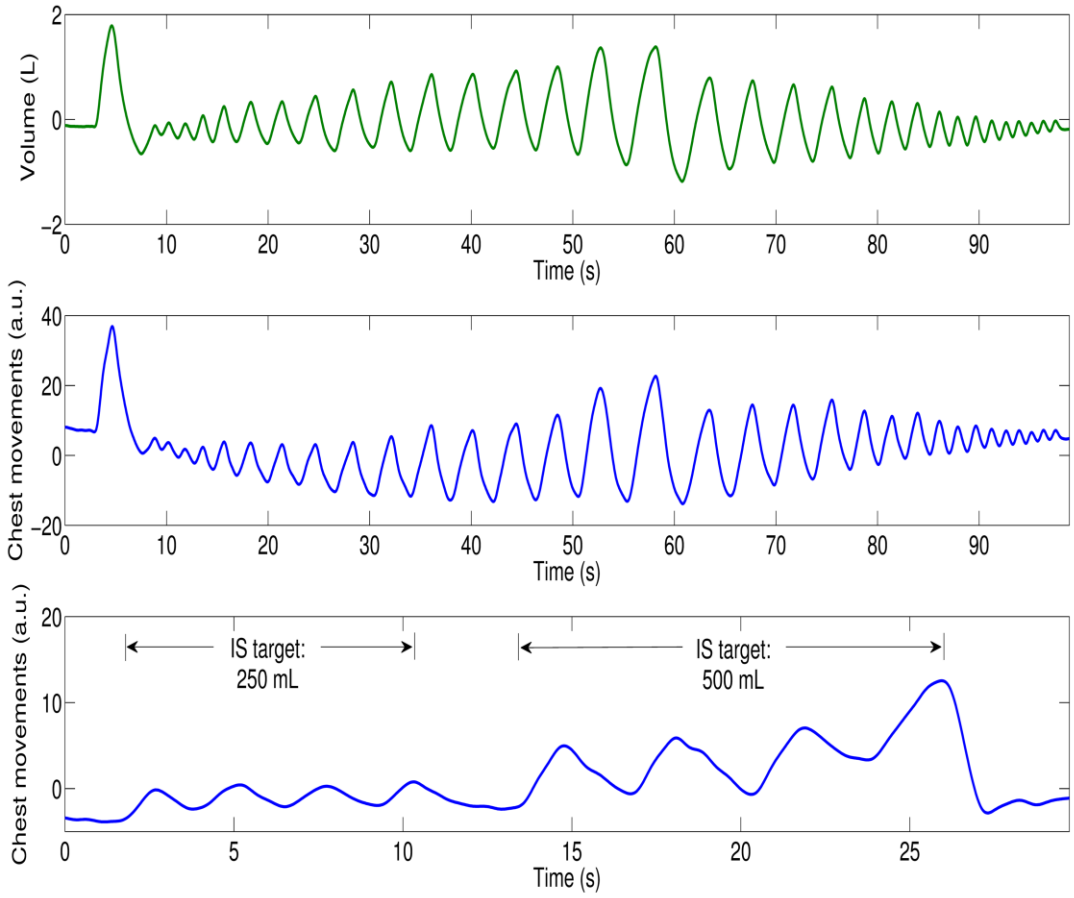

Figure 6.2 – Example of acquired signals for the two breathing maneuvers of a subject.
Top: Reference volume from spirometer for the test maneuver. *Middle*: Corresponding chest movement signal for the test maneuver recorded via the proposed smartphone camera app. These two signals from test maneuver were aligned due to different starting times. *Bottom*: Chest movement signal recorded during calibration maneuver while the subject was breathing though the incentive spirometer; four inspirations at 250 mL target, and four inspirations at 500 mL target. Inspirations/expirations correspond to positive/negative deflections in the signals.

6.2.5 Calibration using Incentive Spirometer

The inspiratory segments of the calibration maneuver using IS were located in the chest movement signal. Then, the peak-to-peak amplitude of this signal was computed at each inspiration and matched with the corresponding target volume from the IS. This resulted in two data sets: 1) four data points with ordinate values $V_{IS,1}$ at 250 mL, and 2) four data points with ordinate values $V_{IS,2}$ at 500 mL, with each point having an abscissa Δx equal to the peak-to-peak amplitude of the chest movement signal for that corresponding inspiratory phase.

Next, the median peak-to-peak amplitude of each set was computed so that information from IS maneuver was condensed in two data points, *A* and *B*, as follows:

$$\begin{aligned} A &= \left(\widehat{\Delta x_1}, V_{IS,1}\right) = \left(\widehat{\Delta x_1}, 250\ mL\right) \\ B &= \left(\widehat{\Delta x_2}, V_{IS,2}\right) = \left(\widehat{\Delta x_2}, 500\ mL\right) \end{aligned} \tag{2}$$

where $\widehat{\Delta x_1}$ and $\widehat{\Delta x_2}$ are the median values of the peak-to-peak amplitudes of the chest movement signal for the inspirations at 250 mL target $V_{IS,1}$ and 500 mL target $V_{IS,2}$, respectively. Finally, the calibration curve to map the peak-to-peak amplitudes to tidal volume estimates was obtained using the linear equation given the locations of points *A* and *B*:

$$V_{Tsmartphone} = \left(\frac{V_{IS,2} - V_{IS,1}}{\widehat{\Delta x_2} - \widehat{\Delta x_1}}\right)\left(\Delta x - \widehat{\Delta x_1}\right) + V_{IS,1} \tag{3}$$

which in turn can be written as

$$V_{Tsmartphone} = \left(\frac{250}{\widehat{\Delta x_2} - \widehat{\Delta x_1}}\right)\Delta x + 250\left(1 + \frac{\widehat{\Delta x_1}}{\widehat{\Delta x_2} - \widehat{\Delta x_1}}\right) \tag{4}$$

where $V_{Tsmartphone}$ denotes the tidal volume estimate given the peak-to-peak amplitude of the smartphone-acquired chest movement signal and the data from calibration using IS.

6.2.6 Tidal Volume Estimation using Smartphone

After we applied the calibration linear model obtained from the calibration maneuver, the V_T smartphone estimates were tested considering the tidal volumes measured from spirometer as reference. To this end, the maxima and minima of the reference volume were found and the $V_{Tspirometer}$ was computed as the absolute amplitude difference between two consecutive extrema. The corresponding peak-to-peak amplitudes Δx were found in the smartphone-acquired chest movement signal. Finally, the linear model obtained from IS given by Eq. 4 was applied to each value Δx of the maneuver to obtain the corresponding smartphone-based V_T estimate.

The performance of the estimation was measured on the test data in terms of the root-mean-squared error *RMSE*, given by

$$RMSE = \sqrt{\frac{\sum_{i=1}^{N}\left(V_{T_{spirometer}}(i) - V_{T_{smartphone}}(i)\right)^2}{N}} \tag{5}$$

and its normalized version *NRMSE* with respect to the mean tidal volume of the maneuver given by

$$NRMSE = \frac{RMSE}{\text{mean}\left(V_{T_{spirometer}}\right)} \text{ x } 100\% \tag{6}$$

where $V_{T_{spirometer}}$ indicates the reference tidal volume measured from spirometer, $V_{T_{smartphone}}$ the tidal volume estimated from smartphone-acquired chest movements after calibration from IS model, and *M* is the number of breath-phases of the analyzed breathing maneuver.

In addition, these V_T estimates obtained from calibration via IS data were compared to those V_T obtained when applying a linear regression to the absolute peak-to-peak amplitude of the chest movement signal and the simultaneously recorded reference V_T from spirometer, to see how much the estimates from IS calibration deviates from those obtained with the best estimation model in the least-squares sense.

6.3 Results

Reference tidal volume from spirometer distributed from a minimum of 0.190 ± 0.116 L (mean ± SD), to a maximum of 2.607 ± 0.400 L, with an average of 1.024 ± 0.159 L for the maneuvers performed by all volunteers (N=12). As in our previous study [20], a strong linear correlation between the peak-to-peak amplitude of the chest movement signal from smartphone's camera and the reference V_T from spirometer was found (r^2=0.945 ± 0.037). An example of this relationship for the breathing maneuver of one subject is shown in Figure 6.3. The distribution of r^2 values was not normal as tested using a one-sample Kolmogorov-Smirnov test (p=0.017). The median r^2 was found to be higher than 0.9 as tested by a one-sample Wilcoxon signed rank test (p=0.002). The RMSE and NRMSE errors obtained when mapping the peak-to-peak amplitude of the chest movement signal to V_T quantities using the linear regression is shown in Table 6.1.

To calibrate the peak-to-peak amplitude of the chest movement signal from smartphone, information from the IS was extracted and a linear model was computed to map the smartphone quantities to tidal volumes. An example of the data extracted from the IS maneuver and the corresponding calibration model are shown in Figure 6.3 together with the testing data from simultaneously recorded V_T from spirometer and peak-to-peak amplitude of chest movement signal. Figure 6.4 shows an example of the V_T estimation using the smartphone data calibrated via the IS for the test maneuver of a subject as well as the corresponding estimation errors with respect to reference volume from spirometry. Table 6.1 shown the performance indexes for the V_T estimates from smartphone when the proposed calibration via IS was used.

Table 6.1 – Tidal volume estimation results from smartphone-acquired signals compared to reference volume from spirometer (N=12 subjects).

Parameter		Linear regression of smartphone data			Calibration of smartphone data using IS		
RMSE	[*L*]	0.147	±	0.044	0.189	±	0.074
NRMSE	[*%*]	14.499	±	4.255	18.559	±	6.579

Values presented as mean ± standard deviation

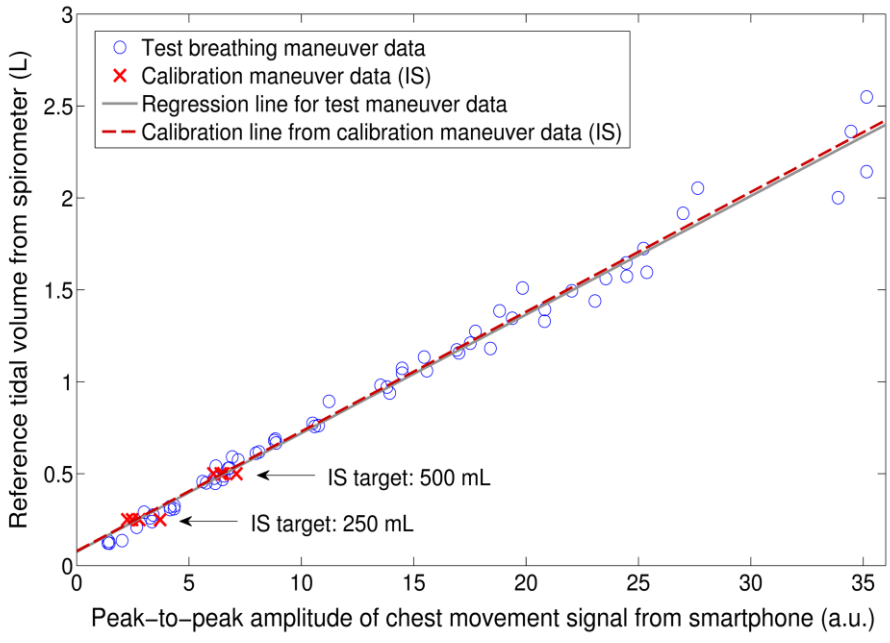

Figure 6.3 – Example of simultaneously acquired data using smartphone camera and spirometer for the experiment of a volunteer.

The solid gray line is the regression line for the test maneuver. Red crosses indicate the data collected during the test maneuver while the subject was breathing at 250 mL and 500 mL targets through the incentive spirometer (IS). The calibration model computed from the IS data is indicated by the red dashed line.

We found that, when calibrated using the IS data, the smartphone-based V_T estimation produced a statistically significant bias of -0.051 liters, and 95% limits of agreements of –0.424 and 0.321 liters as shown in the corresponding Bland-Altman plot of Figure 6.5. In contrast, when the peak-to-peak amplitudes were mapped to volumes using the linear regression of simultaneously acquired spirometer data, no statistically significant bias was found, and the 95% limits of agreements were ±0.292 liters as shown in Figure 6.6.

In our previous study using spirometer data for calibration, the RMSE and NRMSE values of the smartphone-based V_T estimates were found to be 0.182 ± 0.107 L and 14.998 ± 5.171 %, respectively [20]. Those RMSE and NRMSE values did not distribute normally, as tested by a one-sample Kolmogorov-Smirnov test (p=0.008 and p=0.017, respectively). When comparing those prior results to

those obtained in this study, using the best model from the regression of spirometer and smartphone data, no statistically-significant differences (p=0.961) were found. Finally, the estimation errors obtained in this study from the calibration via IS were compared to those from the linear regression by means of a paired-sample t-test and statistically-significant increases in the mean value of the RMSE (p=0.007) and NRMSE (p=0.004) using IS were found.

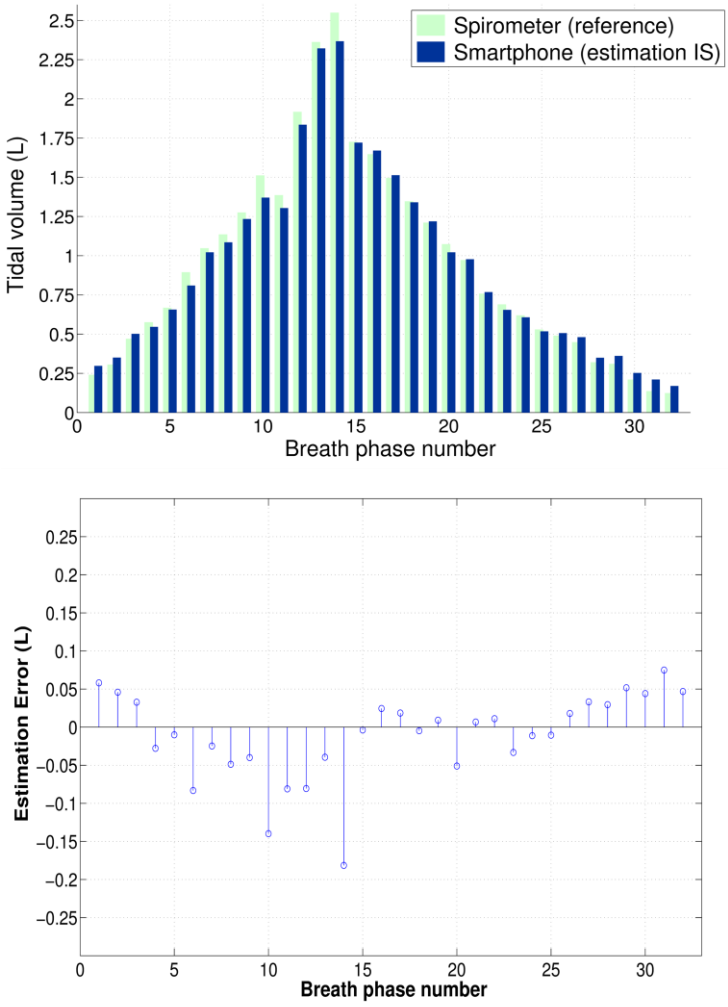

Figure 6.4 – Example of tidal volume estimation using the smartphone-acquired chest movement signal calibrated with an incentive spirometer (IS) for the test maneuver performed by one volunteer.

For visualization purposes, only data from inspiratory phases are displayed. *Top*: Side-to-side tidal volumes. *Bottom*: Corresponding estimation errors of smartphone-system with respect to spirometry.

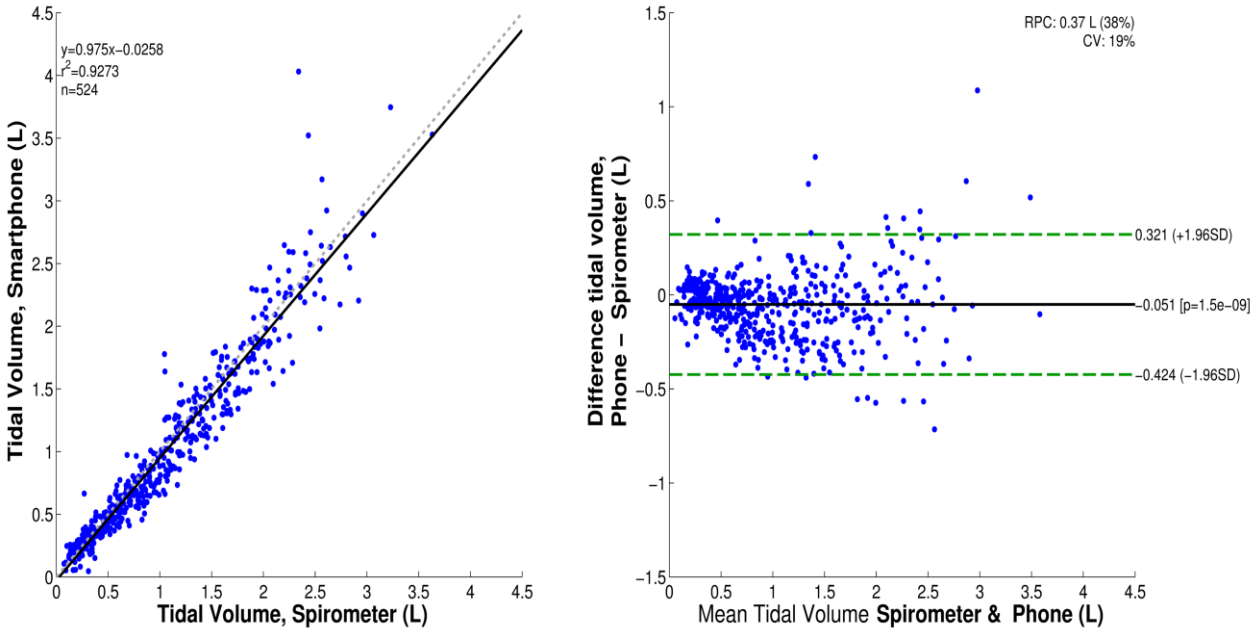

Figure 6.5 – Tidal volume estimation from smartphone-acquired chest movement signal calibrated using incentive spirometer (*N*=12 subjects).
Left: Regression curve. Grey dashed line indicates the identity line and the solid black the regression line. *Right*: Bland-Altman plot. Solid black line indicates the bias and dashed green lines indicate the 95% limits of agreement.

Four screenshots of the smartphone app are shown in Figure 6.7 for the task of V_T estimation with calibration via IS. Figure 6.7a shows the main menu of the Android app. Figure 6.7b shows the settings screen for the calibration maneuver with IS which allows the user to adjust the number of breaths and corresponding target volumes in IS. Figure 6.7c shows an example of the calibration model computed from the breathing data through an IS. Once the calibration model is computed, it is stored for further measurement of V_T. Figure 6.7d shows an example of calibrated V_T estimates from the smartphone's chest movement signal, where the figure on top displays the processed waveform and detected breath phase onsets, and the figure at the bottom displays the corresponding V_T estimates during inspiratory phases. The average RR and average V_T are also displayed on this screen.

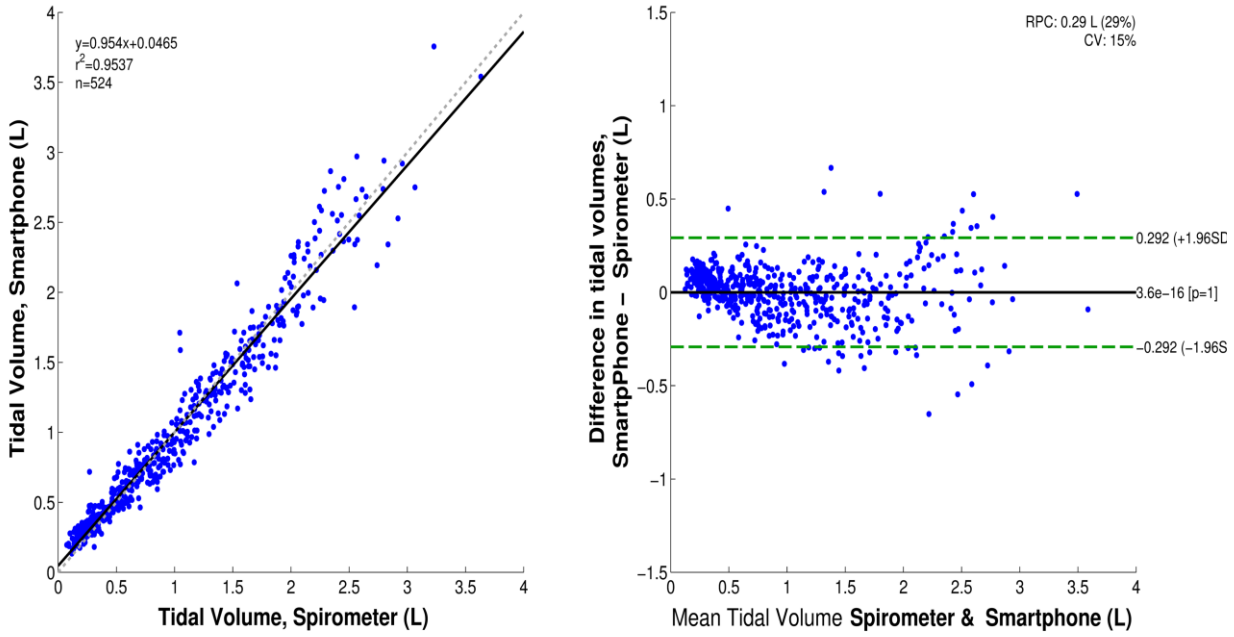

Figure 6.6 – Tidal volume estimated via linear regression of smartphone-acquired data and reference tidal volume from spirometer (*N*=12 subjects).
Left: Regression curve. Grey dashed line indicates the identity line and the solid black the regression line. *Right*: Bland-Altman plot. Solid black line indicates the bias and dashed green lines indicate the 95% limits of agreement.

6.4 Discussion and Conclusions

This dissertation chapter is an extension of our previous work that proposed the estimation of V_T directly on a smartphone by processing video recording information to obtain a chest movement signal correlated with reference V_T from a spirometer. Here, we innovated a simple and attainable calibration procedure to easily allow V_T estimation on a daily basis without the use of specialized devices. To calibrate the data from the smartphone-acquired signal, we propose using a widely-available volumetric incentive spirometer, of the sort that patients are often sent home with after hospitalization for a surgery. We further designed and implemented a smartphone application on an HTC One M8 Android smartphone which allows recording of the chest movement signal, its calibration, and final V_T estimation. We tested the performance of the proposed approach by simultaneously recording a reference volume signal from a spirometer.

Figure 6.7 – Screenshots of the developed Android smartphone application for tidal volume estimation using camera and calibration with an incentive spirometer (IS).

(a) Main menu of the Android application. (b) Calibration setup which allows adjustment of number of inspirations and target volumes. Red dots indicate the first IS target (250 mL) and white dots the second target (500 mL). (c) Example of calibration model computed while the subject breathed through the IS. (d) Example of tidal volume estimates after calibration. Top waveform indicates the chest movement signal from smartphone camera. Bottom graph displays the estimated tidal volume of each inspiration. Average respiratory rate and tidal volume are also displayed.

In agreement with our previous study [20], we found that the peak-to-peak amplitude of the smartphone-acquired chest movement signal is highly linearly correlated to tidal volume as measured by a spirometer system for twelve healthy volunteers. When the linear regression equation was used to normalize the smartphone data to tidal volume estimates, we found an RMSE of 0.147 ± 0.044 L which corresponded to a NRMSE of 14.499 ± 4.255 % when normalized to the mean value of the reference V_T. In turn, these errors were not statistically significantly different from those found in our previous study. At this stage, the proposed method for V_T estimation using a smartphone's camera has provided an average error of approximately 15% when calibrated using spirometry data as reference. However, it should be noted for normal ranges of tidal volume (~400-500 mL), the absolute error value is smaller than for the high tidal volume range (>1.5 L) as seen in Figures 6.4 and 6.6.

A limitation of our previous study [20] was noted to be that our approach has to be calibrated using a spirometer device; this specialized device is not commonly available outside research and clinical settings. In order to deal with this calibration restriction, here we proposed to take advantage of the highly linear correlation between the chest movement signal and reference tidal volumes, to obtain a linear calibration model using only two sets of data points gathered while the volunteers breathed through an IS. The IS device is a cheap device that is currently widely used in practice in many hospitals and nursing homes for the purpose of rebuilding diaphragm muscles for those subjects who have been on a respirator or immobilized for several days due to surgery. Each data set consisted of the peak-to-peak amplitudes of the chest movement signal during inspirations at 250 mL and 500 mL targets marked on the IS. To minimize the effect of a possible outlier when breathing at IS targets, the median value of each data set was taken as representative to compute the calibration model. We found that when calibrated using the linear model from the first IS maneuver, the smartphone-based V_T estimation provided a RMSE of 0.189 ± 0.074 L equivalent to 18.559 ± 6.579 % when normalized. This error represents a statistically-significant increment of around 4% compared to the NRMSE error obtained from calibration using a spirometer. Also, in contrast to the V_T estimation obtained from calibration via spirometer, we found a statistically-significant fixed bias of -51 mL when the calibration was performed using data from the IS

maneuver. This higher estimation error and systematic V_T underestimation could be attributable to limitations of the IS which does not offer a more precise estimation of the inspired volume due to its coarse volume scale as well as to the increase in airway resistance when using it, which in turn increases the chest movements due to a higher breathing effort and hence shifting of the peak-to-peak of chest movement signal to higher values from which the calibration model is constructed. Besides this performance degradation, and even when calibration should be performed *on-site* prior estimating V_T for a given breathing maneuver, the proposed calibration procedure is easy-to-perform and does not employ a specialized nor expensive device. The calibration procedure itself, both maneuver and calculation takes less than 30 seconds and is automatically performed by the smartphone app, with the option to be remotely started and completed via a wireless controller.

Despite the easy calibration procedure proposed here, we recognize the limitations of our study. First, breathing data was collected while the healthy subjects were standing still, *i.e.*, performance of the V_T estimation during motion, postural changes, and airway obstruction was not explored. Second, only a limited area of the anterior chest wall was monitored, *i.e.*, the rig cage area using a rectangular ROI, and this could ignore small contributions of other compartments and anatomical distortions in other areas. Both limitations are topics of further exploration in our research group. In particular, we are interested in the implementation of algorithms to deal with body motion artifacts, as proposed in the literature for RR monitoring [19], [25]. The implementation of image processing techniques to monitor a ROI beyond a simple rectangular area is also pending work. Note however that scenarios including motion artifacts are less likely to occur when measuring V_T during a short maneuver but it would become an important issue if continuous monitoring is intended. In addition, analyzing the performance of the smartphone-based estimator in different postures including supine, when the abdominal mechanical degree of freedom is expected to dominate the contribution to V_T, is pending. Currently, our research group is exploring other applications for the developed smartphone-based monitor in the area of respiratory sound analysis where a temporal reference would be helpful to classify and characterize the recorded sounds, particularly in patients presenting adventitious respiratory sounds.

The development of an inexpensive and portable breathing monitoring system for on-demand V_T and RR estimation capabilities is still pending for the general population. The near-ubiquity of smartphones and their owners' high reliance on them makes them an attractive alternative to develop a system with those characteristics. Although several advances have been made regarding cardiac monitoring using smartphones, a limited number of studies have addressed their applications to respiratory monitoring, and most of them have focused on respiratory rate estimation despite the importance of monitoring respiratory depth. The results found in this dissertation support the feasibility of developing a smartphone-based breathing monitor that provides V_T estimates when calibrated using a simple, affordable, and widely-accessible external device. Development of such a system would advance on-demand monitoring by providing another breathing parameter in addition to the number of breaths-per-minute.

6.5 References

[1] B. M. Koeppen and B. A. Stanton, *Berne & Levy Physiology, Updated Edition*. Elsevier Health Sciences, 2009.

[2] K. Ashutosh, R. Gilbert, J. H. Auchincloss, J. Erlebacher, and D. Peppi, "Impedance pneumograph and magnetometer methods for monitoring tidal volume," *J Appl Physiol*, vol. 37, no. 6, pp. 964–966, 1974.

[3] P. Grossman, M. Spoerle, and F. H. Wilhelm, "Reliability of respiratory tidal volume estimation by means of ambulatory inductive plethysmography," *Biomed. Sci. Instrum.*, vol. 42, pp. 193–198, 2006.

[4] A. Johansson and P. P. Å. Öberg, "Estimation of respiratory volumes from the photoplethysmographic signal. Part I: experimental results," *Med. Biol. Eng. Comput.*, vol. 37, no. 1, pp. 42–47, Jan. 1999.

[5] Y. S. Lee, P. N. Pathirana, C. L. Steinfort, and T. Caelli, "Monitoring and Analysis of Respiratory Patterns Using Microwave Doppler Radar," *IEEE J. Transl. Eng. Health Med.*, vol. 2, pp. 1–12, 2014.

[6] G. Li, N. C. Arora, H. Xie, H. Ning, W. Lu, D. Low, D. Citrin, A. Kaushal, L. Zach, K. Camphausen, and R. W. Miller, "Quantitative prediction of respiratory tidal volume based on the external torso volume change: a potential volumetric surrogate," *Phys. Med. Biol.*, vol. 54, no. 7, pp. 1963–1978, Apr. 2009.

[7] M. R. Miller, J. Hankinson, V. Brusasco, F. Burgos, R. Casaburi, A. Coates, R. Crapo, P. Enright, C. P. M. van der Grinten, P. Gustafsson, and others, "Standardisation of spirometry," *Eur. Respir. J.*, vol. 26, no. 2, pp. 319–338, 2005.
[8] C.-L. Que, C. Kolmaga, L.-G. Durand, S. M. Kelly, and P. T. Macklem, "Phonospirometry for noninvasive measurement of ventilation: methodology and preliminary results," *J. Appl. Physiol. Bethesda Md 1985*, vol. 93, no. 4, pp. 1515–1526, Oct. 2002.
[9] O. Sayadi, E. H. Weiss, F. M. Merchant, D. Puppala, and A. A. Armoundas, "An Optimized Method for Estimating the Tidal Volume from Electrocardiographic Signals: Implications for Estimating Minute Ventilation," *Am. J. Physiol. - Heart Circ. Physiol.*, vol. 307, pp. H426–H436, 2014.
[10] B. J. Semmes, M. J. Tobin, J. V. Snyder, and A. Grenvik, "Subjective and objective measurement of tidal volume in critically ill patients.," *Chest*, vol. 87, no. 5, pp. 577–579, 1985.
[11] M. Bartula, T. Tigges, and J. Muehlsteff, "Camera-based system for contactless monitoring of respiration," in *2013 35th Annual International Conference of the IEEE Engineering in Medicine and Biology Society (EMBC)*, 2013, pp. 2672–2675.
[12] M.-Z. Poh, D. J. McDuff, and R. W. Picard, "Advancements in Noncontact, Multiparameter Physiological Measurements Using a Webcam," *IEEE Trans. Biomed. Eng.*, vol. 58, no. 1, pp. 7–11, Jan. 2011.
[13] L. Tarassenko, M. Villarroel, A. Guazzi, J. Jorge, D. A. Clifton, and C. Pugh, "Non-contact video-based vital sign monitoring using ambient light and auto-regressive models," *Physiol. Meas.*, vol. 35, no. 5, p. 807, 2014.
[14] H.-Y. Wu, M. Rubinstein, E. Shih, J. Guttag, F. Durand, and W. Freeman, "Eulerian Video Magnification for Revealing Subtle Changes in the World," *ACM Trans Graph*, vol. 31, no. 4, pp. 65:1–65:8, Jul. 2012.
[15] F. Zhao, M. Li, Y. Qian, and J. Z. Tsien, "Remote Measurements of Heart and Respiration Rates for Telemedicine," *PLoS ONE*, vol. 8, no. 10, p. e71384, Oct. 2013.
[16] Y. Nam, Y. Kong, B. Reyes, N. Reljin, and K. H. Chon, "Monitoring of Heart and Respiratory Rates using Dual Cameras on a Smartphone," vol. In revision, 2015.
[17] G. Ferrigno, P. Carnevali, A. Aliverti, F. Molteni, G. Beulcke, and A. Pedotti, "Three-dimensional optical analysis of chest wall motion," *J. Appl. Physiol. Bethesda Md 1985*, vol. 77, no. 3, pp. 1224–1231, Sep. 1994.
[18] S. J. Cala, C. M. Kenyon, G. Ferrigno, P. Carnevali, A. Aliverti, A. Pedotti, P. T. Macklem, and D. F. Rochester, "Chest wall and lung volume estimation by optical reflectance motion analysis," *J. Appl. Physiol.*, vol. 81, no. 6, pp. 2680–2689, Dec. 1996.
[19] D. Shao, Y. Yang, C. Liu, F. Tsow, H. Yu, and N. Tao, "Noncontact Monitoring Breathing Pattern, Exhalation Flow Rate and Pulse Transit Time," *IEEE Trans. Biomed. Eng.*, vol. 61, no. 11, pp. 2760–2767, Nov. 2014.
[20] B. A. Reyes, N. Reljin, and K. H. Chon, "Tidal Volume Estimation Using Smartphones," *IEEE J. Biomed. Health Inform.*, vol. In revision, 2015.
[21] C. Scully, J. Lee, J. Meyer, A. M. Gorbach, D. Granquist-Fraser, Y. Mendelson, and K. H. Chon, "Physiological parameter monitoring from optical recordings with a mobile phone," *Biomed. Eng. IEEE Trans. On*, vol. 59, no. 2, pp. 303–306, 2012.
[22] J. Lee, B. A. Reyes, D. D. McManus, O. Mathias, and K. H. Chon, "Atrial Fibrillation Detection Using an iPhone 4S," *IEEE Trans. Biomed. Eng.*, vol. 60, no. 1, pp. 203–206, 2013.
[23] Y. Nam, J. Lee, and K. H. Chon, "Respiratory Rate Estimation from the Built-in Cameras of Smartphones and Tablets," *Ann. Biomed. Eng.*, vol. 42, no. 4, pp. 885–898, Nov. 2013.
[24] N. Reljin, B. A. Reyes, and K. H. Chon, "Tidal Volume Estimation Using the Blanket Fractal Dimension of the Tracheal Sounds Acquired by Smartphone," *Sensors*, vol. 15, no. 5, pp. 9773–9790, 2015.

[25] Y. Sun, S. Hu, V. Azorin-Peris, S. Greenwald, J. Chambers, and Y. Zhu, “Motion-compensated noncontact imaging photoplethysmography to monitor cardiorespiratory status during exercise,” *J. Biomed. Opt.*, vol. 16, no. 7, pp. 077010–077010, 2011.

Chapter 7: Automatic Breath-Phase Classification using Smartphones to Develop a Mobile Phonopneumogram

(B. A. Reyes, N. Reljin, Y. Kong, Y. Nam, S. Ha, and K. H. Chon, "Towards the Development of a Mobile Phonopneumogram: Automatic Breath-Phase Classification using Smartphones,"; Under revision, December 2015)

7.1 Introduction

As mentioned in previous chapters of this dissertation, the use of CORSA systems has overcome some limitations of the mechanical stethoscope and accelerated the interest in respiratory sound analysis over the last decades [1]. For example, employment of CORSA systems now allows quantification of changes in respiratory sound characteristics, correlation of these sounds to other physiological signals, and generation of data representations useful in the diagnosis and treatment of patients with pulmonary diseases [2]. Even with these advantages, pulmonary auscultation with the stethoscope still guides in diagnosis when other tests are not available [3]. Ubiquity, low-cost, mobility, ease-of-use, and non-invasiveness are some characteristics that made the stethoscope the most widely used instrument in clinical practice. Such characteristics should remain when aiming for the development of a CORSA system.

The advanced state-of-the-art of smartphones and their near-ubiquity make them an attractive option for developing a CORSA system that provides more useful information than the stethoscope. Employment of smartphones has advantages over other architectures in terms of implementation and integration with other health monitoring technologies given their hardware and software capabilities. Nowadays, smartphone vital sign applications have been found to be accurate and robust in areas such as cardiac and respiratory monitoring [4], [5].

Automatic classification of breath phases, *i.e.*, automatic labeling of a breath phase as inspiration or expiration, attracts particular interest in applications requiring the timing of breath phases, *e.g.* when

studying the breathing modulation of flow in the heart [6], or during acoustical airflow [7] and volume estimation [8] to correctly assign the polarity of the estimated signals.

In the field of respiratory sounds, discriminating between inspiratory and expiratory phases is also important when analyzing breathing (base) sounds as well as adventitious sounds. The timing of crackle sounds –short duration (discontinuous) with an explosive character [9]- must be characterized and it has been found to differ between different pulmonary disorders, reflecting different pathophysiology [10]. For example, late inspiratory crackles have been associated with restrictive pulmonary diseases while early inspiratory crackles with severe airway obstruction [11]; early timing of crackles in COPD was found not to overlap with late inspiratory crackles in fibrosing alveolitis [12]. Expiratory crackles can be found in many respiratory diseases [10], *e.g.* low-frequency expiratory crackles occur especially in chronic airway obstruction, but in general they are less frequent than inspiratory crackles [13]. Similarly, the relationship of continuous adventitious sounds such as wheezes –long duration sounds with a musical character [9]- to the breath phase is useful for their characterization [14]. The severity of bronchial obstruction has been found to be less in asthmatic patients with only expiratory wheezes than in patients with both inspiratory and expiratory wheezes [15]. Inspiratory short duration wheezes (squawks) are commonly heard in pulmonary fibrosing diseases and pneumonia [16], [17]. Regarding base lung sounds, statistically-significant differences were found between healthy and extrinsic allergic alveolitis patients [18], where the differences were more consistent during the expiratory phase presumably due to the more central source of the expiratory sounds that could carry out more information. Classically, by using phonopneumography –simultaneous presentation of respiratory sound and airflow or volume signals- the timing or volume level of occurrences of adventitious sounds and breath phases can be performed accurately [10]. However, outside clinical and research settings these airflow or volume signals cannot always be taken for granted.

The idea of developing a portable system for respiratory sound analysis is not new [19], [20], nor is the idea of using smartphones for such purposes [21]. Recently, our research group also proposed a smartphone-based system for tracheal sound acquisition purposes [22]. That study was intended to show

that smartphones allow acquisition of tracheal sounds that resemble the main characteristics reported in the classical literature [23]–[27], such as temporal intensity variation that correlates with airflow, similar frequency content of breath phases at similar airflow peaks, and their use for breath-phase onset detection and respiratory rate estimation. We analyzed the acquired sounds employing a Shannon entropy estimator together with a joint time-frequency technique in order to obtain time-varying respiration rate estimates, which were found to correlate well when compared to reference values from spirometer-acquired signals [22]. The breath-phase onset estimates based on smartphone-acquired tracheal sounds were found to be around 52 ± 51 ms (mean ± SD), which are adequate for research involving heart function coupled to respiration [6]. Automatic breath-phase classification was not performed in that previous study.

Use of tracheal sound measurements for estimating ventilation parameters is of particular interest in the CORSA field, *e.g.* phonospirometry provides fairly accurate estimates of airflow [7] and tidal volume [8]. Recently, our research group applied a fractal analysis approach for tidal volume estimation from smartphone-acquired tracheal sounds, and it was found that reasonable estimates could be obtained even for measurements five days after calibration using a simple bag at a known volume [28]. Besides the promising results in phonospirometry using tracheal sounds, airflow and volume estimators share a necessary step involving the correct classification of the inspiratory and expiratory phases which is usually performed via an additional signal, *e.g.* airflow from a spirometer.

Previous studies using a multichannel CORSA system addressed the classification of breath phases using only respiratory sounds. By employing tracheal sounds for breath-phase onset detection and lung sounds for breath-phase classification, via the inspiratory/expiratory power difference, even 100% accuracy was achieved [29]. However, the recording of an additional channel was required in order to achieve this. Hence, this former approach is not feasible in a single channel scenario. Its implementation in a smartphone-based CORSA system would require additional hardware to simultaneously acquire two sound channels if intended for tracheal sound analysis. On the other hand, the use of only tracheal sounds for both breath-phase onset detection and breath-phase classification has also been attempted [24], [30]–

[32]. By taking advantage of fast changes in tracheal sound intensity, classification has been performed in prior studies using both time and frequency analyses [32]. Unfortunately, the accuracy was not reported in the latter case. More recent studies on this classification task have also reported the use of only tracheal sounds, recorded either over the trachea or close to the nostrils or mouth in agreement with current definitions [9]. By applying a ratio of frequency magnitudes at high and low frequency bands to discriminate between inspiratory and expiratory phases, 97% of 436 phases were correctly classified when compared to respiratory inductance plethysmography [31]. An accuracy of 95.6% was obtained by extracting features from the logarithm of the variance and comparing the current phase to the prior and post phases, with the results being independent of the airflow levels [24]. A 90% accuracy for inhalation and exhalation classification was achieved by applying a threshold level to Mel-frequency cepstral coefficients extracted from tracheal sounds [30]. As was pointed out by other authors, breath-phase detection is a relatively easy task if lung sounds are used; however, as can be noticed from the reported accuracy results, ranging from 90 to 97%, it is still a topic of ongoing research exploration when employing only tracheal sound recordings. Certainly, there are applications when only recording a single respiratory signal is desirable, and classification of breath phases only from tracheal sounds is advantageous; however, more often other physiological signals are simultaneously recorded in order not only to enhance the performance of the monitoring system but also to gain a deeper knowledge of the phenomena under analysis.

This dissertation is intended as a step forward towards the development of a mobile CORSA system that takes advantage of smartphone capabilities. Given that smartphones now have a broad collection of sensors, it is natural to question if the employment of additional smartphone-acquired respiratory signals would be helpful when developing a mobile CORSA system. Therefore, as an alternative to the approach of classifying breath phases using only tracheal sounds we propose to acquire an additional respiratory-related signal that can be used as a temporal reference, as it is done in classic phonopneumography, without the need to plug additional hardware into the smartphone. In particular, we propose using a smartphone-acquired optical signal that tracks chest movements from which the correct

detection of the inspiratory and expiratory phases could be achieved by a simple processing technique directly on the smartphone.

Optical approaches have been used for monitoring cardiac and respiratory parameters [33]–[35]. Recently, a breathing pattern tracking algorithm was implemented on a personal computer by detecting shoulder displacements via webcam and image processing techniques [36]. In contrast to that study, our research group implemented an application directly on an Android smartphone that recorded chest movements for average respiratory rate estimation [37]. Similar to the study by Shao *et al*. [36], we noticed that smartphone-based optical signals resemble the spirometry-based volume with the uphill and downhill segments corresponding to the inspiratory and expiratory phases. The proposed smartphone application was previously developed by our research group for non-contact respiratory rate estimation [37], and this dissertation is an extension to that work which now intends to perform automatic breath-phase classification for respiratory sound analysis. Here, as a reference to compare the classification results, spirometer-based airflow and volume signals were simultaneously collected with the chest movement signal recorded remotely from the smartphone's camera. Tracheal sounds were also simultaneously acquired via smartphone as proposed in our previous study [22] during noise-free recordings and also while the subjects made non-breath noise (swallow, cough, and talk) and performed both regular (alternate phases) and irregular breathing patterns to analyze the performance of the proposed classification method in such scenarios.

7.2 Material and Methods

7.2.1 Subjects

Thirteen (N=13) healthy and non-smoker volunteers (twelve males), ages ranging from 19 to 52 years (27.77±9.41, mean±SD), weights 70.77±8.39 kg, and heights 175.31±6.28 cm, were recruited for this study. Students and staff members from the University of Connecticut (UConn), USA, constituted the group of volunteers. Subjects with previous pneumothorax, with chronic respiratory illnesses such as

asthma, and anyone who was currently ill (*e.g.* common cold or upper respiratory infection) were excluded from participation. The Institutional Review Board of UConn approved the study protocol which was provided to each volunteer for his/her agreement and signature.

7.2.2 Respiration Signals Acquisition

Equipment and Chest Movement Algorithm

Three types of signals were recorded during the breathing maneuvers of each volunteer: airflow and volume signals via a spirometer, chest movement signals via a smartphone video camera, and tracheal sounds via an acoustical sensor plugged into a smartphone audio input. The spirometer system used for recording the respiratory airflow, and corresponding volume via integration over time, consisted of a respiration flow head connected to a differential pressure transducer (MLT1000L, FE141 Spirometer, ADInstruments, Inc., Dunedin, New Zealand). A 16-bit A/D converter (PowerLab/4SP, ADInstruments, Inc.) was used to sample the analog airflow and volume signals at 1 kHz. Each volunteer received a new disposable filter, reusable mouthpiece, and disposable nose clip compatible with the spirometer system (MLA304, MLA1026, MLA1008, ADInstruments, Inc.). Prior to each volunteer's experiment, the spirometer system was calibrated using a 3.0 liter calibration syringe (Hans Rudolph, Inc., KS, USA), following instructions in the manufacturer's manual. The digitized volume signal was regarded as a reference for breath-phase classification.

At the same time that the airflow and volume signals were being recorded, each volunteer's chest movement signal was also recorded, using the frontal camera of an HTC One M8 smartphone (HTC Corporation, Taiwan), which consisted of a 5 MP camera with 1080p full HD video recording at 30 frames-per-second (fps) and wide-angle lens. An algorithm was implemented in the smartphone by our research group that recorded chest wall motion at a sampling frequency of 25 Hz during the volunteer's maneuvers [37].

It has been shown that during breathing, as in all mechanical systems involving volume displacement, a relationship between volume displacement and linear motion exists, where the rib cage

and abdomen compartments of the chest wall are the major contributors [38]. Chest wall movements in the anteroposterior direction are greater than those in the vertical or transverse directions, with an increase of around 3 cm in the anteroposterior diameter over the vital capacity range [38]. In optical non-contact monitoring of breathing, a video camera captures the changes in the intensity of reflected light caused by these chest wall movements as they modify the path length of the illumination light [39]. The algorithm implemented by our research group averages the intensities of the red, green and blue (RGB) channels of the video within a rectangular region of interest (ROI) at each time instant *t* as follows

$$I(t) = \left(\frac{1}{3D}\right)\left(\sum_{\{m,n\}\in ROI} i_R(m,n,t) + \sum_{\{m,n\}\in ROI} i_G(m,n,t) + \sum_{\{m,n\}\in ROI} i_B(m,n,t)\right) \quad (1)$$

where *D* refers to the number of pixels in the ROI, and $i_x(m,n,t)$ refers to the intensity value of the pixel at the *m*-th row and *n*-th column of the ROI for the corresponding RGB channel. The ROI was focused on the rib cage area of the subject and consisted of 49 × 90 pixels selected, *i.e.*, *D*=4410 pixels, in a resolution of 320 × 240 pixels. In order to obtain the chest movement signal *I(t)*, the video data was first converted in the smartphone from YUV420SP format to RGB using the Open Source Computer Vision library [40]. The implemented app saved the recorded chest movement signal *I(t)* and time vector of the maneuvers in a text file for further analysis in Matlab (R2012a, The Mathworks, Inc., MA, USA).

A Galaxy S4 smartphone (Samsung Electronics Co., Seoul, South Korea) was employed to acquire tracheal sounds via a cabled acoustical sensor composed of a subminiature electret microphone BT-21759-000 (Knowles Electronics, IL, USA) encased in a plastic bell. A double-sided adhesive ring (BIOPAC Systems, CA, USA) was used to affix the acoustical sensor to the volunteers' necks, at the level of the anterior cervical triangle. The Galaxy S4, as well as the HTC One, was running on Android v4.4.2 (KitKat) operating system. The acoustical sensor used in this dissertation was developed by our colleagues at the Metropolitan Autonomous University at Mexico City, and has been successfully used in respiratory sound analysis [18]. The minimum requirements recommended by the European Respiratory Society Task Force Report [2] are satisfied by the Galaxy S4 high-fidelity audio system, and we found

that the characteristics and information that can be extracted from this kind of smartphone-acquired sound signal are in agreement with those using regular CORSA systems [22]. After smartphone acquisition of the tracheal sounds at 44.1 kHz and 16-bit per sample, the recorded audio files were transferred to a personal computer for further processing in Matlab.

Maneuver

Each volunteer was asked to breathe through the spirometer system at airflow levels ranging from around 0.5 to 2 L/s, first increasing their volumetric flow rates with each breath for around 1 minute, and then decreasing volumetric flow rates with each breath for another minute. These airflow levels cover similar ranges as the ones used in other studies when acquiring tracheal sounds at 'low', 'medium', and 'high' airflow levels [8], [24], [29]. Precise minimum and maximum peak airflows varied between volunteers depending on their own manageable limits. For alignment purposes between the different types of recordings, volunteers were asked to perform initial inspiratory and final expiratory apneas of approximately 5 s each and to take a forced respiratory cycle after initial apnea before performing the described maneuver. The airflow signal from the spirometer was displayed on a 40" monitor placed in front of the volunteers to provide them with visual feedback. During the maneuver, volunteers were in standing still posture and wore nose clips to clamp their nostrils. In order to record the chest movement signal, the smartphone was held in a 3-pronged clamp placed in front of the volunteers at approximately 60 cm from their thorax level so that the central portion of their rib cage areas was captured by the ROI. In a real-world application, the distance from the camera to the subject's thorax would be affected by their body proportions, so it would be necessary to ensure that the ROI's vertical borders do not exceed the anterior axillary line. We have found that a reliable chest movement signal could be obtained even when the ROI captures a smaller area than that defined by the midclavicular lines. Experiments were performed in a regular dry laboratory, not an anechoic chamber, illuminated with ordinary fluorescent ceiling lights. The laboratory was held quiet during each volunteer's maneuvers. Volunteers were asked

not to wear loose clothes but they were free to wear any pattern, *e.g.*, plain or stripes, and any color of clothing during the maneuvers. Figure 7.1 shows an example of the setup during a maneuver acquisition.

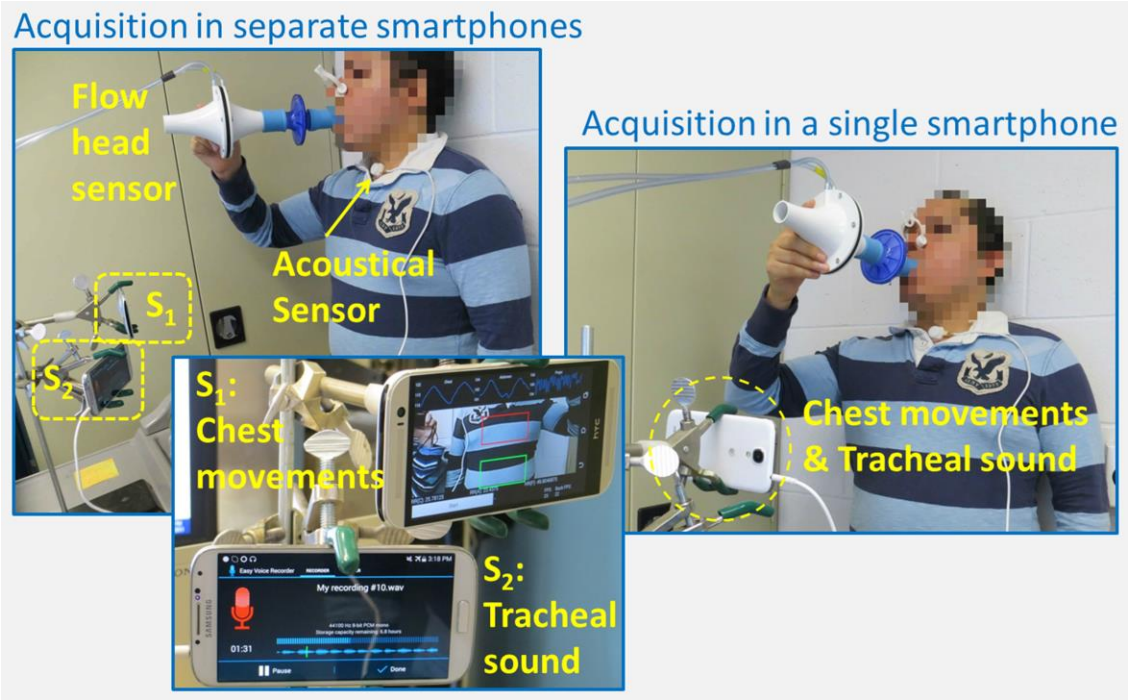

Figure 7.1 – Recording of tracheal sounds and chest movement signals via smartphone during the maneuver of a volunteer.

A smartphone was placed in front of the volunteer at his/her thorax level in order to record the chest movements directly on this device. Tracheal sounds were acquired with an acoustical sensor plugged into the smartphone. Two separate devices were employed to acquire tracheal sounds and chest movement signals in the first stage of the study. Acquisition of both signals was performed with a single smartphone in the second stage. Airflow and volume signals were also acquired via a spirometer system and regarded as temporal reference. Actual breath-phases of the maneuver were obtained from volume signal.

7.2.3 Data Preprocessing

Airflow and volume signals from the spirometer were down-sampled to 25 Hz, and then lowpass filtered at 2 Hz with a 4th-order Butterworth filter applied in a forward and backward scheme to produce zero-phase distortion and minimize start and end transients. Due to fluctuations around the sampling frequency encountered during data acquisition, the chest movement signal was interpolated at 25 Hz via a cubic spline algorithm to obtain a fixed sampling rate. The same lowpass filter at 2 Hz applied to spirometer signals was applied to the chest movement signal to minimize high frequency components not

related to the respiratory maneuver. Acquired tracheal sounds were down-sampled to 6300 Hz. To minimize heart sounds and muscle interference, the down-sampled tracheal sounds were filtered using a 4th-order Butterworth bandpass filter between 100 to 3000 Hz and applied in a forward and backward scheme.

Due to differences in starting times and delays between the spirometer system and the smartphones, alignment of smartphone-acquired signals was performed with respect to spirometry. For the chest movement signal, a segment of 20 seconds duration was extracted from each recording at the central portion of the maneuver. The cross-correlation sequence between volume and chest movement segments was computed and the sample lag for which the cross-correlation value resulted in a maximum was used to shift the smartphone-acquired signal accordingly. For the alignment of tracheal sounds, the Shannon entropy (SE) signal was employed as it resembles a rectified version of the airflow signal [7], with the breath-phase onsets being indicated by its minima. SE was computed in a moving window scheme via the Parzen's density estimation method with a Gaussian kernel [41] using the parameters detailed in our previous study [22]. Then, the tracheal sound was shifted in time so that its initial breath-phase onset after apnea, computed from SE, matched the corresponding onset from the reference volume signal.

Although the manufacturer's instructions were followed, we found a drift in the spirometer-based volume signals. A drift was also found in the smartphone-acquired chest movement signals. Hence, a detrending step based on the Empirical Mode Decomposition (EMD) was applied to both types of signals in order to facilitate their further analysis [42], [43]. EMD employs a sifting process that decomposes the original signal in terms of its intrinsic oscillatory modes (IMFs), based only on the original signal, by analyzing the different time scales presented in it. After the sifting process, the original signal $s(t)$ can be represented as

$$s(t) = \sum_{k=1}^{K} IMF_k\,(t) + r_K(t) \tag{2}$$

where K is the total number of IMFs, and $r_K(t)$ is the residual signal. The EMD sifting process is intended to obtain IMFs without riding waveforms and to produce close to zero mean value as defined by their upper and lower envelope signals [43]. As a result of the sifting process, the first IMFs contain the higher frequency components (lower scales), and hence the trend is contained in the last IMFs. Figure 7.2 shows an example of raw signals acquired using smartphone and spirometer systems during the breathing maneuver of a volunteer. Observe that even with the baseline drift, the inspiratory/expiratory phases can be noticed as the local increasing/decreasing segments in both the chest movement and reference volume signals. However, signal detrending as done here with EMD, or with a more conventional high-pass digital filter, simplifies the further processing including the automatic onset detection. An example of the preprocessing results is shown in Figure 7.3.

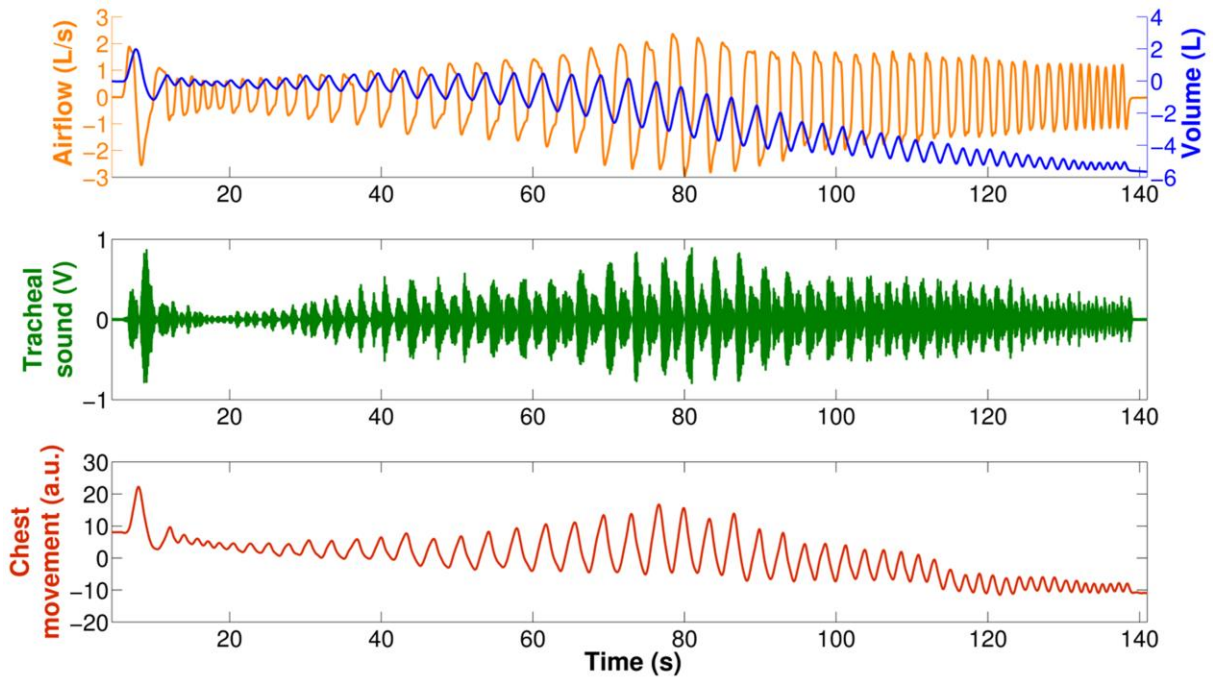

Figure 7.2 – Example of the acquired signals during the respiration maneuver of a volunteer.
Top: spirometer-acquired airflow (orange) and volume (blue) signals. *Middle*: smartphone-acquired tracheal sounds. *Bottom*: smartphone-acquired chest movement signal. Observe that despite of the baseline drift and different starting times, the breath-phase onsets are noticeable in both reference volume from spirometer and chest movement signal from smartphone's camera.

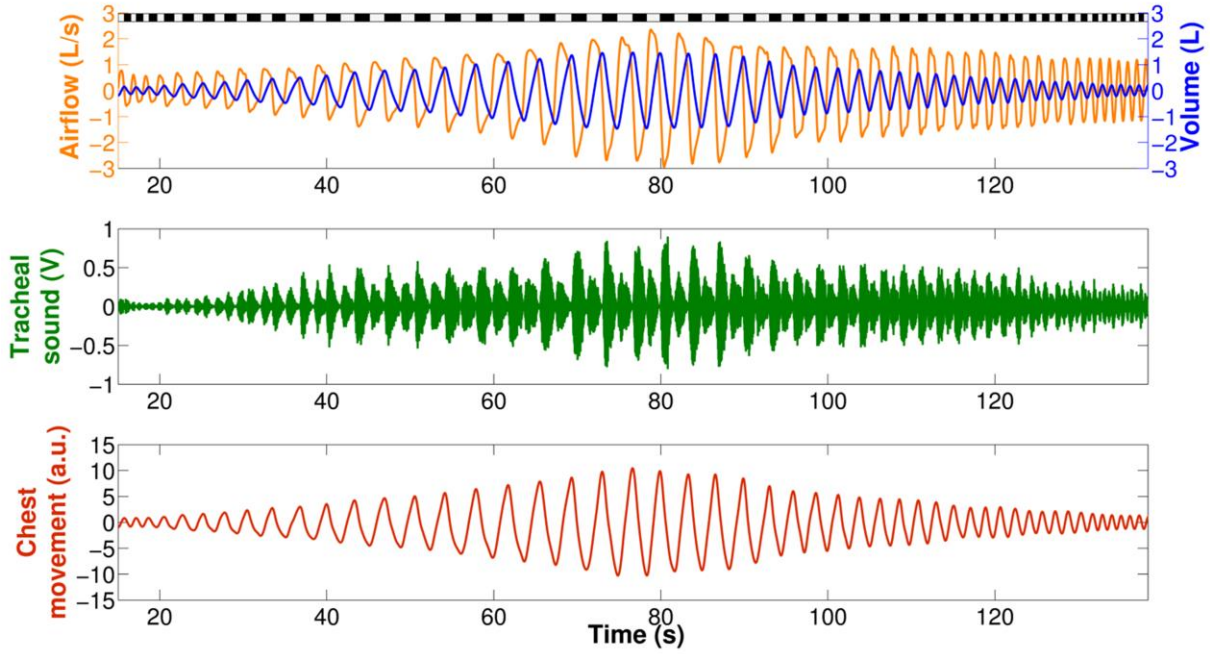

Figure 7.3 – Example of preprocessed signals during the breathing maneuver of a volunteer.
Top: spirometer-acquired airflow signal (orange) and volume signal (blue) after detrending. *Middle*: smartphone-acquired tracheal sounds. *Bottom*: smartphone-acquired chest movement signal with the baseline drift removed after detrend. Gray and black bars displayed on top of spirometer signals indicate the inspiratory and expiratory phases, respectively. Both types of smartphone-acquired signals were aligned in time with respect to reference volume from spirometer.

7.2.4 Breath-Phase Classification using Smartphone Camera Signals

As a reference to test the performance of the proposed breath-phase classification, the spirometer's volume signal was used to obtain the actual breath phases during the maneuver. First, the corresponding breath-phase onsets were found via its local maxima and minima. Then, the breath phase between two consecutive onsets was labeled as inspiration or expiration in accordance to the sign of a linear least-squares model [44] fitted on the volume data in that segment (positive: inspiratory phase, negative: expiratory phase).

For the automatic classification of the breath phases using the smartphone-acquired chest movement signal, we propose to take advantage of the linear correlation between the detrended chest

movement and the spirometer-based volume signals. As the basis of the proposed method is that the chest movement signal from a smartphone's camera and the spirometer-based volume signal are highly correlated, we quantify this linear correlation during the breathing maneuver by computing the cross-correlation index ρ, defined as:

$$\rho = \frac{\sum_{i=1}^{P} chest_{smartphone}(i) \cdot volume_{spirometer}(i)}{\sqrt{\sum_{i=1}^{P}\left(chest_{smartphone}(i)\right)^2 \cdot \sum_{i=1}^{P}\left(volume_{spirometer}(i)\right)^2}} \quad (3)$$

where $chest_{smartphone}$ denotes the smartphone-acquired chest movement signal, $volume_{spirometer}$ the spirometer-acquired volume signal, and P is the total number of samples of the analyzed signals. If both signals were the same, ρ would equal unity. Hence, values close to 1 indicate high correlation between the signals under analysis. Note that if a high linear correlation between smartphone-acquired chest movement and the reference volume signal is found, it would imply that we could easily obtain accurate breath-phase labels from only the chest movement signal. To this end, the chest movement signal was processed in the same way as the volume signal, *i.e.*, the breath-phase onsets were automatically found in the chest movement signal, then each segment between two consecutive onsets was labeled as inspiration if the sign of the linear least-squares model fitted on the chest movement signal was positive, or as expiration if the corresponding sign was negative, *i.e.*,

$$Breath\ phase = \begin{cases} Inspiration, & if\ \ sign\{\beta\} > 0 \\ Expiration, & if\ \ sign\{\beta\} < 0 \end{cases} \quad (4)$$

where $sign\{\cdot\}$ refers to the sign function, and β corresponds to the slope of the regression line for the corresponding segment of smartphone data under analysis. For simplicity of notation, let us consider that for every two consecutive breath-phase onsets we have a set of M pairs of smartphone data points denoted by $\{(t_m, y_m)\}_{m=1,\ldots,M}$, where $\{y_m\}_{m=1,\ldots,M}$ refers to the chest movement data from a smartphone, and $\{t_m\}_{m=1,\ldots,M}$ refers to their corresponding time locations at a uniform sampling rate f_s, hence the best linear fit in the least-squares sense has the form $y = \beta t + \alpha$, where the slope β is given by [44]

$$\beta = \frac{\sum_{m=1}^{M}(t_m \cdot y_m) - \frac{1}{M}(\sum_{m=1}^{M} t_m) \cdot (\sum_{m=1}^{M} y_m)}{\sum_{m=1}^{M}(t_m{}^2) - \frac{1}{M}(\sum_{m=1}^{M} t_m)^2} \tag{5}$$

Without loss of generality, the relationship between the equidistant time points and the sampling frequency can be used, *i.e.*, $t_m = m \cdot \frac{1}{f_s}$ for $m = 1, \ldots, M$ sample indexes, to rewrite the slope of the linear fit as

$$\beta = \frac{\frac{1}{f_s}\sum_{m=1}^{M}(m \cdot y_m) - \frac{1}{Mf_s}(\sum_{m=1}^{M} m) \cdot (\sum_{m=1}^{M} y_m)}{\frac{1}{f_s{}^2}\sum_{m=1}^{M} m^2 - \frac{1}{Mf_s{}^2}(\sum_{m=1}^{M} m)^2} \tag{6}$$

Either Equation (5) or (6) could be used for breath-phase classification purposes. However, as our interest is only in the sign of the slope it would be more convenient to reduce computational burden when implemented on the smartphone. Using the closed forms of the finite summations given by

$$\sum_{m=1}^{M} m = \frac{M(M+1)}{2} \tag{7}$$
$$\sum_{m=1}^{M} m^2 = \frac{M(M+1)(2M+1)}{6}$$

the Equation of the slope β could be simplified as follows

$$\beta = \left(\frac{6fs}{M(M-1)}\right)\left(\left(\frac{2}{M+1}\right)\sum_{m=1}^{M}(m \cdot y_m) - \sum_{m=1}^{M} y_m\right) \tag{8}$$

In turn, by recognizing that in our case the first term in Equation (8) is always positive, the sign of the slope β can be easily computed by

$$sign\{\beta\} = sign\left\{\frac{2\sum_{m=1}^{M}(m \cdot y_m)}{M+1} - \sum_{m=1}^{M} y_m\right\} \tag{9}$$

Finally, the results of the proposed classification scheme using the smartphone-acquired signal can be expressed in terms of the confusion matrix, where the columns are the actual breath-phases as obtained from spirometry, and the rows are the labeled breath-phases from the chest movement signal from smartphone's camera. The accuracy was obtained from the confusion matrix as

$$Accuracy = \frac{TP + TN}{P + N} \tag{10}$$

where *TP* refers to the number of actual inspirations correctly labeled as inspirations, *TN* to the number of actual expirations correctly labeled as expirations, and *P* and *N* to the total number of actual inspirations and expirations, respectively.

7.3 Results

Table 7.1 contains statistics about breath-phase duration, peak airflow, and tidal volume for the breathing maneuvers performed by N=13 volunteers, as measured from spirometer-based airflow and volume signals. The analyzed database was composed of n_1=419 inspirations and n_2=430 expirations.

The smartphone-acquired chest movement signal follows the temporal variations of the spirometer-based volume signal during the breathing maneuvers, as shown from the raw data in Figure 7.2 and more clearly in Figure 7.3 after alignment and detrending. We found a high linear relationship between both detrended signals for all volunteers as measured by the cross-correlation index, ρ=0.960±0.025. Figure 7.4 shows an example of the proposed method for automatic breath-phase classification using the smartphone-acquired chest movement signal. Table 7.2 presents the classification results of the breath phases, as a confusion matrix, for all breathing phases performed by volunteers, where the actual breath phases were obtain from spirometer-acquired volume signals. 100% classification accuracy was achieved as can be seen from the confusion matrix shown in Table 7.2. The distribution of the slope feature extracted from the smartphone's camera signal for the breathing maneuver of all subjects is presented in Figure 7.5. Observe that the use of the sign of the slope for classification of the breath phases corresponds to a threshold equal to 0. Due to the non-overlapping between the slope features for the inspiratory and expiratory data, the correct classification of all breath phases of this stage could be achieved even by using other threshold values but the sign of the slope offers the advantage of an easy computation as derived in the previous section. The receiver operating characteristic (ROC) curve is presented in Figure 7.6.

Table 7.1 – Distribution of breath phases' duration, tidal volume, and peak airflow obtained from spirometer during breathing maneuvers (*N*=13 subjects. Number of expirations=430. Number of inspirations=419).

Parameter		Minimum	Maximum	Mean	Median
Phase duration	*[s]*	0.739 ± 0.317	3.211 ± 1.160	1.749 ± 0.586	1.720 ± 0.670
Inspiration					
Peak airflow	*[L/s]*	0.478 ± 0.176	2.232 ± 1.127	1.107 ± 0.286	1.022 ± 0.263
Tidal volume	*[L]*	0.268 ± 0.131	2.986 ± 0.651	1.292 ± 0.222	1.090 ± 0.215
Expiration					
Peak airflow	*[L/s]*	-0.426 ± 0.203	-2.144 ± 0.875	-1.064 ± 0.361	-0.976 ± 0.346
Tidal volume	*[L]*	-2.972 ± 0.683	-0.236 ± 0.114	-1.261 ± 0.213	-1.062 ± 0.225

Values are presented as mean ± standard deviation

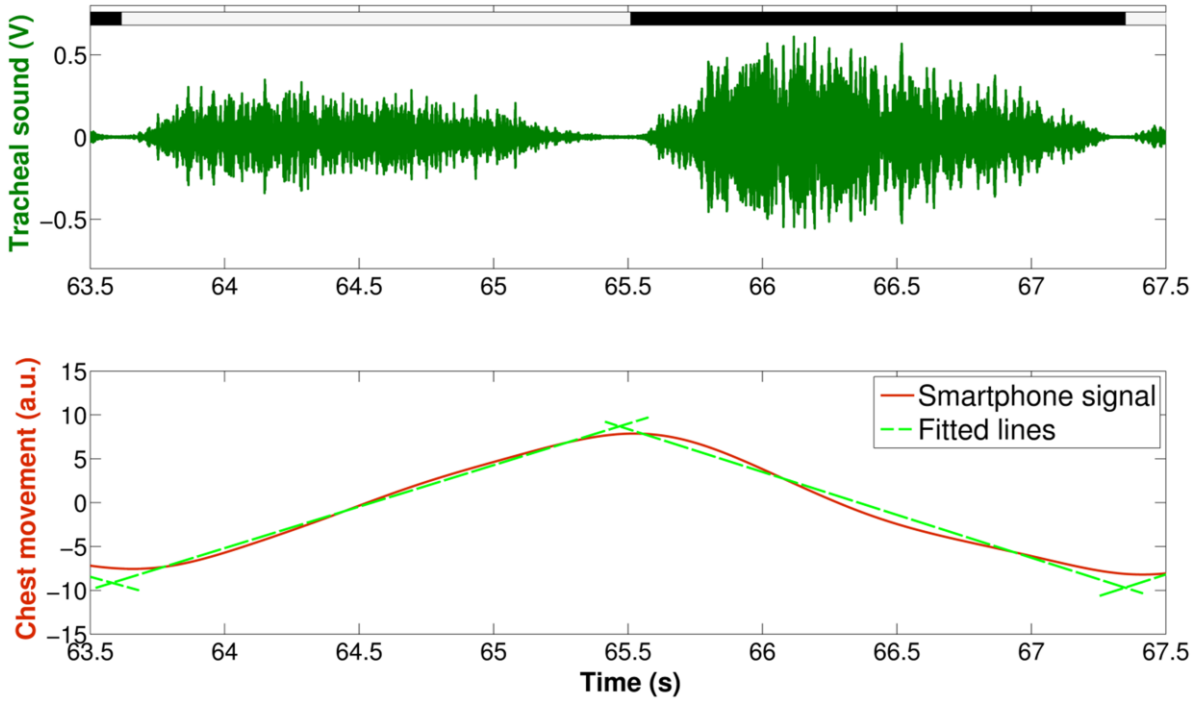

Figure 7.4 – Example of automatic breath-phase classification using smartphone-acquired chest movement signal.

Top: smartphone-acquired tracheal sound signal. Gray and black bars displayed on top indicate the inspiratory and expiratory phases, respectively, as measured from reference volume signal from spirometry. *Bottom*: smartphone-acquired chest movement signal. Superimposed dashed green lines indicate the fitted lines computed via least-squares method. Positive and negative slopes of fitted lines were used to label the segment as inspiration and expiration, respectively.

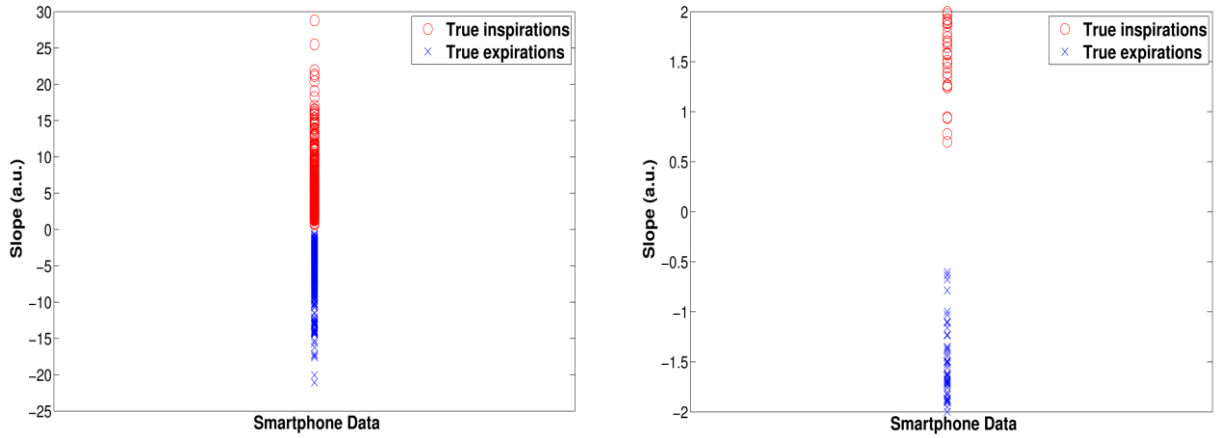

Figure 7.5 – Distribution of the slope of the least-squares fitting line of the smartphone-based chest movement signal.

Left: Slope of the fitted lines for all the inspiratory and expiratory phases for the maneuvers of all volunteers. *Right*: Zoom view around the origin.

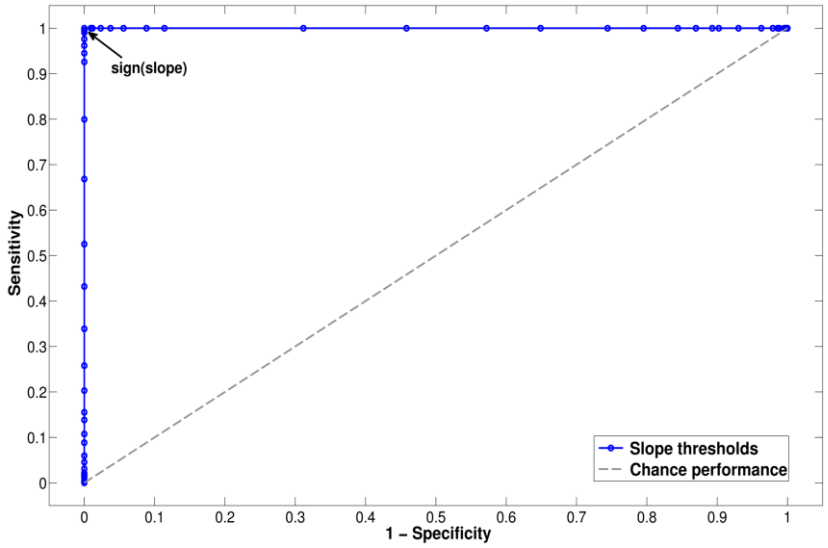

Figure 7.6 – Receiver operating characteristic (ROC) curve for the smartphone-based classification of breath phases.

ROC curve was computed by varying the threshold values of the slope used for labeling of the breath phases. Note that this ROC behavior reflects the non-overlapping between the slope features of the two classes. Although a range of threshold values could be used, a threshold equal to 0 simplifies the computational burden in terms of the sign of the slope.

Table 7.2 – Breath-phase classification results using smartphone-acquired chest movement signal (*N*=13 subjects. Number of actual expirations=430. Number of actual inspirations=419).

		Actual Breath Phase (Spirometer)	
		Expiration	**Inspiration**
Classified Breath phase (Smartphone)	**Expiration**	430	0
	Inspiration	0	419

In addition to the previous breathing maneuvers, a couple of volunteers were asked to perform additional breathing patterns according to different scenarios plausible to occur during respiratory recordings, as has been pointed out [24]. Additional recordings included the following scenarios: non-breath noise immersed in regular or irregular breathing, and successive inhalations or exhalations. The scenario with alternating breathing phases with different durations (inspiration-expiration-inspiration-expiration) was not explicitly performed at this time because it was already achieved during the main breathing maneuvers performed by all volunteers. At this stage of the dissertation, the chest movement algorithm was already implemented on the Samsung S4 smartphone so that only this device was employed for both tracheal sounds and chest movements recording. The Samsung S4 frontal camera -2 MP, 1080p video recording @ 30 fps- was employed for chest movement recording. As before, the native resolution of the Samsung S4 device was not used due to computational burden; its resolution was reduced to 320 × 240 pixels and the ROI was set to 49 × 90 pixels to match those parameters used in the HTC One smartphone. Examples of recorded signals from two volunteers performing different breathing scenarios with non-breathing noises are shown in Figures 7.7 and 7.8. Examples of signals acquired while the volunteers breathed in successive phases are presented in Figure 7.9. In Figures 7.7-7.9, airflow and volume signals are displayed for temporal reference; gray and black bars displayed on top indicate the inspiratory and expiratory phases, respectively. Fitted lines are superimposed on chest movement signals from the smartphone to show the phase labeling outside the noise event as determined by the corresponding slopes. In Figures 7.7 and 7.8, the noise events are indicated by a red bar. These events were labeled by examining the sound replay and waveform display of the tracheal sounds simultaneously

with the chest movement signal from the smartphone, similar to the common practice in respiratory sound analysis, *e.g.*, when labeling adventitious sound events using phonopneumography. Observe that in these cases, the classification of the breath phases is concerned with the phases surrounding the noise events. In Figure 7.9, the occurrence of successive inspirations and expirations are also indicated by a red bar, where classification of these breath phases is of concern. By employing the slope of the smartphone signal, these successive phases will be correctly classified with the same phase label given the monotonically increasing (or decreasing) chest movement waveform in such segments.

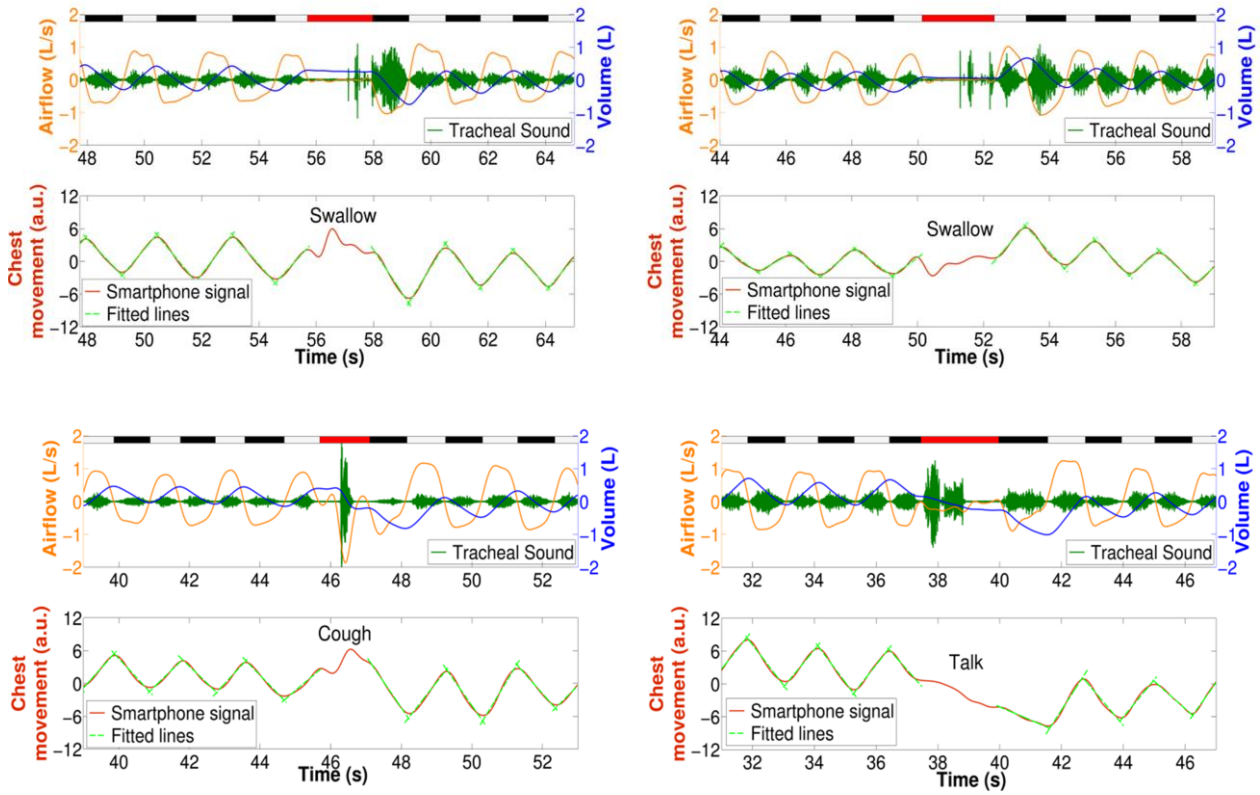

Figure 7.7 – Example of smartphone-acquired signals during different scenarios of breathing patterns.
Top left panel: non-breath noise event (swallow) immersed in regular breathing patterns. *Top right panel*: non-breath noise event (swallow) immersed in irregular breathing. *Bottom left panel*: non-breath event noise (cough) immersed in regular breathing. *Bottom right panel*: non-breath noise event (talk) immersed in irregular breathing.
For each of the four panels, the upper graph displays the airflow (orange), volume (blue), and tracheal sound (dark green) signals, while the bottom graph displays the chest movement signal (red) and the fitted lines computed via least-squares (dashed green lines). Gray/black bars displayed on top indicate the actual inspiratory/expiratory phases measured from spirometry, while the red bar indicates the location of the non-breath noise event.

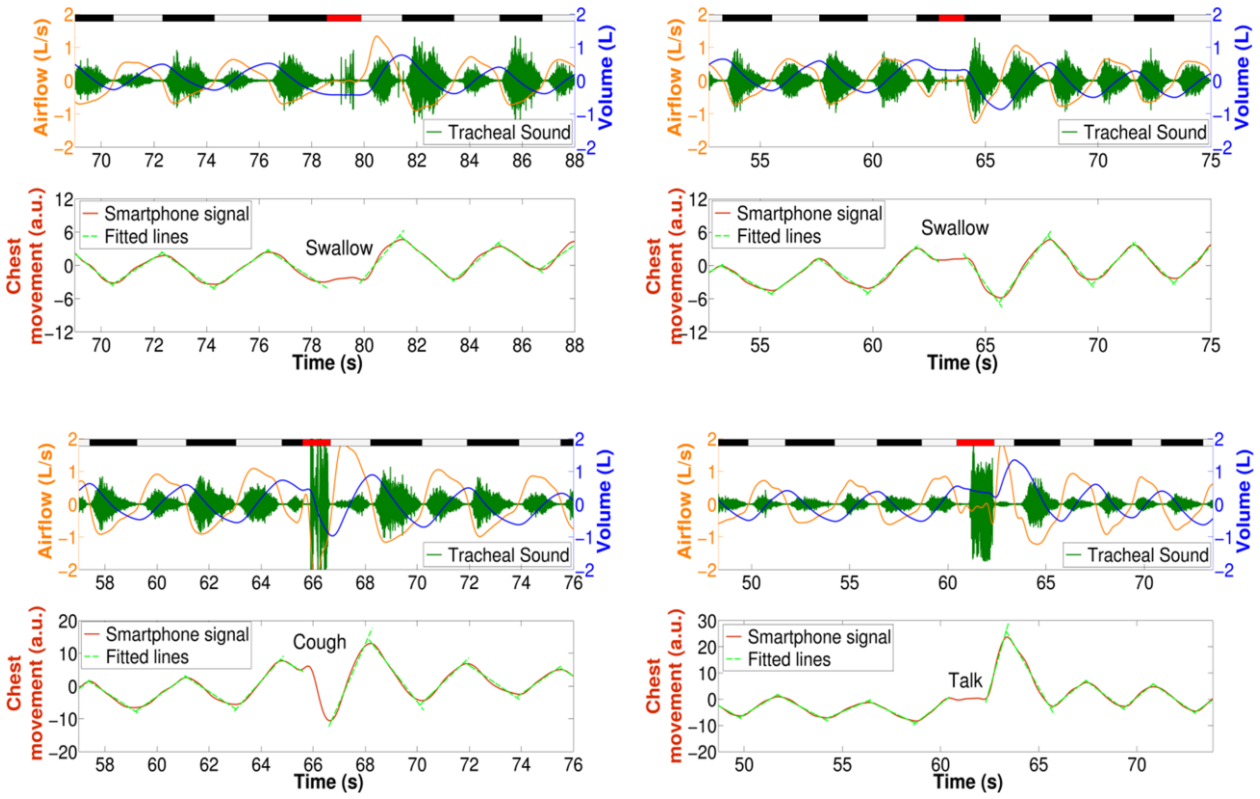

Figure 7.8 – Example of smartphone-acquired signals during different scenarios of breathing patterns of a second volunteer.
Top left panel: non-breath noise event (swallow) immersed in regular breathing patterns. *Top right panel*: non-breath noise event (swallow) immersed in irregular breathing. *Bottom left panel*: non-breath noise event (cough) immersed in regular breathing. *Bottom right panel*: non-breath noise event (talk) immersed in irregular breathing. For each of the four panels, the upper graph displays the airflow (orange), volume (blue), and tracheal sound (dark green) signals, while the bottom graph displays the chest movement signal (red) and the fitted lines computed via least-squares (dashed green lines). Gray/black bars displayed on top indicate the actual inspiratory/expiratory phases measured from spirometry, while the red bar indicates the location of the non-breath noise event.

7.4 Discussion and Conclusions

In this dissertation we propose the automatic classification of inspiratory and expiratory phases from a smartphone-acquired optical recording as an extension to the acquisition of tracheal sounds via smartphones. The app we developed allowed real time recording of chest movements during breathing maneuvers directly on the smartphone. For this dissertation, the app was implemented on two Android smartphones, the HTC One M8 and the Samsung Galaxy S4. During the initial stage of the dissertation,

recordings of chest movements and tracheal sounds were obtained on two separate smartphones, *i.e.*, the HTC One recorded chest movements and the Galaxy S4 recorded tracheal sounds, as each corresponding smartphone was proposed for that particular use in our previous studies [22], [37]. In the second stage of this dissertation, both types of recordings were performed on the same smartphone, *i.e.*, the Galaxy S4 simultaneously recorded chest movements and tracheal sounds.

Previously we studied the employment of smartphones for developing a CORSA system [22]. Results found in that study motivated us to keep working toward the development of a low-cost, easy-to-upgrade, and reliable portable CORSA system. In a subsequent study, our research group aimed for tidal volume estimation using smartphone-acquired tracheal sounds together with novel signal processing techniques and a simple calibration method that does not involve expensive or specialized devices such as spirometers [28]. Although the results are promising, the proposed methods require the correct identification of the inspiratory and expiratory phases.

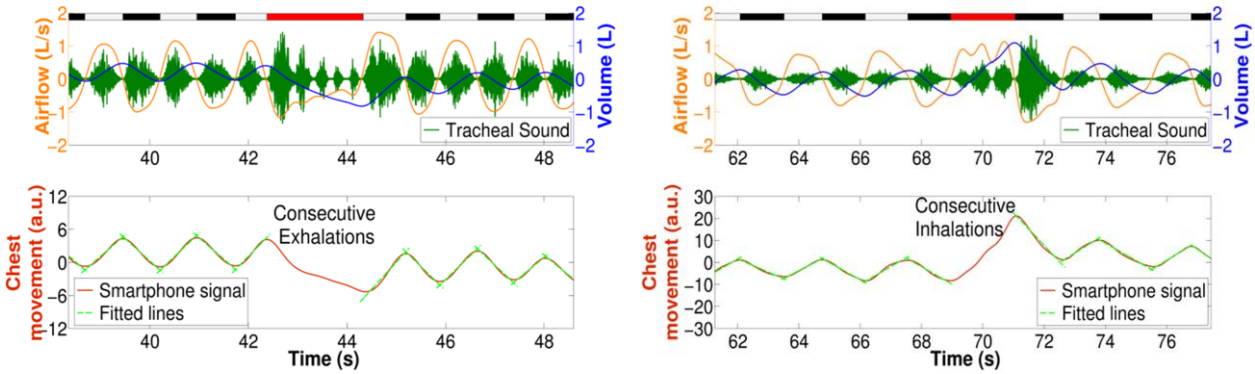

Figure 7.9 – Example of acquired respiratory signals while two volunteers were taking successive breaths.

Left: consecutive exhalations. *Right*: consecutive inhalations. For each of the two panels, the upper graph displays the airflow (orange), volume (blue), and tracheal sound (dark green) signals, while the bottom graph displays the chest movement signal (red) and the fitted lines computed via least-squares (dashed green lines). Gray/black bars displayed on top indicate the actual inspiratory/expiratory phases measured from spirometry, while the red bar indicates the location of the successive breaths event.

Phonopneumography has been useful in the field of respiratory sound analysis. When available, it is used as temporal reference for detection and classification of breath phases as well as diverse time events occurring during the breathing maneuver. Accordingly, the correct classification of breath phases proves to be relevant when performing automatic analysis of respiratory sounds containing adventitious sounds [10], [14], as well as for applications involving airflow or volume estimation from tracheal sounds [6]–[8]. Given the promising estimation of ventilation parameters, the use of only tracheal sounds has been proposed to address the automatic classification of breath phases [24], [30]–[32]. Although this approach has advantages, *e.g.*, greater user acceptance of the acoustical sensors in comparison to nasal cannulas or facemasks used to measure airflow, its accuracy results for breath-phase classification have not matched those found when using an additional lung sound channel.

Given the importance of the correct breath-phase classification in the CORSA field, and as a more-accurate alternative to using only tracheal sounds, we studied the employment of an additional respiration-related signal that could easily upgrade a mobile smartphone-based system. In this dissertation, instead of attempting the classification of breath phases from tracheal sounds, we employed an optical approach to perform this task. Previously, our research group implemented an algorithm that allows the estimation of average respiratory rate from a smartphone-acquired chest movement signal [37], and we noticed that this signal resembles the spirometer-acquired volume signal. To investigate our previous visual observations, in this dissertation were compared the spirometer-based volume and the smartphone-based chest movement signal using the cross-correlation index. The chest movements and tracheal sounds were recorded on separate smartphones at the initial stage of the dissertation because the optical algorithm had been only implemented on a different smartphone from the one used to record tracheal sounds in our previous studies. We found that both types of signals were highly correlated (ρ=0.960±0.025, mean±SD), corroborating our initial observations. These results indicate that our smartphone-based monitor is able to capture the intensity changes in the reflected light caused by the chest motion, linearly related to volume, while breathing. According to Konno and Mead [38], this motion-volume linear relationship is attributable to the relative smaller diameter changes while breathing

in comparison to the absolute diameter of the chest wall, and to the larger contribution of the anteroposterior diameter changes compared to the vertical or transversal. This linearity appears to hold in the recorded optical chest movement signal from a smartphone's camera. Hence, the volume signal was employed to label the phases of the respiratory maneuvers, while the chest movement signal was processed using a simple linear regression to label the uphill segments as inspirations and downhill segments as expirations based on the slope of the computed model. We found 100% accuracy for the task of breath-phase classification, *i.e.*, all inspiratory phases (n_1=419) were detected as inspirations and all expiratory phases (n_2=430) were detected as expirations, for the maneuvers performed by the volunteers in standing still posture, while breathing at different cycle durations ranging from 700 milliseconds to 3 seconds, and different airflow levels with peaks ranging from 0.5 to 2.0 L/s.

The second stage of the dissertation was intended to analyze the performance of the chest movement signal for the automatic classification of breath phases during different scenarios of breathing patterns that included non-alternate inspiratory and expiratory phases, as well as non-breathing related noises like swallowing, talking and coughing. At this point, the optical algorithm was already implemented on the same smartphone tested for tracheal sound acquisition, so that in this stage only a single smartphone was employed. As stated by other authors, these different breathing patterns are the most challenging in respiratory phase detection [24]. We found that the proposed classification scheme can be used to correctly classify the breath phases in such scenarios. For the non-breath events immersed in typical alternate breathing (*e.g.*, inspiration-noise-expiration) or in irregular breathing (*e.g.*, expiration-noise-expiration), the algorithm was able to classify the breath phases surrounding these noise events as indicated by the corresponding slopes of the chest movement signal from the smartphone. During the scenarios involving consecutive inspirations or consecutive expirations, the tracheal sounds involved were correctly classified as the same phase given the fitted slope for the chest movement signal in that time interval.

Besides the above-mentioned results, we recognize limitations of this dissertation. First, subjects were instructed to stand still while performing the breathing maneuvers, and hence, the performance deterioration due to body motion artifacts, not related to the breathing maneuver, was not explored. Incorporation of body tracking and artifact removal algorithms similar to those proposed in the literature to reduce such motion effects –for example in [36], [45]- is a topic of further exploration towards the development of our mobile system. Second, we only explored recordings with the subjects in standing posture. Recordings in supine posture were not performed. We foresee that the proposed scheme would bring similar classification results to the ones reported here when the visual field of the smartphone's camera is focused on the area with the most dominant contribution to volume while breathing, *e.g*., the abdominal compartment in supine posture [38]. Third, recordings were performed in a regular indoor laboratory, and hence further experiments are required to analyze the usability of the proposed portable system in different outdoor environments to fully take advantage of its mobility.

This dissertation represents a step forward in the development of a mobile system for the analysis of respiratory sounds that takes advantage of additional sensors already existing in smartphones. The obtained results show that simultaneous recordings of tracheal sounds and chest movements are useful for both automatic classification of the breath phases and correct timing of events such as the ones shown in this dissertation. An interesting alternative to our proposed approach and a topic for future exploration involves the use of accelerometers for respiratory sound recording [46], [47] with the potential benefit that information regarding the breath phase could be extracted, especially for lung sound recordings, in addition to the respiratory sound itself. Currently, motivated by the high linear correlation obtained between the chest movement signal from the smartphone's camera and the reference volume from spirometry, we are working on a study involving the feasibility of estimating tidal volume via the smartphone-acquired chest movement signal so that estimation of this parameter could be easily performed outside research and clinical settings. Finally, we consider that the smartphone approach proposed in this dissertation, as well as similar ones for respiratory monitoring, has the potential to be

readily accepted by users due to its simplicity and comfort as well as potential to reach populations and geographic areas where it is difficult to study respiratory sounds with current computerized methods.

7.5 Acknowledgments

This work is supported in part by the US Army Medical Research and Material Command (US-AMRMC) under grant No. W81XWH-12-1-0541.

The authors would like to thank Professors Sonia Charleston-Villalobos, Tomas Aljama-Corrales, and Ramon Gonzalez-Camarena for introducing an acoustical sensor used in this dissertation.

7.6 References

[1] A. R. A. Sovijarvi, J. Vanderschoot, and J. E. Earis, "Standardization of computerized respiratory sound analysis," *Eur. Respir. Rev.*, vol. 10, no. 77, pp. 585–585, 2000.

[2] J. E. Earis and B. M. G. Cheetham, "Current methods used for computerized respiratory sound analysis," *Eur. Respir. Rev.*, vol. 10, no. 77, pp. 586–590, 2000.

[3] H. Pasterkamp, C. Carson, D. Daien, and Y. Oh, "Digital respirosonography. New images of lung sounds.," *Chest*, vol. 96, no. 6, pp. 1405–1412, Dec. 1989.

[4] J. Lee, B. A. Reyes, D. D. McManus, O. Mathias, and K. H. Chon, "Atrial Fibrillation Detection Using an iPhone 4S," *IEEE Trans. Biomed. Eng.*, vol. 60, no. 1, pp. 203–206, 2013.

[5] Y. Nam, J. Lee, and K. H. Chon, "Respiratory Rate Estimation from the Built-in Cameras of Smartphones and Tablets," *Ann. Biomed. Eng.*, vol. 42, no. 4, pp. 885–898, Nov. 2013.

[6] C. Xiong, B. Hök, T. Strömberg, D. Loyd, B. Wranne, and P. Ask, "A bioacoustic method for timing of respiration at cardiac investigations," *Clin. Physiol.*, vol. 15, no. 2, pp. 151–157, 1995.

[7] A. Yadollahi and Z. M. K. Moussavi, "Acoustical Respiratory Flow," *IEEE Eng. Med. Biol. Mag.*, vol. 26, no. 1, pp. 56–61, 2007.

[8] C.-L. Que, C. Kolmaga, L.-G. Durand, S. M. Kelly, and P. T. Macklem, "Phonospirometry for noninvasive measurement of ventilation: methodology and preliminary results," *J. Appl. Physiol. Bethesda Md 1985*, vol. 93, no. 4, pp. 1515–1526, Oct. 2002.

[9] A. R. A. Sovijarvi, F. Dalmasso, J. Vanderschoot, L. P. Malmberg, G. Righini, and S. A. T. Stoneman, "Definition of terms for applications of respiratory sounds," *Eur. Respir. Rev.*, vol. 10, no. 77, pp. 597–610, 2000.

[10] P. Piirila and A. R. Sovijarvi, "Crackles: recording, analysis and clinical significance," *Eur. Respir. J.*, vol. 8, no. 12, pp. 2139–2148, Dec. 1995.

[11] A. R. Nath and L. H. Capel, “Inspiratory crackles—early and late,” *Thorax*, vol. 29, no. 2, pp. 223–227, Mar. 1974.
[12] P. Piirilä, A. R. Sovijärvi, T. Kaisla, H. M. Rajala, and T. Katila, “Crackles in patients with fibrosing alveolitis, bronchiectasis, COPD, and heart failure,” *Chest*, vol. 99, no. 5, pp. 1076–1083, May 1991.
[13] A. Vyshedskiy, R. M. Alhashem, R. Paciej, M. Ebril, I. Rudman, J. J. Fredberg, and R. Murphy, “Mechanism of inspiratory and expiratory crackles,” *Chest*, vol. 135, no. 1, pp. 156–164, Jan. 2009.
[14] N. Meslier, G. Charbonneau, and J. L. Racineux, “Wheezes,” *Eur. Respir. J.*, vol. 8, no. 11, pp. 1942–1948, Nov. 1995.
[15] C. S. Shim and M. H. Williams, “Relationship of wheezing to the severity of obstruction in asthma,” *Arch. Intern. Med.*, vol. 143, no. 5, pp. 890–892, May 1983.
[16] J. E. Earis, K. Marsh, M. G. Pearson, and C. M. Ogilvie, “The inspiratory ‘squawk’ in extrinsic allergic alveolitis and other pulmonary fibroses.,” *Thorax*, vol. 37, no. 12, pp. 923–926, Dec. 1982.
[17] R. Paciej, A. Vyshedskiy, D. Bana, and R. Murphy, “Squawks in pneumonia,” *Thorax*, vol. 59, no. 2, pp. 177–178, Feb. 2004.
[18] S. Charleston-Villalobos, L. Albuerne-Sanchez, R. Gonzalez-Camarena, M. Mejia-Avila, G. Carrillo-Rodriguez, and T. Aljama-Corrales, “Linear and Nonlinear Analysis of Base Lung Sound in Extrinsic Allergic Alveolitis Patients in Comparison to Healthy Subjects,” *Methods Inf. Med.*, vol. 52, no. 3, pp. 266–276, Apr. 2013.
[19] L. Guangbin, C. Shaoqin, Z. Jingming, C. Jinzhi, and W. Shengju, “The development of a portable breath sounds analysis system,” in *Proceedings of the 14th Annual International Conference of the IEEE Engineering in Medicine and Biology Society*, 1992, vol. 6, pp. 2582–2583.
[20] K. Hung, B. L. Luk, W. H. Choy, B. Tai, and S. K. Tso, “Multifunction stethoscope for telemedicine,” in *Proceedings of the 2003 IEEE International Workshop on Computer Architectures for Machine Perception*, 2004, pp. 87–89.
[21] D. Oletic, B. Arsenali, and V. Bilas, “Towards Continuous Wheeze Detection Body Sensor Node as a Core of Asthma Monitoring System,” in *Wireless Mobile Communication and Healthcare*, K. S. Nikita, J. C. Lin, D. I. Fotiadis, and M.-T. A. Waldmeyer, Eds. Springer Berlin Heidelberg, 2012, pp. 165–172.
[22] B. A. Reyes, N. Reljin, and K. H. Chon, “Tracheal Sounds Acquisition Using Smartphones,” *Sensors*, vol. 14, no. 8, pp. 13830–13850, Jul. 2014.
[23] R. Beck, G. Rosenhouse, M. Mahagnah, R. M. Chow, D. W. Cugell, and N. Gavriely, “Measurements and Theory of Normal Tracheal Breath Sounds,” *Ann. Biomed. Eng.*, vol. 33, no. 10, pp. 1344–1351, Oct. 2005.
[24] S. Huq and Z. Moussavi, “Acoustic breath-phase detection using tracheal breath sounds,” *Med. Biol. Eng. Comput.*, vol. 50, no. 3, pp. 297–308, Feb. 2012.
[25] V. A. McKusick, J. T. Jenkins, and G. N. Webb, “The acoustic basis of the chest examination; studies by means of sound spectrography,” *Am. Rev. Tuberc.*, vol. 72, no. 1, pp. 12–34, Jul. 1955.
[26] H. Pasterkamp, S. S. Kraman, and G. R. Wodicka, “Respiratory Sounds: Advances Beyond the Stethoscope,” *Am. J. Respir. Crit. Care Med.*, vol. 156, no. 3, pp. 974–987, Sep. 1997.
[27] G. Sierra, V. Telfort, B. Popov, M. Pelletier, P. Despault, R. Agarwal, and V. Lanzo, “Comparison of respiratory rate estimation based on tracheal sounds versus a capnograph,” in *Proceedings of the Annual International Conference of the IEEE Engineering in Medicine and Biology Society*, 2005, vol. 6, pp. 6145–6148.

[28] N. Reljin, B. A. Reyes, and K. H. Chon, “Tidal Volume Estimation using Blanket Fractal Dimension of the Tracheal Sounds Acquired by Smartphone,” *Sensors*, vol. In revision for publication, 2015.
[29] Z. K. Moussavi, M. T. Leopando, H. Pasterkamp, and D. G. Rempel, “Computerised acoustical respiratory phase detection without airflow measurement,” *Med. Biol. Eng. Comput.*, vol. 38, no. 2, pp. 198–203, Mar. 2000.
[30] A. Abushakra and M. Faezipour, “Acoustic signal classification of breathing movements to virtually aid breath regulation,” *IEEE J. Biomed. Health Inform.*, vol. 17, no. 2, pp. 493–500, Mar. 2013.
[31] H. Alshaer, G. R. Fernie, and T. D. Bradley, “Monitoring of breathing phases using a bioacoustic method in healthy awake subjects,” *J. Clin. Monit. Comput.*, vol. 25, no. 5, pp. 285–294, Sep. 2011.
[32] P. Hult, B. Wranne, and P. Ask, “A bioacoustic method for timing of the different phases of the breathing cycle and monitoring of breathing frequency,” *Med. Eng. Phys.*, vol. 22, no. 6, pp. 425–433, Jul. 2000.
[33] S. J. Cala, C. M. Kenyon, G. Ferrigno, P. Carnevali, A. Aliverti, A. Pedotti, P. T. Macklem, and D. F. Rochester, “Chest wall and lung volume estimation by optical reflectance motion analysis,” *J. Appl. Physiol.*, vol. 81, no. 6, pp. 2680–2689, Dec. 1996.
[34] M.-Z. Poh, D. J. McDuff, and R. W. Picard, “Advancements in Noncontact, Multiparameter Physiological Measurements Using a Webcam,” *IEEE Trans. Biomed. Eng.*, vol. 58, no. 1, pp. 7–11, Jan. 2011.
[35] L. Tarassenko, M. Villarroel, A. Guazzi, J. Jorge, D. A. Clifton, and C. Pugh, “Non-contact video-based vital sign monitoring using ambient light and auto-regressive models,” *Physiol. Meas.*, vol. 35, no. 5, p. 807, 2014.
[36] D. Shao, Y. Yang, C. Liu, F. Tsow, H. Yu, and N. Tao, “Noncontact Monitoring Breathing Pattern, Exhalation Flow Rate and Pulse Transit Time,” *IEEE Trans. Biomed. Eng.*, vol. 61, no. 11, pp. 2760–2767, Nov. 2014.
[37] Y. Nam, Y. Kong, B. Reyes, N. Reljin, and K. H. Chon, “Monitoring of Heart and Respiratory Rates using Dual Cameras on a Smartphone,” vol. In revision, 2015.
[38] K. Konno and J. Mead, “Measurement of the separate volume changes of rib cage and abdomen during breathing,” *J. Appl. Physiol.*, vol. 22, no. 3, pp. 407–422, Mar. 1967.
[39] F. Zhao, M. Li, Y. Qian, and J. Z. Tsien, “Remote Measurements of Heart and Respiration Rates for Telemedicine,” *PLoS ONE*, vol. 8, no. 10, p. e71384, Oct. 2013.
[40] “Open CV. Open Source Computer Vision Library.” .
[41] R. O. Duda, P. E. Hart, and D. G. Stork, *Pattern Classification*. New York, NY, USA: Wiley-Interscience, 2000.
[42] P. Flandrin, P. Goncalves, and G. Rilling, “Detrending and denoising with empirical mode decomposition,” in *Proceedings of the European signal processing conference (EUSIPCO’04)*, 2004, vol. 2, pp. 1581–1584.
[43] N. E. Huang, Z. Shen, S. R. Long, M. C. Wu, H. H. Shih, Q. Zheng, N.-C. Yen, C. C. Tung, and H. H. Liu, “The empirical mode decomposition and the Hilbert spectrum for nonlinear and non-stationary time series analysis,” *Proc. R. Soc. Lond. Ser. Math. Phys. Eng. Sci.*, vol. 454, no. 1971, pp. 903–995, 1998.
[44] G. Lindfield and J. Penny, *Numerical Methods: Using MATLAB*. Academic Press, 2012.
[45] Y. Sun, S. Hu, V. Azorin-Peris, S. Greenwald, J. Chambers, and Y. Zhu, “Motion-compensated noncontact imaging photoplethysmography to monitor cardiorespiratory status during exercise,” *J. Biomed. Opt.*, vol. 16, no. 7, pp. 077010–077010, 2011.

[46] Y. Hu, E. G. Kim, G. Cao, S. Liu, and Y. Xu, “Physiological acoustic sensing based on accelerometers: a survey for mobile healthcare,” *Ann. Biomed. Eng.*, vol. 42, no. 11, pp. 2264–2277, Nov. 2014.
[47] L. Vannuccini, J. E. Earis, P. Helisto, B. M. G. Cheetham, M. Rossi, A. R. A. Sovijarvi, and J. Vanderschoot, “Capturing and preprocessing of respiratory sounds,” *Eur. Respir. Rev.*, vol. 10, no. 77, pp. 616–620, 2000.

Chapter 8: Conclusions and Future Work

8.1 Conclusions

This thesis explored the use of smartphones for the noninvasive monitoring of breathing parameters including instantaneous respiratory rate (IRR) and tidal volume (V_T) via acoustical and noncontact optical approaches. In addition to estimate these parameters, we explored the development of a portable phonopneumogram directly on a smartphone by combining both approaches. Diverse research groups, including ours, have proposed the employment of smartphones for healthcare applications particularly in the area of cardiac monitoring [1]–[6]. The smartphones' applications for respiratory monitoring are more reduced and they have focused on the estimation of average respiratory rate [7]–[11]. On the other hand, the employment of smartphones for respiratory sound analysis has been also proposed [12]–[16], particularly for screening sleep-related disorders, but those studies have not questioned the acquisition step of real respiratory sounds itself neither the extraction of the abovementioned breathing parameters, in particular V_T, from the smartphone-acquired respiratory sounds. The methods proposed in this thesis were designed to take advantage of the hardware and software capabilities of smartphones found nowadays in the general market. Methodology of this thesis first explored the acquisition of real tracheal sounds using smartphones aided with an acoustical sensor, to subsequently use these smartphone-acquired sounds for the estimation of IRR and V_T. Next, estimation of these parameters was performed without the need of plugin an additional sensor to the smartphone via a noncontact optical approach. In both approaches, simple calibration procedures were proposed so that they can be easily performed by the general population. Finally, we combined the acoustical and optical approaches to perform the automatic classification of tracheal sounds directly on a smartphone without relying on a non-always available external reference signal. We consider that the methods developed in this thesis would allow the development of a mobile device from which more breathing information, in addition to together with IRR and V_T, could be obtained on a daily basis and being of particular interest in the area of respiratory sound analysis. Figure 8.1 outlines the smartphone-based breathing monitoring methods proposed in this thesis.

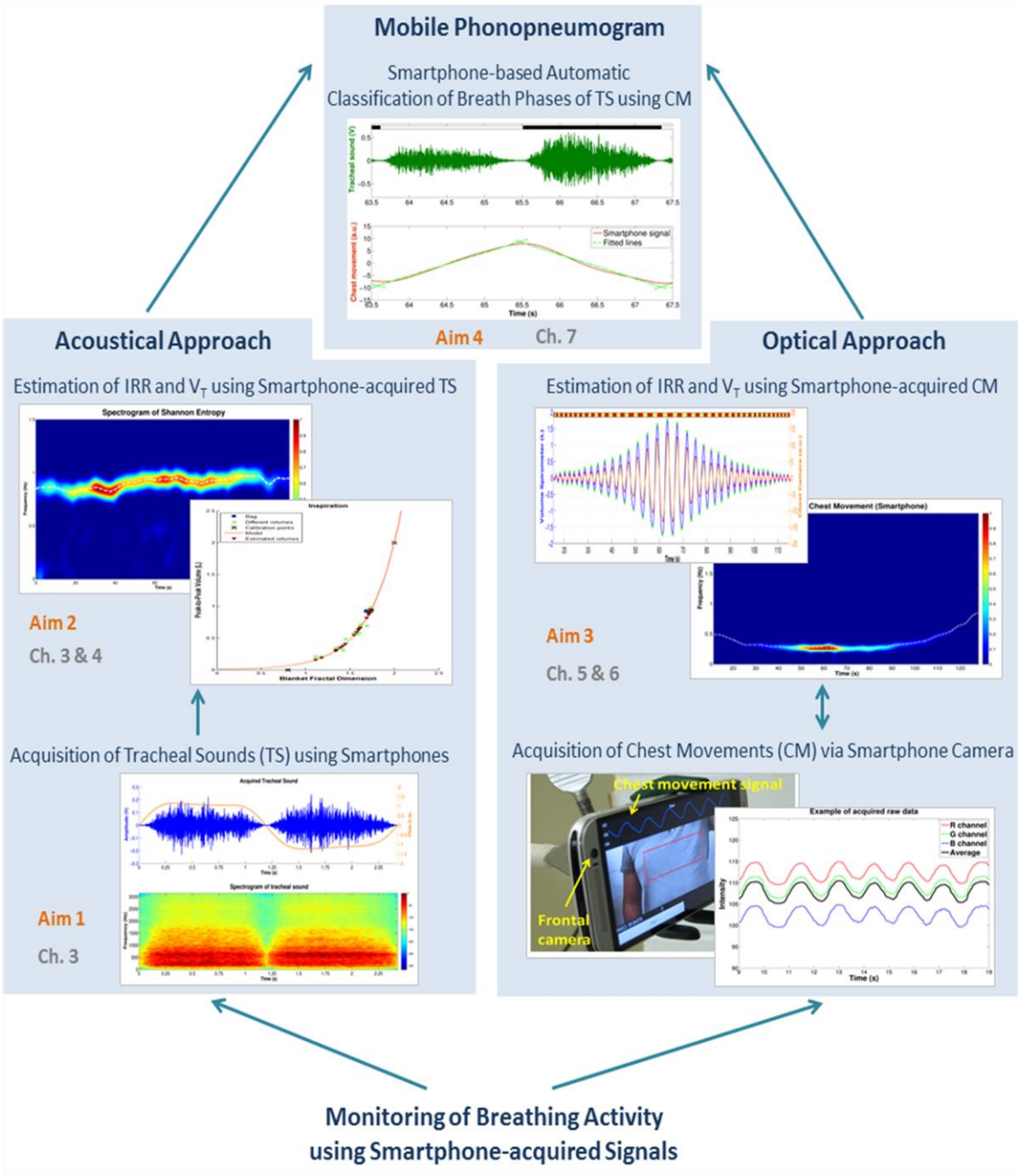

Figure 8.1 – Smartphone-based breathing monitoring methods proposed in this thesis

Two general approaches were explored: the acoustical and the optical. In the acoustical approach, respiratory tracheal sounds were acquired and their characteristics analyzed to use them later for the tasks of tracking respiratory rate (IRR) and tidal volume (V_T) estimation. In the optical approach, this estimation was performed directly on the smartphone without external sensors. Finally, both approaches were jointed to automatically classify the breath phases of the tracheal sounds directly on the smartphone without using an external reference signal from a specialized device or another respiratory sound channel.

In Aim 1, we questioned if real tracheal sounds could be acquired using smartphones. A specific designed acoustical sensor developed for respiratory sound analysis was plugged to the standard audio input of the smartphone with a simple passive circuit. We found that the proposed system allowed the acquisition of tracheal sounds whose temporal and spectral characteristics resemble those reported in the classical literature in the field of respiratory sound analysis, *e.g.*, they exhibited a temporal intensity variation related to respiratory airflow in a power law, their breath phases exhibit similar frequency content at similar airflow peaks, they possess well defined phases such that the breath-phase onsets could be extracted from them with a temporal error lower than the required for cardiorespiratory research.

Having verified that the smartphone-acquired sounds correspond to real tracheal sounds, in Aim 2 we employed signal processing techniques to extract breathing parameters from them. Regarding the respiratory rate estimation, we applied the classical time-frequency in the field respiratory sound analysis, *i.e.*, the spectrogram (SP) also called respirosonogram, to the tracheal sound's Shannon entropy (SE) signal estimated via Parzen's probability density function method applied in a moving window scheme. The fact that the SE of the acquired tracheal sounds resembled the positive rectified airflow signal of the breathing maneuver allowed us to obtain smartphone-based IRR estimates highly correlated with spirometry-based reference and with an average error lower than 1 breath-per-minute (bpm). Next, we investigated a novel signal processing technique for V_T estimation based on the fractal analysis. In general, due to the tracheal sound intensity-airflow relationship, a higher airflow produces a tracheal sound with higher temporal variations due to higher turbulences in the tracheobronchial tree and presumably a more chaotic process. To quantify this nonlinear process, the blanket fractal dimension (BFD) was estimated from the smartphone-acquired tracheal sounds. We found that an exponential model, between reference V_T and BFD from tracheal sound, is suitable to obtain rough estimates of V_T after an easy calibration done while breathing through a fixed volume bag. The acoustical estimation of V_T proposed in this thesis had the advantage of been used for multiple days after calibration and do not

rely on specialized devices. However, in order to obtain V_T as well as IRR estimates, an external sensor should be plugged to the smartphone in the acoustical approach.

To overcome the need of an additional sensor, we investigated if IRR and V_T estimates could be directly obtained in the smartphone. To this end, we employed a noncontact optical approach in Aim 3. It has been found that the external displacements of the chest wall are linearly correlated to reference tidal volume as measured from spirometry or inductance plethysmography. In this research we analyzed if the linearity between tidal volume and chest wall displacements could be captured in real time by a noncontact optical monitoring method implemented on a smartphone. We found that the developed smartphone application was effective in capturing the intensity changes of the reflected light due to breathing and provided a waveform linearly related to reference volume from spirometry, *i.e.*, there was a linear relationship between the smartphone's signal and the chest displacements which in turn are linearly related to reference tidal volume. With the knowledge of this linear relationship, we could easily perform the estimation of IRR via applying a high-resolution time-frequency representation, the smoothed pseudo Wigner-Ville distribution (SPWVD), and we found an average error lower than 1 bpm. Regarding the V_T estimation, we found that rough estimates could be directly obtained in the smartphone when calibrated on an individual basis. Initially, calibration of the optical approach was performed via spirometry. However, as this device is not generally available outside research and clinical settings, we searched for a device that allowed us to take advantage of the linearity of the optical smartphone system previously found. To this end, we investigated if a linear model could be successfully obtained by breathing at two different target volumes through a commercial volume-oriented incentive spirometer (IS). We found that a fast calibration procedure could be done and it can be implemented on a smartphone so that V_T estimation can be fully performed in the device. In contrast to the spirometer, the IS device is inexpensive and widely available but the performance of the V_T estimation deteriorated when it was used.

The results obtained in this dissertation using the acoustical and noncontact optical monitoring approaches in the smartphone are summarized in Table 8.1 for the tasks of IRR and V_T estimation.

Table 8.1 – Summary of estimation results for instantaneous respiratory rate (IRR) and tidal volume (V_T) parameters using smartphones.

Parameter		Values		
Acoustical approach				
IRR estimation				
Range of measurements	[*bpm*]	15	to	35
RMSE	[*bpm*]	0.73	±	0.29
NRMSE	[*%*]	3.21	±	1.30
Bias	[*bpm*]		0.11 *	
95% limits of agreement	[*bpm*]	−1.41	to	1.64
V_T estimation (calibration using Spirobag®)				
Range of measurements	[*L*]	0.2	to	1.0
NRMSE	[*%*]	15.88	±	9.25
Bias	[*L*]		0.023 *	
95% limits of agreement	[*L*]	-0.16	to	0.20
Noncontact optical approach				
IRR estimation				
Range of measurements	[*bpm*]	7	to	50
RMSE	[*bpm*]	0.41	±	0.18
NRMSE	[*%*]	3.03	±	2.87
Bias	[*bpm*]		-0.024 *	
95% limits of agreement	[*bpm*]	-0.85	to	0.80
V_T estimation (calibration using spirometer)				
Range of measurements	[*L*]	0.3	to	3.0
RMSE	[*L*]	0.18	±	0.11
NRMSE	[*%*]	14.99	±	5.17
Bias	[*L*]		0.014	
95% limits of agreement	[*L*]	-0.35	to	0.38
V_T estimation (calibration using incentive spirometer)				
Range of measurements	[*L*]	0.3	to	3.0
RMSE	[*L*]	0.19	±	0.07
NRMSE	[*%*]	18.56	±	6.58
Bias	[*L*]		-0.051 *	
95% limits of agreement	[*L*]	-0.42	to	0.32

Values presented as mean ± standard deviation
* indicates statistically significant differences from a zero bias (p<0.05)

Given the knowledge learned during the acoustical and optical approaches using smartphones, *i.e.*, the reliable acquisition of tracheal sounds and the linearity of the captured chest wall displacements signals and reference volume, we investigated if accurate breath-phase classification of tracheal sounds could be automatically performed in the smartphone by using the optical acquired signal in Aim 4. In the field of respiratory sound analysis, it is well known that the timing of events and the relationship of these sounds with respect to the breath phase is relevant. We found that the chest movement signal provided by our smartphone algorithm was highly linear correlated to reference volume signal from spirometry. Hence, we used this smartphone signal as a surrogate of the spirometer-based volume which is not always granted for the general population or even the general practitioner when performing pulmonary auscultation. We found that the breath phases of the tracheal sounds were correctly classified using the optical approach during noise-free and regular breathing conditions. We also found that the classification can be performed during different breathing scenarios that include non-breathing related events like coughing, swallowing or talking, and during irregular or non-alternate breathing phases. Due to the linearity of the smartphone-acquired chest movement signal and the reference volume, the classification task was performed as it could be done in classical phonopneumography, *i.e.*, first detecting the breath-phase onsets and then analyzing the slope of the data in between two consecutive onsets. As the objective is to develop a mobile phonopneumography, effort was put to simplify the computational burden of the classification method.

Through this thesis, we presented general methods for the extraction of breathing parameters from smartphone-acquired acoustical and optical signals. The methods developed in this research were meant for general use but having in mind the respiratory sound analysis. The results presented here point out to the feasibility of developing a mobile phonopneumogram based on commercially available smartphones. It is not the intention of this research to replace any existing breathing monitoring method, including the human observation and auscultation with the mechanical stethoscope, but only to provide additional tools to the general practitioner, or for on-demand monitoring, so that the computerized

respiratory sound analysis can be translated outside specialized research and clinical centers for the benefit of the general population. We recognize that despite achieving the proposed aims, this research is still under ongoing exploration and possesses several limitations that need to be addressed. The areas of future development and applications of the methods of this research are presented next.

8.2 Future Work

Regarding the smartphone-based acoustical monitoring of breathing parameters presented in this dissertation, future work includes the acquisition and analysis of tracheal sounds in different postures and involving head movements. Previous studies have addressed some of these questions using classical computerized analysis of respiratory sounds [17]. Additional studies have to be done to test the performance of the smartphone-based estimation of IRR and V_T when the head moves during the maneuvers as well as when moving from a posture to the other, *e.g.*, from standing to supine or seating. If intended for short-term recordings, head movements and postural changes maybe can be avoided but they can still become an issue when working with children who tend not to collaborate during the breathing maneuvers. In addition, studies outside regular dry laboratories are required to test the performance of the smartphone-based system under everyday situations and the results obtained would pointed out to the modification of the system to deal with noise. If successful, that research would expand the usability of the proposed system and enable the acquisition of large-samples studies in locations not easily accessible nowadays with the current acoustical respiratory monitoring systems. Regarding the calibration procedure, the use of a Spirobag allowed us to not rely on specialized devices like a spirometer or an inductance plethysmography. However, the Spirobag is an instrument that could be improved, if not substituted by another one, to obtain a more reliable fixed volume. Finally, although not limited to the proposed smartphone-based breathing monitoring, an acoustical sensor should be connected to the main data acquisition and processing system. In this dissertation, they were connected via a standard audio cable and a passive circuit. Future studies could explore the implementation and testing of wireless communications in the smartphone-based system.

The employment of a noncontact optical approach in the smartphone allowed us to overcome the use of an external sensor to estimate IRR and V_T. Future studies similar to the ones discussed above for the acoustical approach should be performed to analyze the performance of smartphone-based optical approach. Breathing maneuvers should be recorded in different postures to establish if the monitored area should still be focused on the rib cage or, as expected for the supine posture, it should be focused on the abdominal area. The use of two monitoring areas should also be explored to analyze if the sum of the rib cage and abdominal contributions provides a more accurate estimation of V_T. The use of advanced image processing techniques that allows the definition and tracking of a region of interest delimited by the thorax borders is also a topic that should be explored so that all the anterior chest wall area visible to the smartphone could be used to obtain the chest movement signal from which V_T is estimated. The implementation of body tracking and motion noise artifact removal algorithms is another area of future exploration. In particular, our research group has been pursuing and developing motion noise artifact detection and reconstruction algorithms for photoplethysmogram and electrocardiogram applications [18], [19]. It would be interesting to implement such algorithms in the smartphone and test their performance for the tasks of IRR and V_T estimation as well as for the automatic classification of breath phases. The effect of illumination changes during the acquisition should be studied. Of particular interest will be the recording of signals in environments different to the regular office or dry laboratory in order to explore the usability of the proposed system in situations that take advantage of smartphone's mobility.

As being a mixture of the acoustical and optical approaches, the future work of the mobile phonopneumogram involves those mentioned above for such approaches. It is worth mentioning that besides the results obtained by the acoustical approach in this research, the proposed method for V_T estimation relied on the labeling and segmentation of the breath phases of the acquired tracheal sounds. At that stage, the phases were labeled using the reference volume from inductance plethysmography. However, such limitation can be overcome by employing the smartphone-optical acquired signal proposed in this thesis. Currently, our research group is working on the implementation of a smartphone

application able to simultaneously acquire and process the tracheal sounds and the chest movement signals directly on the device. The smartphone application is being designed so that it allows the automatically classification of the breath phases as well as to perform classical temporal, spectral and joint time-frequency analysis of the acquired tracheal sounds. Although the waveform of the smartphone-acquired chest movement signal was employed for automatic breath-phase classification given the linearity of this signal and the reference volume from spirometry, this waveform was mainly studied for IRR and V_T estimation purposes. Hence, further studies are required to analyze if the smartphone-acquired chest movement signal could be used to detect different types of breathing patterns [20], *e.g.*, ataxic breathing, dysrhythmic breathing, Cheyne-Stokes respiration, or central sleep apnea, so that it provides more information than the respiratory rate or breathing depth parameters by themselves.

8.2.1 Envisioned application

This research was focused on the development of general smartphone-based breathing monitoring methods and for this purpose we only acquired signals during the maneuvers performed by healthy volunteers and not by patients with respiratory diseases. As mentioned before, the computerized respiratory sound analysis interests our and our collaborators research groups. An application for the methods developed in this dissertation regards with the automatic analysis of adventitious respiratory sounds directly on the smartphone. Nowadays, most of practitioners perform the pulmonary auscultation via mechanical stethoscope where the analysis of the heard sounds is based on their own experience and auditory capabilities, *i.e.*, this procedure does not allow a quantitative analysis of the sounds heard from the patients. The results of this dissertation point out that a smartphone-based system could provide information regarding the breathing frequency and depth of breath in addition to the acquired respiratory sounds of interest. Also, the proposed smartphone system appears to provide a volumetric surrogate from which information about the timing and level of occurrence of respiratory sounds events can be labeled. Therefore, we consider that this technology could be useful to complement the information obtained by the classical pulmonary auscultation. Among other benefits, a smartphone-based system allows an easy

integration of other methods of analysis, *e.g.*, the embedding of signal processing algorithms for respiratory sounds such as automatic adventitious sounds detection and analysis. Also, the use of smartphones provides our proposed system with the characteristic of being readily adopted by other users. This adoptability becomes relevant when providing the system to researchers in other institutes to study respiratory diseases.

In an initial effort towards this long-term goal, our collaborators, Drs. Sonia Charleston-Villalobos, Tomas Aljama-Corrales and Ramon Gonzalez-Camarena, acquired respiratory sounds at the National Institute of Respiratory Diseases in Mexico City (Instituto Nacional de Enfermedades Respiratorias) using the proposed acoustical approach of this research. An example of the smartphone-acquired respiratory sound is shown in Figure 8.2. This respiratory sound recording was obtained in a patient diagnosed with pulmonary fibrosis. The acoustical sensor corresponded to the one used in this research and was coupled to the smartphone as detailed in Chapter 3 of this dissertation. The acoustical sensor was placed on the posterior right surface of the chest wall at the basal level of the mid-clavicular line according to the array of sensors designed by our collaborators [21]. At this location, the physician heard more discontinuous adventitious lung sounds (crackles) during the inspiratory phase when performing the pulmonary auscultation via the mechanical stethoscope. An automatic crackle detection algorithm based on the time-varying autoregressive modeling was applied to the acquired signal [22]. As can be seen in Figure 8.2, the smartphone-acquired tracheal sounds were able to capture the crackle sounds from this patient. The triangular markers displayed on top of the sound indicate the detected location of the crackles. Crackles were detected only during the inspiratory phases in agreement with the initial findings of the physician. This preliminary result is promising and we are currently working together on a protocol to acquire lung sounds from patients with diverse stages of pulmonary fibrosis and other related respiratory diseases. The proposed smartphone-based system can be updated with this and similar algorithms so that general practitioners can take advantage of the computerized analysis of respiratory sounds directly at the primary healthcare points.

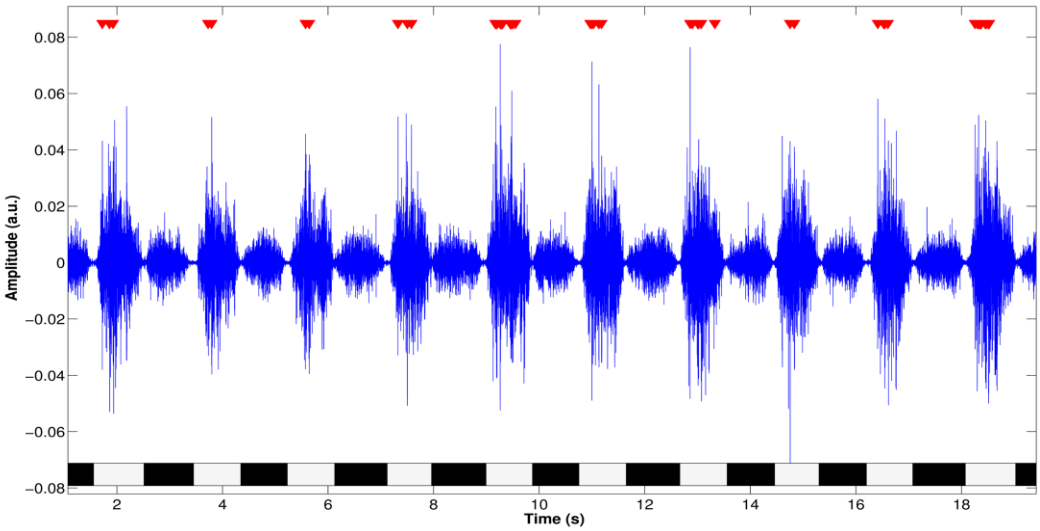

Figure 8.2 – Smartphone-acquired lung sounds of a patient with pulmonary fibrosis.
Grey and black boxes at the bottom of the signal indicate the inspiratory and expiratory breath phases, respectively. Triangular markers on top of the signal indicate the location of the crackles as detected via an automatic algorithm. Observe that crackles were only detected during the inspiratory phases as initially noted by the physician prior recording via smartphone.

A disease that commonly exhibits crackles and could lead in long-term to pulmonary fibrosis is the extrinsic allergic alveolitis (EAA), also called hypersensitivity pneumonitis. EAA is an important respiratory disease affecting mainly female adults [23], [24]. EAA is a progressive disease caused in response to repeated inhalation of a large variety of antigens that elicit an immunologically induced inflammation of the lung parenchyma, peripheral airways and surrounding interstitial tissue [25]. Acute, sub-acute and chronic are the three phases of EAA [26]. The chronic form of EAA has an insidious onset over a period of months, with increasing cough and exertional dyspnea and with predominant fatigue and weight loss [27]. Persistent low-level exposure tends to cause this chronic form which often portends a progressive and irreversible disease due to progressive deposition of fibrotic tissue [26]. Early and accurate diagnosis of this disease is important because EAA could be reversed if diagnosed in its early stages [28]. However, nowadays diagnosis of EAA is challenging and long. The first approach employed in the diagnosis is the clinical examination of the pulmonary function that includes clinical history and

auscultation of the lungs [29]. Clinical history often arise suspicion of EAA via an exhaustive occupational, hobbies, and home environmental questioning section [26], [30]. During the auscultation procedure with the traditional stethoscope, adventitious lung sounds are expected to be heard in subjects with EAA [27], [31]–[34]. The most predominant type of adventitious lung sounds heard in subjects with EAA is the crackle [34]. It has been found that these crackles are more frequent in patients in the chronic phase than in patients in the acute or sub-acute phase [24]. In diffuse interstitial pulmonary diseases like EAA, crackles first appear in the basal areas of the lungs and later, as the disease progress, also in the upper zones of the lungs [35], [36]. It has been recently proposed that the surrounding base lung sounds, to which the crackles are superimposed, also change its characteristics during EAA [37]. Other important diagnostic tools include pulmonary function test, chest radiography and high-resolution computed tomography, precipitating antibodies test, bronchoalveolar lavage, provocation test [25], [28]. However, not all these techniques are available in the clinical centers [25]. A definitive diagnosis of EAA will usually require surgical lung biopsy [38]. Biopsy at chronic phase has shown that lung fibrosis, or scarring of the lung, is the important hallmark [33]. Lung fibrosis is associated with reduced survival in patients with EAA [39].

As mentioned above, the early and accurate detection of EAA plays a key role to provide prompt treatment and to avoid further exposure to causative antigens that could lead to progressive and irreversible phases [40]. Although not definitive to make a diagnosis, auscultation is a tool used by the physicians since the first contact with the patient. We consider that this auscultation step could benefit from the use of a smartphone-based system as the one presented in this thesis. Application of a mobile computerized system for respiratory sound analysis could also help to study the actual prevalence of EAA. It is believed that the prevalence of EAA is low, but this low prevalence may be artificial because the large number of individuals with EAA that are not detected or are misdiagnosed [25]. Reports based on hospital admissions where a definite diagnosis can be made using radiologic evaluation, bronchoalveolar lavage, and lung biopsy are likely to identify the most severe cases only and thus

underestimate the true prevalence of this disease [27]. Nevertheless, despite the low prevalence, EAA negatively impacts the quality of life and productivity of individuals, causes an increase in costs of occupational illness, and due to its progressive nature may result in permanent dysfunction that may lead to disability or death [25], [30], [41]. Future studies employing smartphone-based systems are required and will bring light regarding their clinical relevance in detecting adventitious respiratory sounds during EAA and similar respiratory diseases.

Finally, it is worth mentioning that our research group is pursuing the development of a wearable device for long-term cardiac monitoring. A key role of this development is played by the electrocardiogram (ECG) electrode. To this end, our research group has designed and tested a carbon-based dry, flexible, and reusable electrode able to collect ECG signals under different conditions [42]. The goal of our research group is to integrate this wearable monitor with a smartphone system containing the methods described in this dissertation so that the simultaneous monitoring of ECG, breathing-parameters, and respiratory sounds could be performed directly on the smartphone.

8.3 References

[1] C. Scully, J. Lee, J. Meyer, A. M. Gorbach, D. Granquist-Fraser, Y. Mendelson, and K. H. Chon, "Physiological parameter monitoring from optical recordings with a mobile phone," *Biomed. Eng. IEEE Trans. On*, vol. 59, no. 2, pp. 303–306, 2012.

[2] J. Lee, B. A. Reyes, D. D. McManus, O. Mathias, and K. H. Chon, "Atrial Fibrillation Detection Using an iPhone 4S," *IEEE Trans. Biomed. Eng.*, vol. 60, no. 1, pp. 203–206, 2013.

[3] M. J. Gregoski, M. Mueller, A. Vertegel, A. Shaporev, B. B. Jackson, R. M. Frenzel, S. M. Sprehn, and F. A. Treiber, "Development and Validation of a Smartphone Heart Rate Acquisition Application for Health Promotion and Wellness Telehealth Applications," *Int J Telemed. Appl*, vol. 2012, pp. 1:1–1:1, Jan. 2012.

[4] E. Jonathan and M. Leahy, "Investigating a smartphone imaging unit for photoplethysmography," *Physiol. Meas.*, vol. 31, no. 11, p. N79, Nov. 2010.

[5] R.-C. Peng, X.-L. Zhou, W.-H. Lin, and Y.-T. Zhang, "Extraction of heart rate variability from smartphone photoplethysmograms," *Comput. Math. Methods Med.*, vol. 2015, p. 516826, 2015.

[6] J. A. J. Heathers, "Smartphone-enabled pulse rate variability: An alternative methodology for the collection of heart rate variability in psychophysiological research," *Int. J. Psychophysiol.*, vol. 89, no. 3, pp. 297–304, Sep. 2013.

[7] J. Lazaro, Y. Nam, E. Gil, P. Laguna, and K. H. Chon, "Smartphone-camera-acquired pulse photoplethysmographic signal for deriving respiratory rate," in *2014 8th Conference of the European Study Group on Cardiovascular Oscillations (ESGCO)*, 2014, pp. 121–122.
[8] Y. Nam, J. Lee, and K. H. Chon, "Respiratory Rate Estimation from the Built-in Cameras of Smartphones and Tablets," *Ann. Biomed. Eng.*, vol. 42, no. 4, pp. 885–898, Nov. 2013.
[9] Y. Nam, B. Reyes, and K. Chon, "Estimation of Respiratory Rates Using the Built-in Microphone of a Smartphone or Headset," *IEEE J. Biomed. Health Inform.*, vol. PP, no. 99, pp. 1–1, 2015.
[10] A. R. Fekr, M. Janidarmian, K. Radecka, and Z. Zilic, "A Medical Cloud-Based Platform for Respiration Rate Measurement and Hierarchical Classification of Breath Disorders," *Sensors*, vol. 14, no. 6, pp. 11204–11224, Jun. 2014.
[11] J. Lázaro, Y. Nam, E. Gil, P. Laguna, and K. H. Chon, "Respiratory rate derived from smartphone-camera-acquired pulse photoplethysmographic signals," *Physiol. Meas.*, vol. 36, no. 11, p. 2317, 2015.
[12] D. Oletic, B. Arsenali, and V. Bilas, "Towards Continuous Wheeze Detection Body Sensor Node as a Core of Asthma Monitoring System," in *Wireless Mobile Communication and Healthcare*, K. S. Nikita, J. C. Lin, D. I. Fotiadis, and M.-T. A. Waldmeyer, Eds. Springer Berlin Heidelberg, 2012, pp. 165–172.
[13] D. Oletic, M. Skrapec, and V. Bilas, "Monitoring Respiratory Sounds: Compressed Sensing Reconstruction via OMP on Android Smartphone," in *Wireless Mobile Communication and Healthcare*, B. Godara and K. S. Nikita, Eds. Springer Berlin Heidelberg, 2013, pp. 114–121.
[14] K. Hung, B. L. Luk, W. H. Choy, B. Tai, and S. K. Tso, "Multifunction stethoscope for telemedicine," in *Proceedings of the 2003 IEEE International Workshop on Computer Architectures for Machine Perception*, 2004, pp. 87–89.
[15] M. Al-Mardini, F. Aloul, A. Sagahyroon, and L. Al-Husseini, "Classifying obstructive sleep apnea using smartphones," *J. Biomed. Inform.*, vol. 52, pp. 251–259, Dec. 2014.
[16] J. Behar, A. Roebuck, J. S. Domingos, E. Gederi, and G. D. Clifford, "A review of current sleep screening applications for smartphones," *Physiol. Meas.*, vol. 34, no. 7, p. R29, 2013.
[17] C.-L. Que, C. Kolmaga, L.-G. Durand, S. M. Kelly, and P. T. Macklem, "Phonospirometry for noninvasive measurement of ventilation: methodology and preliminary results," *J. Appl. Physiol.*, vol. 93, no. 4, pp. 1515–1526, Oct. 2002.
[18] J. W. Chong, D. K. Dao, S. M. A. Salehizadeh, D. D. McManus, C. E. Darling, K. H. Chon, and Y. Mendelson, "Photoplethysmograph Signal Reconstruction Based on a Novel Hybrid Motion Artifact Detection–Reduction Approach. Part I: Motion and Noise Artifact Detection," *Ann. Biomed. Eng.*, vol. 42, no. 11, pp. 2238–2250, Aug. 2014.
[19] S. M. A. Salehizadeh, D. K. Dao, J. W. Chong, D. McManus, C. Darling, Y. Mendelson, and K. H. Chon, "Photoplethysmograph Signal Reconstruction based on a Novel Motion Artifact Detection-Reduction Approach. Part II: Motion and Noise Artifact Removal," *Ann. Biomed. Eng.*, vol. 42, no. 11, pp. 2251–2263, May 2014.
[20] G. Yuan, N. A. Drost, and R. A. McIvor, "Respiratory rate and breathing pattern," *McMaster Univ Med J*, vol. 10, pp. 23–28, 2013.
[21] S. Charleston-Villalobos, G. Martinez-Hernandez, R. Gonzalez-Camarena, G. Chi-Lem, J. G. Carrillo, and T. Aljama-Corrales, "Assessment of multichannel lung sounds parameterization for two-class classification in interstitial lung disease patients," *Comput. Biol. Med.*, vol. 41, no. 7, pp. 473–482, Jul. 2011.
[22] S. Charleston-Villalobos, G. Dorantes-Méndez, R. González-Camarena, G. Chi-Lem, J. G. Carrillo, and T. Aljama-Corrales, "Acoustic thoracic image of crackle sounds using linear and nonlinear processing techniques," *Med. Biol. Eng. Comput.*, vol. 49, no. 1, pp. 15–24, Jan. 2011.
[23] M. L. Bustos, S. Frías, S. Ramos, A. Estrada, J. L. Arreola, F. Mendoza, M. Gaxiola, M. Salcedo, A. Pardo, and M. Selman, "Local and Circulating Microchimerism Is Associated with Hypersensitivity Pneumonitis," *Am. J. Respir. Crit. Care Med.*, vol. 176, no. 1, pp. 90–95, Jul. 2007.

[24] F. Morell, À. Roger, L. Reyes, M. J. Cruz, C. Murio, and X. Muñoz, "Bird Fancier's Lung: A Series of 86 Patients," *Medicine (Baltimore)*, vol. 87, no. 2, pp. 110–130, Mar. 2008.
[25] J. N. Fink, H. G. Ortega, H. Y. Reynolds, Y. F. Cormier, L. L. Fan, T. J. Franks, K. Kreiss, S. Kunkel, D. Lynch, S. Quirce, C. Rose, R. P. Schleimer, M. R. Schuyler, M. Selman, D. Trout, and Y. Yoshizawa, "Needs and Opportunities for Research in Hypersensitivity Pneumonitis," *Am. J. Respir. Crit. Care Med.*, vol. 171, no. 7, pp. 792–798, Apr. 2005.
[26] A. M. Patel, J. H. Ryu, and C. E. Reed, "Hypersensitivity pneumonitis: Current concepts and future questions," *J. Allergy Clin. Immunol.*, vol. 108, no. 5, pp. 661–670, Nov. 2001.
[27] Y. Lacasse and Y. Cormier, "Hypersensitivity pneumonitis," *Orphanet J. Rare Dis.*, vol. 1, no. 1, p. 25, Jul. 2006.
[28] A. L. Chan, M. M. Juarez, K. O. Leslie, H. A. Ismail, and T. E. Albertson, "Bird Fancier's Lung: A State-of-the-Art Review," *Clin. Rev. Allergy Immunol.*, vol. 43, no. 1–2, pp. 69–83, Aug. 2012.
[29] F. Dalmay, M. T. Antonini, P. Marquet, and R. Menier, "Acoustic properties of the normal chest," *Eur. Respir. J.*, vol. 8, no. 10, pp. 1761–1769, Oct. 1995.
[30] R. L. Jacobs, C. P. Andrews, and J. J. Coalson, "Hypersensitivity pneumonitis: beyond classic occupational disease–changing concepts of diagnosis and management," *Ann. Allergy. Asthma. Immunol.*, vol. 95, no. 2, pp. 115–128, Aug. 2005.
[31] Y. Cormier and Y. Lacasse, "Keys to the diagnosis of hypersensitivity pneumonitis: the role of serum precipitins, lung biopsy, and high-resolution computed tomography," *Clin. Pulm. Med.*, vol. 3, no. 2, p. 77, 1996.
[32] M. Schuyler and Y. Cormier, "The diagnosis of hypersensitivity pneumonitis," *CHEST J.*, vol. 111, no. 3, pp. 534–536, 1997.
[33] T. Takemura, T. Akashi, Y. Ohtani, N. Inase, and Y. Yoshizawa, "Pathology of hypersensitivity pneumonitis," *Curr. Opin. Pulm. Med.*, vol. 14, no. 5, pp. 440–454, Sep. 2008.
[34] Y. Lacasse, M. Selman, U. Costabel, J.-C. Dalphin, M. Ando, F. Morell, R. Erkinjuntti-Pekkanen, N. Müller, T. V. Colby, M. Schuyler, and Y. Cormier, "Clinical Diagnosis of Hypersensitivity Pneumonitis," *Am. J. Respir. Crit. Care Med.*, vol. 168, no. 8, pp. 952–958, Oct. 2003.
[35] G. R. Epler, C. B. Carrington, and E. A. Gaensler, "Crackles (rales) in the interstitial pulmonary diseases," *Chest*, vol. 73, no. 3, pp. 333–339, Mar. 1978.
[36] P. Piirila and A. R. Sovijarvi, "Crackles: recording, analysis and clinical significance," *Eur. Respir. J.*, vol. 8, no. 12, pp. 2139–2148, Dec. 1995.
[37] S. Charleston-Villalobos, L. Albuerne-Sanchez, R. Gonzalez-Camarena, M. Mejia-Avila, G. Carrillo-Rodriguez, and T. Aljama-Corrales, "Linear and Nonlinear Analysis of Base Lung Sound in Extrinsic Allergic Alveolitis Patients in Comparison to Healthy Subjects," *Methods Inf. Med.*, vol. 52, no. 3, pp. 266–276, Apr. 2013.
[38] H. Sahin, K. K. Brown, D. Curran-Everett, V. Hale, C. D. Cool, J. S. Vourlekis, and D. A. Lynch, "Chronic Hypersensitivity Pneumonitis: CT Features—Comparison with Pathologic Evidence of Fibrosis and Survival," *Radiology*, vol. 244, no. 2, pp. 591–598, Aug. 2007.
[39] V. Hanak, J. M. Golbin, and J. H. Ryu, "Causes and Presenting Features in 85 Consecutive Patients With Hypersensitivity Pneumonitis," *Mayo Clin. Proc.*, vol. 82, no. 7, pp. 812–816, Jul. 2007.
[40] T. Ismail, C. Mcsharry, and G. Boyd, "Extrinsic allergic alveolitis," *Respirology*, vol. 11, no. 3, pp. 262–268, 2006.
[41] American Lung Association, "Occupational Lung Diseases," *Lung Dis. Data*, 2008.
[42] B. A. Reyes, H. F. Posada-Quintero, J. R. Bales, A. L. Clement, G. D. Pins, A. Swiston, J. Riistama, J. P. Florian, B. Shykoff, M. Qin, and K. H. Chon, "Novel electrodes for underwater ECG monitoring," *IEEE Trans. Biomed. Eng.*, vol. 61, no. 6, pp. 1863–1876, Jun. 2014.